INVESTIGATION OF PRE-CLINICAL AND PHASE II CLINICAL STUDIES OF VLP-58-1023-AL-K3-PII VACCINE FOR ALPHA VARIANT

A THESIS SUBMITTED TO

THE GRADUATE SCHOOL OF ENGINEERING AND SCIENCE

OF BILKENT UNIVERSITY

IN PARTIAL FULFILLMENT OF THE REQUIREMENTS FOR

THE DEGREE OF

MASTER OF SCIENCE

IN

MOLECULAR BIOLOGY AND GENETICS

By

Berfu Saraydar

August 2022

INVESTIGATION OF PRE-CLINICAL AND PHASE II CLINICAL STUDIES OF VLP-58-1023-AL-K3-PII VACCINE FOR ALPHA VARIANT

By Berfu Saraydar

August 2022

We certify that we have read this dissertation and that in our opinion it is fully adequate in scope and in quality, as a thesis for the degree of Master of Science.

_____

Prof. Dr. İhsan Gürsel

(Advisor)

_____

Dr. Serkan Belkaya

_____

Prof. Dr. Kamil Can Akçalı

Approved for Graduate School of Engineering and Science

_____

Orhan Arıkan

Director of the Graduate School of Engineering and Science

To my beloved family…

ABSTRACT

INVESTIGATION OF PRE-CLINICAL AND PHASE II CLINICAL STUDIES OF VLP-58-1023-AL-K3-PII VACCINE FOR ALPHA VARIANT

Berfu Saraydar

M.Sc. in Molecular Biology and Genetics

Advisor: Prof. Dr. İhsan Gürsel

August 2022

In the late December of 2019, SARS-CoV-2, a new coronavirus, was discovered in Wuhan, China and described as the causative agent of Coronavirus Disease 2019 (COVID-19). The disease has spread rapidly across the world due to its high transmissibility and has been declared a pandemic by the World Health Organization (WHO). The development of an effective vaccine has become the most significant issue to constrain the pandemic. Several COVID-19 vaccines have been authorized for human use and others are in clinical trials. Although SARS-CoV-2 encodes four structural proteins, which are Spike (S), Nucleocapsid (N), Membrane (M) and Envelope (E), most of the current vaccines used only Spike as antigen in order to generate antibodies for preventing the virus entry and replication. However, concerns have raised about Spike-based vaccines with the emerging of variants as they can moderately escape from neutralizing antibodies. For these purposes, we developed Virus-like particle (VLP) vaccine which displays hexaproline prefusion-stabilized spike (S-6p), N, M, E proteins, and adjuvanted with Alum and K3-CpG ODN. Rather than using wild type, we preferred to use the sequence of Alpha variant because of its high mortality risk and selection advantages. At the beginning of the study, we designed three different vaccine formulations and based on the results of humoral immune response in mice we determined the optimal formulation and dosage for human use. Our pre-clinical studies revealed that the best vaccine combination was high dose antigen and low dose adjuvants. Next, we wondered whether a 3rd dose has an impact on long-lasting immunity or enhancing immunogenicity in mice so that its applicability to humans could be determined. It was found that 3rd dose injection increased the antibody levels much higher than 2nd dose administration and prevented humoral immunity from decreasing after a certain amount of time. Further, both humoral and cellular immunity were studied

with serum and PBMC samples from 117 volunteers who participated in the Phase II clinical trial. All IgG ELISA experiments indicated that VLP-58-1023-AL-K3-PII vaccine induced great amount of humoral immune responses against S,N proteins and WT, Alpha, Delta RBDs. In terms of T cell responses, it is known that Alum-induced robust Th2 response can be redirected to the Th1 axis with the use of CpG ODN. So, we investigated whether Th1 or Th2 type of cell response was dominant after vaccination. All cytokine levels specific to SARS-CoV-2 peptides demonstrated that the vaccine elicited Th1-biased responses. Taken together, this study revealed that VLP-58-1023-AL-K3-PII vaccine for Alpha variant successfully elicited both humoral and cellular immune responses, its effectiveness against other variants was indicated and the efficiency of vaccine could be increased with the administration of 3rd dose, in terms of ensuring long-lasting immunity.

Keywords: SARS-CoV-2, Virus-like particles, vaccines, CpG ODN, Alum, humoral immunity, cellular immunity

ÖZET

VLP-58-1023-AL-K3-PII AŞISININ ALFA VARYANTI İÇİN KLİNİK ÖNCESİ VE FAZ II KLİNİK ÇALIŞMALARININ ARAŞTIRILMASI

Berfu Saraydar

Moleküler Biyoloji ve Genetik, Yüksek Lisans

Tez Danışmanı: Prof. Dr. İhsan Gürsel

Ağustos 2022

2019 yılının aralık ayının sonlarında, yeni bir koronavirüs olan SARS-CoV-2, Çin'in Wuhan kentinde keşfedildi ve Coronavirus Hastalığı 2019'un (COVID-19) etken maddesi olarak tanımlandı. Hastalık, bulaşıcılığının yüksek olması nedeniyle tüm dünyaya hızla yayılmış ve Dünya Sağlık Örgütü (DSÖ) tarafından pandemi ilan edilmiştir. Etkili bir aşının geliştirilmesi, pandemiyi sınırlamak için en önemli konu haline geldi. Birkaç COVID-19 aşısı insan kullanımı için yetkilendirilmiştir ve diğerleri klinik deneyler aşamasındadır. SARS-CoV-2, Spike (S), Nükleokapsid (N), Membran (M) ve Kılıf (E) olmak üzere dört yapısal proteini kodlasa da mevcut aşıların çoğu, virüs girişini ve replikasyonunu önlemek amacıyla antikorlar oluşturmak için antijen olarak yalnızca Spike'ı kullandı. Ancak, ortaya çıkan varyantların nötralize edici antikorlardan belli derecede kaçabildiklerinden Spike bazlı aşılar konusunda endişeler arttı. Bu amaçlar doğrultusunda, heksaprolin prefüzyonla stabilize edilmiş Spike (S-6p), N, M, E sergileyen ve Alum ve K3-CpG ODN ile adjuvanlanmış Virüs benzeri parçacık (VLP) aşısı geliştirdik. Yabani tip kullanmak yerine, yüksek ölüm riski ve seçim avantajları taşıdığından Alfa varyantı dizilimini kullanmayı tercih ettik. Çalışmanın başında üç farklı aşı formülasyonu tasarladık ve farelerde hümoral bağışıklık yanıtın sonuçlarına dayanarak insan kullanımı için optimal formülasyonu ve dozu belirledik. Klinik öncesi çalışmalarımız, en iyi aşı kombinasyonunun yüksek doz antijen ve düşük doz adjuvanlar olduğunu ortaya koydu. Daha sonra, insanlara uygulanabilirliğinin belirlenebilmesi için 3. dozun uzun süreli bağışıklık üzerinde veya farelerde immünojenisiteyi artırmada bir etkisi olup olmadığını merak ettik. 3. doz enjeksiyonun 2. doz uygulamasından çok daha fazla antikor seviyesini arttırdığı ve belli bir süre zaman geçtikten sonra hümoral bağışıklığın azalmasını engellediği bulundu. Daha sonra, Faz II klinik çalışmasına katılan 117 gönüllüden alınan serum ve PBMC numuneleri ile hem hümoral hem de hücresel bağışıklık incelendi. Tüm IgG ELISA deneyleri, VLP-58-1023-AL-K3-PII aşısının S, N

proteinlerine ve WT, Alpha, Delta RBD'lere karşı büyük miktarda hümoral bağışıklık yanıtına neden olduğunu gösterdi. T hücresi yanıtları açısından, Alum kaynaklı güçlü Th2 yanıtının, CpG ODN kullanımı ile Th1 eksenine yeniden yönlendirilebileceği bilinmektedir. Bu nedenle, aşılamadan sonra Th1 mi yoksa Th2 tipi hücre yanıtının mı baskın olup olmadığını araştırdık. SARS-CoV-2 peptitlerine özgü tüm sitokin seviyeleri, aşının Th1 yanlı tepkileri ortaya çıkardığını gösterdi. Bütün sonuçlar ele alındığında, Alfa varyantlı VLP-58-1023-AL-K3-PII aşısının hem hümoral hem de hücresel bağışıklık yanıtlarını başarılı bir şekilde ortaya çıkardığını, diğer varyantlara karşı etkinliğinin belirtildiğini ve uzun süreli bağışıklık açısından 3.doz uygulaması ile aşının etkinliğinin arttırılabileceğini ortaya koymuştur.

Anahtar sözcükler: SARS-CoV-2, virüs benzeri parçacıklar, aşılar, CpG ODN, Alum, hümoral bağışıklık, hücresel bağışıklık

ACKNOWLEDGEMENTS

I would like to express my greatest gratitude to Prof. Dr. İhsan Gürsel who always shows me fatherly love, cherish and thinks of his students more than himself. You are much more than being my supervisor and I feel so lucky to have had the opportunity to work with you, to be, in your words your " right-hand man". I know you will always be in my life but know that I will miss you very much. I also would like to thank Prof. Dr. Mayda Gürsel for giving me great inspiration in this field, it was a huge honor to work with her.

I also want to thank the jury members of my thesis defense, Dr. Serkan Belkaya and Prof. Dr. Kamil Can Akçalı for their interest and valuable suggestions.

İrem Evcili and Naz Bozbeyoğlu, my dear friends, who welcomed me most sincerely when I first came to this laboratory, I am so glad to have you. The value we give to each other and the memories we share since the first day are priceless to me. Nilsu Turay and Bilgehan Ibibik, I am very happy to get to know you and made two beautiful friends like you, thanks for everything. Oğuzhan Tarman, I am so grateful to you for helping me with my endless questions, bringing color to my life with your character. Honestly, I will even miss you imitating my smile. Aslı Bartan and Tuğçe Bildik, you are beyond words, and I cannot describe how much I love and care about you. Working with you and being friends with you for these three years is among my best. We have gathered lots of memories we will always cherish in such a short time that I don't know what I would do without you for the rest of my career. You are my best friends, and you will always be. Also, I would like to thank all Thorlab members for their friendship and help.

I am so grateful to my mother Aylin Saraydar and my father Selçuk Saraydar who always believed in me and supported me. I really appreciate everything that you have done for me. Also, I would like to thank my brother Baran Saraydar who is my biggest chance in this life, I will always have your back as you have always had mine . My fiancée Kerem Gölcüklü, thank you very much for helping me overcome every problem, never letting me give up and always trying to lead me to the right path. I feel so lucky to have Hande Gölcüklü and Can Gölcüklü who have always seen me as their daughter, and I am very pleased to you for always supporting me. My dear family, I love you more than anything and anyone.

Lastly, I would like to thank TÜBİTAK for the financial support of my studies with the T1004 (18AG020) grant.

TABLE OF CONTENTS

LIST OF FIGURES

LIST OF TABLES

ABBREVIATIONS

ACE2	Angiotensin-converting enzyme 2
AP-1	Activator protein
APCs	Antigen-presenting cells
BCR	B cell receptor
BLA	Biologics license application
CDC	Center for Disease Control
CLRs	C-type lectin receptors
COVID-19	Coronavirus disease 2019
CTD	C-terminal domain
DAMPs	Danger-associated molecular patterns
DCs	Dendritic cells
E	Envelope
ELISA	Enzyme-linked immunosorbent assay
ERGIC	ER-Golgi intermediate complex
FDA	Food and drug administration
FP	Fusion peptide
HBV	Human B virus
HCV	Human C virus
HEV	Human E virus
HIV	Human immunodeficiency virus
HR1	Heptapeptide repeat sequence 1
HSCs	Hematopoietic stem cells
IFNs	Interferons
Ig	Immunoglobulin

IgG2a	Immunoglobulin G2a
IL-12	Interleukin 12
ILCs	Innate lymphoid cells
IND	Investigational new drug
IRF	Interferon regulatory factor
ISCOMs	Immune-stimulating complexes
ISGs	Interferon-stimulated genes
LPS	Lipopolysaccharide
LRR	Leucine-rich-repeat
M	Membrane
MAVS	Mitochondrial antiviral signaling protein
MDA5	Melanoma differentiation-associated protein 5
MERS-CoV	Middle east respiratory syndrome-CoV
MHC	Major histocompatibility complex
MTD	Maximum tolerated dosage
N	Nucleocapsid
NETs	Neutrophil extracellular traps
NF-κB	Nuclear factor κ-light-chain-enhancer of activated T cells
NLRP3	NOD-like receptor protein 3
NLRs	NOD-like receptors
NTD	N-terminal domain
ODNs	oligodeoxynucleotides
ORFs	Open reading frames
PAMPs	Pathogen-associated molecular patterns
PBMCs	Peripheral blood mononuclear cells
PCs	Plasma cells

pDCs	plasmacytoid DCs
PNPP	p-nitrophenyl phosphate
PRRs	Pathogen recognition receptors
RBD	Receptor-binding domain
RIG	Retinoic acid-inducible gene
RLRs	RIG-I-like receptors
RLU	Relative light unit
RNP	Ribonucleocapsid
ROR-t	Retinoic acid receptor-related orphan receptor t
RT	room temperature
RTC	Replication transcription complexes
S	Spike
S-6p	hexaproline prefusion-stabilized spike
s.c	Subcutaneous
SA-PE	PE-conjugated streptavidin
SARS-CoV-2	Severe acute respiratory syndrome 2
SOCS-1	Suppressor of cytokine signaling-1
ssRNA	single-stranded RNA
TCR	T cell receptor
Tfh	Follicular helper T
Th	T-helper
Th1	T helper 1
TLRs	Toll-like receptors
TM	Transmembrane
TNF-α	Tumor necrosis factor-α
Treg	regulatory T

VLPs	Virus-like particles
VOC	Variants of concern
VOHC	Variants of high consequence
VOI	Variants of interest
WHO	World Health Organization

CHAPTER 1

INTRODUCTION

1.1. Immune System

The body has to protect itself against infections by pathogens such as bacteria, viruses, and fungi. As a result of this, the immune system, which is a sophisticated network of cells and proteins, defends the body with various and numerous strategies. The mammalian immune system can be divided into two interrelated systems which are innate and adaptive. These two immune systems are built on the activities of the immune cells, also termed leukocytes, and emerge from pluripotent hematopoietic stem cells (HSCs) in the bone marrow. HSCs produce myeloid and lymphoid lineages. B- and T-lymphocytes, natural killer cells and innate lymphoid cells (ILCs) rise from the lymphoid lineage whereas the myeloid lineage encompasses neutrophils, eosinophils, basophils, monocytes, platelets, erythrocytes, mast cells, macrophages and monocytes. Dendritic cells (DCs) can both arise from myeloid and lymphoid progenitor cells [1].

Both the innate and adaptive immune systems have developed sensing mechanisms that allow them to identify and discriminate detrimental pathogens from the host's own cells, as well as beneficial organisms [2]. As the first line of the defense mechanism, pattern recognition receptors (PRRs) in the innate system identify certain microbial kinds or patterns which are absent within the host [3]. The adaptive system, on the other hand, is more effective and specific line of defense against pathogens. The antigen-specific receptors on T- and B- cells are capable of recognizing and responding specifically to any pathogens and even their variants. In addition to antibody secretion, adaptive immune system generates an immunological memory so that it can recognize and eliminate faster when it encounters the same pathogen at another time [4].

1.1.1. Innate Immune System

The innate immune system recognizes and eliminates pathogens so quickly, even within minutes. Atomic and chemical barriers such as mucosal and epithelial surfaces try to prevent the entry of pathogen [5]. Antimicrobial proteins, that are secreted from epithelial cells and phagocytes, are causing bacteria and fungal cell walls and membranes to be disrupted. Besides, pathogens are targeted by the complement system, which is composed of plasma proteins, for both lysis and phagocytosis [6]. If pathogens pass through the physical and chemical barriers, the immune cells are activated by PRRs which detect pathogen-associated molecular patterns (PAMPs) or danger-associated molecular patterns (DAMPs). After recognition, phagocytic cells like macrophages and neutrophils can kill pathogens. If innate immunity fails, the adaptive immune system can be initiated by the production of chemokines, cytokines and upregulation of co-stimulatory molecules.

1.1.1.1. Pathogen Recognition Receptors (PRR)

In order to recognize pathogens such as bacteria and viruses, the immune system has receptors called PRRs which are trained to detect PAMPs and DAMPs. Some PRRs are located on the cell surface where they can identify extracellular pathogens like bacteria and fungi by macrophages and neutrophils. Other PRRs can be found in the endosomes where they detect intracellular pathogens like viruses [1]. Also, they can be situated in the cytosol as well as in the bloodstream and intestinal fluids. PRRs can be classified into four families: Toll-like receptors (TLRs), C-type lectin receptors (CLRs), Retinoic acid-inducible gene (RIG)-I-like receptors (RLRs) and NOD-like receptors (NLRs) [7]. PRRs can be expressed in antigen-presenting cells (APCs) like macrophages and dendritic cells and also other immune and non-immune cells. Once they are activated, they trigger an inflammatory response which activate the induction of type I interferons (IFNs), chemokines, anti-microbial proteins and pro-inflammatory cytokines [8].

1.1.1.1.1. Toll-Like Receptors (TLRs)

Toll, which is a receptor transmembrane glycoprotein, was first identified in Drosophila melanogaster as it is responsible for embryonic dorso-ventral polarity development. Later, 10 human and 12 mice TLRs was discovered that each TLR recognizes different patterns of pathogens [7]. Some TLRs (TLRs 1, 2, 4, 5, and 6) are located on the cell surface and other TLRs (TLRs 3, 7, 8, and 9) can be found on the endosomal membrane [9]. Extracellular domains of TLRs contain different number of leucine-rich-repeat (LRR) motifs and TIR domain in their cytoplasmic tail. When TLRs are activated, TIR-domain containing adaptors such as Myd88 and TIRAP are recruited to the receptor and a signaling cascade become triggered. The signaling events lead to the activation of activator protein (AP-1) transcription factor, which is significant for the expression of cytokines, and interferon regulatory factor (IRF), nuclear factor κ-light-chain-enhancer of activated T-cells (NF-κB) which induce proinflammatory cytokines and type I IFNs [6]. TLR signaling pathway is illustrated in Figure 1.1.1..

TLR1, TLR2, TLR4, TLR5 and TLR6 are known as mammalian cell surface TLRs. TLR2 heterodimerizes either with TLR1 or TLR6 and they recognize triacylated lipopeptides of Gram-negative bacteria and diacylated lipopeptides of Gram-positive bacteria respectively [10]. They are expressed in monocytes, DCs, eosinophils, basophils, and mast cells. TLR4, which is the receptor for lipopolysaccharide (LPS), requires an accessory protein MD-2 and found on macrophages, DCs, eosinophils and mast cells [11]. TLR5 detects flagellin, which is a protein of bacterial flagella, and expressed on intestinal epithelium, macrophages and DCs [10]. TLR3, TLR7, TLR8 and TLR9 are known as mammalian endosomal membrane TLRs and recognize nucleic acids [12]. TLR3 senses double-stranded RNA of viruses and is found in conventional dendritic cells, macrophages and intestinal epithelial cells [13]. Both TLR7 and TLR9 are located in plasmacytoid DCs (pDCs), macrophages, eosinophils and B cells whereas TLR8 is expressed in macrophages and neutrophils [12]. TLR7 and TLR8 function as receptors for single-stranded RNA (ssRNA) [14] . Unmethylated CpG in bacterial DNA is recognized by TLR9 [15]. Detailed explanation of CpG was given in Section 1.5.2 as it was used as an adjuvant in this study.

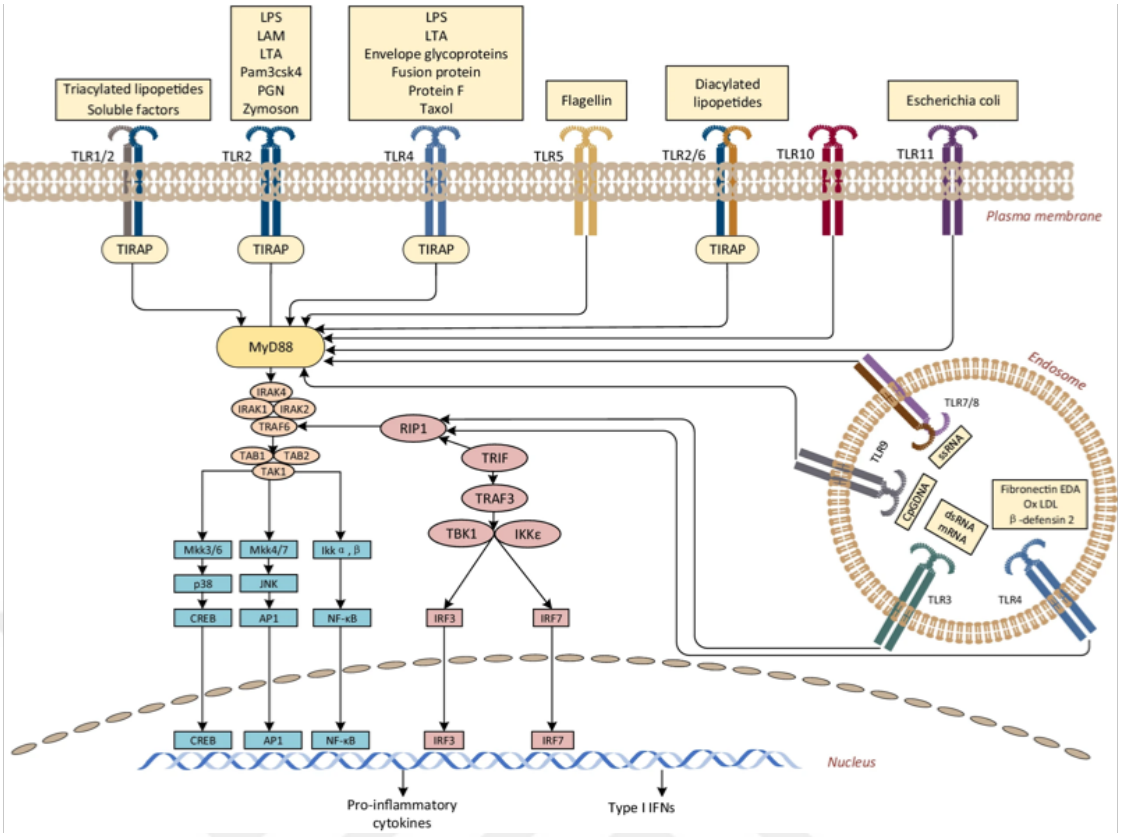

Figure 1.1.1. TLR Signaling pathway [16].

1.1.2. Adaptive Immune Systems

Although the innate immune system has evolved to detect and eliminate pathogens, pathogens may overwhelm this defense mechanism. The adaptive immune system has been counter-evolved due to incredibly high diversity of antigen epitopes and the capacity of pathogens to quickly change their antigenic phenotype. The main functions of the adaptive immune system include recognizing “non-self” antigens and identifying them from “self” antigens, eliminating pathogens and pathogen-infected cells by providing specific effector pathways and developing an immunological memory [4]. This complex defense mechanism relies on B and T lymphocytes (B and T cells), which readjust specific DNA sequences in different combinations during development, thus B and T cell receptors and antibodies can be produced in an almost infinite diversity by the cells [17].

T cells develop from bone marrow and mature in the thymus. They express T cell receptor (TCR) in their membrane and recognize antigens by APCs. In order to activate TCR, major histocompatibility complex (MHC), found on the surface of APCs, requires forming a complex with antigen so that cytokines can be secreted by T cells for

controlling the immune response [4]. T cells differentiate into either cytotoxic T cells (CD8+ cells) or T-helper (Th) cells (CD4+ cells) as a result of antigen-presentation. Cytotoxic T cells secrete granzymes and perforins in order to kill infected cells by undergoing apoptosis [5]. T-helper cells contribute to the activation of cytotoxic T cells, B cells in producing antibody response, macrophages and dendritic cells [18]. A subset of T-helper cells called regulatory T (Treg) cells prohibit other immune cells by producing suppressive proteins [19].

B cells both develop from and mature in bone marrow. They express antigen-binding receptor on their membrane; therefore, they do not need APCs to recognize antigens [4]. The generation of antigen-specific immunoglobulin (Ig) targeted against pathogens is mediated by B cells. Once they are activated by antigens, B cells, with the assistance of T cells, can differentiate into IgM-secreting plasma cells. These cells are short-lived but with class-switch recombination, IgG, IgA and IgE can be produced [20]. Also, B cells can differentiate into memory B cells, thus immune system can react quickly when it exposes to the same pathogens.

1.1.2.1. CD8+ T cells

Virus-infected or malignantly transformed cells are ingested by phagocytic cells and their material was breakdown, peptide antigens were presented in both class I and class II MHC alleles. CD8+ T cells encounter with these phagocytic cells in the lymph nodes. CD8+ T cell differentiation begin when they are activated by the interaction of peptide-MHC class I complexes with TCR [21]. In order to exit the circulation and enter tissues, CD8+ cells alter their integrin and chemokine receptor expression and search for host cells expressing the same antigen that triggered CTL activation by the APC [22]. Once they found, TCR of the CTL is triggered again by peptide-MHC class I complex on the target cells. CD8+ T cells kill infected cells by three different ways: indirect killing, inducing apoptosis and direct killing. Firstly, they can destroy infected cells by releasing cytokines such as IFN-γ and tumor necrosis factor-α (TNF-α). Inhibition of viral replication, increase of MHC class I expression, which enhance the stimulation of TCR by the cells, are provided by IFN-γ. TNF-α binds its receptor on the target cell to activate caspase cascade which causes apoptosis. Also, it synergizes with IFN-γ to activate macrophages. Secondly, when Fas ligand, which is expressed on the surface of CD8+ T cells, binds to Fas on the surface of target cells, this binding leads to apoptosis through caspase cascade activation [23]. Thirdly, CD8+ T cells contain specialized granules which consist of effector proteins such as perforins and granzymes. When CTL releases

these cytotoxic granules, perforin assists the entry of granzyme to the target cell by forming a pore in the membrane of target cell and granzyme promotes cell-death [24].

1.1.2.2. CD4+ T cells

CD4+ T cells have many roles in the function of the immune system. They assist B cells in the production of antibodies, improve the response of CD8+ T cells, regulate the function of macrophages and coordinate immune response against pathogens and are critical for immunological memory [21]. Unlike CD8+ T cells, CD4+ T cells are activated by the interaction of antigen and MHC Class II molecules [26]. When they are activated, they can differentiate into various subsets of effector T cells: T helper 1 (Th1), Th2, Th17, Treg and follicular helper T (Tfh) cells. Th1 cells are significant for inflammation and the activation of macrophage whereas Th2 cells are critical for allergic responses. Th17 cells has a role in inflammation and Treg cells function in regulating and suppressing inflammatory responses [21]. Tfh cells provides germinal center help.

CD4+ T cell subsets are primarily determined by transcription factors. Type I IFN and interleukin 12 (IL-12), which express T-bet transcription factor, stimulate Th1 response and produce IFN-γ and TNF [26]. Th2 differentiation is significantly determined by the cytokine IL-4. Th2 express GATA3 transcription factor and IL-4, IL-5, and IL-13 are markers for these cells [27]. IL-6 and TGF- β promotes Th17 differentiation and they are defined by the expression of the retinoic acid receptor–related orphan receptor t (ROR-t) and they produce IL-17A, IL-17F and IL-22 [28]. Treg differentiation is mediated by IL-2 and TGF- β, they express FOXP3 transcription factor and produce IL-10. Tfh cells are described by expression of BCL-6 and production of IL-4, IL-21. CD4+ T cell subsets are illustrated in Figure 1.1.2..

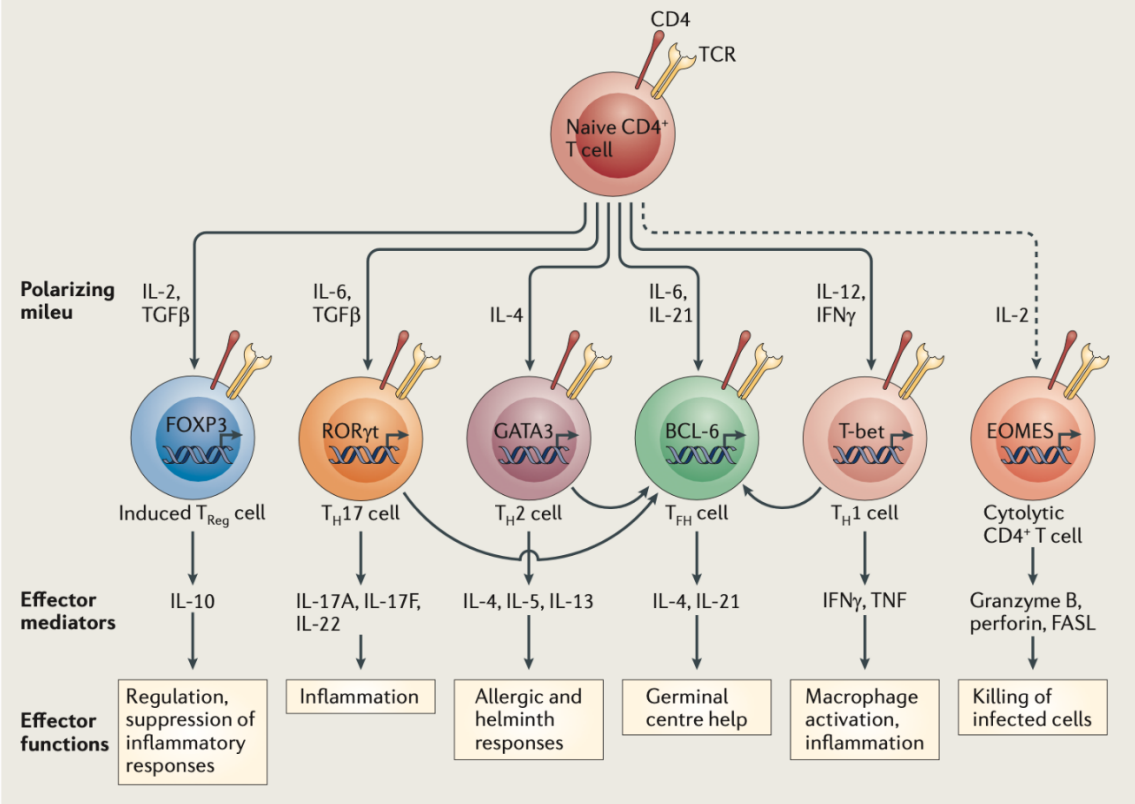

Figure 1.1.2. T cell subsets of CD4+ T cells [26].

1.1.2.2.1. Th1 Pathway Cellular Immune Response

In order to fight with intracellular pathogens, Th1 cells activate natural killer cells, macrophages and also CD8+ T cells. Th1 cells also trigger immunoglobulin class switching in B cells, resulting in the generation of immunoglobulin G (IgG) antibodies which facilitate viral and extracellular bacterial clearance [29]. Antigen features, cytokine microenvironment and co-stimulatory signals that are presented by APCs support Th1 differentiation. IFN-γ and IL-12 are the two signature cytokines that promote differentiation of Th1 cells. Th1 cells mainly produce IL-2, IFN- γ and TNF. IL-2 increases CD8+ T cell proliferation and the development of a cytolytic phenotype. Aside from its activity as a T cell growth factor, IL-2 was discovered to enhance the formation of CD8+ memory cells following antigen priming, hence contributing to a powerful secondary immunological response [30]. IFN-γ can act as a signal transducer and activate STAT-1 transcription pathway, resulting in the production of T-bet which increases IFN-γ expression and the downregulation of IL-4 expression that enhances Th2 differentiation [31]. Also, IFN-γ has impacts on APCs which activate macrophages to contribute the production of IL-12. As a result, a positive feedback loop is formed which IL-12 drives

developing Th1 cells to release IFN-γ, which in turn promotes APCs to make more IL-12. IL-12 is a potent heterodimeric cytokine released largely by activated macrophages in response to infection by viruses and bacteria [28]. The binding of IL-12 to its receptor triggers the STAT4 signaling pathway, resulting in the generation of IFN-γ. The IL12/STAT4 pathway promotes IL-18R expression. IL12, in conjunction with IL18, stimulates IFN-γ production regardless of TCR activation, hence establishing a mechanism for improving Th1 response [24].

1.1.2.2.2. Th2 Pathway Humoral Immune Response

Th2 cells, which produce IL-4, IL-5, IL-6, IL-9 and IL-13, are essential for the immune response to extracellular parasites [32]. When naive T cells are exposed to IL-4 during T-cell priming, Th2 responses are produced. Once IL-4 binds to its receptor, it triggers STAT6 transcription pathway, resulting in the production of GATA-3 which increases IL-4, IL-5, and IL-13 expression [33]. Since eosinophils and their precursors have substantially greater levels of IL-5R expressed on their surface, IL-5 primarily targets them, resulting in prevention of apoptosis. IL-6 can stimulate CD4+T cells to generate IL-4, which may act in an autocrine fashion to enhance Th2 differentiation. Th1 development is inhibited by IL6-induced increase of suppressor of cytokine signaling-1 (SOCS-1) expression, which inhibits STAT1 activation [33]. IL-9 has a role in the immunopathogenesis of asthma. It stimulates the activity mast cells, B cells, eosinophils, neutrophils, and airway epithelial cells. IL-13 receptor comprises the IL-4Rα chain, and it signals through STAT6 [31]. Besides, IL-13 can partially replace IL-4 in enabling isotype flipping to IgE and IgG1 in B cells.

1.2. COVID-19 Disease

In December 2019, a new coronavirus known as severe acute respiratory syndrome coronavirus 2 (SARS-CoV-2) was first found in Wuhan, China and triggered an outbreak of atypical viral pneumonia. This new coronavirus disease, also known as coronavirus disease 2019 (COVID-19), has spread rapidly over the world due to its high transmissibility [34]. In March 2020, World Health Organization (WHO) was declared COVID-19 as a pandemic.

SARS-CoV-2 has a lot in common with SARS-CoV and Middle East respiratory syndrome-CoV (MERS-CoV), which are its closest homologs. The virus–host contact of SARS-CoV-2 is identical to that of SARS-CoV, and utilizes the same receptor,

angiotensin-converting enzyme 2 (ACE2) [35]. The virus transmits from person to person mostly by respiratory secretions, such as droplets produced by coughing, sneezing or talking [36]. COVID-19 has a wide spectrum of clinical features, from asymptomatic or moderate illness to severely ill individuals in life-threatening situations. Fever, shortness of breath, dyspnea, cough, and exhaustion are the most common symptoms of the disease [37].

1.3. Severe Acute Respiratory Syndrome 2 (SARS-CoV-2)

SARS-CoV-2 is a single-stranded positive-sense RNA virus of approximately 30 kB in size, belongs to the Coronaviridae family, in the order of Nidovirales [37]. It has 79% similar genome sequence with SARS-CoV and 50% with MERS-CoV. There are six open reading frames (ORFs) that are positioned from 5' to 3' in the following order: replicase (ORF1a/ORF1b), spike (S), envelope (E), membrane (M), and nucleocapsid (N) [34]. SARS-CoV-2 virions are spherical and vary in size from 60 to 140 nanometers and the S proteins reside on the surface, lipidic envelope contains M and E proteins, while the genetic material that causes replication is located inside the virion and is attached together with N protein [35].

The SARS-CoV-2 infection and life cycle begin when then the virus binds specifically to the cell membrane of the host. The interaction between S protein of the virus and cell surface receptor ACE2, together with S protein priming by the serine protease, TMPRSS2, allow viral uptake and fusion at the cellular membrane [38]. Following entrance, genomic RNA is uncoated and released into cytosol and immediate translation of ORF1a and ORF1b, which are two major open reading frames, starts. Then, replication transcription complexes (RTC) are formed by this translation and polyprotein processing. To preserve the nascent genome and newly generated sub-genomic mRNAs, the replicase complex begins to synthesize viral RNA in a microenvironment created by intracellular vesicular structures. The production of accessory proteins for the suppression of antiviral host cell responses is provided by these sub-genomic mRNAs. When the nucleocapsid-nascent genomic RNA complex is produced, translated structural proteins translocate to the endoplasmic reticulum membrane to be destined to the ER-Golgi intermediate complex (ERGIC) for initializing virion formation [39]. The newly generated genomic RNA leads to budding into the lumen of the secretory vesicle compartment [36]. Finally, exocytosis allows virions to be secreted from the infected cell.

1.3.1. Structural Proteins of SARS-CoV-2

SARS-CoV-2 genome encodes four structural proteins which are Spike, Nucleocapsid, Membrane and Envelope. All of these proteins are necessary to generate a structurally complete virus particle and they have different functions. S proteins are found on the surface of the virus whereas M and E proteins are embedded in the lipid bilayer of the host membrane which encapsulate the helical nucleocapsid containing viral RNA [40]. Structure of the SARS-CoV-2 is depicted in Figure 1.3.1..

The 180-200 kDa Spike protein is composed of the extracellular N-terminus, the transmembrane (TM) domain, and the intracellular C-terminus. It is usually in a metastable pre-fusion conformation; nevertheless, when the virus contacts with the host cell, the S protein undergoes substantial structural rearrangement, enabling the virus to merge with the cell membrane of the host. To avoid being detected by the host immune system upon entrance, spikes are coated with polysaccharide molecules. SARS-CoV-2 S is comprised of the S1 and S2 subunits, as well as a signal peptide at the N-terminus. The S1 subunit has an N-terminal domain and a receptor-binding domain (RBD), whereas the S2 subunit has the fusion peptide (FP), heptapeptide repeat sequence 1 (HR1), HR2, TM domain, and cytoplasm domain [41]. The S protein promotes virus entrance by attaching the S1 subunit to the host cell receptor, ACE2, via S1 RBD, whereas the S2 subunit promotes viral-cell fusion between the viral membrane and the cell membrane [42]. The Nucleocapsid is one of the abundantly expressed protein in host cells and highly conserved among other types of Coronaviruses. The N-terminal domain (NTD) and C-terminal domain (CTD) of the N protein bind to the virus RNA and assist ribonucleocapsid (RNP) packaging which is significant for virion formation. Moreover, N protein has diverse significant activities in host cellular machinery such as inhibition of interferon, apoptosis and RNA interference, hence plays a regulatory function in viral life cycles [43]. The Membrane proteins are abundantly expressed in the viral membrane, and interact with other viral components including S, N and viral RNA. The M protein assists to stabilize N proteins which facilitates viral assembly, interacts with E protein for virion release [44]. Also, it mediates inflammatory responses in hosts by forming ribonucleoproteins [45]. The Envelope protein is a small integral membrane protein comprised of NTD, hydrophobic domain, and a C terminal chain. The majority of the protein is found at the intracellular trafficking site, where it helps viral budding and also viral assembly by forming viroporins and budding [46].

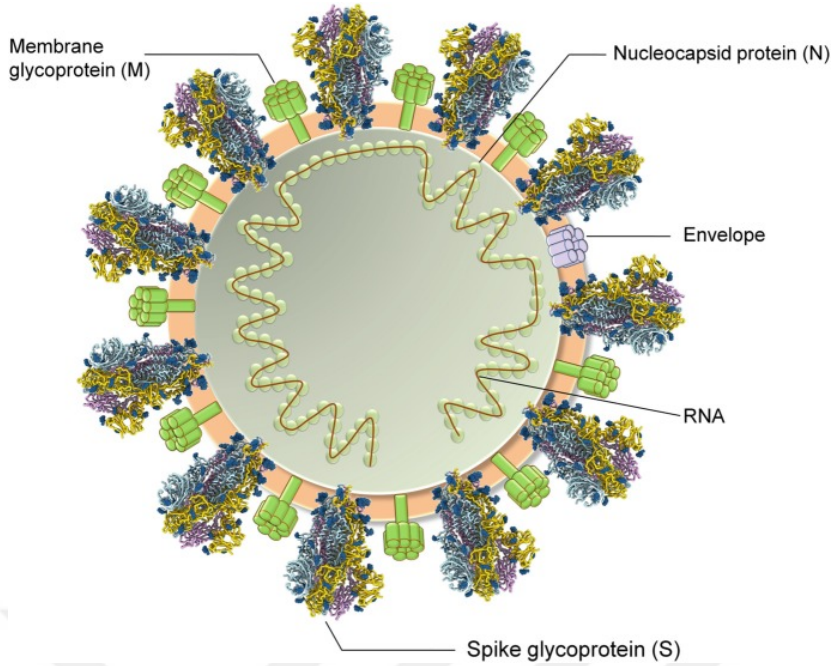

Figure 1.3.1. Structure of the SARS-CoV-2 [40].

1.3.2. SARS-CoV-2 Variants

New variants that are either more or less infectious than the original form emerged due to rapid transmission and circulation of SARS-CoV-2 across the world. The Center for Disease Control (CDC) classifies SARS-CoV-2 variations into three groups: variants of interest (VOI), variants of concern (VOC), or variants of high consequence (VOHC), based on their risk of developing severe disease with significant death, high infectivity rate, or diminished SARS-CoV-2 antibodies response derived from past infection or immunization [47]. To date, there are five variants which are classified as variants of concern: B.1.1.7 (UK, Alpha variant), B.1.351 (South Africa, Beta variant), P.1 (Brazil, Gamma variant), B.1.617.2 (India, Delta), and B.1.1.529 (Omicron variant).

The B.1.1.7 variant contains 23 mutations which the most significant mutations, that alter the biological features of the virus, are D614G, N501Y and P681H in the Spike protein [48]. These mutations cause an increase in the interaction between ACE2 receptor and RBD, and also 56% more transmissibility because of the enhanced viral replication and cleavage of Spike protein [49] [50]. The S RBD mutations K417N, E484K, and N501Y and five N terminal domain mutations are shared by B.1.351 and P.1 variants [51]. These mutations provide an advantage to escape from neutralization and increase

transmission rate to the SARS-CoV-2 [52]. Besides, these variants are associated with decreased vaccine efficiency [53]. B.1.617.2 variant has L452R, T478K mutation at RBD, D614G mutation at S1 subunit and P681R at Furin cleavage site [54]. With the emergency of this variant, the hospitalization rates, transmissibility and viral load increased [55]. Recently, a new variant which is B.1.1.529 was discovered with more than 30 mutations in S protein, in total 50 mutations [56]. Although the virus improves its evolutionary advantages in order to boost the ACE2-RBD binding affinity and to avoid antibody protection, the variant does not affect the severity of the disease and hospitalization rate [57].

Since the diversity of SARS-CoV-2 variants expands and shifts faster than epidemiological investigations, the need for vaccines which provide protection against reinfection among vaccinated people and variant-specific neutralizing activity become the highest priority.

1.3.3. Immune Responses against SARS-CoV-2

SARS-CoV-2 can be detected by TLR3, TLR7, and TLR8 or cytosolic RNA sensors, such as the retinoic acid-like receptors, RIG-I and melanoma differentiation-associated protein 5 (MDA5), which then activate the mitochondrial antiviral signaling protein (MAVS), resulting in the generation of an antiviral response [58]. TLRs trigger the NF-κB pathway, as well as a large variety of pro-inflammatory cytokines, which play a key role in virus-induced inflammation, chemokines and IFNs [59]. A substantial IFN production is required for the innate immune response to protect the host against the virus during the early stages of infection. Once IFNs are released, binding of the interferon receptors (IFNAR1/2) activate JAK1-STAT1/2 dependent transcription of chemokines and interferon-stimulated genes (ISGs), resulting in systemic immunity and limiting the virus replication [60]. Moreover, a controlled cytokine release is essential for infection resolution, but excessive levels of proinflammatory and antiviral mediators such as IL-6, IL-8, IL-17, TNF-α and IFN-γ can result in a cytokine storm, which causes severe symptoms in SARS-CoV-2 patients [61].

When SARS-CoV-2 reaches the respiratory epithelial cells, T cells recognize viral peptides via MHC Class I molecules to generate CD8+ T cells which in turn proliferate and produce virus-specific effector and memory T cells [62]. Infected cells can be lysed by CD8+ T cells with the help of perforin and granzymes. Antigen-presenting cells, mostly dendritic cells and macrophages, identify entire virus and viral particles for a short

period and through the interaction of TCR and MHC Class II molecules CD4+ T cells recognize viral peptides and induce T cell differentiation [63]. Additionally, CD4+ T cells assist the development of B cells, which can recognize S, N, RBD and accessory proteins of the SARS-CoV-2, into plasma cells (PCs) and enhance the generation of virus-specific antibodies of the IgM, IgA, and IgG isotypes [64]. Since T cells play role in the production of neutralizing antibodies, which are thought to be significant adaptive immunity mediators for viral clearance and infection prevention, levels of neutralizing antibodies after vaccination are regarded to be the gold standard for determining efficacy of vaccine [65].

1.4. Current Vaccines against SARS-CoV-2

When the vaccine is injected into the muscle, the protein antigen is picked up by dendritic cells, which are triggered by the adjuvant through PRRs, and subsequently transported to the draining lymph node. T cells are activated by the interaction between TCR and MHC molecules, which present peptides of the vaccine antigen, on dendritic cells. Then, T cells stimulate B cell growth in the lymph node in conjunction with soluble antigen signaling through the B cell receptor (BCR). The maturation of the antibody response improves antibody affinity and induce distinct antibody isotypes occurs as a result of B cell growth. Within two weeks, serum antibody levels rise rapidly due to the development of plasma cells that generate antibodies specific for the vaccine protein [66]. Memory B cells, CD8+ effector and memory T cells are also generated. The process of a vaccination eliciting an immunological response is depicted in Figure 1.4.1..

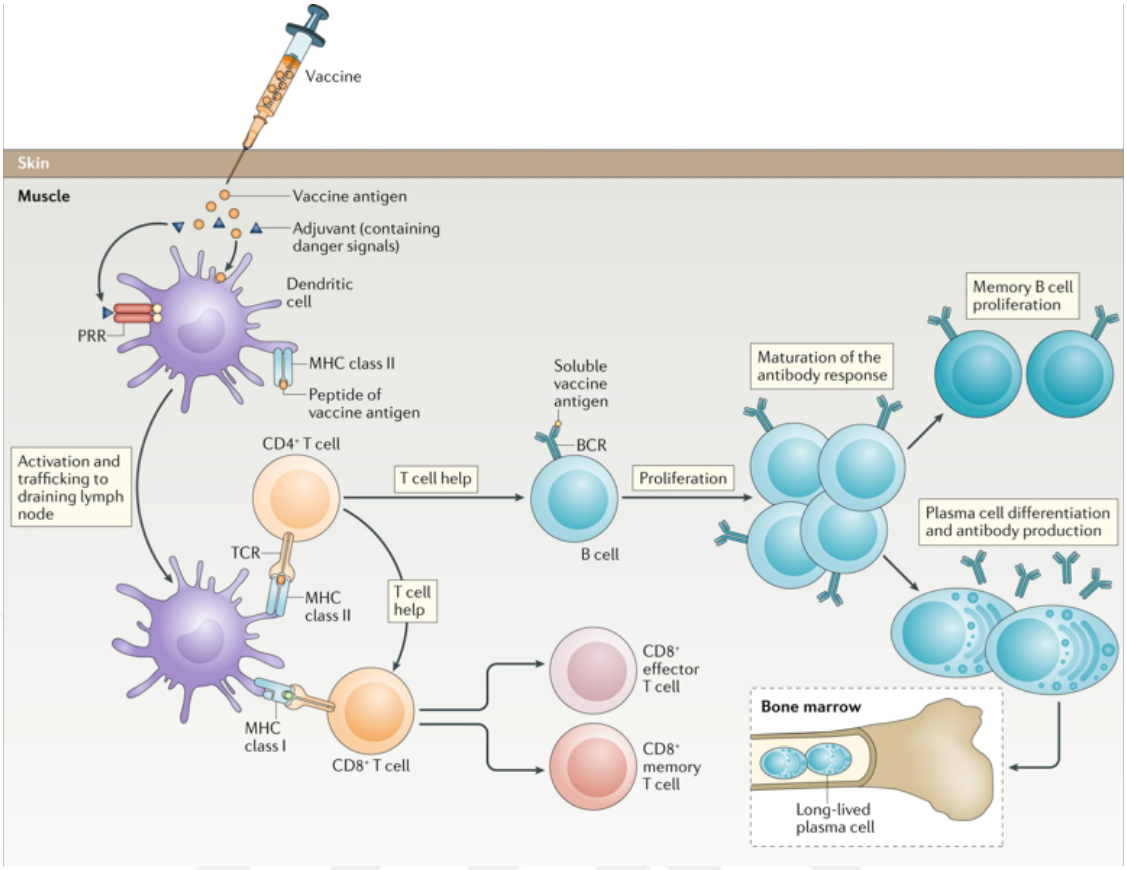

Figure 1.4.1. The process of a vaccination eliciting an immunological response [66].

COVID-19 vaccines have been trying to be developed by researchers all over the world since the pandemic began. According to WHO, there are currently 149 vaccines are in clinical development and 195 vaccines are in pre-clinical development (Figure 1.4.2) [67]. During the COVID-19 pandemic, several vaccine candidates have been developed utilizing various platforms. These candidates are divided into different platforms, which include traditional techniques like inactivated or live attenuated viruses, protein subunits, virus-like particles and next-generation technologies like viral vectors and nucleic acid-based antigens like DNA and mRNA [68]. CoronaVac (Sinovac Biotech, China) is an inactivated vaccine adjuvanted with Alum that is made by generating the SARS-CoV-2 virus, which S protein is expressed on the surface of the vector, in cell culture and then chemically inactivating it [69]. Novavax (NVX-CoV2373, US) is an example of protein subunit vaccine which generated from full-length Spike protein, that has been stabilized in a prefusion conformation, and adjuvanted with Matrix-M [70]. There are four replication-incompetent vector vaccine candidates against SARS-CoV-2: Ad5-nCOV (CanSino Biologics, China), Sputnik V (Gamaleya, Russia), Ad26.COV2.S

(Janssen/Johnson & Johnson, The Netherlands, US), ChAdOx1 nCoV-19 (University Oxford/Astra Zeneca, UK). These candidate vaccines express Spike protein and use non-replicating Ad5 vector, recombinant serotype 26 and serotype 5 adenoviral vectors, non-replicating Ad5 vector and chimpanzee adenovirus vaccine vector respectively [71] [72]. BNT162b1/BNT162b2 (BioNTech/Pfizer, Germany/US) and mRNA-1273 (Moderna, US) use mRNA technology for developing the SARS-CoV-2 vaccine. BNT162b1 encodes RBD of the Spike protein whereas BNT162b2 and mRNA-1273 codes for prefusion stabilized Spike protein and all of them are formulated with lipid nanoparticles [73] [74]. Clinical trials of these mRNA vaccines demonstrate that they have higher efficacy, 95% and 94.50% respectively, among 149 candidate vaccines who are in clinical trials [75].

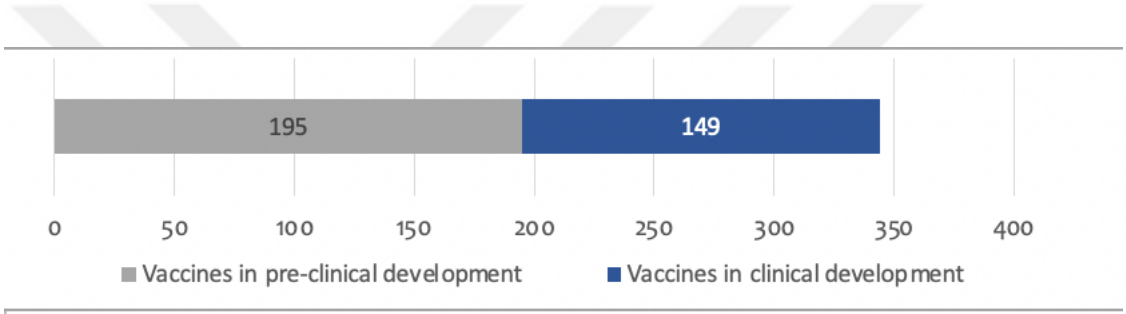

Platform		Candidate vaccines (no. and %)	
PS	Protein subunit	48	32%
VVnr	Viral Vector (non-replicating)	21	14%
DNA	DNA	16	11%
IV	Inactivated Virus	21	14%
RNA	RNA	27	18%
VVr	Viral Vector (replicating)	4	3%
VLP	Virus Like Particle	6	4%
VVr + APC	VVr + Antigen Presenting Cell	2	1%
LAV	Live Attenuated Virus	2	1%
VVnr + APC	VVnr + Antigen Presenting Cell	1	1%
BacAg-SpV	Bacterial antigen-spore expression vector	1	1%

Figure 1.4.2. COVID-19 tracker data summary [67].

1.4.1. Virus-Like Particles (VLPs) and VLP vaccines

Virus-like particles (VLPs) are virus-derived nanostructures composed of one or more proteins that can assemble themselves, resemble the shape and size of a virus particle. Since VLPs do not contain the genetic material of the virus, they cannot infect the host cell [76]. Besides, their size varies, mostly ranging from 20 to 200 nm which is ideal for draining themselves into lymphatic nodes and uptaking by APCs. VLPs are divided into two categories: enveloped and non-enveloped. Non-enveloped VLPs do not

have lipid envelope and are generally composed of single or several self-assembled pathogen or viral protein structures constituents [77]. On the other hand, enveloped VLPs are made up of an envelope, which is derived from the host cell, and viral proteins on the outside surface. Also are more adaptable since they address antigenic epitopes from the same or different viruses [78]. VLPs can significantly trigger humoral and cellular immunity. DCs are activated in the first stage by binding VLPs to PRRs. After that, VLPs are internalized in the cytoplasm of DCs and introduced to cytotoxic T cells and helper T cells via MHC class I and class II molecules, respectively [79]. Also, they can stimulate the proliferation of CD4+ and CD8+ cells as well as B cells, which regulate the antibody response (Figure 1.4.3.)

In principle, there are three phases to produce of VLP-based vaccines: First, the interested viral structural genes are cloned and viral proteins, that has the ability to self-assemble, expressed in an appropriate expression platform such as HEK293T cell line [80]. Then, harvested and lysed cells were clarified to eliminate cell debris and aggregates [81]. Additional purification processes such as ion-exchange chromatography and ultracentrifugation are required to acquire intact and pure VLPs [82]. After removing any remaining host cell proteins and nucleic acids, product is filtered and formulated for developing an effective candidate vaccine [80]. Previously, VLP technology was used to target several viruses such as human immunodeficiency virus (HIV), Hepatitis E virus (HEV), Hepatitis B virus (HBV) and Hepatitis C virus (HCV) [83]. During the SARS-CoV-2 outbreak, VLP is one of the platforms for developing a candidate vaccine. To date, there are six vaccines which are in clinical development. Among them, CoVLP (Medicago Inc.), which is a plant-based VLP vaccine and consists of the full-length S glycoprotein of SARS-CoV-2, is under phase III clinical trials [84]. Another candidate VLP vaccine was developed by Middle East Technical University/Bilkent University which consist of all four proteins of SARS-CoV-2 and completed Phase II clinical trial [85].

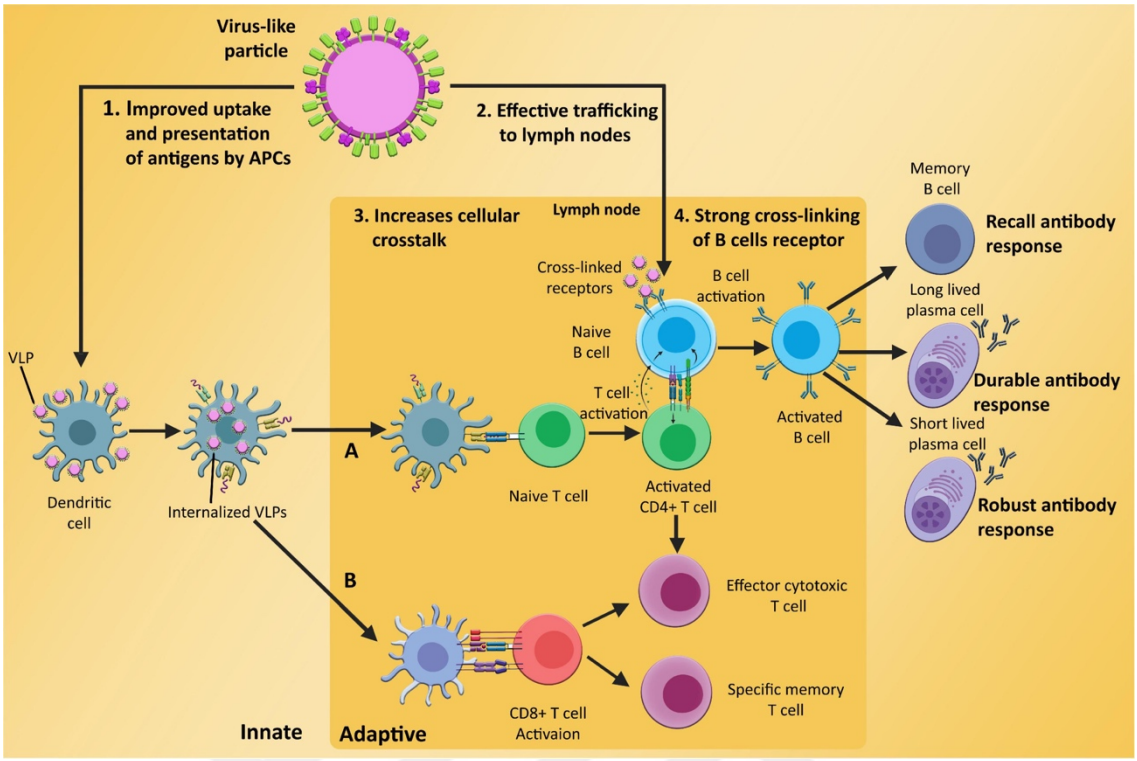

Figure 1.4.3. Induction of Humoral and Cellular Immune Responses by VLPs [77].

1.5. ADJUVANTS

Adjuvants are components which able to boost and/or alter antigen-specific immune responses in the context of vaccines [86]. Adjuvants may exploit the activation of the innate immune system to improve or regulate antigen-specific immunity. They increase local proinflammatory cytokine production through stromal cells, activate local mast cells, and induce localized apoptosis which all lead to increased antigen-specific adaptive immune responses as a result of activation and improved trafficking of APCs and lymphocytes to the draining lymph node [87]. The physical and chemical natures of the vaccine antigen, intended immune response, the age of the target group, and vaccine administration route can all influence adjuvant and formulation decision [88]. Adjuvants with specific characteristics may be required depending on the intended properties of vaccine. There are several different types of adjuvants being used in vaccines, which are categorized based on their composition and how they interact with the immune system, include: Alum, liposomes, virosomes, emulsions, cytokines, Toll-receptor agonists and immune-stimulating complexes (ISCOMs) [89]. Since the vaccine candidate in this study was adjuvanted with Alum and CpG, which is a Toll-receptor agonist, we will focus on these two adjuvants.

1.5.1. Alum

Aluminum salts, which are made up of crystalline nanoparticles that aggregate to produce a heterogeneous distribution of particles measuring several microns, have been used as adjuvants in human vaccinations for decades [88]. They have a high charge and are good at adsorbing antigens and immunomodulatory chemicals. Alum serves as an antigen depot, antigens in vaccines bind to Alum and elute from it after being injected into the host [90]. It works as a mild irritant, inducing leukocytes recruitment to the injection site, which is required for the formation of an immunological response [91]. Antigen adsorption on to Alum enhances immunogenicity and antibody response. Th-2 type responses including IL-4, IL-5, IL-6, and IgG1 secretion are induced by Alum [92]. Besides, it may contribute to the stimulation of proinflammatory cytokines by generating inflammasome and targeting NOD-like receptor protein 3 (NLRP3) in macrophages and DCs [93]. Antibody responses were mediated by a mechanism independent of TLR signaling [94]. Alum can also boost adaptive immunity by generating tissue damage that activates inflammatory DCs through uric acid [95]. Alum injection attracts neutrophils which generate chromatin-based neutrophil extracellular traps (NETs) [96]. It causes apoptosis, which releases DNA and activates STING–IRF3, which is required for IgE antibody and Th2 cell responses [97].

.

1.5.2. CpG ODN

TLR9, which is expressed by B lymphocytes, DCs, and macrophages, recognizes unmethylated CpG in bacterial DNA [62]. Synthetic oligodeoxynucleotides (ODNs) with unmethylated CpG patterns mimic bacterial DNA's capacity to trigger the innate immune system via TLR9 [63]. There are four types of synthetic CpG ODN, each with its own structural and biological features. K-type ODNs induce pDCs differentiation and TNF-α production, as well as B cell proliferation and IgM secretion [98]. D-type ODNs stimulate the maturation of pDCs and the secretion of IFN-α but have no impact on B cells [99]. C-type ODNs induce B cell for IL-6 secretion and pDCs for IFN-α production [100]. When compared to C-type ODNs, P-type ODNs activate B cells and pDCs and produce much more IFN-production [101]. In this study K-type CpG ODN was used because of its scalability and efficacy for immunological activation.

Mature B cells enter the G1 phase of the cell cycle after the activation of TLR9 by K-type CpG ODN which leads to IgG2a class-switching, secretion of proinflammatory cytokines and production of antibodies independently of T cells [102]. Besides, B cells are stimulated by CpG activation to express more Fc receptors and co-stimulatory

molecules such as class II MHC, CD80, and CD86 [98]. CpG ODN can boost naïve B-cell survival by triggering IgM production [103]. Furthermore, K-type CpG ODN promotes pDCs to express more MHC class II, ICAM-1, CD40, CD54, CD80, and CD86 on their surfaces and also trigger the production of numerous cytokines and chemokines such as TNF-α, IL-6, IL-8, IP-10 [102]. TLR9 is expressed on DCs and Langerhans cells originating from the bone marrow, and it is triggered by K-type CpG ODN to produce IL-12 and IL-6 [104]. As a result, in the secondary lymphoid organs, K-type CpG establish a Th1-biased immunological environment that boost cross-priming of cytotoxic T cells, promotes NK cell activation, and enhances Ab responses [105] [106].

1.6. Clinical Phase Trials

Vaccine development takes 10-15 years, and the process starts with years of experimental work on vaccine formulation and assessment in animal models. This is followed by the design of the vaccine production, toxicological studies which takes 2-4 years [107]. After applying for an investigational new drug (IND), clinical trials consisting of 4 phases begin. These phases are used to determine a drug's safety and maximum tolerated dosage (MTD), as well as human pharmacokinetics and pharmacodynamics, and also drug–drug interactions [108]. After successfully completed each phase, a biologics license application (BLA) is summitted which is reviewed by the regulatory agencies and finally large-scale production starts.

Clinical trials are a type of study that analyzes the effects of novel tests and treatments on human health outcomes. Besides, these trials involve volunteers to evaluate medical interventions such as drugs, vaccines, and other biological products, surgical processes and behavioral therapies [109]. Additionally, clinical trials are often carried out in stages that build on one other [110]. Each step is intended to provide answers to specific questions.

Human tests of a vaccine candidate's acceptable safety and reactogenicity are carried out in 'Phase I' clinical trials [111]. As the primary outcome in this phase, safety and tolerability are assessed at both the local and systemic levels. The study is conducted to determine the maximum dose of a new medication that may be safely administered without generating serious adverse effects, therefore, dose-ranging (low dose, high dose) experiments are carried out [112]. These studies are frequently designed as single-center, randomized, double-blind, placebo-controlled investigations [113]. Because the trials only involve a limited number of individuals (20-80), the statistical analysis is mostly descriptive and exploratory.

A vaccine candidate is then progressed into phase II clinical trials if the findings are promising, and the candidate is found to be safe. The purpose of this phase is to indicate the immunogenicity of the relevant active component(s) and the safety profile of a candidate vaccine in the target population, as well as to determine the best dosage and starting schedule [113] [114]. The dose and number of doses, the time between doses, and the administration route are all determinants of therapeutically relevant vaccination regimens [108]. Statistical studies are carried out, and the proportion of responders should be specified and characterized using predetermined immune response criteria such as antibodies and/or cell-mediated immunity.

The effectiveness and safety of formulation(s) of the immunologically active component(s) must be examined in the large-scale target population in a Phase III study, which is designed to produce a critical conclusion required for marketing authorization [115]. Phase III clinical trials enroll 300 to 3000 volunteers and efficacy trials are randomized, double-blind and placebo-controlled [116]. The clinical result is highly suggested as a criterion for evaluating effectiveness. As a result, serological data is often gathered at predetermined intervals from at least a portion of the vaccinated population. Phase IV studies are conducted after a country's permission, and more testing in a large population over a longer period of time is required.

The SARS-CoV-2 pandemic needed immediate action and vaccine development in an extraordinary period. Because of the unprecedented speed, governments have had to create a new approval procedure in order to assure the safety, efficacy, and controlled quality of new vaccines [117]. Preclinical data from vaccine candidates for SARS-CoV and MERS-CoV allowed the first phase of investigational vaccine design to be abandoned entirely, saving a significant amount of time. Clinical stages overlapped and trial commencement were staggered in the studies, with initial phase I/II trials followed by quick transition to phase III trials after intermediate review of phase I/II results [107]. Several vaccine manufacturers have already begun production of vaccines despite the lack of findings from phase III studies. The whole process decreased 15 years to 1.5 years. The comparison of vaccine development process for traditional and SARS-CoV-2 vaccine development is illustrated in Figure 1.6.1..

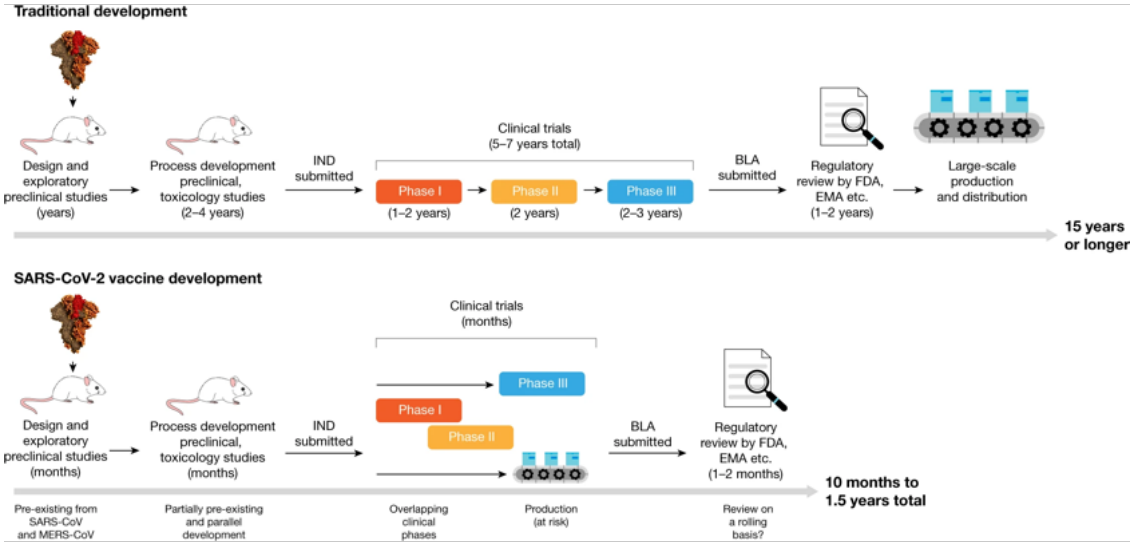

Figure 1.6.1. Vaccine development processes, both traditional and accelerated [107].

1.7. Aim and Outline of the Study

In order to control the COVID-19 pandemic, effective vaccines need to be developed quickly. Several highly efficient SARS-CoV-2 vaccines have been authorized for human use, and others are presently being tested in clinical trials. A candidate VLP vaccine was development by our (Prof. Dr. İhsan Gürsel, Bilkent University) and Prof. Dr. Mayda Gürsel's group (Middle East Technical University). VLPs were produced to express the structural proteins N, M, and E and hexaproline prefusion-stabilized Spike (S-6p) of SARS-CoV-2, and were adsorbed with Alum and mixed with a K3 CpG ODN as vaccine adjuvants to increase immunogenicity and promote both humoral and cellular immunity [85]. Since the SARS-CoV-2 mutates and generates new variants naturally, the efficacy of vaccines decreases. The first aim of this study is to determine the optimal formulation of the vaccine which induces the most effective immune responses by injecting 2 doses of the vaccine for Alpha variant to mice. Since volunteers in Phase II clinical trial received 2 doses of VLP-58-1023-AL-K3-PII vaccine for Alpha variant, the second aim is to investigate how a third dose affect the production of antibodies in mice so that it can be applied to human as well. The third aim of this study is to characterize both cellular and humoral immune responses of 117 volunteers who received 2 subcutaneous (s.c) doses of VLP-58-1023-AL-K3-PII vaccine for Alpha variant in Phase II clinical trial.

For the purposes summarized above, to determine immune responses in mice subcutaneously injected with three different formulations of vaccines, we measured IgG antibody levels produced against Spike and Nucleocapsid proteins of SARS-CoV-2. Additionally, we analyzed the production of IgG antibodies against WT, Alpha and Delta RBD to confirm if vaccine is still efficient on different variants.

Although the protection of 2 dose vaccines has been proven, the efficacy of the vaccines has tendency to decrease after 2 months. Therefore, The U.S Food and Drug Administration (FDA) has recently approved COVID-19 vaccination boosters and additional vaccine doses. We injected an additional booster dose to mice with 2 doses of VLP-Alpha vaccine and examine the positive effects of the 3rd dose on humoral immune response.

It has been revealed that in addition to humoral immune response, cellular immunity has a great significance in protection against COVID-19. For this reason, in the phase 2 study, we tried to understand whether Th1 or Th2 cellular response was dominant in volunteers who were administered 2 doses of VLP-Alpha vaccine by analyzing the cytokines production.

MATERIALS AND METHODS

1.1. Materials

1.1.1. Cell Culture Media and Buffers

RPMI 1640 with L-Glutamine and Phenol Red (#01-100-1A), high glucose DMEM with L-Glutamine and Phenol Red (#01-052-1A), FBS (#04-127-1A), Sodium Pyruvate (100mM, # 03-042-1B), Penicillin-Streptomycin (# 03-031-1B), DPBS (#02-023-1A), HEPES buffer (1M, #03- 025-1B), Ultrapure Cell Culture Water (#01-869-1A), MEM Non-Essential Amino Acids Solution (#01-340-1B) were purchased from Biological Industries (USA). Lymphocyte Separation Medium (density 1.077 g/ml, #LSM-A) for PBMCs isolation was obtained from Capricorn (Germany). Dimethyl sulfoxide (DMSO, #A3672,0250) was from AppliChem (Germany).

The recipes of homemade buffers and reagents were given in APPENDIX B.

1.1.2. Kits, Antibodies and Reagents

Table 1.1.1. Human and mouse-specific ELISA antibodies, reagents and kits used throughout the study.

Product	Brand	#Catalogue Number	Working concentration
Homemade recombinant Spike	Bilkent University	-	6 µg/ml for human 4 µg/ml for mice
Homemade recombinant Nucleocapsid	Bilkent University	-	4 µg/ml for human 1 µg/ml for mice
Homemade recombinant RBD	Bilkent University	-	4 µg/ml for both human and mice
Convalescent sera	Marmara University	-	-
RBD Domain	Proteogenix	PX-COV- P046-100	1 µg/ml for both human and mice
SARS-CoV-2 RBD of Spike protein, N501Y – B 1.1.7 lineage – UK Alpha Variant	Proteogenix	PX-COV- P052-100	1 µg/ml for both human and mice

SARS-CoV-2 RBD of Spike protein, L452R, T478K – lineage B.1.617.2 – Indian Delta Variant	Proteogenix	PX-COV- P061-100	1 µg/ml for both human and mice
Goat Anti Human IgG-AP	Southern Biotech	2040-04	1:1000
Goat Anti Mouse IgG-AP	Southern Biotech	1030-04	1:1000
PNPP Tablets	Thermo Scientific	34047	1 tablet/plate
Substrate Buffer 5X	Thermo Scientific	34064	1 ml/plate
CORONAHUNTER ELISA Kit	Matriks Biotek	COR-QNS-IGG-STRIM	N/A*
SARS-CoV-2 IgG II Quant	Abbott	6S60-32	N/A
LEGENDplexTM HU Th Cytokine Panel (12-plex) w/ VbP	Biolegend	741028	N/A
SARS-CoV-2 SNMO defined peptide pool	Mabtech	3622-1	N/A
Anti-SARS-CoV-2 Verification Panel for Serology Assays	NIBSC	20/B770	N/A
First WHO International Reference Panel for anti-SARS-CoV-2 immunoglobulin	NIBSC	20/268	N/A

*N/A: not-applicable

1.2. Methods

1.2.1. Animal Experiments

BALB/c mice were maintained in the Department of Molecular Biology and Genetics' Animal Facility at Bilkent University. Mice were subjected to 12-hour light/dark cycles at a temperature of 22°C with unlimited food and drink. The Bilkent University Animal Ethics Committee authorized all experimental protocols.

1.2.1.1. Immunization

Animal studies were conducted with prior approval of the animal ethics committee of Bilkent University. Three different formulations of VLP vaccine for Alpha variant were designed. For the first group, VLP (2.5 μg/mice) were formulated with Alum (120 μg/mice) and K3-CpG ODN (60 μg/mice). For the second group, 5 μg VLP was absorbed onto 120 μg Alum and adjuvanted with 60 μg K3-CpG ODN. Third group were injected with 5 μg VLP vaccine containing 60 μg Alum and 30 μg K3-CpG ODN. Groups of female mice (BALB/c, 6–8 weeks old) were subcutaneously (s.c.) injected with 100 μl VLP vaccine 2 weeks apart (on 0 and 14 days). Before the day of booster and 2 weeks post-booster injection, mice were bled, and sera were stored at −20°C until further use.

1.2.2. Clinical Trial

Phase 2 study of VLP-58-1023-AL-K3-PII vaccine were conducted with prior approval of the ethics committee of Dr. Abdurrahman Yurtaslan Ankara Oncology Training and Research Hospital (Approval no: NCT04962893).

1.2.2.1. Cohort

Volunteers aged between 18-59 years with no history of COVID-19, with negative PCR and SARS-CoV-2 IgG/IgM antibody test and with no chronic diseases were enrolled at three centers which are Dr. Abdurrahman Yurtaslan Ankara Oncology Training and Research Hospital, Clinical Research Center, Kocaeli University Infectious Diseases Clinic and Health Sciences University Yedikule Chest Diseases and Thoracic Surgery Training and Research Hospital in TURKEY. 117 participants received VLP vaccine for Alpha variant subcutaneously on days 0 and 21. 40 μg VLP-Alpha absorbed onto 600 μg Alum and adjuvanted with 300 μg CpG ODN-K3 and participants received 1 ml dose for each injection. In order to check cellular and humoral response of participants at day 0, 21, 35, 49 and 90 after first injection, their bloods were collected.

1.2.2.2. Serum Isolation

Collected SST blood tubes (BD Biosciences, USA) were centrifuged at 2500 g for 10 min. Isolated serum samples were aliquoted as 500 µl x 5 vials and stored at -80°C for further experiments.

1.2.3. Cell Culture

1.2.3.1. Peripheral Blood Mononuclear Cells (PBMCs) Isolation from Whole Blood

8 ml peripheral blood from (VLP-58-1023-AL-K3-PII vaccine Phase II clinical trial) volunteers were collected into K2-EDTA (BD Biosciences, USA). Collected bloods were diluted 1:1 ratio with 1X DPBS which was lowered to room temperature (RT). Diluted blood samples were layered onto the room temperature lymphocyte separation medium (Capricorn Scientific, Germany) at 3:2 ratio. After layering, samples were centrifuged for 30 minutes at 540 g and 21°C. In order not to disrupt formed cell layers, rate of deacceleration was set to zero. After centrifugation, four distinct layers which are plasma, PBMCs, granulocytes and red blood cells can be observed respectively. PBMCs, which can be seen as a cloudy layer, were collected with sterile Pasteur pipette into 50 ml falcon. Collected PBMCs were washed twice with 2% FBS containing RPMI-1640 medium and were centrifuged for 10 minutes at 540 g. Then, cell pellets were resuspended in 500 µl of Fetal Bovine Serum (Biological Industries, USA) to count the cells in Flow Cytometry which was explained in Section 1.2.3.2..

1.2.3.2. Cell counting

10 µl of isolated PBMCs, which were suspended in 500 µl Fetal Bovine Serum, was diluted in 990 µl 2% FBS containing RPMI-1640 media. A sample of 50 µl of the suspension was taken and analyzed using Novocyte 3000 flow cytometer. The number of the living cells were measured by positioning events to FSC and SSC. Gating was used to remove detritus and apoptotic cells. The total PBMCs count in 1 ml suspension was calculated by multiplying the dilution factor, which was 2000 for that experiment, by the number of counted events.

1.2.4. Recombinant Production

His-tagged pVitro2-S and pVitro1-N plasmids were transfected into the HEK293 cell line. Cells were incubated for 96-120 hours after being transfected with PEIpro. Then, cell supernatant was collected and centrifuged for 10 minutes at 500 g to eliminate dead cells before purifying full-length thermostable (6p) trimeric Spike and his-tagged recombinant Nucleocapsid of SARS-CoV-2. The harvest was filtered by Filtropur S 0.2

μm filtration unit (Sarstedt, Germany). ÄKTA go fast protein liquid chromatography system (Cytiva, U.S.A.), which is an affinity chromatography, was used to purify the his-tagged proteins. Briefly, equilibrated His-Trap excel 1 mL pre-packed IMAC column (Cytiva, U.S.A.) was used, and samples are applied. After washing step, his-tagged proteins were eluted with imidazole buffer. Desalting step was then conducted using HiPrep™ 26/10 Desalting column (Cytiva, U.S.A.) to remove the imidazole from the recombinant proteins' buffer. D-PBS (Biological Industries, U.S.A.) was used to exchange the buffer. After concentrating the recombinant proteins with Vivaspin 20 Ultrafiltration unit (Sartorius, Germany), the concentration of recombinant nucleocapsid and full-length thermostable (6p) trimeric Spike proteins of SARS-CoV-2 were quantified via Nanodrop One (Thermo-Fischer, U.S.A.) and BCA assay. Also, SDS-PAGE Western Blotting and Silver Staining were performed for confirmation. Spike and Nucleocapsid recombinant proteins production and characterization were explained in detail in İpekoğlu, E. M. (2022) [118].

1.2.5. Quantitative Analyses

1.2.5.1. IgG Enzyme-Linked Immunosorbent Assay (ELISA)

1.2.5.1.1. Mouse ELISA

2HB Maxi binding immunoplates (SPL Life Sciences, South Korea) were coated with 50 μl/well homemade recombinant Spike (4 μg/ml), homemade recombinant Nucleocapsid (1 μg/ml), in-house WT RBD (4 μg/ml), commercial UK Alpha variant RBD (1 μg/ml) and commercial Delta variant RBD (1 μg/ml) in 1X PBS (non-commercial, see Appendix B) at 4°C for overnight. Next day, plates were blocked with 200 μl/well Blocking buffer (see Appendix) for 5 hours at RT. Plates were washed 4 times with Wash buffer and finally were rinsed 2 times with ddH2O. 50x diluted mice sera were 5-fold serially diluted with Blocking buffer into wells. After coating the plates with sera as 50 μl/well and incubating at 4°C overnight, plates were washed as in described previously. Then ALP conjugated anti-mouse IgG antibody (Southern Biotech, USA) were plated as 50 μl/well at a 1:100 dilution and incubated for 2 hours at RT. After washing the plates, p-nitrophenyl phosphate (PNPP, Thermo, USA) substrates were added as 50 μl/well and development of plates were observed. Optical density values were measured at 405 nm by using ELISA plate reader (Molecular Devices, USA).

1.2.5.1.2. Human ELISA

2HB Maxi binding immunoplates (SPL Life Sciences, South Korea) were coated with 50 µl/well homemade recombinant Spike (6 µg/ml), homemade recombinant Nucleocapsid (4 µg/ml), commercial RBD (1 µg/ml), commercial UK Alpha variant RBD (1 µg/ml) and commercial Indian Delta variant RBD (1 µg/ml) in 1X PBS (non-commercial, see Appendix) at 4°C for overnight. Next day, plates were blocked with 200 µl/well Blocking buffer (see Appendix) for 3 hours at RT. Plates were washed 4 times with Wash buffer and finally were rinsed 2 times with ddH2O. For recombinant Spike and Nucleocapsid 1:100 diluted volunteers' sera were 3 times 6-fold diluted and for commercial RBDs 1:100 diluted volunteers' sera were 4 times 4-fold diluted with Blocking buffer. Additionally, 35 samples convalescent sera, Anti-SARS-CoV-2 verification panel and First WHO International Reference Panel for anti-SARS-CoV-2 immunoglobulin were used as controls. After coating the plates with sera as 50 µl/well and incubating at 4°C overnight, plates were washed as in described previously. Then, ALP conjugated goat anti-human IgG antibody (Southern Biotech, USA) were plated as 50 µl/well at a 1:100 dilution and incubated for 2 hours at RT. After washing the plates, PNPP (Thermo, USA) substrates were added as 50 µl/well and development of plates were observed. Optical density values were measured at 405 nm by using ELISA plate reader (Molecular Devices, USA).

1.2.5.2. CORONAHUNTER^{TM} Anti-SARS-Cov-2 SPIKE IgG ELISA

In order to quantify Spike Trimer antibodies from serum samples, CORONAHUNTER^{TM} Anti-SARS-Cov-2 SPIKE IgG ELISA was used. Isolated serum samples of Phase 2 volunteers from Day 0, 21, 35, 49, 90, convalescent plasma samples, NIBSC standards and samples were studied. Before performing the kit, according to manufacturer's instructions, serum samples were diluted 1:100 with Assay buffer. Then, 100 µl Assay buffer was plated into each well and 20 µl of standards, low level control, high level control and serum samples were pipetted. After incubating the plates for 1 hour at RT, plates were washed 3 times with Wash buffer. 100 µl of conjugate was pipetted and incubated for 30 minutes at RT. Plates were washed again, 100 µl Substrate was added and incubated for 20 minutes in dark at RT. As blue color develops, 100 µl Stop solution was added to stop the reaction. Optical density was recorded at 450 nm with ELISA Plate Reader (Molecular Devices, USA).

1.2.5.3. Cytometric bead array for measurement of CD4+ helper T responses

Since Th cytokine expression measurement is significant for understanding the regulation of immune response, LEGENDplex™ HU Th Cytokine Panel (12-plex) w/ VbP kit (Biolegend, U.S.A.) was used for this purpose. The kit allows us to quantify 12 different cytokines which are IL-2, 4, 5, 6, 9, 10, 13, 17A, 17F, 22, IFN-γ and TNF-α. Before performing the kit, collected PBMCs from the volunteers at day 35 after first injection were thawed. PBMCs were rested in 2 ml %20 FBS containing RPMI-1640 for 1 hour in CO2 incubator at 37°C. After counting cells by using NovoCyte 3000 flow cytometer (ACEA Biosciences, USA) as described in section 2.2.3.2, 100 µl SARS-CoV-2 SNMO defined peptide pool (2 µg/ml) (Mabtech, Sweden) was layered to 96 well V-bottom plate, 100 µl (750.000 cells/well) rested cells were added and incubated for 48 hours at 37°C. Then, supernatant was collected, centrifuged for 5 min at 300 g and kit was performed according to the manufacturer's instructions. Firstly, standards, beads, wash buffer and reagents were prepared. 25 µl of samples, standards were placed into V-bottom plate and 25 µl mixed beads were added. After sealing the plate with aluminum foil, the plate was incubated for 2 hours at room temperature on a shaker. The plate was centrifuged for 5 minutes at 250 g and the supernatant was discarded immediately. The plate was washed twice with 200 µl of Wash buffer and centrifuged again. 25 µl of Detection antibody was added, the plate was sealed and incubated for 1 hour as described before. PE-conjugated streptavidin (SA-PE) was added as 25 µl and the plate was incubated for 30 minutes. After washing step, the plate was centrifuged for 5 minutes at 250 g. Finally, resuspension of beads was done by 150 µl Wash buffer and samples were read by using Novocyte 3000 flow cytometer (ACEA Biosciences, USA). Data analysis was accomplished with LEGENDplex™ Data Analysis Software (Biolegend, U.S.A.).

1.2.5.4. SARS-CoV-2 IgG II Quant Assay (Abbott)

In order to both qualify and quantify SARS-CoV-2 IgG antibodies in volunteers' serums, Abbott Architect system (USA), which is a chemiluminescent microparticle immunoassay (CMIA), was used. Serums of day 0, 21 ,35 ,49 and 90 after the first injection of vaccine collected from volunteers were studied. The process was carried out according to manufacturer's protocol thanks to a cooperation with Deren Laboratory (Ankara, Turkey). Paramagnetic microparticles were S1 subunit of RBD SARS-CoV-2 coated, and samples and assay diluents were added onto it and incubated. After washing the mixture, anti-human IgG acridinium-labeled conjugate was added and incubated again. Pre-Trigger and Trigger solutions were applied after washing step. The chemiluminescent reaction that results is quantified as a relative light unit (RLU). The number of SARS-CoV-2 IgG antibodies in the samples and the RLU measured by the system optics have a direct connection. Positive values were decided using a cut off of 50.0 AU/ml which indicates recordings higher than 50.0 AU/ml considered positive in production of antibody.

1.2.6. Statistical Analyses

One-way ANOVA with Dunnett's multiple comparison test was used to compare various treatment groups to a control group. GraphPad Prism 7 (GraphPad Software Inc., San Diego, USA) was used to conduct all statistical analyses and plots.

CHAPTER 2

RESULTS

2.1. Pre-Clinical Studies

Pre-clinical studies encompass all parts of testing such as characterization of products, immunogenicity studies, and safety testing in animals undertaken prior to clinical testing of the product in humans. These studies are significant in order to find the optimal dose to produce an immune response in appropriate animal models which can offer useful information about the immunological response that can be expected in humans, and to evaluate whether the candidate vaccine will be efficient and favorable to both the human study participant and the general population. Therefore, we designed three different formulations of our vaccine which the amount of VLP as well as adjuvants (Alum and K3-CpG-ODN) varies (See Table 2.1.1). The experimental design was done with 7 female Balb/c mice in a cage for each group, and prepared vaccines were injected subcutaneously at 14-day intervals. An additional third dose was given subcutaneously 2 months after the second dose. A placebo group which does not receive any injection was used as a negative control. Tail bleeding was performed after 2 weeks of 1st injection, 2 weeks of 2nd injection, 2 months of 2nd injection and 2 weeks of 3rd injection in order to evaluate humoral immune responses. Antibody levels were measured against S, N proteins and WT, Alpha, Delta RBD variants by ELISA.

Table 2.1.1. Three different vaccine formulations that are used in animal experiments.

Group Name	Vaccine Formulation
A	2.5 µg VLP + 120 µg Alum + 60 µg K3-CpG ODN
B	5 µg VLP + 120 µg Alum + 60 µg K3-CpG ODN
C	5 µg VLP + 60 µg Alum + 30 µg K3-CpG ODN

An increase in the level of IgG antibodies against S protein was observed in sera taken from group A mice 2 weeks after the second dose. Also, the antibody level in the sera taken 2 months after the second injection decreased to the same level as the sera taken 2 weeks after the first injection. However, contrary to what we expected, second boosting did not cause any positive increase. In group B, the IgG antibody levels has continued to increase steadily after each vaccination. Compared to other groups, in group C mice, much higher humoral antibody responses were observed. Although there was a slight immune response decrease 2 months after 2nd injection in other groups, the antibody levels remained constant, and an even increase was observed with the 3rd dose in group C (Figure 2.1.1).

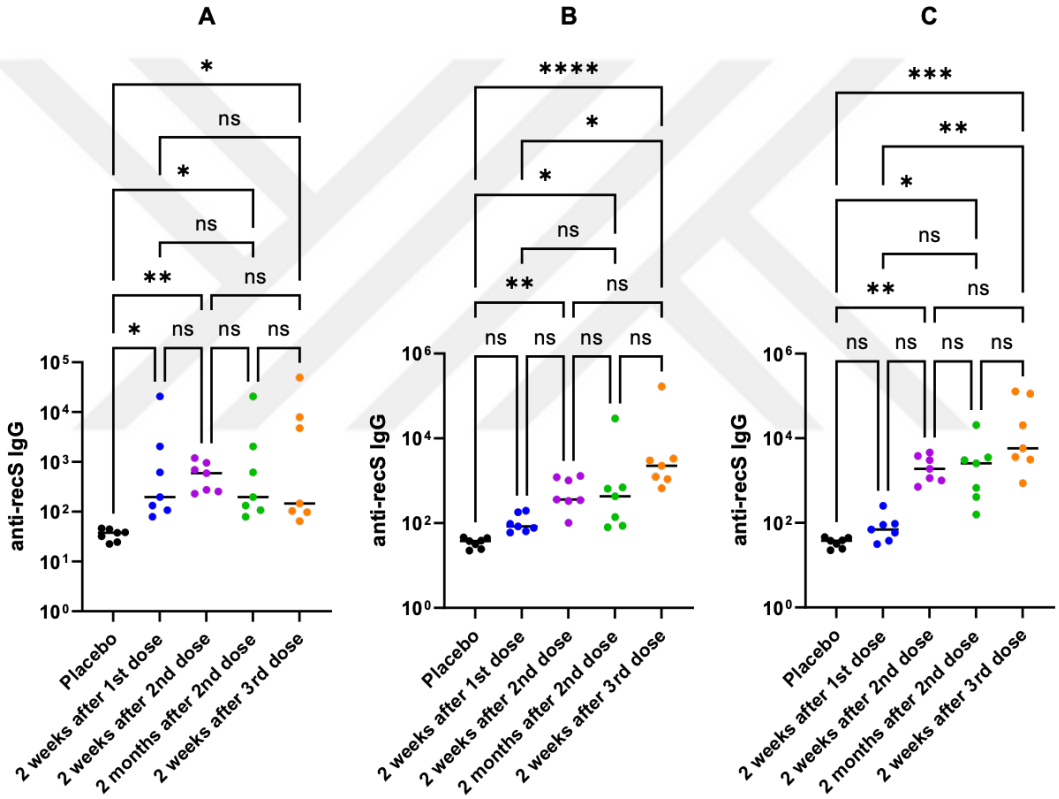

Figure 2.1.1. Evaluation of IgG antibody levels of mice against in-house trimeric S protein. ELISA plates were coated with in-house trimeric S protein and IgG antibody production of mice (N=7/group) sera from 2 weeks after 1st dose, 2 weeks after 2nd dose, 2 months after 2nd dose and 2 weeks after 3rd dose were measured. Placebo group were used as a negative control. Kruskal-Wallis test and Dunn's multiple comparison correction were performed. (ns:non-significant, *p≤0.05, **p≤0.01, ***p≤0.001, ****p≤0.0001.) (A: 2.5:120:60, VLP:Alum:CpG, B: 5:120:60, C: 5:60:30)

As it was mentioned in Section 1.2.4, Nucleocapsid recombinant protein was produced in our laboratory. We used two different batches that one of them was used in the sera from 2 weeks after 1st dose, and the other one was used in other serum samples. Since the affinity binding of the recombinant protein from the last batch was higher than the first one, which increase the detection rate, higher levels of IgG antibody against N protein were detected (Figure 2.1.2). It can be seen that one dose vaccine provides IgG antibody production for all groups and those immune responses increased after the 2nd dose. Although there was no decrease after 2 months of 2nd vaccination, third dose maintained the antibody levels high.

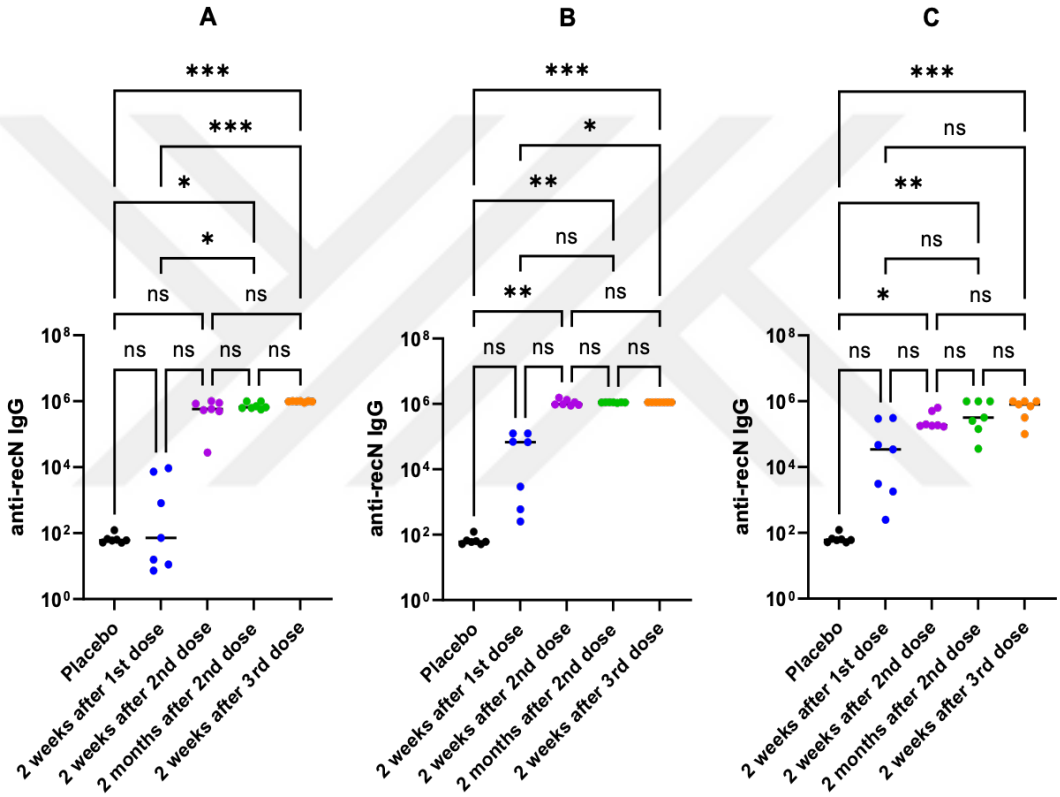

Figure 2.1.2. Evaluation of IgG antibody levels of mice against in-house N protein. ELISA plates were coated with in-house N protein and IgG antibody production of mice (N=7/group) sera from 2 weeks after 1st dose, 2 weeks after 2nd dose, 2 months after 2nd dose and 2 weeks after 3rd dose were measured. Placebo group were used as a negative control. Kruskal-Wallis test and Dunn's multiple comparison correction were performed. (ns:non-significant, *p≤0.05, **p≤0.01, ***p≤0.001, ****p≤0.0001.) (A: 2.5:120:60, VLP:Alum:CpG, B: 5:120:60, C: 5:60:30)

Although the SARS-CoV-2 mutates in the course of time and new variants were developed, we would like to evaluate whether our candidate vaccine can provide the production of IgG antibodies against the original (WT) RBD protein. According to the results, 2nd dose was effective to generate humoral immune responses for all groups. The antibody levels that had dropped in the 2 months after 2nd dose became high again after injecting the 3rd dose. When a general comparison is made between the groups, it was observed that the antibody titer levels of the mice in group C were higher than the mice in the other two groups (Figure 2.1.3).

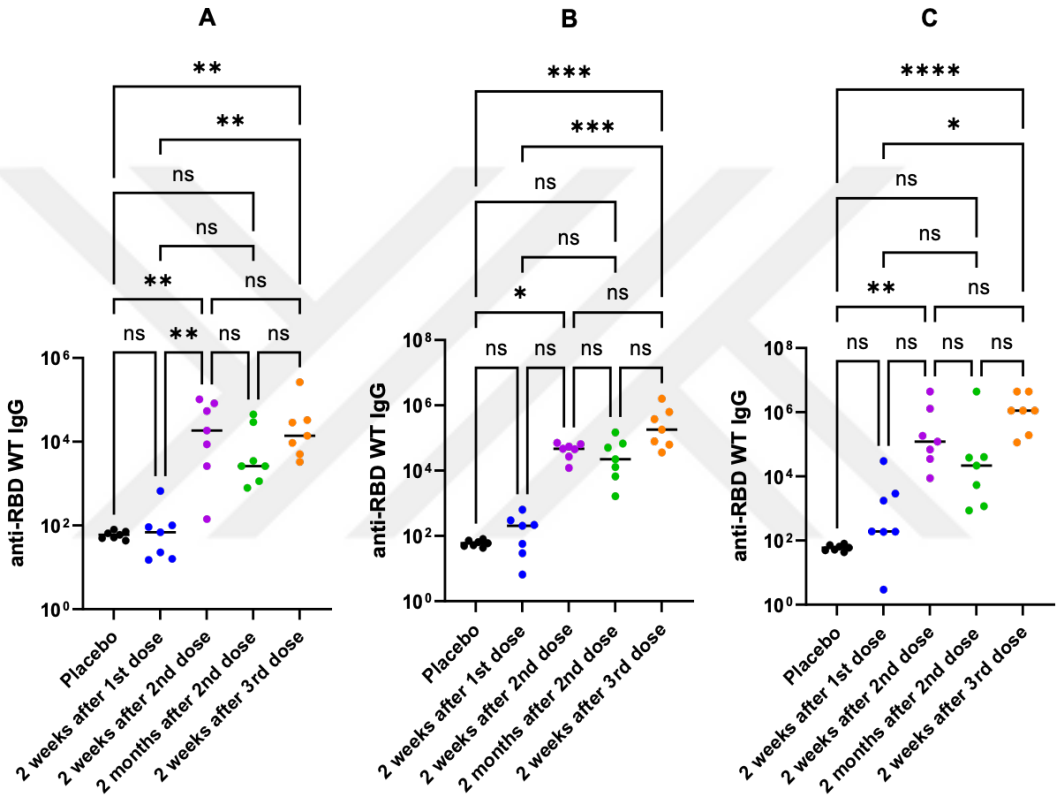

Figure 2.1.3. Evaluation of IgG antibody levels of mice against in-house WT RBD protein. ELISA plates were coated with in-house WT RBD protein and IgG antibody production of mice (N=7/group) sera from 2 weeks after 1st dose, 2 weeks after 2nd dose, 2 months after 2nd dose and 2 weeks after 3rd dose were measured. Placebo group were used as a negative control. Kruskal-Wallis test and Dunn's multiple comparison correction were performed. (ns:non-significant, *p≤0.05, **p≤0.01, ***p≤0.001, ****p≤0.0001.) (A: 2.5:120:60, VLP:Alum:CpG, B: 5:120:60, C: 5:60:30)

Humoral immune responses against Alpha RBD protein demonstrated that there was no antibody production occurred after the 1st dose in all groups, but a gradual increase was observed after the 2nd dose. Although the third vaccination did not make a noticeable difference in groups A and B when compared to the serum levels taken in the second month after 2nd dose, it positively affected the antibody levels of mice in group C (Figure 2.1.4). Overall, it can be said that high dose VLP and low dose adjuvants combination ensures the maximum humoral immune responses.

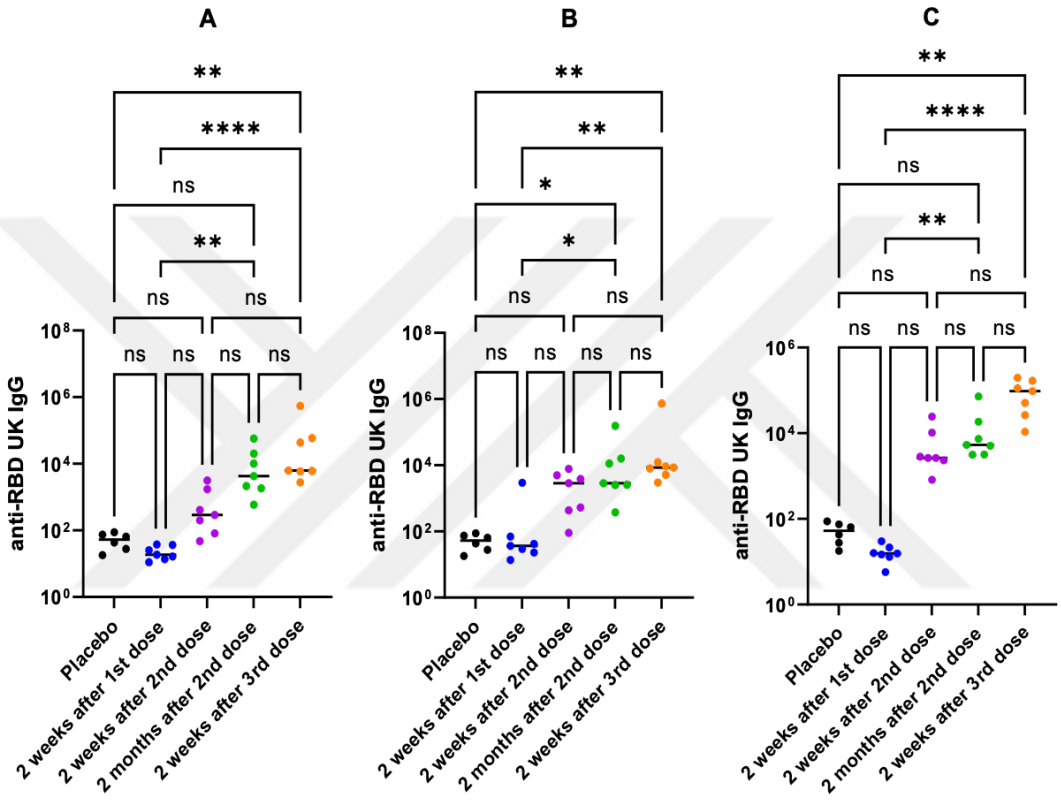

Figure 2.1.4. Evaluation of IgG antibody levels of mice against commercial Alpha RBD protein. ELISA plates were coated with commercial Alpha RBD protein and IgG antibody production of mice (N=7/group) sera from 2 weeks after 1st dose, 2 weeks after 2nd dose, 2 months after 2nd dose and 2 weeks after 3rd dose were measured. Placebo group were used as a negative control. Kruskal-Wallis test and Dunn's multiple comparison correction were performed. (ns:non-significant, *p≤0.05, **p≤0.01, ***p≤0.001, ****p≤0.0001.) (A: 2.5:120:60, VLP:Alum:CpG, B: 5:120:60, C: 5:60:30)

Interestingly, there was no antibody production against Delta RBD protein after two vaccinations in group A. Although IgG levels were detected after the 2nd dose, the responses of group B were lower compared to group C. Additionally, there was no decrease observed after 2 months of 2nd dose. As with the two dose vaccination results, the third vaccination was not sufficient for group A to generate a high immune response. The third dose positively affected the IgG antibody production in groups B and C. Taken together, these results suggest that similar to other RBD variants (WT and Alpha), mice in group C were able to produce higher levels of antibodies (Figure 2.1.5).

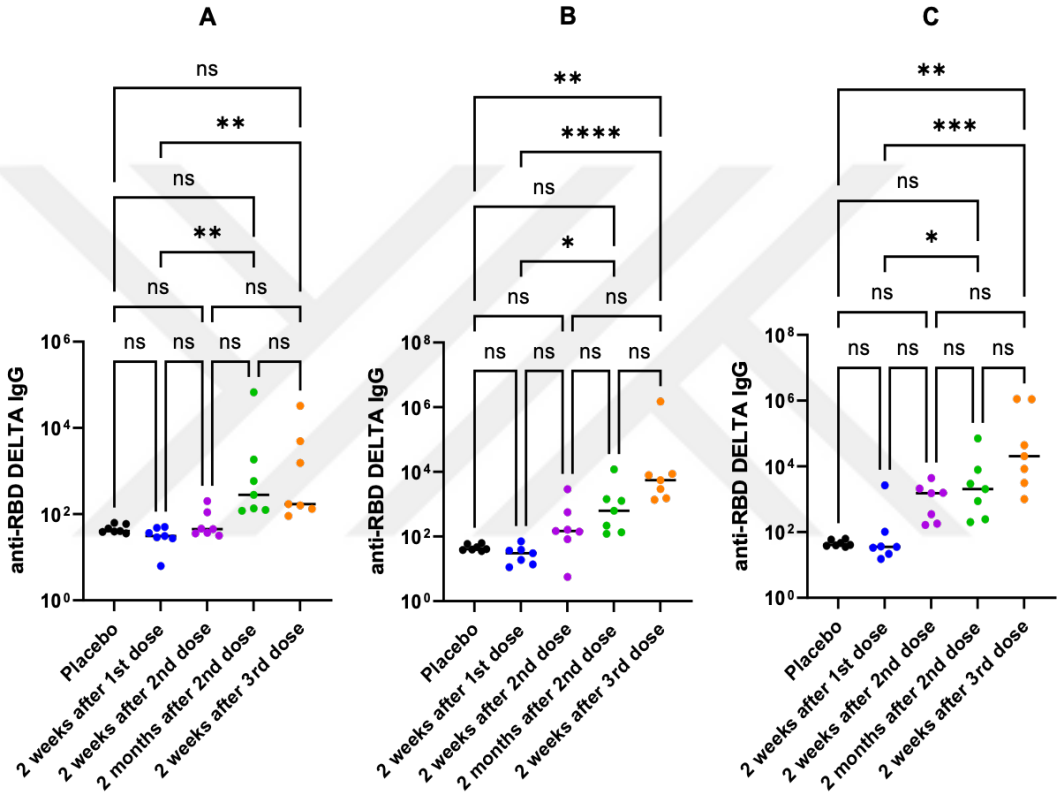

Figure 2.1.5. Evaluation of IgG antibody levels of mice against commercial Delta RBD protein. ELISA plates were coated with commercial Delta RBD protein and IgG antibody production of mice (N=7/group) sera from 2 weeks after 1st dose, 2 weeks after 2nd dose, 2 months after 2nd dose and 2 weeks after 3rd dose were measured. Placebo group were used as a negative control. Kruskal-Wallis test and Dunn's multiple comparison correction were performed. (ns:non-significant, *p≤0.05, **p≤0.01, ***p≤0.001, ****p≤0.0001.) (A: 2.5:120:60, VLP:Alum:CpG, B: 5:120:60, C: 5:60:30)

2.2. Clinical Studies

There are several research groups have used the VLP technology for developing SARS-CoV-2 vaccine. They mainly used full-length Spike or its RBD for antigenic component, and showed a high immunogenicity, production of neutralizing antibodies and cellular responses in clinical trials [119]. However, none of them tried using all structural four proteins, which are S,N,M and E, of SARS-CoV-2 as antigenic components. Therefore, our aim was to acquire higher long-term antibody production and cellular response by using all structural proteins and proper adjuvants.

In December 2020, a new SARS-CoV-2 variant was confirmed in United Kingdom and listed as “Alpha” in the category of VOC. Since it was linked to a higher infection rate and reduced neutralizing antibodies than other variants, in Phase 2 clinical study of VLP-58-1023-AL-K3-PII, we decided to produce an effective vaccine especially for Alpha (UK) variant. 117 participants received VLP vaccine (40 µg VLP-UK + 600 µg Alum + 300 µg CpG ODN-K3) subcutaneously on day 0 and 21. In order to check humoral and cellular responses of participants at day 0, 21, 35, 49 and 90 after first injection, their bloods were collected. Unfortunately, during Phase 2 clinical study, several participants had COVID-19. Table 2.2.1 shows which participants had COVD-19 on which day. The infected participants were asymptomatic or had mild symptoms.

Table 2.2.1. Participants who had COVID-19 after a certain period of time.

Participant Number	Days after first injection
1010084	29
1010094	43
1010129	81
1010138	89
1010142	29
1010143	69
1010227	89
1010275	58
1030054	93
1030065	62
1030069	81
1030084	32
1030096	97
1030104	68

2.2.1. Determination of Humoral Immune Responses of Phase II Clinical Trial Volunteers Vaccinated with VLP-58-1023-AL-K3-PII SARS-COV-2 for Alpha Variant

To determine humoral immune responses of vaccinated volunteers, we measured IgG antibody levels against S,N proteins, and also three different RBD variants (WT, Alpha, Delta) at specific time intervals by ELISA technique. In order to make a comparison, we used 35 convalescent sera received from Marmara University, 37 NIBSC plasma samples including 23 positive and 14 negative, and 5 NIBSC standards which are negative (20/142), low (20/140), mid (20/148), low anti-S/high anti-N (20/144), high (20/150).

In Figure 2.2.1., it is shown that there was a slight increase in IgG antibody levels produced against S protein after 1st injection of 115 participants. After the 2nd vaccination, antibody responses elevated gradually until 90th day. Although IgG levels of positive NIBSC plasma samples are higher than serum samples taken from participants on certain days, it can be clearly seen that there was no significance when convalescent samples and NIBSC standards are compared with participant serum taken from day 49 and 90. This graph demonstrates that 2 doses of VLP-Alpha vaccine have successfully enabled the production of IgG antibody against Spike protein of SARS-CoV-2. The OD graphs of each participant for each day are shown in APPENDIX A. There were few people got COVID-19 during the clinical trial, and we excluded those volunteers from the measurement of antibody responses against Spike in Figure A6 so that we could understand whether these COVID-19 positive volunteers affected the efficiency of our vaccine. Unsurprisingly, there was no change in the efficacy of the vaccine or IgG antibody levels.

According to researches, SARS-CoV-2 N protein plays significant role in triggering T cell proliferation and cytotoxic activity [120]. Therefore, we wanted to check whether our candidate vaccine can successfully produce IgG antibody in vaccinated participants. As shown in Figure 2.2.2., the antibody levels started to increase after 2nd injection, but the majority of participants remained below the convalescent samples and NIBSC standards. When pre-vaccination IgG antibody levels against N protein compared with 90 days post-vaccination, a large amount of antibody production was observed.

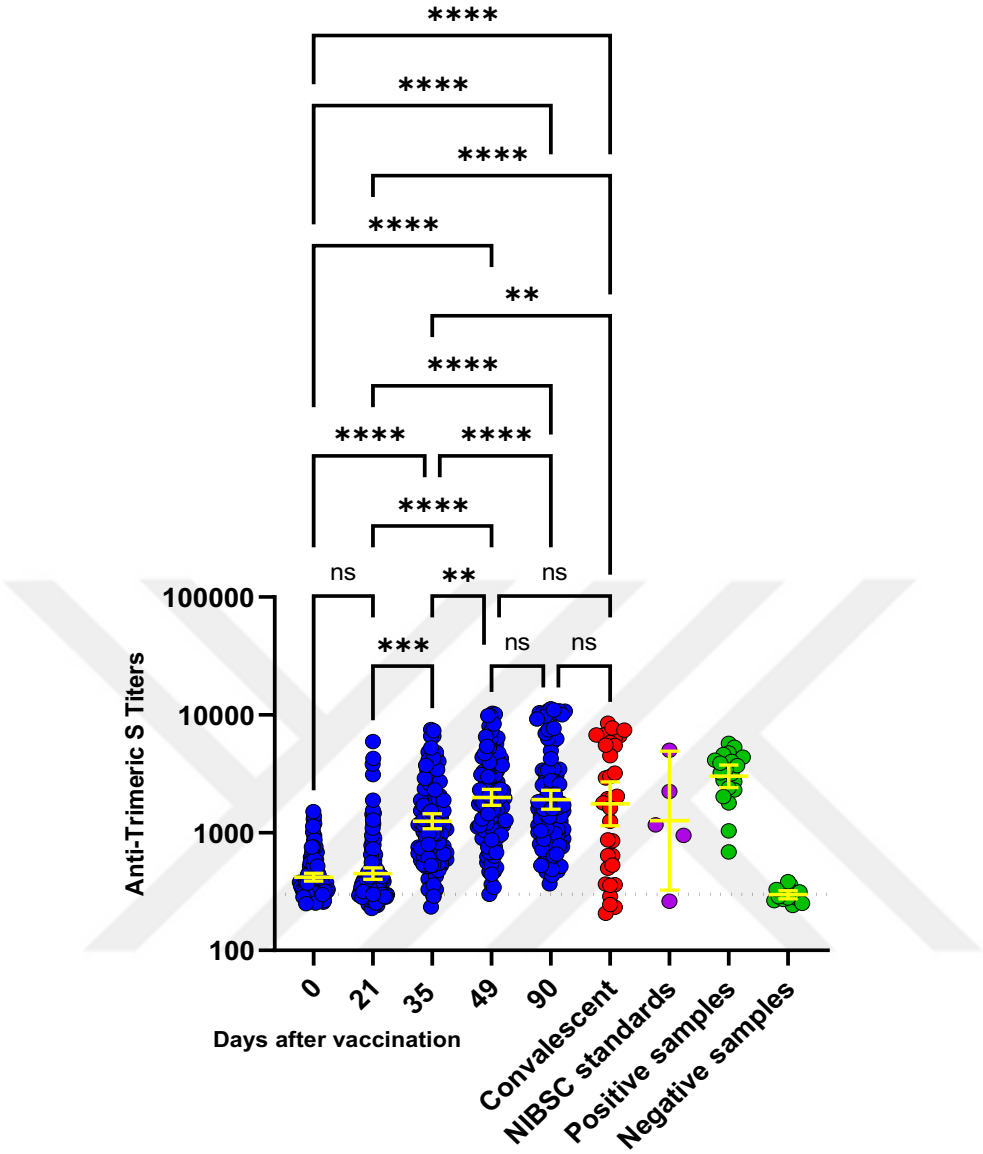

	0	21	35	49	90	Convalescent
Number of values	115	115	115	114	106	35
Geometric mean	418.4	449.1	1248	1993	1903	1756
Geometric SD factor	1.505	1.849	2.239	2.317	2.635	3.485
Lower 95% CI of geo. mean	388.0	400.9	1075	1705	1579	1143
Upper 95% CI of geo. mean	451.2	503.0	1448	2330	2294	2696

Figure 2.2.1. Measurement of anti-Spike IgG responses of vaccinated volunteers and comparison with convalescent sera. ELISA plates were coated with in-house trimeric S protein and IgG antibody production of serum samples of volunteers from Day:0, 21, 35, 49 and 90 and convalescent sera (N=35) along with NIBSC samples (N=37) and NIBSC standards (N=5) were measured. Kruskal-Wallis test and Dunn's multiple comparison correction were performed. (ns:non-significant, *p≤0.05, **p≤0.01, ***p≤0.001, ****p≤0.0001.)

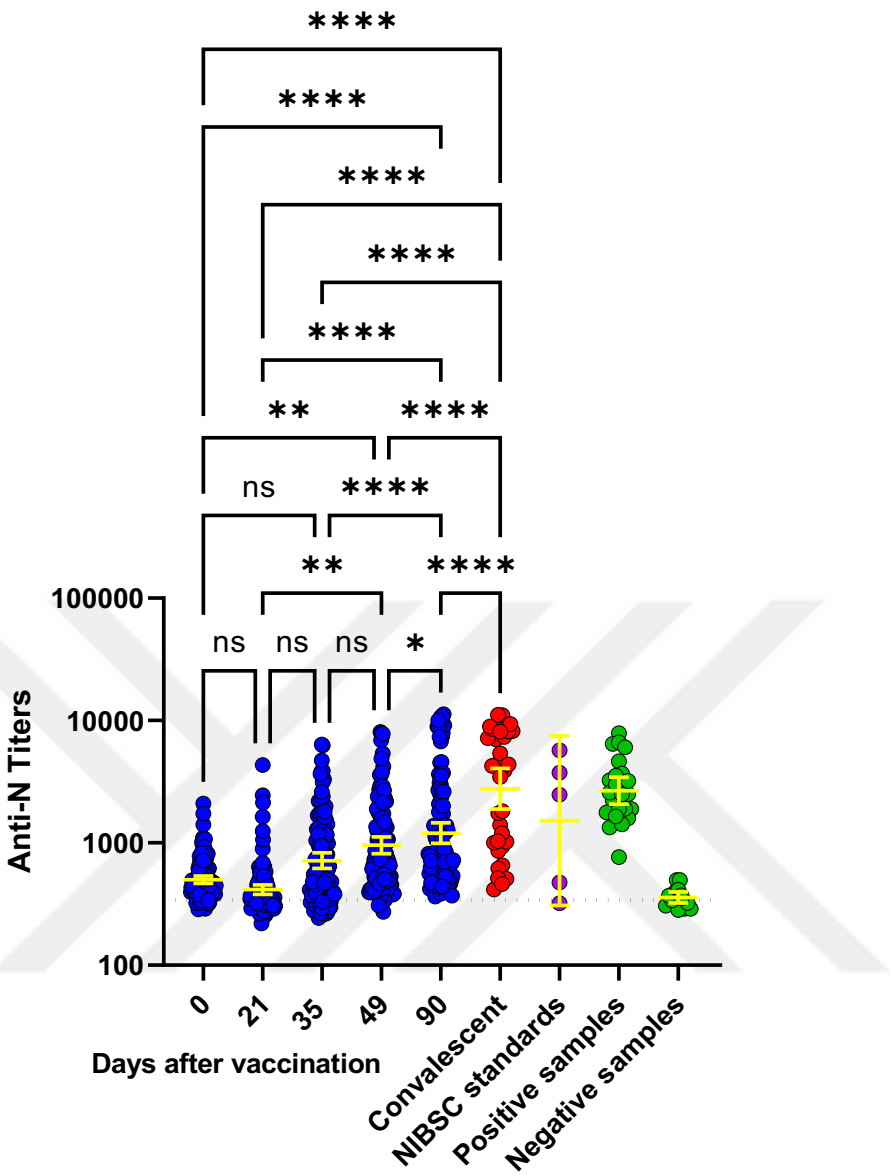

	0	21	35	49	90	Convalescent
Number of values	115	115	115	114	106	35
Geometric mean	498.9	414.6	716.0	956.4	1202	2770
Geometric SD factor	1.458	1.603	2.187	2.338	2.741	3.054
Lower 95% CI of geo. mean	465.3	380.0	619.7	817.0	989.8	1887
Upper 95% CI of geo. mean	534.9	452.4	827.4	1120	1459	4064

Figure 2.2.2. Measurement of anti-Nucleocapsid IgG responses of vaccinated volunteers and comparison with convalescent sera. ELISA plates were coated with in-house Nucleocapsid protein and IgG antibody production of serums samples of volunteers from Day:0, 21, 35, 49 and 90 and convalescent sera (N=35) along with NIBSC samples (N=37) and NIBSC standards (N=5) were measured. Kruskal-Wallis test and Dunn's multiple comparison correction were performed. (ns:non-significant, *p≤0.05, **p≤0.01, ***p≤0.001, ****p≤0.0001.)

With the emerging variants, concerns began to arise about whether the effectiveness of vaccines is decreasing. Therefore, we measured the IgG antibody levels against WT, Alpha and Delta variants in order to observe how the vaccine we made using the sequences of Alpha variant had a protective effect against other variants.

In Figure 2.2.3., from the 35th to the 90th day, the humoral immune responses gradually increased. While the serums of the volunteers remained above the negative standards, they were below the positive standards. Furthermore, it is understood that there was no significant difference between convalescents and volunteers' serums. The results were above the five NIBSC samples used. As expected, IgG levels produced against Alpha (UK) RBD are higher compared to the Wuhan (WT). When the antibody levels on the 49th and 90th days were examined, it can be seen that there was no significance with the convalescents used as controls and was higher than the NIBSC standards (Figure 2.2.4). ELISA results show that the developed vaccine was also effective against the Delta variant. As with the Alpha RBD results, antibody levels on the 49th and 90th day demonstrate that no significancy was observed with the convalescents. In addition, the IgG levels of the participants were also above the NIBSC standards (Figure 2.2.5).

Taken together, these results suggest that VLP-58-1023-AL-K3-PII vaccine was successfully elicited anti-WT, Alpha, Delta RBD IgG 2 weeks after 2nd dose, especially in 49th and 90th days humoral immunity was much higher. These data also provide positive impacts of the effectiveness of the vaccine against variants that may occur later.

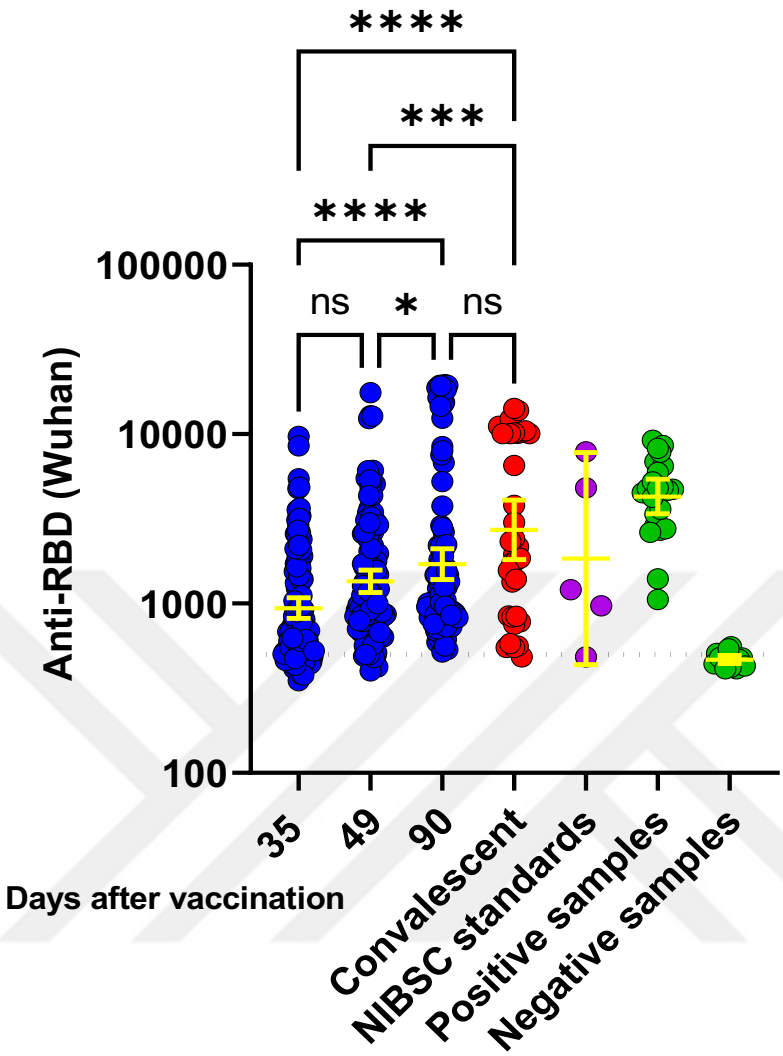

	35	49	90	Convalescent
Number of values	114	114	105	35
Geometric mean	939.2	1353	1709	2719
Geometric SD factor	2.115	2.271	2.928	3.235
Lower 95% CI of geo. mean	817.4	1162	1388	1817
Upper 95% CI of geo. mean	1079	1575	2104	4070

Figure 2.2.3. Measurement of anti-RBD (WT) IgG responses of vaccinated volunteers and comparison with convalescent sera. ELISA plates were coated with commercial WT RBD and IgG antibody production of serums samples of volunteers Day:0, 21, 35, 49 and 90 and convalescent sera (N=35) along with NIBSC samples (N=37) and NIBSC standards (N=5) were measured. Kruskal-Wallis test and Dunn's multiple comparison correction were performed. (ns:non-significant, *p≤0.05, **p≤0.01, ***p≤0.001, ****p≤0.0001.)

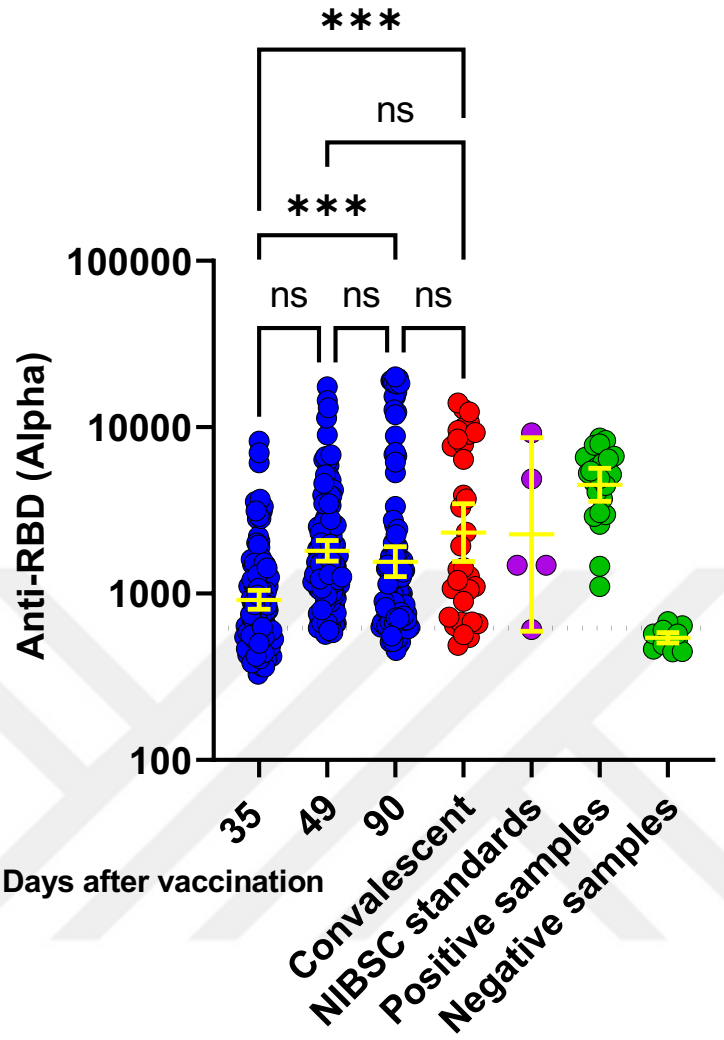

	35	49	90	Convalescent
Number of values	114	114	106	35
Geometric mean	917.7	1806	1555	2325
Geometric SD factor	2.042	2.148	2.928	3.193
Lower 95% CI of geo. mean	803.9	1567	1264	1560
Upper 95% CI of geo. mean	1048	2082	1912	3465

Figure 2.2.4. Measurement of anti-RBD (Alpha) IgG responses of vaccinated volunteers and comparison with convalescent sera. ELISA plates were coated with commercial UK RBD and IgG antibody production of serums samples of volunteers Day:0, 21, 35, 49 and 90 and convalescent sera (N=35) along with NIBSC samples (N=37) and NIBSC standards (N=5) were measured. Kruskal-Wallis test and Dunn's multiple comparison correction were performed. (ns:non-significant, *p≤0.05, **p≤0.01, ***p≤0.001, ****p≤0.0001.)

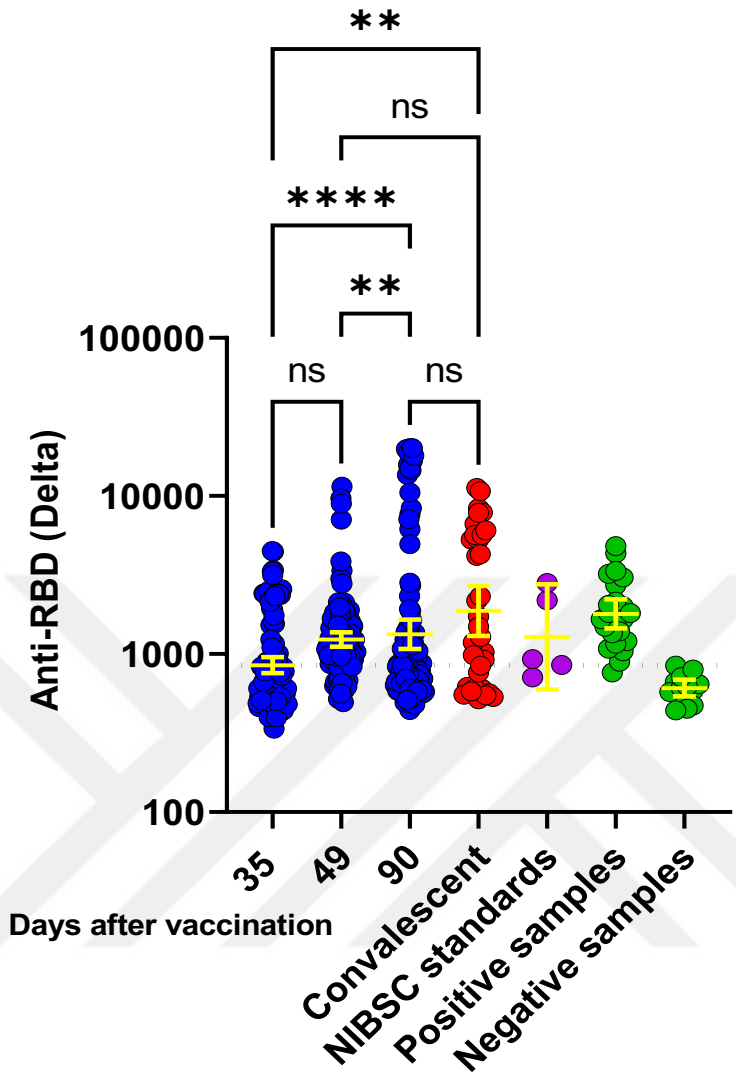

	35	49	90	Convalescent
Number of values	114	114	106	35
Geometric mean	850.3	1236	1334	1874
Geometric SD factor	1.890	1.741	3.028	2.884
Lower 95% CI of geo. mean	755.5	1115	1078	1303
Upper 95% CI of geo. mean	956.9	1370	1651	2697

Figure 2.2.5. Measurement of anti-RBD (Delta) IgG responses of vaccinated volunteers and comparison with convalescent sera. ELISA plates were coated with commercial Delta RBD and IgG antibody production of serums samples of volunteers from Day:0, 21, 35, 49 and 90 and convalescent sera (N=35) along with NIBSC samples (N=37) and NIBSC standards (N=5) were measured. Kruskal-Wallis test and Dunn's multiple comparison correction were performed. (ns:non-significant, *p≤0.05, **p≤0.01, ***p≤0.001, ****p≤0.0001.)

In order to confirm the reliability of our results, we wanted to support it with a purchased kit and a neutralizing antibody kit made in an accredited laboratory (Deren Laboratory, Ankara, Turkey). We used the CoronaHunter kit to determine the IgG antibody levels against the Trimeric S protein. The results show that after the second vaccination there was a significant humoral immune responses formation (Figure 2.2.6). Additionally, these responses persisted at a high level until the 90th day. When comparing with convalescent sera, no significant difference was observed. All samples after the 21st day were above the NIBSC negative samples, and 5 NIBSC standards.

The results of neutralizing antibodies performed with the Abbott show that high levels of antibody responses were observed in all samples, with the exception of serum samples taken 21 days after the 1st dose (Figure 2.2.7). Also, the responses were above the threshold, which was 50 according to the manufacturer's protocol, and they continued to increase slightly until the 90th day. There was no significant difference in neutralizing antibody levels on the 49th and 90th day compared to convalescent samples.

It has been understood that the results acquired from the kits are compatible with our other ELISA results. Although some humoral immune responses were below what we were expected, after the 2nd dose, IgG antibody production against Spike, Nucleocapsid and WT, Alpha, Delta RBD proteins was successfully achieved in most of our participants.

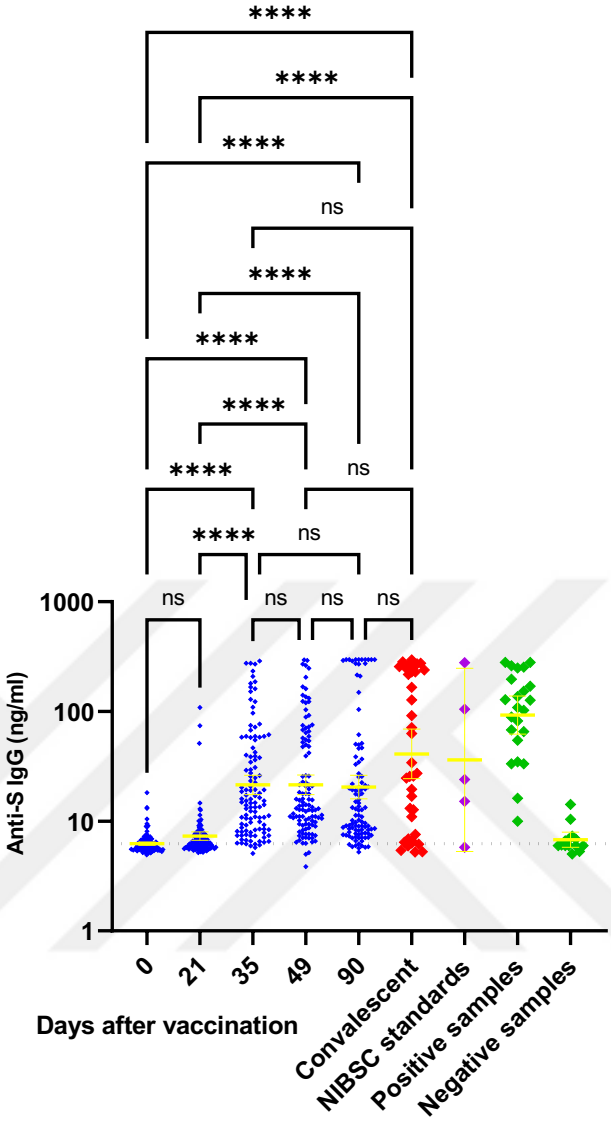

	0	21	35	49	90	Convalescent	NIBSC standards	Positive samples	Negative samples
Geometric mean	6.242	7.311	21.42	21.48	20.47	41.01	36.15	92.78	6.768
Geometric SD factor	1.219	1.616	2.993	3.021	3.612	4.748	4.700	2.511	1.316
Lower 95% CI of geo. mean	6.018	6.690	17.48	17.47	15.98	24.40	5.293	62.31	5.775
Upper 95% CI of geo. mean	6.475	7.989	26.25	26.42	26.21	68.94	247.0	138.1	7.931

Figure 2.2.6. Determination of anti-Spike IgG antibody responses by using CoronaHunter kit. Serums taken from participants on certain days (0,21,35,49,90), convalescent sera, NIBSC standards and samples were studied. Kit was carried out according to manufacturer's instructions. Kruskal-Wallis test and Dunn's multiple comparison correction were performed. (ns:non-significant, *p≤0.05, **p≤0.01, ***p≤0.001, ****p≤0.0001.)

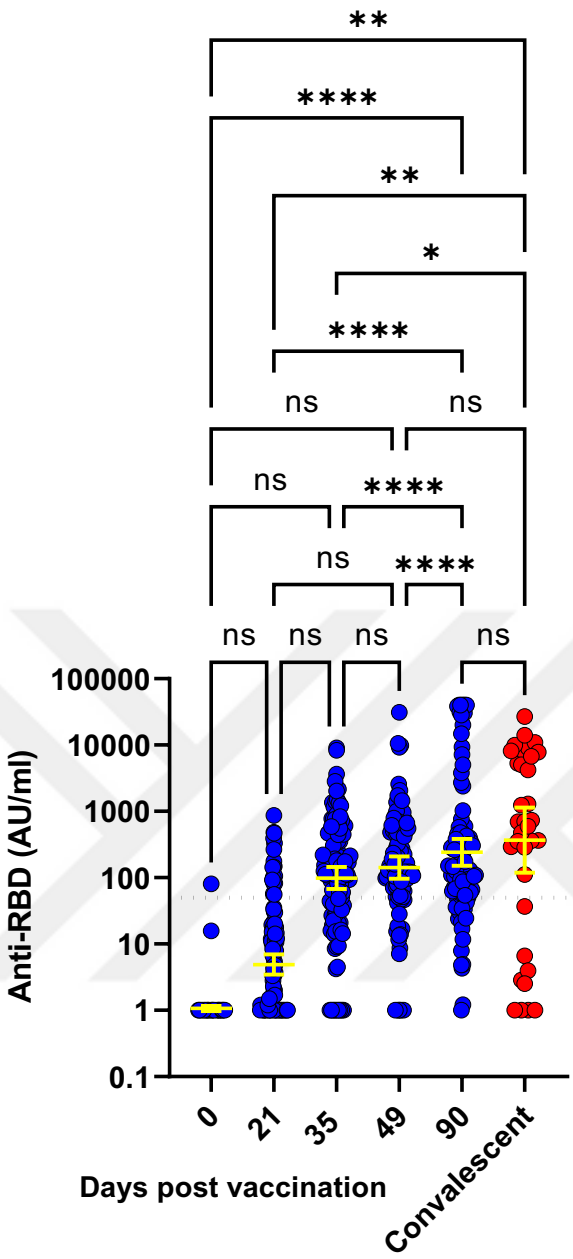

	0	21	35	49	90	Convalescent
Number of values	113	116	114	106	104	35
Geometric mean	1.065	4.896	98.87	142.3	241.4	367.4
Geometric SD factor	1.625	6.645	7.704	7.380	11.06	26.71
Lower 95% CI of geo. mean	0.9731	3.456	67.69	96.82	151.3	118.9
Upper 95% CI of geo. mean	1.166	6.936	144.4	209.1	385.1	1136

Figure 2.2.7. Determination of neutralizing antibody levels of vaccinated volunteers and comparison with convalescent sera by Abbott. Serums samples of participants from Day:0, 21, 35, 49, 90 and convalescent sera were studied. The assay was conducted in Deren Laboratory. Kruskal-Wallis test and Dunn's multiple comparison correction were performed. (ns:non-significant, *p≤0.05, **p≤0.01, ***p≤0.001, ****p≤0.0001.)

2.2.2. Determination of Cellular Immune Responses of Phase II Clinical Trial Volunteers Vaccinated with VLP-58-1023-AL-K3-PII SARS-COV-2 for Alpha Variant

In addition to humoral immune responses, cellular immune responses have significant role in protection against SARS-CoV-2. T cell responses specific to SARS-CoV-2 are required for clearance of virus, might inhibit infection without seroconversion, contribute strong memory, and facilitate SARS-CoV-2 variant detection [121]. Besides, they may also be triggered after vaccination, which they can prevent serious illness and mortality. Therefore, it is critical to obtain high T cell responses from our vaccinated volunteers. Here, our aim was to analyze cytokine levels and show that VLP-58-1023-AL-K3-PII vaccine trigger Th1-biased T cell responses.

Th1 responses are mainly comprised of IFN-γ, IL-2 and TNF-α cytokines. As seen in Figure 2.2.8, there was a significant increase in the production of these three cytokines. Especially, PBMCs taken from volunteers showed a 11.1-fold increase in IFN-γ levels. Also, IL-2 and TNF-α cytokines levels increased 7.6-fold and 2.6-fold respectively. This result indicates that vaccinated volunteers successfully triggered a strong Th1 responses after stimulation with S,N,M,O peptide pool.

Since Th2 cells are produced by IL-4, IL-5, IL-9 and IL-13, we measured those cytokines levels after peptide stimulation. Our vaccine elicited more IL-13 cytokine production, 7.5-fold, compared to other three cytokines. Figure 2.2.9 indicates that IL-4, IL-5 and IL-9 increased 1.2-fold, 4-fold and 2.9-fold respectively. In general, Th2 immune response was generated in our vaccinated volunteers but it is not high as Th1 response.

We wondered whether other Th subsets were triggered after immunization. For instance Th17 cells have indirect role in inducing neutrophils and macrophages. As shown in Figure 2.2.10., the detection of Th17 responses and IL-17A, IL-17F and IL-22 were studied for that purpose. It is illustrated that the increases in IL-17A and IL-27F were almost the same, 1.8-fold and 2.1-fold respectively. IL-22 showed a 3.8-fold increase after the stimulation of PBMCs taken from volunteers with S,N,M,O peptide pool.

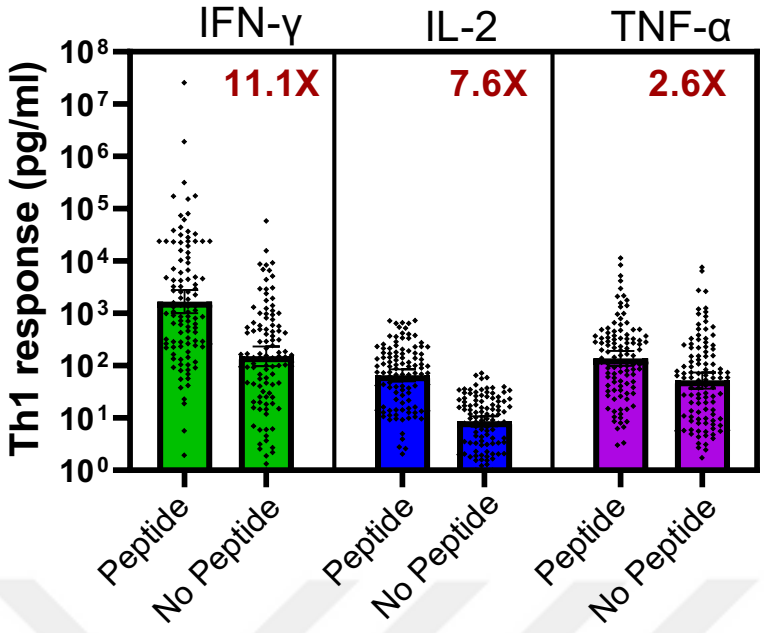

	IFN-γ		IL-2		TNF-α	
	A:1	A:2	B:1	B:2	C:1	C:2
Number of values	107	107	107	107	107	107
Geometric mean	1675	150.2	65.61	8.634	137.7	52.22
Geometric SD factor	14.43	9.516	4.008	3.177	5.433	6.428
Lower 95% CI of geo. mean	1004	97.53	50.28	6.918	99.56	36.55
Upper 95% CI of geo. mean	2794	231.3	85.61	10.77	190.5	74.59

Figure 2.2.8. CBA measurement of Th1 responses of volunteers before and after peptide stimulation. PBMCs from the volunteers at day 35, that were stimulated with SARS-CoV-2 SNMO defined peptide pool, were labeled as “Peptide” and non-stimulated PBMCs were labeled as “No Peptide”. IFN-γ, IL-2 and TNF-α cytokine production were studied and categorized as Th1 response. The rate of increase in the level of each cytokine after peptide stimulation is shown by the number of "X"-fold.

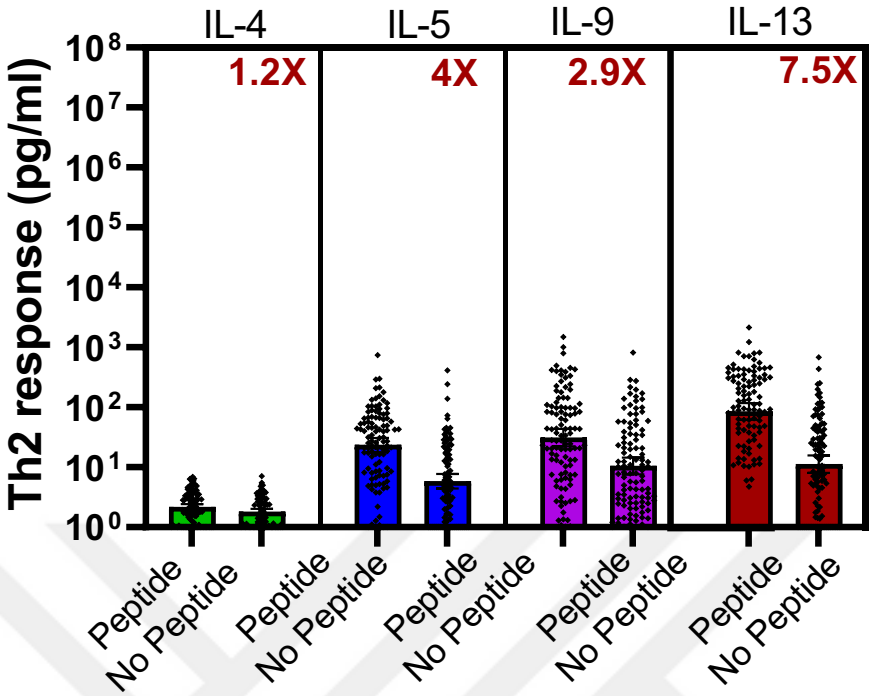

	IL-4		IL-5		IL-9		IL-13	
	A:1	A:2	B:1	B:2	C:1	C:2	D:1	D:2
Number of values	107	107	107	107	107	107	107	107
Geometric mean	2.155	1.817	23.46	5.809	31.07	10.48	84.80	11.23
Geometric SD factor	1.820	1.726	4.200	4.290	5.823	5.294	5.272	5.715
Lower 95% CI of geo. mean	1.921	1.636	17.82	4.394	22.17	7.612	61.66	8.043
Upper 95% CI of geo. mean	2.417	2.017	30.88	7.679	43.55	14.42	116.6	15.69

Figure 2.2.9. CBA measurement of Th2 responses of volunteers before and after peptide stimulation. PBMCs from the volunteers at day 35, that were stimulated with SARS-CoV-2 SNMO defined peptide pool, were labeled as “Peptide” and non-stimulated PBMCs were labeled as “No Peptide”. IL-4, IL-5, IL-9 and IL-13 cytokine production were studied and categorized as Th2 response. The rate of increase in the level of each cytokine after peptide stimulation is shown by the number of "X"-fold.

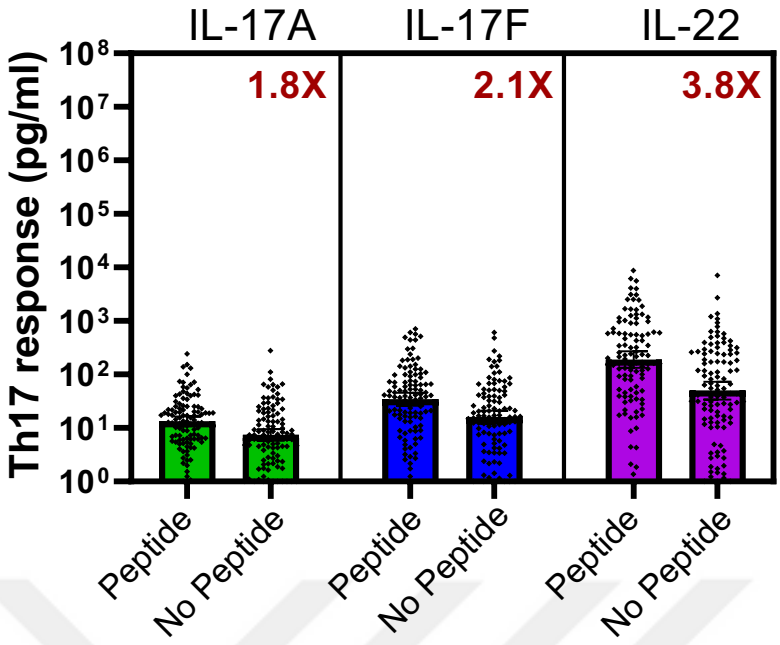

	IL-17A		IL-17F		IL-22	
	A:1	A:2	B:1	B:2	C:1	C:2
Number of values	107	107	107	107	107	107
Geometric mean	13.29	7.405	34.22	15.98	189.9	49.91
Geometric SD factor	2.984	3.604	4.282	4.396	6.320	7.449
Lower 95% CI of geo. mean	10.78	5.792	25.89	12.03	133.3	33.97
Upper 95% CI of geo. mean	16.39	9.468	45.22	21.22	270.3	73.34

Figure 2.2.10. CBA measurement of Th17 responses of volunteers before and after peptide stimulation. PBMCs from the volunteers at day 35, that were stimulated with SARS-CoV-2 SNMO defined peptide pool, were labeled as “Peptide” and non-stimulated PBMCs were labeled as “No Peptide”. IL-17A, IL-17F and IL-22 cytokine production were studied and categorized as Th17 response. The rate of increase in the level of each cytokine after peptide stimulation is shown by the number of "X"-fold.

Tregs inhibit a wide range of immune cells, such as CD4+ and CD8+ T cells, DCs, B cells, macrophages, and NK cells and IL-10 plays a significant role in mediating this function [24]. When IL-10 production measured, it was seen that there was almost no induction after peptide stimulation (Figure 2.2.11).

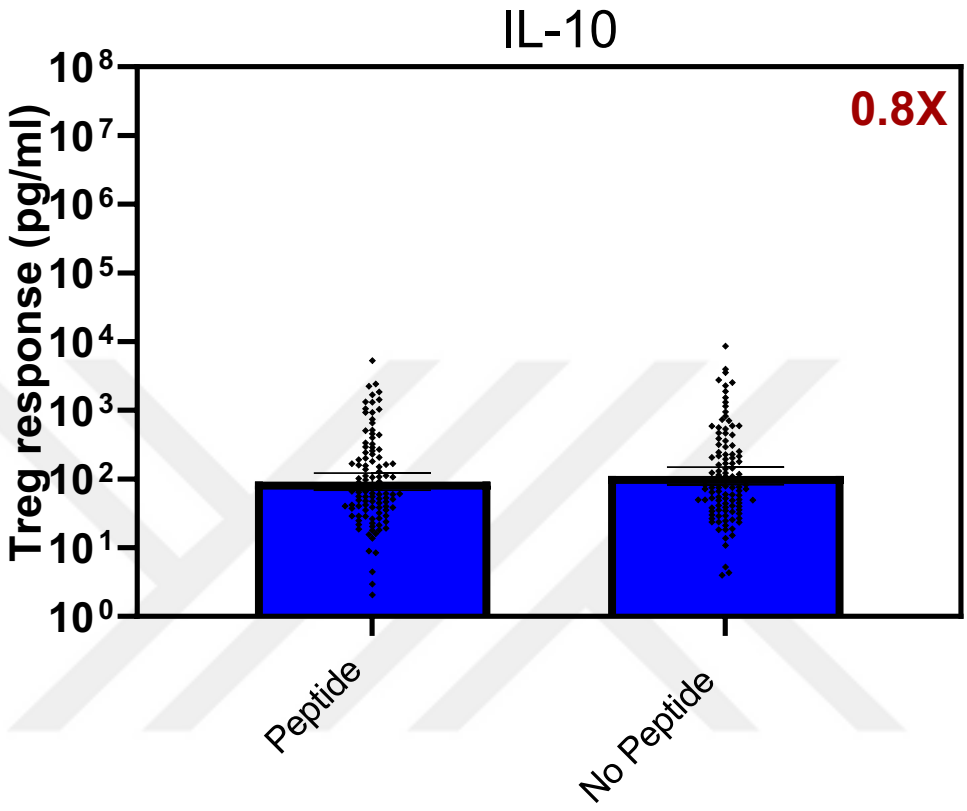

	IL-10	
	A:1	A:2
Number of values	107	107
Geometric mean	91.51	110.8
Geometric SD factor	4.451	4.615
Lower 95% CI of geo. mean	68.73	82.62
Upper 95% CI of geo. mean	121.8	148.5

Figure 2.2.11. CBA measurement of Treg responses of volunteers before and after peptide stimulation. PBMCs from the volunteers at day 35, that were stimulated with SARS-CoV-2 SNMO defined peptide pool, were labeled as “Peptide” and non-stimulated PBMCs were labeled as “No Peptide”. IL-10 cytokine production was studied and categorized as Treg response. The rate of increase in the level of cytokine after peptide stimulation is shown by the number of "X"-fold.

Our goal was to obtain Th1-biased response instead of Th2 hence it is critical to measure the level of IL-6 cytokine since it inhibits Th1 polarization via stimulating CD4+ cells to produce IL-4 or negatively affects the production of IFN-γ which in turn trigger Th2 response. After peptide stimulation, there was no change in the IL-6 cytokine level as depicted in Figure 2.2.12.

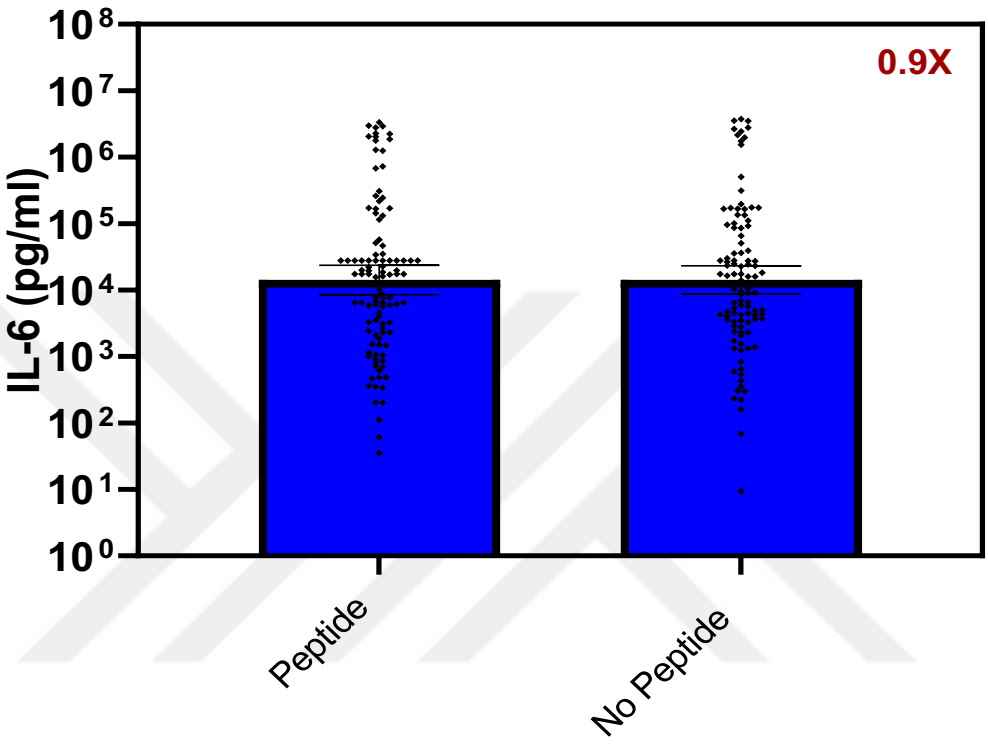

	A:1	A:2
Number of values	107	107
Geometric mean	14182	14223
Geometric SD factor	14.23	12.79
Lower 95% CI of geo. mean	8525	8727
Upper 95% CI of geo. mean	23591	23182

Figure 2.2.12. CBA measurement of IL-6 responses of volunteers before and after peptide stimulation. PBMCs from the volunteers at day 35, that were stimulated with SARS-CoV-2 SNMO defined peptide pool, were labeled as “Peptide” and non-stimulated PBMCs were labeled as “No Peptide”. IL-6 cytokine production was studied and the rate of increase in the level of cytokine after peptide stimulation is shown by the number of "X"-fold.

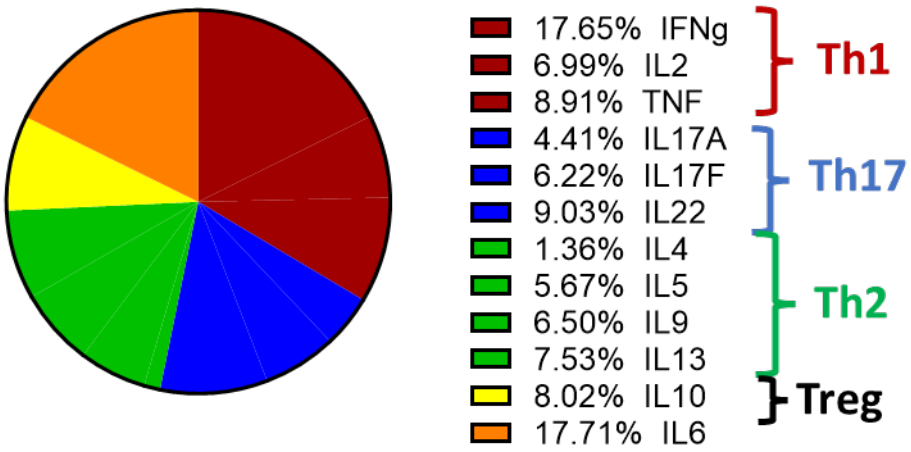

Figure 2.2.13. A pie chart distribution of the secreted effector T cell cytokines. Cytokines responses were classified into T cell subsets and the size of the slices indicates the percentage of secreted cytokines. Th1, Th17, Th2, Treg, and IL-6 responses were shown in red, blue, green, yellow and orange, respectively.

In the pie chart above, the percentages of produced T cell cytokines were shown, and each color indicates different T helper cell subsets, which are Th1, Th2, Th17, Treg, and IL-6. It is illustrated that 33.55% of the total T cell cytokines were Th1 responses. Th2 responses were the second highest proportion with 21.06%. Besides, 19.66% of T helper cell cytokines were produced by Th17 cells. Also, IL-6 secretion accounted for 17.71% while Treg was only 8.02% of the total T cell responses. Overall, Th1-biased cellular immune responses were generated after two doses of VLP-58-1023-AL-K3-PII SARS-COV-2 vaccine. Additionally, other T cell subsets were also induced in a certain amount and these balanced responses were critical for eliciting strong humoral immunity and viral clearance.

CHAPTER 3

DISCUSSION

SARS-CoV-2 is a new beta-coronavirus that first appeared in Wuhan, China in December 2019 and is the cause of the coronavirus disease 2019 (COVID-19) pandemic [122]. WHO has reported more than 500 milion confirmed cases and over 6 million deaths globally [123]. There is an immediate need of efficient vaccines and therapeutics to control the pandemic and return to normal life. Although SARS-CoV-2 encodes four structural proteins, S, N, M, E, most of the vaccine candidates targeted S glycoprotein due to its significant functions in viral entry and ability to neutralize the virus [124]. There are several vaccines that have been developed for COVID-19. The most known vaccines are Pfizer/BioNtech/BNT162b2, mRNA-1273/Moderna, Oxford/AstraZeneca/ AZD1222, Janssen/Ad26.COV2.S and Sinovac/CoronaVac. BNT162b2 and mRNA-1273 are mRNA-based vaccines which uses full-length Spike and prefusion stabilized full-length Spike of SARS-CoV-2 respectively [125]. AZD1222 and Ad26.COV2.S are viral vector vaccines which works against full-length Spike glycoprotein [126]. CoronaVac uses the technology of inactive virus and they encapsulated Spike protein [72].

SARS-CoV-2 encodes four structural proteins; S, N, M, and E but only S protein was attracted attention as a target antigen by the vaccine research groups because of its function and properties. However, other three proteins have also crucial roles in the generation of immune responses. For instance, N protein is involved in both viral replication and assembly, but also elicits a greater immunological response as it is less susceptible to mutations [43]. Besides, E protein not only contributes to viral assembly, budding, and virulence, but it also activates the NLRP3 inflammasome in the host [46]. Additionally, M protein is significant for assembling of virus, trafficking of virus proteins and releasing the virus particles but also it acts as a interferon antagonist like N protein [127]. So, all four proteins are promising target for COVID-19 vaccine. Since Spike protein is not stable and difficult to produce recombinantly in mammalian cells, we prefered to use Hexaproline prefusion-stabilized spike (S-6p). HexaPro is a stable S with six proline substitutions, as well as furin cleavage site mutations and a C-terminal trimerization motif [128]. This form is more stable, has greater expression, enhanced solubility and higher immunogenity compare to S-2P [129].

B.1.1.7 (Alpha, UK) variant was first identified in December 2020 and it became highly frequent, with prevalence rates exceeding 80%, hence, indicating a significant selection advantage over the original strain, which was the most widespread variant at the time. In addition to high transmissibility rate, Alpha variant has been linked to a 35% greater risk of mortality when compared to pre-existing lineages, highlighting the severity of the disease induced by this variant [130]. Besides, it possesses 23 mutations, three of which are significant because they alter the virus's biological features. Therefore, we used B.1.1.7 variant of SARS-CoV-2 instead of wild-type for the design of our vaccine. It would be more advantageous to use Alpha variant, predicting that similar mutations might occur in other variants that may arise, so that the vaccine will be effective for any circumstances.

We decided to develop a candidate COVID-19 vaccine by using the virus-like particle (VLP) technology for several reasons. In addition to its safety as it does not contain any genetic materials, VLPs are considerably more immunogenic than conventional subunit vaccines because they display repeating antigenic epitopes on their surface, which the immune system can identify [77]. Besides, VLP platform can address variety of issues that are commonly found in traditional vaccines such as reversion to lethal form because of the infectious nature of live attenuated vaccines, mutation risks, diminished immunogenicity of inactivated vaccines, toxicity, low yield, and long formulation time [131]. Since VLP’s manufacturing process is fast, a novel VLP vaccine against a particular strain may be generated in 12–14 weeks once the strain has been sequenced, whereas preparation of traditional vaccines take 24–32 weeks. Furthermore, we formulated our VLP vaccine with K3 CpG ODN and Alum which are explained in detail below.

When foreign pathogens attack the human body, the immune system triggers a series of immunological responses in order to eliminate the pathogens. Antibodies against SARS-CoV-2 can neutralize the virus or support cytotoxic T cells in the elimination of virus-infected cells, allowing disease progression to be controlled [132]. In this case, antibodies targeted towards primarily the Spike and Nucleocapsid proteins, which neutralize infected-cells and tissues expressing ACE2, induce humoral immune responses against SARS-CoV-2 [133]. Additionally, the S1 subunit of the Spike has a RBD that intervene viral binding to ACE2 receptors on susceptible cells and it is the key target for neutralizing antibodies against SARS-CoV-2. Thus, antibody titer is a useful way to detect the protective efficiency of antibodies for the virus.

For the pre-clinical studies, three different vaccine formulations were designed, which the amount of VLP and adjuvants varies, so that the optimal formulation can be found. High dose antigen and low dose adjuvants were expected to be the most effective in terms of inducing humoral immune responses. Since the amount of antigen in the formulation of Group C is higher compared to other groups, the amount of leukoyctes recruited by Alum to the injection site are also higher and combination with CpG enhance immunogenity. Results presented in Figure 2.1.1 and Figure 2.1.2 suggest that Group C elicited robust IgG responses against spike and nucleocapsid proteins after 2 doses of vaccine as we expected. When the samples taken after the first and second dose were compared, there was a 2-fold increase. It can be understood that after the first dose, a trigger was generated in the immune system, and a high level of immunogenicity was obtained after the second dose. Moreover, one of the purposes of using VLP technology containing four structural proteins was to acquire long-lasting immunity. IgG responses against spike proteins demonstrates that there was no decrease in the antibody levels two months after the second dose, as in the other groups. In other words, maintaining the IgG antibody levels after several months of second injection shows long-lasting immunity. Furthermore, nucleocapsid results were almost similar for every group. The reason for this was that the purity and the affinity binding of the produced nucleocapsid recombinant protein batch were so high, so the detection rate was also very high.

As in the animal studies, antibody responses against spike and nucleocapsid were examined for clinical phase II study. Similarly, as shown in the Figure 2.2.1 a small amount of response was observed after the first dose, while an effective humoral immunity was obtained after the second dose and this was maintained until the 90th day. Interestingly, anti-N responses after the first dose decreased below the levels of pre-vaccination. This can be because of the any mistakes during performing ELISA experiment such as the concentration of recombinant used for coating, background development and failure of detection of IgG antibody. Moreover, the antibody levels against spike were almost at the same levels with convalescent sera and NIBSC standards but IgG responses to nucleocapsid could not reach their levels. It can be said that VLP-58-1023-AL-K3-PII vaccine elicited higher IgG production against spike than nucleocapsid.

SARS-CoV-2 undergoes mutational alterations throughout time. The spread of the pandemic causes enormous viral replication, raising the possibilities of adaptive mutations, which might lead to selection benefits. Therefore, it is significant that vaccines should provide wide immunity against SARS-CoV-2 variants. In that time, after the emergence of Alpha variant, Delta variant became the new concern because of the ability of rapid spread across the world. Delta has P681R mutation but has no additional mutations in common with Alpha's background lineages. So, it is an exception in that Delta lacks N501Y mutation and the deletion in NSP6, has a slower rate of evolution than the other VOCs, and carries less non-synonymous mutations in its Spike protein but more mutations in other regions of the genome [134]. Although our vaccine was designed for the Alpha variant, its effectiveness against WT and Delta variant can provide insight whether VLP-58-1023-AL-K3-PII will be effective and protective against future variants. Also, it is known that Alpha and Delta variant do not share common mutations except P681R but Beta, Gamma and Omicron variants carry several common mutations with Alpha such as they have N501Y mutation in spike and deletion in NSP6. We hypothesize that if our vaccine will be effective for WT and Delta that do not share common mutations, it can be efficient for other variants that has or has not similar mutations. Therefore, it is significant to measure the humoral immune responses against WT, UK and Delta RBD.

Pre-clinical studies indicate that the antibody responses of half of the mice in group A and B were below the placebo group after the first injection, and the other half reached the same level as placebo for WT, Delta and Alpha. However, IgG levels of the mice in Group C increased slightly above the placebo, except for Alpha which can be due to an injectional mistake, indicating that the immune system had been activated. Moreover, Group C had the highest IgG responses after the second injection for all three RBDs compared to other groups which indicates that the vaccine formulation used in group C was optimal and effective against WT, Alpha and Delta RBD. It can be concluded that as with the spike and nucleocapsid results, an effective vaccine has been developed by using high antigen and low adjuvants dose, as we predicted.

In Phase II clinical trials, it was shown that neutralizing antibody levels of the volunteers for WT, Alpha and Delta variants increased over time. The responses reached a level comparable to convalescent and NIBSC standards which means the vaccine succesfully neutralize the virus. Besides, Hirabara et al. indicates that a decrease in neutralizing antibody activity of vaccines were detected even 14 days after the second dose [50]. However, this is not the case for us, in contrary, neutralizing antibody responses consistently increased untill 90 days after first dose. Therefore, it can be assumed that VLP-58-1023-AL-K3-PII vaccine is capable of neutralizing the virus and effective against future variants.

Humoral immune responses were measured by ELISA technique that in-house or commercial recombinant proteins were used for coating the plates. However, we also wanted to detect anti-S IgG levels by a purchased kit in order to verify our results and quantify the antibody levels in terms of ng/ul. For these reasons, we chose to use CoronaHunter anti-spike Trimer IgG kit which allows us to measure the absolute values of IgG against full-length spike protein. Besides, they used NIBSC 20/B770 panel samples from WHO to determine a cut off as we did. Since the kit is manufactured in Turkey, it can be delivered within 10 days after ordering which provides an advantage in terms of completing clinical trial analysis in a short time. In-house anti-S IgG ELISA results were very similar and consistent with the study performed with the CoronaHunter kit. While a low response was seen in both methods after the first dose, there was a constantly increasing response after the second dose. Moreover, there is only one small difference between two experiments that 49th and 90th days samples were higher than the convalescent and standards levels in the in-house ELISA but according to CoronaHunter, samples reached at a close level with controls. It can be deduced that the results of two different experiments were compatible with each other and it was understood that VLP-58-1023-AL-K3-PII vaccine elicited huge extent of humoral immune responses against spike.

SARS-CoV-2 IgG II Quant (Abbott) assay was used for detecting anti-RBD IgG responses, neutralizing antibodies, and performed in an accredited laboratory (Deren Laboratory, Ankara). According to manufacturer’s protocol, its cut off was 50 AU/ml and results below that value were considered as negative. Although some volunteers could not exceed the threshold value, majority of them succesfully produced neutralizing antibodies against the virus. Also antibody levels continued to increase, instead of decrease, over time which underpin the long-lasting immune effect of the vaccine.

Besides, the authenticity of the results were supported by convalescent samples and were compatible with commercial RBD ELISA experiments.

In summary, humoral immune response results obtained in animal studies showed that the formulation used in group C was the optimal and most effective vaccine formulation. Therefore, it was reasonable to increase the dosage 8-10 times in order to be administered in humans. In general, both anti-spike and anti-nucleocapsid IgG and neutralizing antibody responses for WT, Alpha and Delta were successfully produced in both mice and humans. Besides, the continued increase in humoral immune responses 90 days after the first injectiction indicates long-lasting efficacy of the vaccine. Finally, developing immunity not only against the wild-type strain, but also against other variants, elucidates that VLP-58-1023-AL-K3-PII vaccine may also be effective against other variants that may emerge in the future.

Existing vaccines for COVID-19 are administered as two doses, but the need for a third dose arose as the protection of the vaccines decreased over time. For instance, there was a study which efficiency of third dose BNT162b2 was investigated and indicated that the third dose showed greater than 95% relative vaccine efficacy over any residual protection from the two-dose series [135]. Additionally, an effective third dose has significant possible benefits in addition to decreasing the disease, such as avoiding COVID-19 complications following the progress of infections, enhancing the efficacy against the Omicron variant and it might decrease the transmission to unvaccinated people [136] [137] [138]. For this purpose, two months after the 2nd dose, the mice were injected with the 3rd dose. It can be clear that without the third dose, all antibody responses were started to decrease after a certain period of time. The highest humoral immune responses were obtained with the administration of the third dose.

In addition to humoral immunity, cellular immune response has an essential role in long-term immunological protection against COVID-19 disease which provide a recall for following infection and vaccination. Although high titer neutralizing antibodies develop an immunity and protect from SARS-CoV-2, T cells can decrease the severity of the disease, shorten the infection duration and enhance recovery. Besides, Th1/Th2 balance is critical in terms of generating various pathologies and development of SARS-CoV-2 infection. For instance, overproduction of cytokines lead to cytokine storm which generate Th2 response with a poor diagnosis. Also, Th2-biased responses can cause vaccine-associated enhanced disease (VAED) such as eosinophil infiltration. According to Martonik et al., uncontrolled IL-17 and IL-23 cytokine production, which are associated

with Th17 response, contribute to cytokine released syndrome (CRS) [139]. It is known that at the optimum levels, increased cytokine expression prevents the host from SARS-CoV-2 and substantially regulates viral replication which can be achieved with an efficient Th1 immune response. The study of BNT162b1, mRNA-1273, GX-19, S-Trimer and many other SARS-CoV-2 vaccines demonstrates Th1-biased responses and low or undetectable Th2 responses [140]. So, both Th1-biased responses and neutralizing antibodies are required to obtain an effective COVID-19 vaccine and also these two requirements would diminish the risk of VAED or antibody-dependent amplification of replication [141].

Although many of the candidate vaccines used Spike as the main antigen, we targeted all four SARS-CoV-2 antigens (S, N, M, E) in our vaccine. The COVID-19 vaccine containing only Spike induce CD4+ T cell responses that are similar to those seen in natural COVID-19 disease, however, other structural SARS-CoV-2 proteins such as N and M would more closely resemble the natural SARS-CoV-2-specific CD4+ T cell response seen in mild to severe COVID-19 infection because they are not subjected to the same selection pressure as the Spike RBD, they are less susceptible to mutation [142] [143]. Besides, it has been revealed that the Spike protein was not dominant in targeting CD8+ T cell responses, but significant reactivity and equally strong recognition was reported for M and N proteins. Grifoni et al. demonstrates that potential COVID-19 vaccines attempting to generate CD8+ T cell responses against the spike protein will induce a relatively restricted CD8+ T cell response in comparison to the natural CD8+ T cell response seen in mild to severe COVID-19 disease [143]. Therefore, these two structural SARS-CoV-2 proteins can be used to induce greater CD8+ T cell responses. Thus, we wanted to take advantage of not only Spike but also Nucleocapsid, Membrane and Envelope proteins in VLP-58-1023-AL-K3-PII vaccine and much higher and long-lasting T cell responses were expected.

Two adjuvants, Alum and CpG were used in VLP-58-1023-AL-K3-PII vaccine, and they have different effects on cellular immune responses. Alum has been demonstrated to primarily serve as a transport method for antigen, trapping it at the injection site by creating macromolecular aggregates, allowing for gradual release and absorption by APCs [144]. Also, it is known that Alum trigger NLRP3 pathway which in turn stimulate Th2 immune responses. For COVID-19 vaccine, combination of Alum and PRR-based adjuvant were used to improve the immunogenicity, eliciting balanced Th1/Th2 responses and long-lasting immunity. To address this, we combined Alum with K3-CpG ODN which is an effective adjuvant for generating Th1 responses, stimulating

the production of cytotoxic T lymphocytes and IFN-γ [145]. However, the dosage of both Alum and CpG must be carefully determined since Alum can absorb the ability of CpG to induce Th1 responses. So, we expected to generate Th1-biased immune response and reduce the risk of Th2 and Th17-induced immunopathology.

In this thesis, we used a Th human cytokine panel which allowed us to study IL-2, 4, 5, 6, 9, 10, 13, 17A, 17F, 22, IFN-γ and TNF-α. PMBCs were stimulated with the SARS-CoV-2 SNMO peptide pool which consists peptides from S,N,M, ORF-3a and ORF-7a proteins so that T cell responses specific to SARS-CoV-2 were determined. The results were categorized according to T cell subsets (Th1, Th2, Th17, Treg, IL-6) and depicted in Figure 2.2.8, Figure 2.2.9, Figure 2.2.10, Figure 2.2.11 and Figure 2.2.12. Since IFN-γ is a key cytokine for triggering intracellular antiviral pathways and most effective activator of macrophages, it is significant to get a robust release of IFN-γ. Additionally, IL-4 is known to be the driving force for Th2 differentiation, hence, low or undetectable level of IL-4 is critical to obtain Th1-biased response. Therefore, expression of these two cytokines, IFN-γ and IL-4, were expected to be upregulated and downregulated in our vaccinated volunteers respectively. In addition to Th1 and Th2 responses, Th17, Treg and IL-6 responses were studied.

The results show strong release of IFN- γ (11.1-fold), IL-2 (7.6-fold) and low expression of TNF-α (2.6-fold) after peptide stimulation. On the other hand, low detection of IL-4, IL-5 and IL-9 was observed which indicates the generation of Th1-biased response after vaccination. Besides, although excess IL-13 damage to airway homeostasis, in the appropriate milieu, IL-13 expression help efficient differentiation of antibody [146]. So, 7.5-fold increase of IL-13 is not harmful, instead it shows a successful recruitment of distinct immune cells such as neutrophils and macrophages. Furthermore, Th17 cells have a significant role in COVID-19 pathogenesis which inhibit Th1 differentiation, trigger Th2 responses and lead to immune-driven lung injury [139]. Unsurprisingly, very low levels of IL-17A, IL-17F, IL-22 were detected as we expected. Moreover, IL-6 was higher than other cytokines before peptide stimulation and this can be explained with its critical role in connecting innate and acquired immune responses which induces naïve CD4+ T cells differentiation [147]. Also, IL-6 expression was observed to be undetectable after peptide stimulation as it was expected because it suppresses IFN-γ gene expression directly and it should be suppressed in order to prevent a cytokine storm [148]. However, there was a certain amount of IL-6 expression before peptide stimulation. The reason for this is that PBMCs were freezed, thawed, incubated and during that time other immune cells such as macrophages and DCs could lead to the secretion of IL-6, hence, this background was not a T-cell dependent

expression. IL-10 is another cytokine that was expected to be undetectable since it reduces the innate inflammatory response to viral particles by preventing the formation of IL-17-producing cells that harm the tissue. Overall, based on the analysis, VLP-58-1023-AL-K3-PII induced Th1-biased response, low Th2 and Th17 response, undetectable Treg and IL-6 as we expected.

In this study, total IgG antibody responses against S,N proteins and WT,Alpha,Delta RBDs were demonstrated. It is known that when antigen and antibody complexed, Fc domain of the antibody facilitates the effector fuction via the FcR engagement which promotes phagocytosis functions of monocytes, NK cells and neutrophils [149]. Therefore, antibody-dependent functional activities such as antibody-dependent monocyte phagocytosis (ADMP), antibody-dependent neutrophil phagocytosis (ADNP), antibody-dependent NK cell activation (ADNKA), and antibody-dependent complement deposition (ADCD) can be measured as future experimental plans. Furthermore, the last reported VOC is Omicron variant, thus, the efficiency of vaccine against Omicron can be detected by neutralizing antibody measurement. Also, the measurement of memory B cells and CD8+ T cells levels of vaccinated volunteers can be studied in order to provide information regarding to long-term protection from SARS-CoV-2. We demonstrated the positive effects of 3rd dose on mice for the long-lasting immunity of the vaccine. The effects of the third dose can be compared with the second dose results if administration to humans allowed. Moreover, VLP technology that we used for the development of the VLP-58-1023-AL-K3-PII vaccine can be easily adapted to other diseases such as influenza, hepatitis and can help preventing future pandemics.

Taken together, this study revealed that VLP-58-1023-AL-K3-PII vaccine elicited robust humoral and cellular immune responses, there were no reported side effects, its efficiency against variants was demonstrated. We proposed that third dose can be administred to humans for long-lasting immunity.

BIBLIOGRAPHY

[1] Kenneth M, Weaver C. *Janeway's Immunobiology*. Vol 1. 9th ed. Garland Science, Taylor & Francis Group, LLC; 2017.

[2] Palm NW, Medzhitov R. Pattern recognition receptors and control of adaptive immunity. *Immunol Rev*. 2009;227(1):221-233. doi:10.1111/j.1600-065X.2008.00731.x

[3] Kaur BP, Secord E. Innate Immunity. *Pediatr Clin North Am*. 2019;66(5):905-911. doi:10.1016/j.pcl.2019.06.011

[4] Marshall JS, Warrington R, Watson W, Kim HL. An introduction to immunology and immunopathology. *Allergy Asthma Clin Immunol*. 2018;14(S2):49. doi:10.1186/s13223-018-0278-1

[5] Parkin J, Cohen B. An overview of the immune system. *The Lancet*. 2001;357(9270):1777-1789. doi:10.1016/S0140-6736(00)04904-7

[6] McDonald DR, Levy O. Innate Immunity. In: *Clinical Immunology*. Elsevier; 2019:39-53.e1. doi:10.1016/B978-0-7020-6896-6.00003-X

[7] Takeuchi O, Akira S. Pattern Recognition Receptors and Inflammation. *Cell*. 2010;140(6):805-820. doi:10.1016/j.cell.2010.01.022

[8] Amarante-Mendes GP, Adjemian S, Branco LM, Zanetti LC, Weinlich R, Bortoluci KR. Pattern Recognition Receptors and the Host Cell Death Molecular Machinery. *Front Immunol*. 2018;9:2379. doi:10.3389/fimmu.2018.02379

[9] Newton K, Dixit VM. Signaling in Innate Immunity and Inflammation. *Cold Spring Harb Perspect Biol*. 2012;4(3):a006049-a006049. doi:10.1101/cshperspect.a006049

[10] Akira S, Uematsu S, Takeuchi O. Pathogen Recognition and Innate Immunity. *Cell*. 2006;124(4):783-801. doi:10.1016/j.cell.2006.02.015

[11] Kawai T, Akira S. The role of pattern-recognition receptors in innate immunity: update on Toll-like receptors. *Nat Immunol*. 2010;11(5):373-384. doi:10.1038/ni.1863

[12] Kumagai Y, Akira S. Identification and functions of pattern-recognition receptors. *J Allergy Clin Immunol*. 2010;125(5):985-992. doi:10.1016/j.jaci.2010.01.058

[13] O'Neill LAJ, Golenbock D, Bowie AG. The history of Toll-like receptors — redefining innate immunity. *Nat Rev Immunol*. 2013;13(6):453-460. doi:10.1038/nri3446

[14] Heil F, Hemmi H, Hochrein H, et al. Species-specific recognition of single-stranded RNA via toll-like receptor 7 and 8. *Science*. 2004;303(5663):1526-1529. doi:10.1126/science.1093620

[15] Medzhitov R. Toll-like receptors and innate immunity. *Nat Rev Immunol*. 2001;1(2):135-145. doi:10.1038/35100529

[16] Li B, Xia Y, Hu B. Infection and atherosclerosis: TLR-dependent pathways. *Cell Mol Life Sci*. 2020;77(14):2751-2769. doi:10.1007/s00018-020-03453-7

[17] Alberts B, Johnson A, Lewis J, et al. *Molecular Biology of the Cell*. Vol 1. 6th edition. Garland Science, Taylor & Francis Group, LLC; 2015.

[18] Mirzaei HR. Adaptive Immunity. In: *Reference Module in Biomedical Sciences*. Elsevier; 2020:B9780128187319001000. doi:10.1016/B978-0-12-818731-9.00028-8

[19] Spiering MJ. Primer on the Immune System. *Alcohol Res Curr Rev*. 2015;37(2):171-175.

[20] Hoffman W, Lakkis FG, Chalasani G. B Cells, Antibodies, and More. *Clin J Am Soc Nephrol*. 2016;11(1):137-154. doi:10.2215/CJN.09430915

[21] Basu R, Hatton RD, Weaver CT. The Th17 family: flexibility follows function. *Immunol Rev*. 2013;252(1):89-103. doi:10.1111/imr.12035

[22] Andersen MH, Schrama D, thor Straten P, Becker JC. Cytotoxic T Cells. *J Invest Dermatol*. 2006;126(1):32-41. doi:10.1038/sj.jid.5700001

[23] Seder RA, Ahmed R. Similarities and differences in CD4+ and CD8+ effector and memory T cell generation. *Nat Immunol*. 2003;4(9):835-842. doi:10.1038/ni969

[24] Carty SA, Riese MJ, Koretzky GA. T-Cell Immunity. In: *Hematology*. Elsevier; 2018:221-239. doi:10.1016/B978-0-323-35762-3.00021-4

[25] Zhu J, Yamane H, Paul WE. Differentiation of Effector CD4 T Cell Populations. *Annu Rev Immunol*. 2010;28(1):445-489. doi:10.1146/annurev-immunol-030409-101212

[26] Swain SL, McKinstry KK, Strutt TM. Expanding roles for CD4+ T cells in immunity to viruses. *Nat Rev Immunol*. 2012;12(2):136-148. doi:10.1038/nri3152

[27] Bonilla FA, Oettgen HC. Adaptive immunity. *J Allergy Clin Immunol*. 2010;125(2):S33-S40. doi:10.1016/j.jaci.2009.09.017

[28] Hohl TM. Cell-Mediated Defense against Infection. In: *Mandell, Douglas, and Bennett's Principles and Practice of Infectious Diseases*. Elsevier; 2015:50-69.e6. doi:10.1016/B978-1-4557-4801-3.00006-0

[29] Annunziato F, Romagnani C, Romagnani S. The 3 major types of innate and adaptive cell-mediated effector immunity. *J Allergy Clin Immunol*. 2015;135(3):626-635. doi:10.1016/j.jaci.2014.11.001

[30] Annunziato F, Romagnani S. Th1 Cells. In: *Encyclopedia of Immunobiology*. Elsevier; 2016:287-293. doi:10.1016/B978-0-12-374279-7.08002-4

[31] Mak TW, Saunders ME. T Cell Differentiation and Effector Function. In: *The Immune Response*. 1st edition. Academic Press; 2005:403-432.

[32] Stetson DB, Voehringer D, Grogan JL, et al. Th2 Cells: Orchestrating Barrier Immunity. In: *Advances in Immunology*. Vol 83. Elsevier; 2004:163-189. doi:10.1016/S0065-2776(04)83005-0

[33] Luckheeram RV, Zhou R, Verma AD, Xia B. CD4 $^{+}$ T Cells: Differentiation and Functions. *Clin Dev Immunol*. 2012;2012:1-12. doi:10.1155/2012/925135

[34] Hu B, Guo H, Zhou P, Shi Z-L. Characteristics of SARS-CoV-2 and COVID-19. *Nat Rev Microbiol*. 2021;19(3):141-154. doi:10.1038/s41579-020-00459-7

[35] Haque SM, Ashwaq O, Sarief A, Azad John Mohamed AK. A comprehensive review about SARS-CoV-2. *Future Virol*. 15(9):625-648. doi:10.2217/fvl-2020-0124

[36] Triggle CR, Bansal D, Ding H, et al. A Comprehensive Review of Viral Characteristics, Transmission, Pathophysiology, Immune Response, and Management of SARS-CoV-2 and COVID-19 as a Basis for Controlling the Pandemic. *Front Immunol*. 2021;12. Accessed March 15, 2022. https://www.frontiersin.org/article/10.3389/fimmu.2021.631139

[37] Lebeau G, Vagner D, Frumence É, et al. Deciphering SARS-CoV-2 Virologic and Immunologic Features. *Int J Mol Sci*. 2020;21(16):5932. doi:10.3390/ijms21165932

[38] Hoffmann M, Kleine-Weber H, Schroeder S, et al. SARS-CoV-2 Cell Entry Depends on ACE2 and TMPRSS2 and Is Blocked by a Clinically Proven Protease Inhibitor. *Cell*. 2020;181(2):271-280.e8. doi:10.1016/j.cell.2020.02.052

[39] V'kovski P, Kratzel A, Steiner S, Stalder H, Thiel V. Coronavirus biology and replication: implications for SARS-CoV-2. *Nat Rev Microbiol*. 2021;19(3):155-170. doi:10.1038/s41579-020-00468-6

[40] Kumar S, Nyodu R, Maurya VK, Saxena SK. Morphology, Genome Organization, Replication, and Pathogenesis of Severe Acute Respiratory Syndrome Coronavirus 2 (SARS-CoV-2). *Coronavirus Dis 2019 COVID-19*. Published online April 30, 2020:23-31. doi:10.1007/978-981-15-4814-7_3

[41] Huang Y, Yang C, Xu X, Xu W, Liu S. Structural and functional properties of SARS-CoV-2 spike protein: potential antivirus drug development for COVID-19. *Acta Pharmacol Sin*. 2020;41(9):1141-1149. doi:10.1038/s41401-020-0485-4

[42] Troyano-Hernáez P, Reinosa R, Holguín Á. Evolution of SARS-CoV-2 Envelope, Membrane, Nucleocapsid, and Spike Structural Proteins from the Beginning of the Pandemic to September 2020: A Global and Regional Approach by Epidemiological Week. *Viruses*. 2021;13(2):243. doi:10.3390/v13020243

[43] Bai Z, Cao Y, Liu W, Li J. The SARS-CoV-2 Nucleocapsid Protein and Its Role in Viral Structure, Biological Functions, and a Potential Target for Drug or Vaccine Mitigation. *Viruses*. 2021;13(6):1115. doi:10.3390/v13061115

[44] Hatmal MM, Alshaer W, Al-Hatamleh MAI, et al. Comprehensive Structural and Molecular Comparison of Spike Proteins of SARS-CoV-2, SARS-CoV and MERS-CoV, and Their Interactions with ACE2. *Cells*. 2020;9(12):2638. doi:10.3390/cells9122638

[45] Satarker S, Nampoothiri M. Structural Proteins in Severe Acute Respiratory Syndrome Coronavirus-2. *Arch Med Res*. 2020;51(6):482-491. doi:10.1016/j.arcmed.2020.05.012

[46] Schoeman D, Fielding BC. Coronavirus envelope protein: current knowledge. *Virol J*. 2019;16(1):69. doi:10.1186/s12985-019-1182-0

[47] CDC. Coronavirus Disease 2019 (COVID-19). Centers for Disease Control and Prevention. Published February 11, 2020. Accessed March 24, 2022. https://www.cdc.gov/coronavirus/2019-ncov/variants/variant-classifications.html

[48] Otto SP, Day T, Arino J, et al. The origins and potential future of SARS-CoV-2 variants of concern in the evolving COVID-19 pandemic. *Curr Biol*. 2021;31(14):R918-R929. doi:10.1016/j.cub.2021.06.049

[49] Davies NG, Abbott S, Barnard RC, et al. Estimated transmissibility and impact of SARS-CoV-2 lineage B.1.1.7 in England. *Science*. 2021;372(6538):eabg3055. doi:10.1126/science.abg3055

[50] Hirabara SM, Serdan TDA, Gorjao R, et al. SARS-COV-2 Variants: Differences and Potential of Immune Evasion. *Front Cell Infect Microbiol*. 2022;11. Accessed March 15, 2022. https://www.frontiersin.org/article/10.3389/fcimb.2021.781429

[51] Focosi D, Maggi F. Neutralising antibody escape of SARS-CoV-2 spike protein: Risk assessment for antibody-based Covid-19 therapeutics and vaccines. *Rev Med Virol*. 2021;31(6):e2231. doi:10.1002/rmv.2231

[52] Tegally H, Wilkinson E, Giovanetti M, et al. Detection of a SARS-CoV-2 variant of concern in South Africa. *Nature*. 2021;592(7854):438-443. doi:10.1038/s41586-021-03402-9

[53] Hoffmann M, Arora P, Groß R, et al. SARS-CoV-2 variants B.1.351 and P.1 escape from neutralizing antibodies. *Cell*. 2021;184(9):2384-2393.e12. doi:10.1016/j.cell.2021.03.036

[54] Tao K, Tzou PL, Nouhin J, et al. The biological and clinical significance of emerging SARS-CoV-2 variants. *Nat Rev Genet*. 2021;22(12):757-773. doi:10.1038/s41576-021-00408-x

[55] Lopez Bernal J, Andrews N, Gower C, et al. Effectiveness of Covid-19 Vaccines against the B.1.617.2 (Delta) Variant. *N Engl J Med*. 2021;385(7):585-594. doi:10.1056/NEJMoa2108891

[56] Callaway E. Heavily mutated Omicron variant puts scientists on alert. *Nature*. 2021;600(7887):21-21. doi:10.1038/d41586-021-03552-w

[57] Chen J, Wang R, Gilby NB, Wei G-W. Omicron Variant (B.1.1.529): Infectivity, Vaccine Breakthrough, and Antibody Resistance. *J Chem Inf Model*. 2022;62(2):412-422. doi:10.1021/acs.jcim.1c01451

[58] Portela Sousa C, Brites C. Immune response in SARS-CoV-2 infection: the role of interferons type I and type III. *Braz J Infect Dis*. 2020;24(5):428-433. doi:10.1016/j.bjid.2020.07.011

[59] Conti P, Ronconi G, Caraffa A, et al. Induction of pro-inflammatory cytokines (IL-1 and IL-6) and lung inflammation by Coronavirus-19 (COVI-19 or SARS-CoV-2): anti-inflammatory strategies. *J Biol Regul Homeost Agents*. 2020;34(2):327-331. doi:10.23812/CONTI-E

[60] Li G, Fan Y, Lai Y, et al. Coronavirus infections and immune responses. *J Med Virol*. 2020;92(4):424-432. doi:10.1002/jmv.25685

[61] Leisman DE, Ronner L, Pinotti R, et al. Cytokine elevation in severe and critical COVID-19: a rapid systematic review, meta-analysis, and comparison with other inflammatory syndromes. *Lancet Respir Med*. 2020;8(12):1233-1244. doi:10.1016/S2213-2600(20)30404-5

[62] Shah VK, Firmal P, Alam A, Ganguly D, Chattopadhyay S. Overview of Immune Response During SARS-CoV-2 Infection: Lessons From the Past. *Front Immunol*. 2020;11. Accessed March 25, 2022. https://www.frontiersin.org/article/10.3389/fimmu.2020.01949

[63] Azkur AK, Akdis M, Azkur D, et al. Immune response to SARS-CoV-2 and mechanisms of immunopathological changes in COVID-19. *Allergy*. 2020;75(7):1564-1581. doi:10.1111/all.14364

[64] Robbiani DF, Gaebler C, Muecksch F, et al. Convergent antibody responses to SARS-CoV-2 in convalescent individuals. *Nature*. 2020;584(7821):437-442. doi:10.1038/s41586-020-2456-9

[65] Khoury DS, Cromer D, Reynaldi A, et al. Neutralizing antibody levels are highly predictive of immune protection from symptomatic SARS-CoV-2 infection. *Nat Med*. 2021;27(7):1205-1211. doi:10.1038/s41591-021-01377-8

[66] Pollard AJ, Bijker EM. A guide to vaccinology: from basic principles to new developments. *Nat Rev Immunol*. 2021;21(2):83-100. doi:10.1038/s41577-020-00479-7

[67] COVID-19 vaccine tracker and landscape. Accessed March 21, 2022. https://www.who.int/publications/m/item/draft-landscape-of-covid-19-candidate-vaccines

[68] van Riel D, de Wit E. Next-generation vaccine platforms for COVID-19. *Nat Mater*. 2020;19(8):810-812. doi:10.1038/s41563-020-0746-0

[69] Gao Q, Bao L, Mao H, et al. Development of an inactivated vaccine candidate for SARS-CoV-2. *Science*. Published online May 6, 2020:eabc1932. doi:10.1126/science.abc1932

[70] Ye T, Zhong Z, García-Sastre A, Schotsaert M, De Geest BG. Current Status of COVID-19 (Pre)Clinical Vaccine Development. *Angew Chem Int Ed*. 2020;59(43):18885-18897. doi:10.1002/anie.202008319

[71] Liu Y, Wang K, Massoud TF, Paulmurugan R. SARS-CoV-2 Vaccine Development: An Overview and Perspectives. *ACS Pharmacol Transl Sci*. 2020;3(5):844-858. doi:10.1021/acsptsci.0c00109

[72] Ahmed S, Khan S, Imran I, et al. Vaccine Development against COVID-19: Study from Pre-Clinical Phases to Clinical Trials and Global Use. *Vaccines*. 2021;9(8):836. doi:10.3390/vaccines9080836

[73] Jeyanathan M, Afkhami S, Smaill F, Miller MS, Lichty BD, Xing Z. Immunological considerations for COVID-19 vaccine strategies. *Nat Rev Immunol*. 2020;20(10):615-632. doi:10.1038/s41577-020-00434-6

[74] Prüβ BM. Current State of the First COVID-19 Vaccines. *Vaccines*. 2021;9(1):30. doi:10.3390/vaccines9010030

[75] Shahcheraghi SH, Ayatollahi J, Aljabali AA, et al. An overview of vaccine development for COVID-19. *Ther Deliv*. 2021;12(3):235-244. doi:10.4155/tde-2020-0129

[76] Swann H, Sharma A, Preece B, et al. Minimal system for assembly of SARS-CoV-2 virus like particles. *Sci Rep*. 2020;10(1):21877. doi:10.1038/s41598-020-78656-w

[77] Tariq H, Batool S, Asif S, Ali M, Abbasi BH. Virus-Like Particles: Revolutionary Platforms for Developing Vaccines Against Emerging Infectious Diseases. *Front*

Microbiol. 2022;12. Accessed June 2, 2022. https://www.frontiersin.org/article/10.3389/fmicb.2021.790121

[78] Kushnir N, Streatfield SJ, Yusibov V. Virus-like particles as a highly efficient vaccine platform: Diversity of targets and production systems and advances in clinical development. *Vaccine*. 2012;31(1):58-83. doi:10.1016/j.vaccine.2012.10.083

[79] Keikha R, Daliri K, Jebali A. The Use of Nanobiotechnology in Immunology and Vaccination. *Vaccines*. 2021;9(2):74. doi:10.3390/vaccines9020074

[80] Nooraei S, Bahrulolum H, Hoseini ZS, et al. Virus-like particles: preparation, immunogenicity and their roles as nanovaccines and drug nanocarriers. *J Nanobiotechnology*. 2021;19(1):59. doi:10.1186/s12951-021-00806-7

[81] Vicente T, Roldão A, Peixoto C, Carrondo MJT, Alves PM. Large-scale production and purification of VLP-based vaccines. *J Invertebr Pathol*. 2011;107:S42-S48. doi:10.1016/j.jip.2011.05.004

[82] Hillebrandt N, Vormittag P, Bluthardt N, Dietrich A, Hubbuch J. Integrated Process for Capture and Purification of Virus-Like Particles: Enhancing Process Performance by Cross-Flow Filtration. *Front Bioeng Biotechnol*. 2020;8:489. doi:10.3389/fbioe.2020.00489

[83] García-Silva I, Colunga-Saucedo M, Almendarez-Rodríguez C, Miranda-López C, Rosales-Mendoza S, Comas-Garcia M. Chapter 10 - Virus-like particle-based vaccines against SARS-CoV-2. In: Rosales-Mendoza S, Comas-Garcia M, Gonzalez-Ortega O, eds. *Biomedical Innovations to Combat COVID-19*. Academic Press; 2022:173-192. doi:10.1016/B978-0-323-90248-9.00005-X

[84] Maharjan PM, Choe S. Plant-Based COVID-19 Vaccines: Current Status, Design, and Development Strategies of Candidate Vaccines. *Vaccines*. 2021;9(9):992. doi:10.3390/vaccines9090992

[85] Yilmaz IC, Ipekoglu EM, Bulbul A, et al. Development and preclinical evaluation of virus-like particle vaccine against COVID-19 infection. *Allergy*. 2022;77(1):258-270. doi:10.1111/all.15091

[86] Shaw AR, Feinberg MB. 92 - Vaccines. In: Rich RR, Fleisher TA, Shearer WT, Schroeder HW, Frew AJ, Weyand CM, eds. *Clinical Immunology (Third Edition)*. Mosby; 2008:1353-1382. doi:10.1016/B978-0-323-04404-2.10092-2

[87] T. Johnson-Weaver B, Abraham SN, Staats HF. Innate Immunity-Based Mucosal Modulators and Adjuvants. In: *Mucosal Vaccines*. Elsevier; 2020:167-183. doi:10.1016/B978-0-12-811924-2.00010-9

[88] Reed SG, Orr MT, Fox CB. Key roles of adjuvants in modern vaccines. *Nat Med*. 2013;19(12):1597-1608. doi:10.1038/nm.3409

[89] Wu Z, Liu K. Overview of vaccine adjuvants. *Med Drug Discov*. 2021;11:100103. doi:10.1016/j.medidd.2021.100103

[90] Pulendran B, Ahmed R. Immunological mechanisms of vaccination. *Nat Immunol*. 2011;12(6):509-517. doi:10.1038/ni.2039

[91] Marrack P, McKee AS, Munks MW. Towards an understanding of the adjuvant action of aluminium. *Nat Rev Immunol*. 2009;9(4):287-293. doi:10.1038/nri2510

[92] Keshavarz-Fathi M, Rezaei N. Chapter 3 - Vaccines, Adjuvants, and Delivery Systems. In: Rezaei N, Keshavarz-Fathi M, eds. *Vaccines for Cancer Immunotherapy*. Academic Press; 2019:45-59. doi:10.1016/B978-0-12-814039-0.00003-5

[93] Franchi L, Núñez G. The Nlrp3 inflammasome is critical for aluminium hydroxide-mediated IL-1beta secretion but dispensable for adjuvant activity. *Eur J Immunol*. 2008;38(8):2085-2089. doi:10.1002/eji.200838549

[94] Gavin AL, Hoebe K, Duong B, et al. Adjuvant-enhanced antibody responses occur without Toll-like receptor signaling. *Science*. 2006;314(5807):1936-1938. doi:10.1126/science.1135299

[95] Kool M, Soullié T, van Nimwegen M, et al. Alum adjuvant boosts adaptive immunity by inducing uric acid and activating inflammatory dendritic cells. *J Exp Med*. 2008;205(4):869-882. doi:10.1084/jem.20071087

[96] Munks MW, McKee AS, MacLeod MK, et al. Aluminum adjuvants elicit fibrin-dependent extracellular traps in vivo. *Blood*. 2010;116(24):5191-5199. doi:10.1182/blood-2010-03-275529

[97] Marichal T, Ohata K, Bedoret D, et al. DNA released from dying host cells mediates aluminum adjuvant activity. *Nat Med*. 2011;17(8):996-1002. doi:10.1038/nm.2403

[98] Bode C, Zhao G, Steinhagen F, Kinjo T, Klinman DM. CpG DNA as a vaccine adjuvant. *Expert Rev Vaccines*. 2011;10(4):499-511. doi:10.1586/erv.10.174

[99] Krug A, Rothenfusser S, Hornung V, et al. Identification of CpG oligonucleotide sequences with high induction of IFN-α/β in plasmacytoid dendritic cells. *Eur J Immunol*. 2001;31(7):2154-2163. doi:10.1002/1521-4141(200107)31:7<2154::AID-IMMU2154>3.0.CO;2-U

[100] Marshall JD, Fearon K, Abbate C, et al. Identification of a novel CpG DNA class and motif that optimally stimulate B cell and plasmacytoid dendritic cell functions. *J Leukoc Biol*. 2003;73(6):781-792. doi:10.1189/jlb.1202630

[101] Samulowitz U, Weber M, Weeratna R, et al. A novel class of immune-stimulatory CpG oligodeoxynucleotides unifies high potency in type I interferon

induction with preferred structural properties. *Oligonucleotides*. 2010;20(2):93-101. doi:10.1089/oli.2009.0210

[102] Kayraklioglu N, Horuluoglu B, Klinman DM. CpG Oligonucleotides as Vaccine Adjuvants. *Methods Mol Biol Clifton NJ*. 2021;2197:51-85. doi:10.1007/978-1-0716-0872-2_4

[103] Bernasconi NL, Onai N, Lanzavecchia A. A role for Toll-like receptors in acquired immunity: up-regulation of TLR9 by BCR triggering in naive B cells and constitutive expression in memory B cells. *Blood*. 2003;101(11):4500-4504. doi:10.1182/blood-2002-11-3569

[104] Gursel M, Klinman DM. Use of CpG Oligonucleotides as Mucosal Adjuvants. In: *Mucosal Immunology*. Elsevier; 2015:1201-1209. doi:10.1016/B978-0-12-415847-4.00062-8

[105] Shirota H, Klinman DM. CpG Oligodeoxynucleotides as Adjuvants for Clinical Use. In: *Immunopotentiators in Modern Vaccines*. Elsevier; 2017:163-198. doi:10.1016/B978-0-12-804019-5.00009-8

[106] Lee Y, Lee YS, Cho SY, Kwon H-J. Chapter Four - Perspective of Peptide Vaccine Composed of Epitope Peptide, CpG-DNA, and Liposome Complex Without Carriers. In: Donev R, ed. *Advances in Protein Chemistry and Structural Biology*. Vol 99. Peptide and Protein Vaccines. Academic Press; 2015:75-97. doi:10.1016/bs.apcsb.2015.03.004

[107] Krammer F. SARS-CoV-2 vaccines in development. *Nature*. 2020;586(7830):516-527. doi:10.1038/s41586-020-2798-3

[108] Umscheid CA, Margolis DJ, Grossman CE. Key Concepts of Clinical Trials: A Narrative Review. *Postgrad Med*. 2011;123(5):194-204. doi:10.3810/pgm.2011.09.2475

[109] Learn About Clinical Studies - ClinicalTrials.gov. Accessed March 20, 2022. https://clinicaltrials.gov/ct2/about-studies/learn#WhatIs

[110] Types and Phases of Clinical Trials | What Are Clinical Trial Phases? Accessed March 19, 2022. https://www.cancer.org/treatment/treatments-and-side-effects/clinical-trials/what-you-need-to-know/phases-of-clinical-trials.html

[111] Goetz KB, Pfleiderer M, Schneider CK. First-in-human clinical trials with vaccines—what regulators want. *Nat Biotechnol*. 2010;28(9):910-916. doi:10.1038/nbt0910-910

[112] The Basics. National Institutes of Health (NIH). Published May 14, 2015. Accessed March 20, 2022. https://www.nih.gov/health-information/nih-clinical-research-trials-you/basics

[113] Han S. Clinical vaccine development. *Clin Exp Vaccine Res*. 2015;4(1):46-53. doi:10.7774/cevr.2015.4.1.46

[114] Vaccine Development, Testing, and Regulation | History of Vaccines. Accessed March 20, 2022. https://www.historyofvaccines.org/multilanguage/content/articles/vaccine-development-testing-and-regulation

[115] Guidelines on clinical evaluation of vaccines: regulatory expectations. Accessed March 20, 2022. https://www.who.int/publications/m/item/WHO-TRS-1004-web-annex-9

[116] Hudgens MG, Gilbert PB, Self SG. Endpoints in vaccine trials. *Stat Methods Med Res*. 2004;13(2):89-114. doi:10.1191/0962280204sm356ra

[117] Peng X-L, Cheng J-S-Y, Gong H-L, et al. Advances in the design and development of SARS-CoV-2 vaccines. *Mil Med Res*. 2021;8(1):67. doi:10.1186/s40779-021-00360-1

[118] İPekoğlu EM. MIDDLE EAST TECHNICAL UNIVERSITY. :147.

[119] Prates-Syed WA, Chaves LCS, Crema KP, et al. VLP-Based COVID-19 Vaccines: An Adaptable Technology against the Threat of New Variants. *Vaccines*. 2021;9(12):1409. doi:10.3390/vaccines9121409

[120] Le Bert N, Tan AT, Kunasegaran K, et al. SARS-CoV-2-specific T cell immunity in cases of COVID-19 and SARS, and uninfected controls. *Nature*. 2020;584(7821):457-462. doi:10.1038/s41586-020-2550-z

[121] Moss P. The T cell immune response against SARS-CoV-2. *Nat Immunol*. 2022;23(2):186-193. doi:10.1038/s41590-021-01122-w

[122] Huang C, Wang Y, Li X, et al. Clinical features of patients infected with 2019 novel coronavirus in Wuhan, China. *The Lancet*. 2020;395(10223):497-506. doi:10.1016/S0140-6736(20)30183-5

[123] WHO Coronavirus (COVID-19) Dashboard. Accessed June 1, 2022. https://covid19.who.int

[124] Heinz FX, Stiasny K. Distinguishing features of current COVID-19 vaccines: knowns and unknowns of antigen presentation and modes of action. *Npj Vaccines*. 2021;6(1):1-13. doi:10.1038/s41541-021-00369-6

[125] Francis AI, Ghany S, Gilkes T, Umakanthan S. Review of COVID-19 vaccine subtypes, efficacy and geographical distributions. *Postgrad Med J*. 2022;98(1159):389-394. doi:10.1136/postgradmedj-2021-140654

[126] Martínez-Flores D, Zepeda-Cervantes J, Cruz-Reséndiz A, Aguirre-Sampieri S, Sampieri A, Vaca L. SARS-CoV-2 Vaccines Based on the Spike Glycoprotein and

Implications of New Viral Variants. *Front Immunol*. 2021;12. Accessed June 1, 2022. https://www.frontiersin.org/article/10.3389/fimmu.2021.701501

[127] Wong NA, Saier MH. The SARS-Coronavirus Infection Cycle: A Survey of Viral Membrane Proteins, Their Functional Interactions and Pathogenesis. *Int J Mol Sci*. 2021;22(3):1308. doi:10.3390/ijms22031308

[128] Hsieh C-L, Goldsmith JA, Schaub JM, et al. Structure-based design of prefusion-stabilized SARS-CoV-2 spikes. *Science*. 2020;369(6510):1501-1505. doi:10.1126/science.abd0826

[129] Seephetdee C, Buasri N, Bhukhai K, et al. Mice Immunized with the Vaccine Candidate HexaPro Spike Produce Neutralizing Antibodies against SARS-CoV-2. *Vaccines*. 2021;9(5):498. doi:10.3390/vaccines9050498

[130] Aleem A, Akbar Samad AB, Slenker AK. Emerging Variants of SARS-CoV-2 And Novel Therapeutics Against Coronavirus (COVID-19). In: *StatPearls*. StatPearls Publishing; 2022. Accessed June 1, 2022. http://www.ncbi.nlm.nih.gov/books/NBK570580/

[131] Mohsen MO, Gomes AC, Vogel M, Bachmann MF. Interaction of Viral Capsid-Derived Virus-Like Particles (VLPs) with the Innate Immune System. *Vaccines*. 2018;6(3):37. doi:10.3390/vaccines6030037

[132] Zheng J, Deng Y, Zhao Z, et al. Characterization of SARS-CoV-2-specific humoral immunity and its potential applications and therapeutic prospects. *Cell Mol Immunol*. 2022;19(2):150-157. doi:10.1038/s41423-021-00774-w

[133] Oliveira-Silva J, Reis T, Lopes C, et al. Humoral response to the SARS-CoV-2 BNT162b2 mRNA vaccine: Real-world data from a large cohort of healthcare workers. *Vaccine*. 2022;40(4):650-655. doi:10.1016/j.vaccine.2021.12.014

[134] Hill V, Plessis LD, Peacock TP, et al. The origins and molecular evolution of SARS-CoV-2 lineage B.1.1.7 in the UK. Published online March 8, 2022:2022.03.08.481609. doi:10.1101/2022.03.08.481609

[135] Moreira ED, Kitchin N, Xu X, et al. Safety and Efficacy of a Third Dose of BNT162b2 Covid-19 Vaccine. *N Engl J Med*. 2022;386(20):1910-1921. doi:10.1056/NEJMoa2200674

[136] Ledford H. Do vaccines protect against long COVID? What the data say. *Nature*. 2021;599(7886):546-548. doi:10.1038/d41586-021-03495-2

[137] Andrews N, Stowe J, Kirsebom F, et al. Covid-19 Vaccine Effectiveness against the Omicron (B.1.1.529) Variant. *N Engl J Med*. 2022;386(16):1532-1546. doi:10.1056/NEJMoa2119451

[138] Shah ASV, Gribben C, Bishop J, et al. Effect of Vaccination on Transmission of SARS-CoV-2. *N Engl J Med*. 2021;385(18):1718-1720. doi:10.1056/NEJMc2106757

[139] Martonik D, Parfieniuk-Kowerda A, Rogalska M, Flisiak R. The Role of Th17 Response in COVID-19. *Cells*. 2021;10(6):1550. doi:10.3390/cells10061550

[140] Aleebrahim-Dehkordi E, Molavi B, Mokhtari M, et al. T helper type (Th1/Th2) responses to SARS-CoV-2 and influenza A (H1N1) virus: From cytokines produced to immune responses. *Transpl Immunol*. 2022;70:101495. doi:10.1016/j.trim.2021.101495

[141] Goyal K, Goel H, Baranwal P, et al. Immunological Mechanisms of Vaccine-Induced Protection against SARS-CoV-2 in Humans. *Immuno*. 2021;1(4):442-456. doi:10.3390/immuno1040032

[142] Wirsching S, Harder L, Heymanns M, et al. Long-Term, CD4+ Memory T Cell Response to SARS-CoV-2. *Front Immunol*. 2022;13. Accessed May 31, 2022. https://www.frontiersin.org/article/10.3389/fimmu.2022.800070

[143] Grifoni A, Weiskopf D, Ramirez SI, et al. Targets of T Cell Responses to SARS-CoV-2 Coronavirus in Humans with COVID-19 Disease and Unexposed Individuals. *Cell*. 2020;181(7):1489-1501.e15. doi:10.1016/j.cell.2020.05.015

[144] Pifferi C, Fuentes R, Fernández-Tejada A. Natural and synthetic carbohydrate-based vaccine adjuvants and their mechanisms of action. *Nat Rev Chem*. 2021;5(3):197-216. doi:10.1038/s41570-020-00244-3

[145] Shi S, Zhu H, Xia X, Liang Z, Ma X, Sun B. Vaccine adjuvants: Understanding the structure and mechanism of adjuvanticity. *Vaccine*. 2019;37(24):3167-3178. doi:10.1016/j.vaccine.2019.04.055

[146] Deimel LP, Li Z, Ranasinghe C. Interleukin-13 as a target to alleviate severe coronavirus disease 2019 and restore lung homeostasis. *J Clin Transl Res*. 2021;7(1):116-120.

[147] Tanaka T, Narazaki M, Kishimoto T. IL-6 in Inflammation, Immunity, and Disease. *Cold Spring Harb Perspect Biol*. 2014;6(10):a016295. doi:10.1101/cshperspect.a016295

[148] Diehl S, Anguita J, Hoffmeyer A, et al. Inhibition of Th1 Differentiation by IL-6 Is Mediated by SOCS1. *Immunity*. 2000;13(6):805-815. doi:10.1016/S1074-7613(00)00078-9

[149] Grunst MW, Uchil PD. Fc effector cross-reactivity: A hidden arsenal against SARS-CoV-2's evasive maneuvering. *Cell Rep Med*. 2022;3(2):100540. doi:10.1016/j.xcrm.2022.100540

APPENDICES

APPENDIX A

Additional Figures

	Day0	Day21	Day35	Day49	Day90
Total Area	509.3	388.5	2243	2162	1748

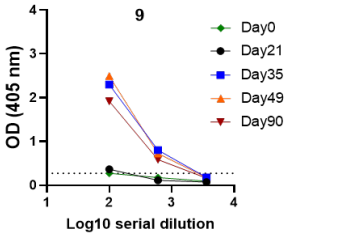

	Day0	Day21	Day35	Day49	Day90
Total Area	615.5	339.8	581.0	467.8	790.3

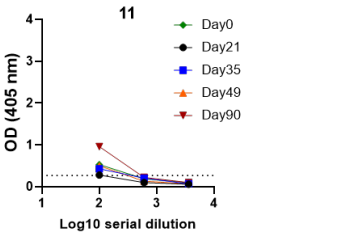

	Day0	Day21	Day35	Day 49	Day90
Total Area	348.0	727.3	2332	4409	10768

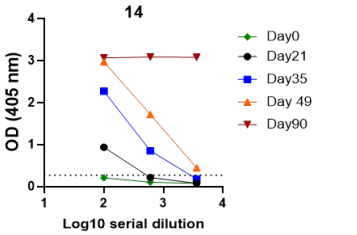

	Day0	Day21	Day35	Day49	Day90
Total Area	657.3	399.8	3288	4278	3403

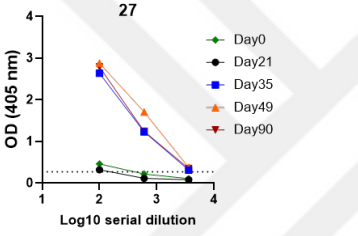

	Day0	Day21	Day35	Day49	Day90
Total Area	419.0	328.0	751.5	753.5	10402

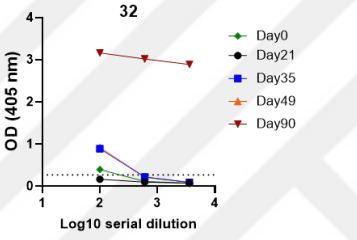

	Day0	Day21	Day35	Day49	Day90
Total Area	448.8	349.5	1190	1428	1260

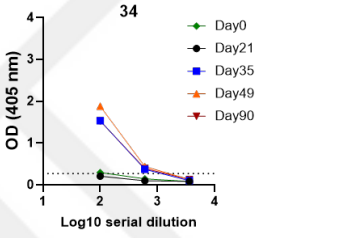

	Day0	Day21	Day35	Day49	Day90
Total Area	371.8	298.3	421.5	465.8	492.3

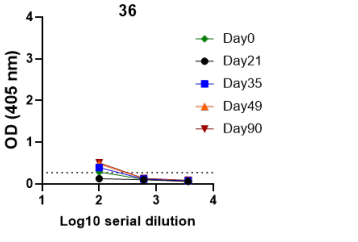

	Day0	Day21	Day35	Day49	Day90
Total Area	661.0	306.0	328.3	505.4	474.3

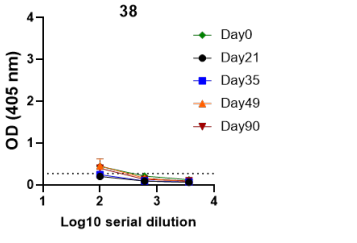

	Day0	Day21	Day35	Day49	Day90
Total Area	361.5	283.5	591.0	782.0	678.8

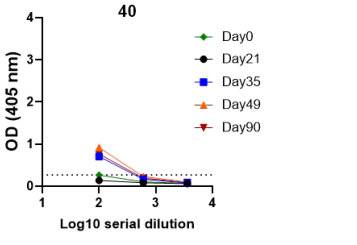

,

	Day0	Day21	Day35	Day49	Day90
Total Area	939.5	524.3	1571	1842	965.0

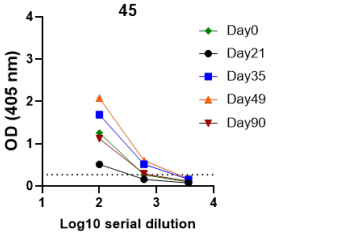

	Day0	Day21	Day35	Day49	Day90
Total Area	536.8	355.5	676.8	770.5	732.0

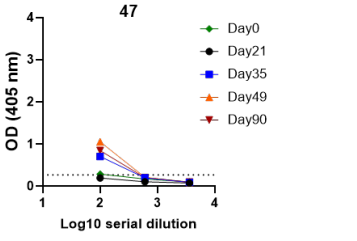

	Day0	Day21	Day35	Day49	Day90
Total Area	552.3	578.5	2509	4240	1595

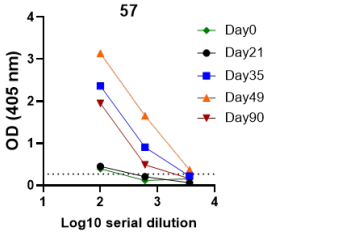

	Day0	Day21	Day35	Day49	Day90
Total Area	1303	933.5	1065	1960	1723

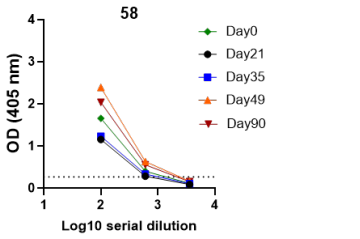

	Day0	Day21	Day35	Day49	Day90
Total Area	344.0	277.5	1134	2076	870.5

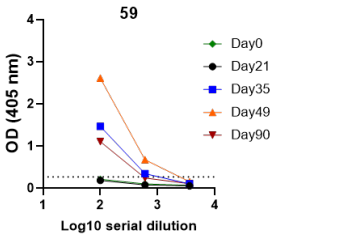

	Day0	Day21	Day35	Day49	Day90
Total Area	393.0	358.8	4692	5046	1768

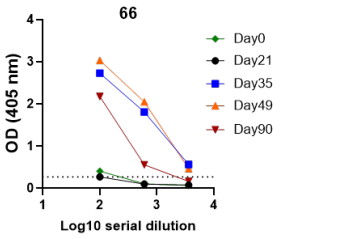

	Day0	Day21	Day35	Day49	Day90
Total Area	489.8	601.5	4832	5830	6011

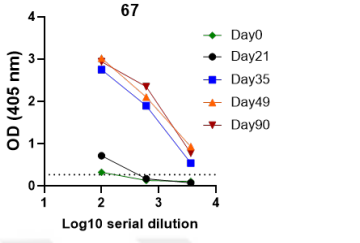

	Day0	Day21	Day35	Day49
Total Area	379.3	299.8	404.3	558.5

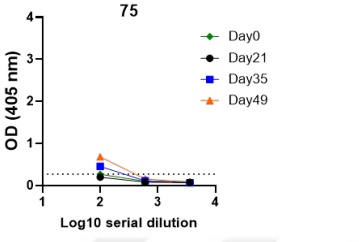

	Day0	Day21	Day35	Day49	Day90
Total Area	478.5	397.3	1284	1515	1252

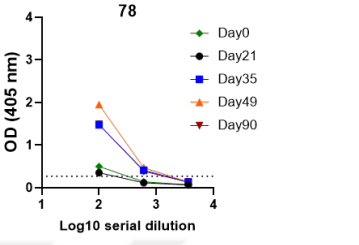

	Day0	Day21	Day35	Day49	Day90
Total Area	351.5	241.5	285.5	372.5	465.8

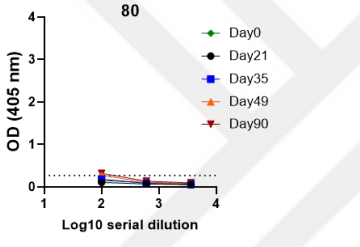

	Day0	Day21	Day35	Day49	Day90
Total Area	424.0	330.3	4379	6382	3632

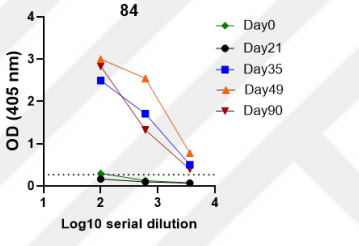

	Day0	Day21	Day35
Total Area	346.5	429.0	1694

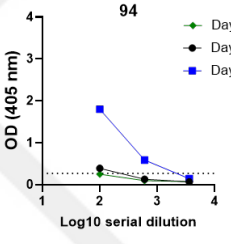

	Day0	Day21	Day35	Day49	Day90
Total Area	257.3	239.3	233.3	300.0	368.5

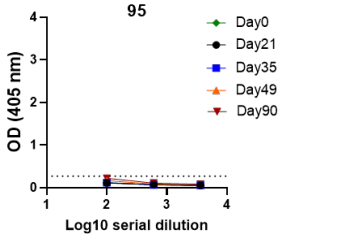

	Day0	Day21	Day35	Day49	Day90
Total Area	589.0	525.0	3761	4952	3290

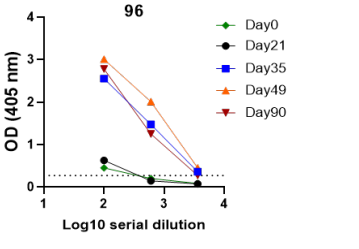

	Day0	Day21	Day35	Day49	Day90
Total Area	688.3	1433	2059	2675	2735

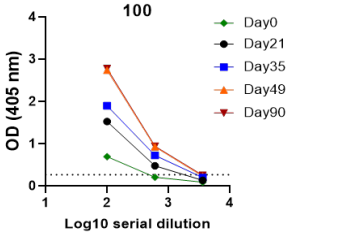

	Day0	Day21	Day35	Day49	Day90
Total Area	370.0	290.5	1094	1191	1270

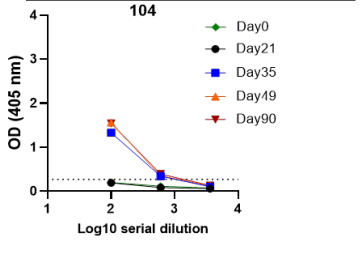

	Day0	Day21	Day35	Day49	Day90
Total Area	473.3	285.5	642.3	623.3	1426

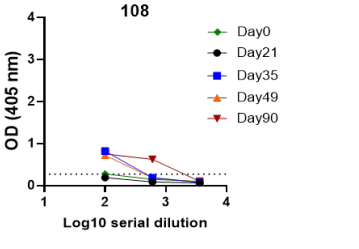

	Day0	Day21	Day35	Day49	Day90
Total Area	448.0	307.5	813.3	882.0	1003

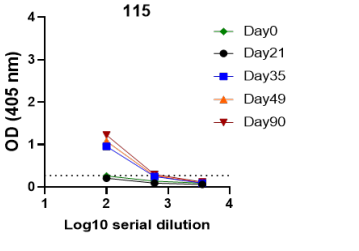

	Day0	Day21	Day35	Day49	Day90
Total Area	415.3	282.5	765.3	958.5	886.0

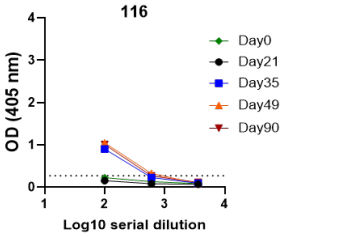

	Day0	Day21	Day35	Day49	Day90
Total Area	404.5	283.8	342.5	342.0	539.3

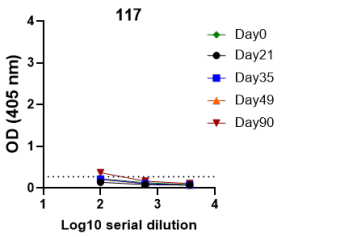

	Day0	Day21	Day35	Day49	Day90
Total Area	377.8	386.3	1427	2272	3076

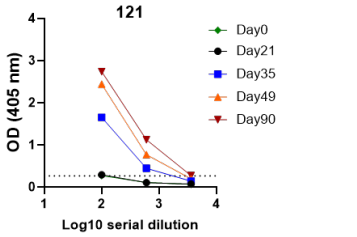

	Day0	Day21	Day35	Day49	Day90
Total Area	283.8	245.0	428.5	548.8	518.3

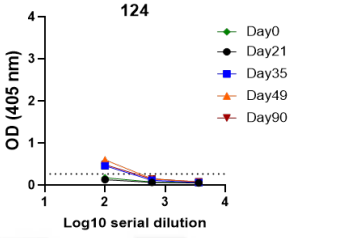

	Day0	Day21	Day35	Day49	Day90
Total Area	1011	353.3	525.0	932.5	1066

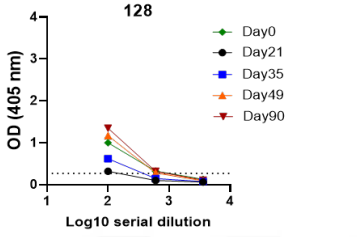

	Day0	Day21	Day35	Day49	Day90
Total Area	338.0	239.0	1534	3391	10838

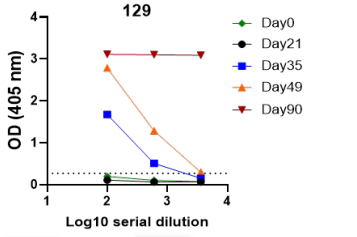

	Day0	Day21	Day35	Day49	Day90
Total Area	332.8	250.0	605.8	630.5	10797

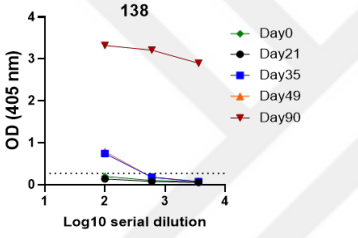

	Day0	Day21	Day35	Day49	Day90
Total Area	681.8	472.3	2211	4400	6001

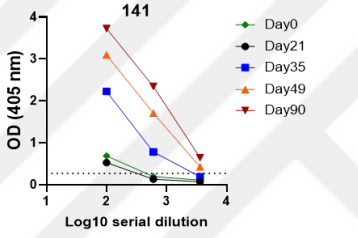

	Day0	Day21	Day35	Day49	Day90
Total Area	339.0	426.8	6583	10295	10258

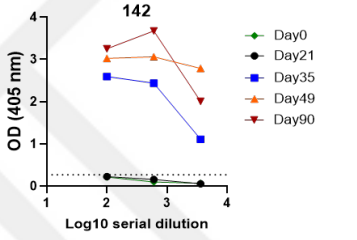

	Day0	Day21	Day35	Day49	Day90
Total Area	387.8	487.8	1017	893.5	10217

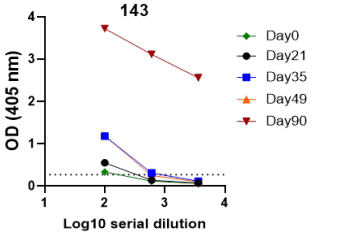

	Day0	Day21	Day35	Day49	Day90
Total Area	519.0	348.8	1118	2981	3461

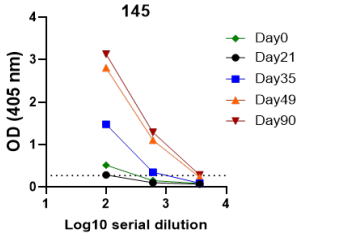

	Day0	Day21	Day35	Day49	Day90
Total Area	850.3	778.8	1883	1966	1361

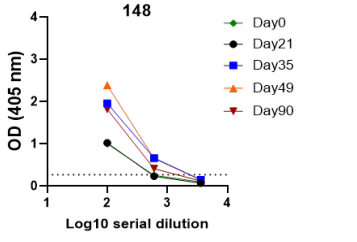

	Day0	Day21	Day35	Day49
Total Area	425.0	446.8	2712	5812

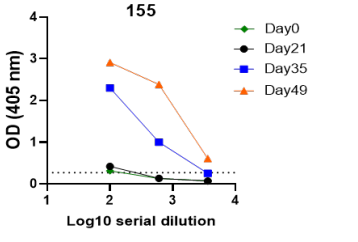

	Day0	Day21	Day35	Day49	Day90
Total Area	332.0	295.0	1169	1117	773.0

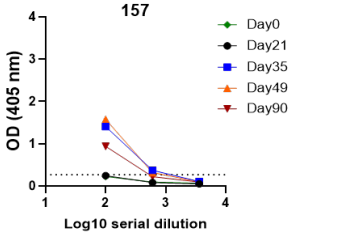

	Day0	Day21	Day35	Day49	Day90
Total Area	379.8	321.5	915.0	1237	1056

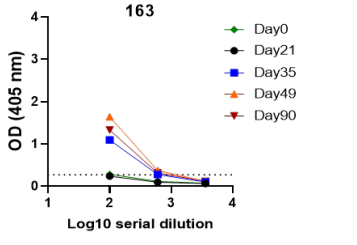

	Day0	Day21	Day35	Day49
Total Area	326.3	281.0	730.3	678.3

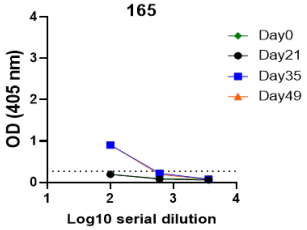

	Day0	Day21	Day35	Day49	Day90
Total Area	268.3	227.5	1614	1842	1148

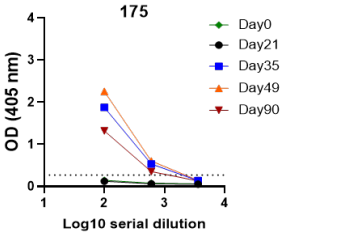

	Day0	Day21	Day35	Day49	Day90
Total Area	294.0	409.8	857.3	1377	597.3

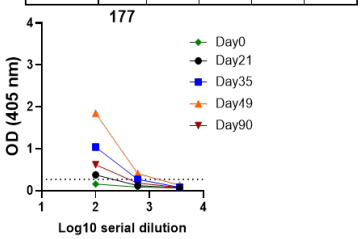

	Day0	Day21	Day35	Day49	Day90
Total Area	344.3	319.3	844.0	1041	1088

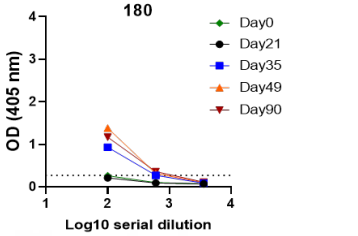

	Day0	Day21	Day35	Day49	Day90
Total Area	335.8	295.8	329.5	678.5	433.8

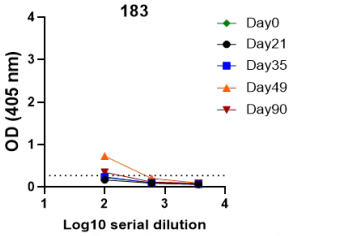

	Day0	Day21	Day35	Day49	Day90
Total Area	460.0	578.0	2435	4018	10598

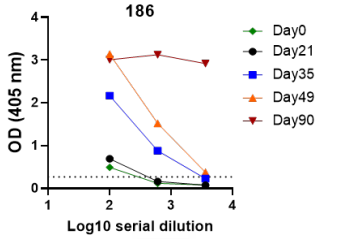

	Day0	Day21	Day35	Day49	Day90
Total Area	337.5	453.5	478.3	444.5	608.8

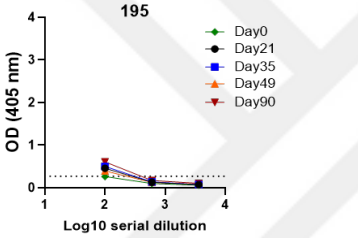

	Day0	Day21	Day35	Day49	Day90
Total Area	307.8	290.0	618.3	1243	1068

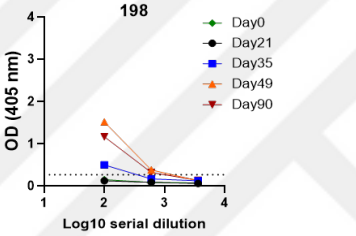

	Day0	Day21	Day35	Day49	Day90
Total Area	762.5	787.8	1598	3301	3457

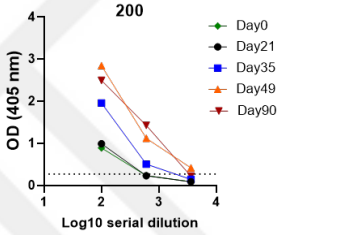

	Day0	Day21	Day35	Day49
Total Area	406.8	860.8	2363	3758

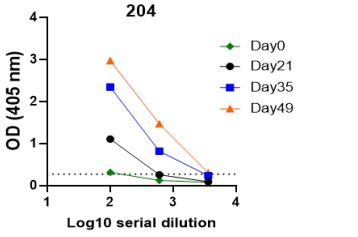

	Day0	Day21	Day35	Day49	Day90
Total Area	296.3	312.5	2460	3644	2670

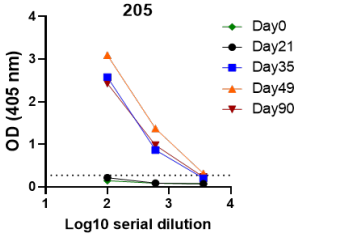

	Day0	Day21	Day35	Day49	Day90
Total Area	352.8	393.8	694.0	1134	831.3

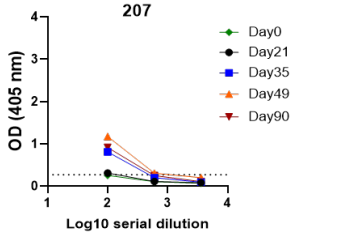

	Day0	Day21	Day35	Day49	Day90
Total Area	297.5	343.8	567.0	1279	968.0

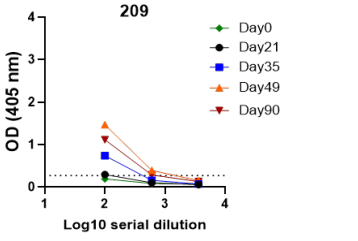

	Day0	Day21	Day35	Day49	Day90
Total Area	1192	362.8	2582	4501	2418

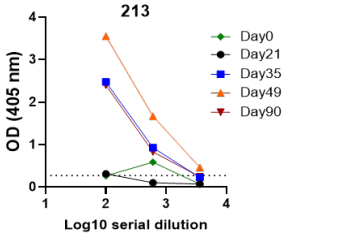

	Day0	Day21	Day35	Day49	Day90
Total Area	381.5	1463	3476	5690	4961

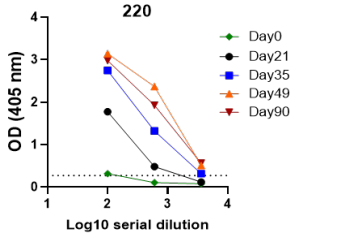

	Day0	Day21	Day35	Day49	Day90
Total Area	675.8	895.8	1630	4382	2527

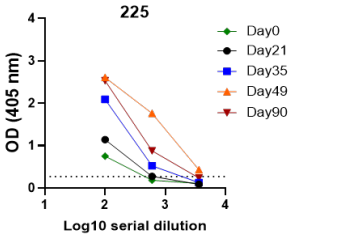

	Day0	Day21	Day35	Day49	Day90
Total Area	293.8	417.0	4155	5183	2669

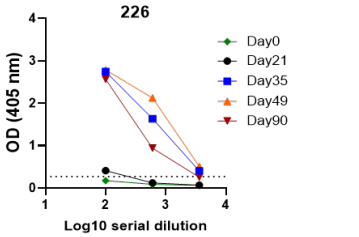

	Day0	Day21	Day35	Day49	Day90
Total Area	396.0	382.0	708.3	889.0	10706

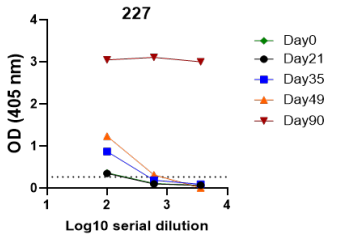

	Day0	Day21	Day35	Day49	Day90
Total Area	377.5	1541	3287	4740	6244

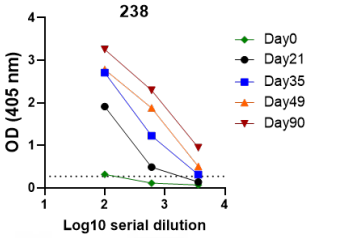

	Day0	Day21	Day35	Day49	Day90
Total Area	582.3	945.8	4018	6421	3375

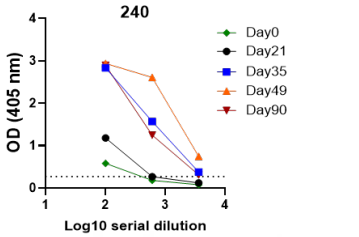

	Day0	Day21	Day35	Day49	Day90
Total Area	347.8	420.0	968.0	1645	1529

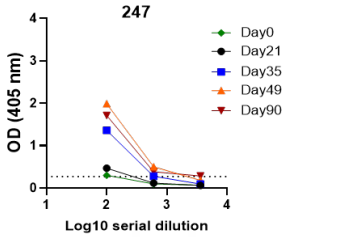

	Day0	Day21	Day35	Day49	Day90
Total Area	287.8	268.5	1706	2639	1003

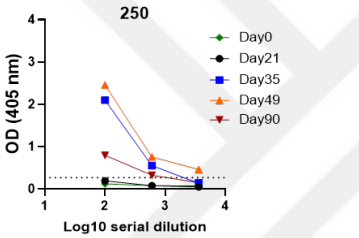

	Day0	Day21	Day35	Day49	Day90
Total Area	325.5	297.5	514.3	1543	1670

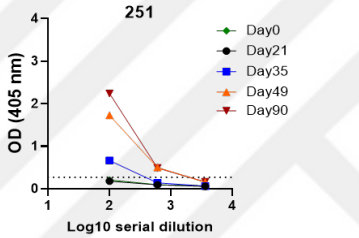

	Day0	Day21	Day35	Day49	Day90
Total Area	314.5	424.0	1208	2005	1456

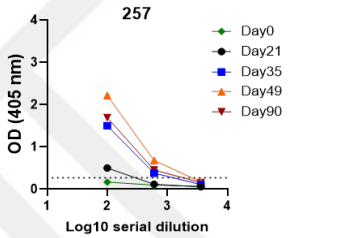

	Day0	Day21	Day35	Day49	Day90
Total Area	352.5	383.5	2712	2995	1067

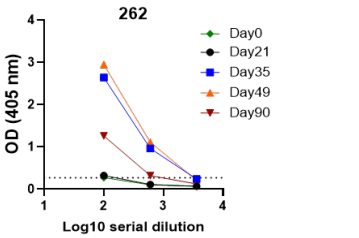

	Day0	Day21	Day35	Day49	Day90
Total Area	280.8	266.3	541.5	1156	1301

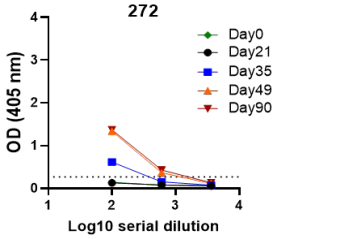

	Day0	Day21	Day35	Day49	Day90
Total Area	286.5	290.0	678.8	926.5	11232

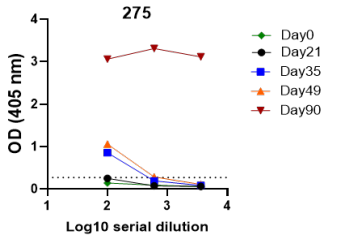

	Day0	Day21	Day35	Day49	Day90
Total Area	554.0	649.0	664.8	1123	1541

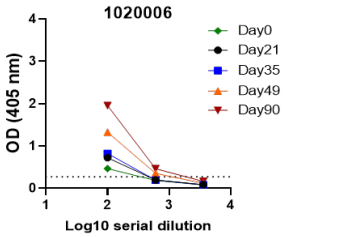

	Day0	Day21	Day35	Day49	Day90
Total Area	328.8	339.0	2045	2456	1410

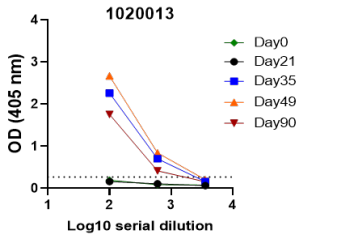

	Day0	Day21	Day35	Day49	Day90
Total Area	338.3	433.0	516.0	752.8	488.3

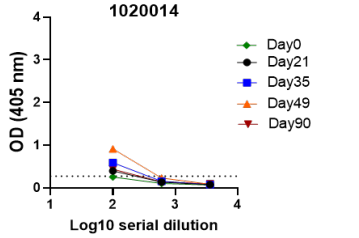

	Day0	Day21	Day35	Day49	Day90
Total Area	1379	1887	3423	8001	7656

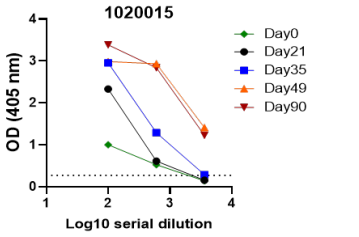

	Day0	Day21	Day35	Day49	Day90
Total Area	284.3	268.8	554.0	1097	758.5

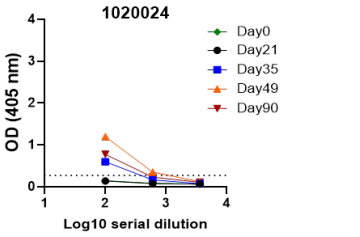

	Day0	Day21	Day35	Day49	Day90
Total Area	1012	650.8	826.3	2206	1751

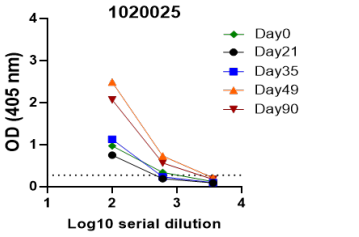

	Day0	Day21	Day35	Day49	Day90
Total Area	471.3	341.0	1327	1662	982.0

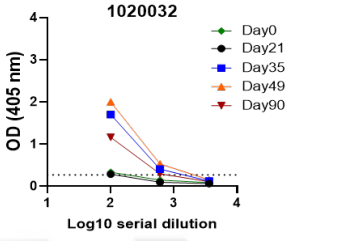

	Day0	Day21	Day35	Day49	Day90
Total Area	347.8	369.5	1294	1315	759.5

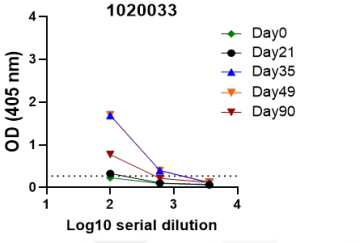

	Day0	Day21	Day35	Day49	Day90
Total Area	372.0	355.0	1162	1743	1383

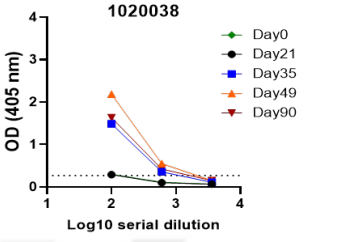

	Day0	Day21	Day35	Day49
Total Area	336.0	293.3	1923	3353

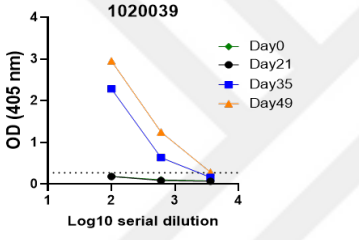

	Day0	Day21	Day35	Day49	Day90
Total Area	367.5	365.5	549.8	1564	10443

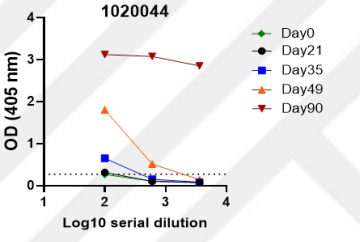

	Day0	Day21	Day35	Day49	Day90
Total Area	413.3	439.8	1367	2320	1667

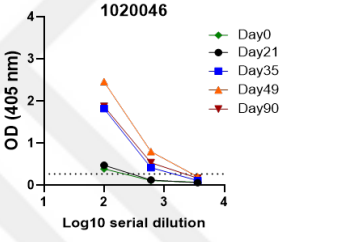

	Day0	Day21	Day35	Day49	Day90
Total Area	316.5	366.5	658.5	3066	1631

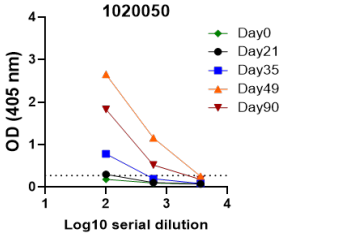

	Day0	Day21	Day35	Day49
Total Area	438.5	353.3	359.8	676.3

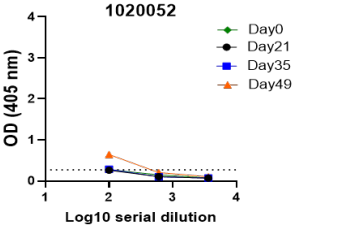

	Day0	Day21	Day35	Day49	Day90
Total Area	436.8	470.5	530.8	2256	2741

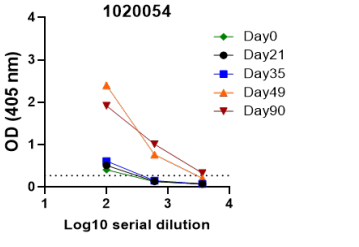

	Day0	Day21	Day35	Day49	Day90
Total Area	869.3	325.5	1221	1863	2200

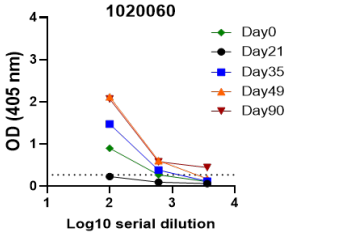

	Day0	Day21	Day35	Day49
Total Area	292.5	299.5	535.3	1275

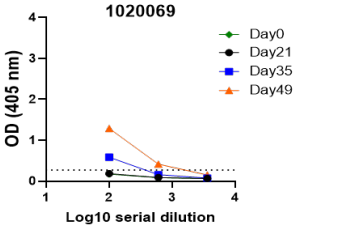

	Day0	Day21	Day35	Day49	Day90
Total Area	757.8	3109	4814	6223	2770

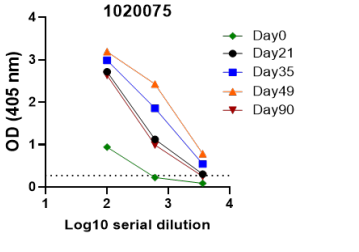

	Day0	Day21	Day35	Day49	Day90
Total Area	525.0	449.5	7515	10139	6274

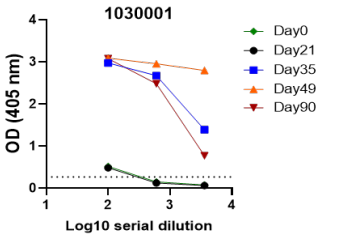

	Day0	Day21	Day35	Day49	Day90
Total Area	264.5	256.0	647.3	1206	525.5

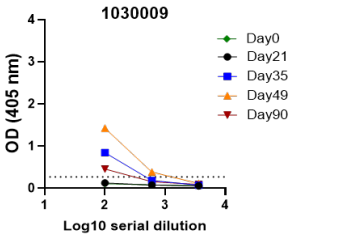

	Day0	Day21	Day35	Day49	Day90
Total Area	305.8	423.0	1182	2095	715.3

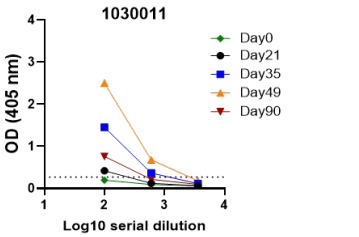

	Day0	Day21	Day35	Day49	Day90
Total Area	268.8	465.5	6583	7331	1788

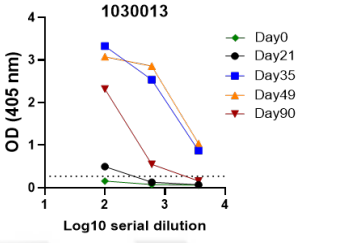

	Day0	Day21	Day35	Day49	Day90
Total Area	282.3	418.8	824.3	1793	633.8

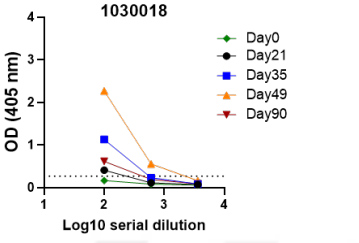

	Day0	Day21	Day35	Day49	Day90
Total Area	338.8	336.0	964.3	3229	875.3

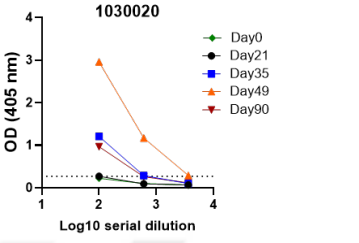

	Day0	Day21	Day35	Day49	Day90
Total Area	312.8	479.5	1294	2964	1088

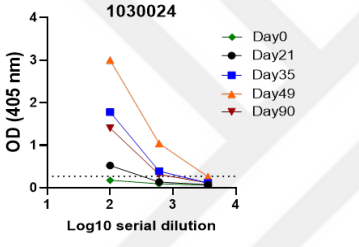

	Day0	Day21	Day35	Day49	Day90
Total Area	271.8	252.3	288.8	9815	6954

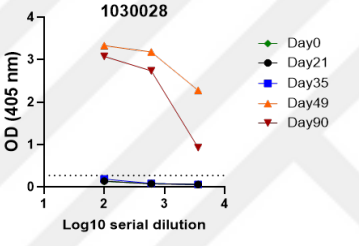

	Day0	Day21	Day35	Day49	Day90
Total Area	318.0	343.8	1914	3729	2040

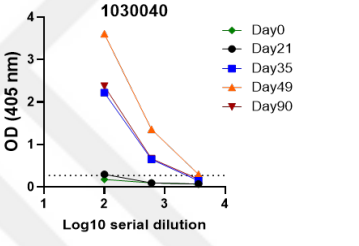

	Day0	Day21	Day35	Day49	Day90
Total Area	305.8	726.8	3431	1151	2567

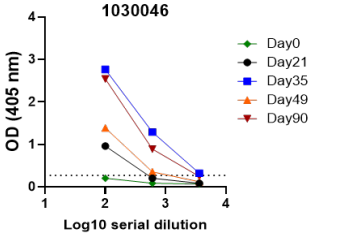

	Day0	Day21	Day35	Day49	Day90
Total Area	307.3	395.0	1216	3127	1359

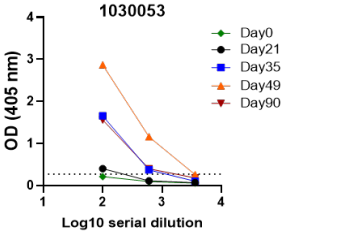

	Day0	Day21	Day35	Day49	Day90
Total Area	301.8	320.8	1534	3099	10007

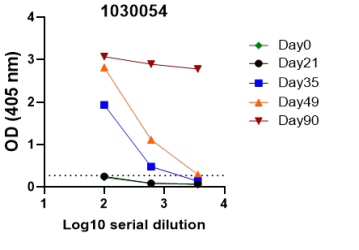

	Day0	Day21	Day35	Day49
Total Area	1506	3808	4256	6529

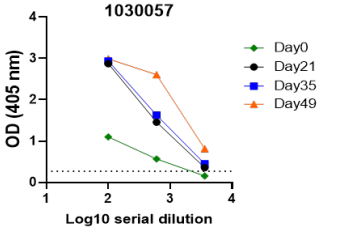

	Day0	Day21	Day35	Day49	Day90
Total Area	590.8	5924	7315	8413	4231

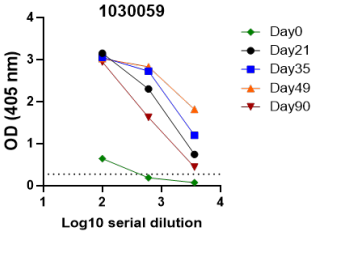

	Day0	Day21	Day35	Day49
Total Area	317.3	559.8	1203	2335

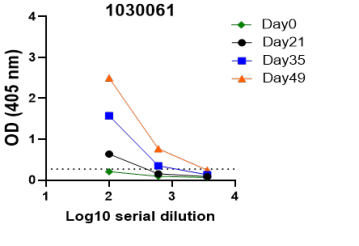

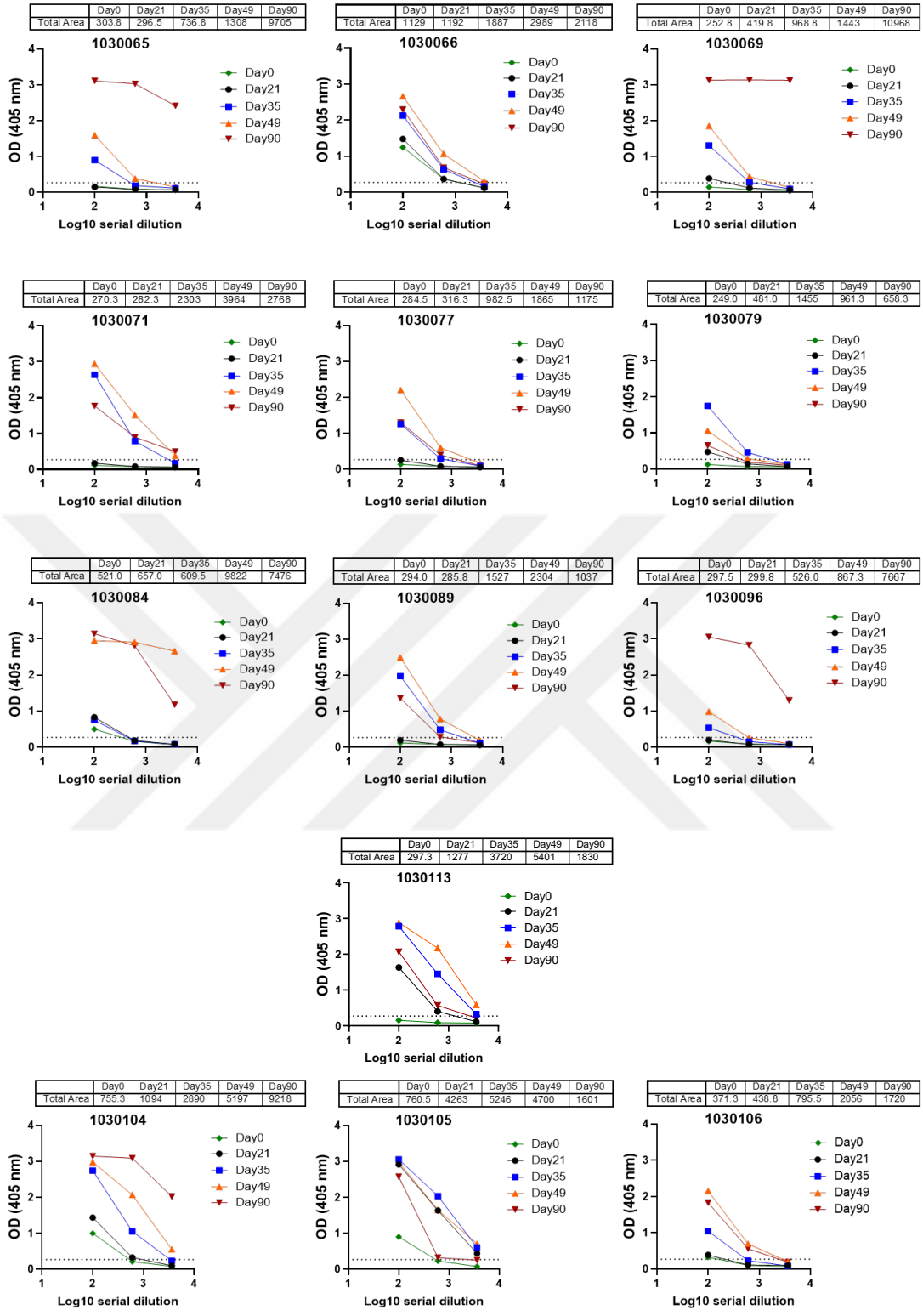

Figure A1. Anti-Spike IgG Titer demonstrations of Phase II clinical trial volunteers. Serum samples taken from volunteers were diluted 1:100, 1:600 and 1:3600-fold. Area under the curve calculations were used to determine titers of OD405 versus log10 reciprocal serial dilutions graphs.

	Day0	Day21	Day35	Day49	Day90
Total Area	749.8	487.3	3295	2502	2084

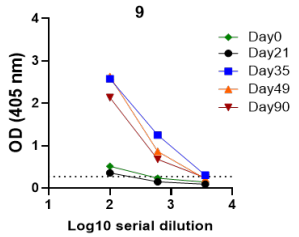

	Day0	Day21	Day35	Day49	Day90
Total Area	726.8	417.8	443.0	442.3	667.8

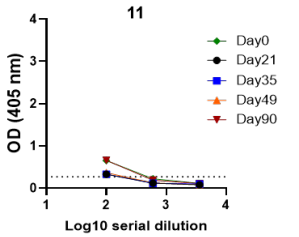

	Day0	Day21	Day35	Day49	Day90
Total Area	486.3	385.0	1561	1733	10682

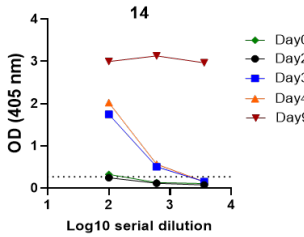

	Day0	Day21	Day35	Day49	Day90
Total Area	613.0	341.8	1291	1259	812.5

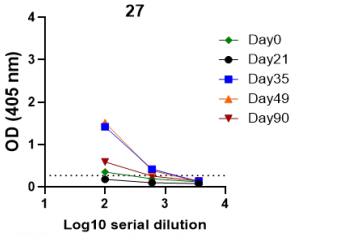

	Day0	Day21	Day35	Day49	Day90
Total Area	428.8	357.8	1526	1016	7386

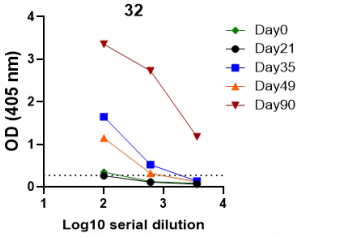

	Day0	Day21	Day35	Day49	Day90
Total Area	778.3	503.5	993.5	1025	1063

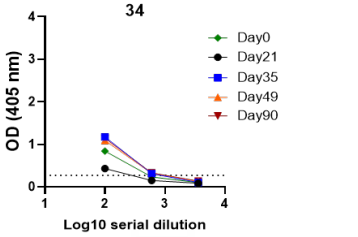

	Day0	Day21	Day35	Day49	Day90
Total Area	439.0	322.0	1984	1250	1042

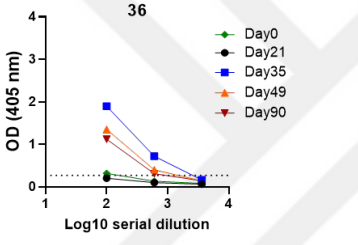

	Day0	Day21	Day35	Day49	Day90
Total Area	753.3	349.3	317.3	452.5	498.5

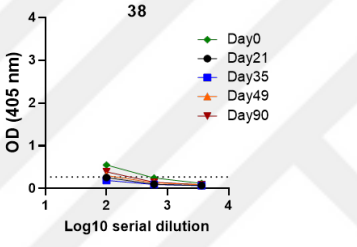

	Day0	Day21	Day35	Day49	Day90
Total Area	869.8	456.8	1423	1049	711.8

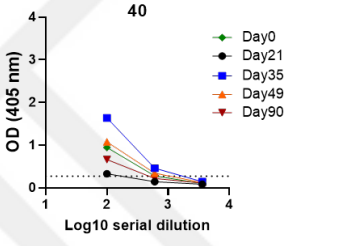

	Day0	Day21	Day35	Day49	Day90
Total Area	451.8	454.3	1675	1069	814.5

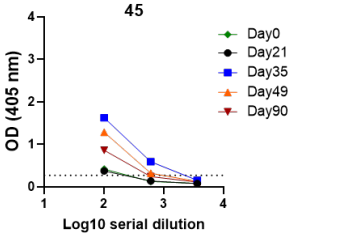

	Day0	Day21	Day35	Day49	Day90
Total Area	494.8	385.5	412.5	414.8	564.5

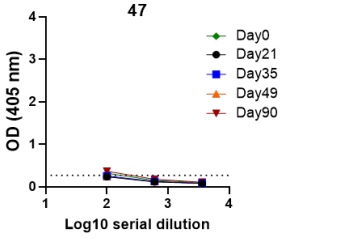

	Day0	Day21	Day35	Day49	Day90
Total Area	417.8	327.3	1420	1393	643.3

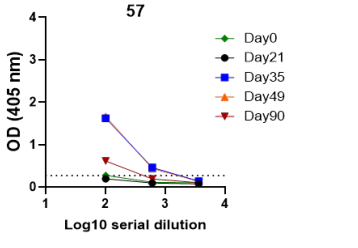

	Day0	Day21	Day35	Day49	Day90
Total Area	363.8	343.0	550.5	489.3	525.8

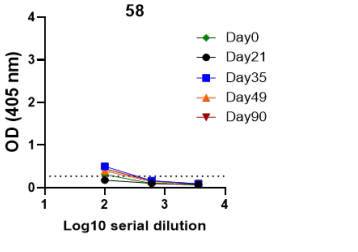

	Day0	Day21	Day35	Day49	Day90
Total Area	1102	891.5	1389	2734	1732

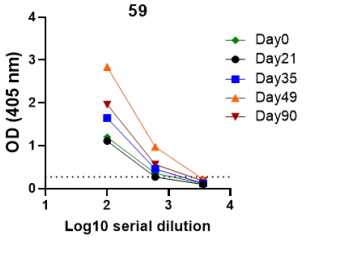

	Day0	Day21	Day35	Day49	Day90
Total Area	975.0	665.5	2198	2318	2470

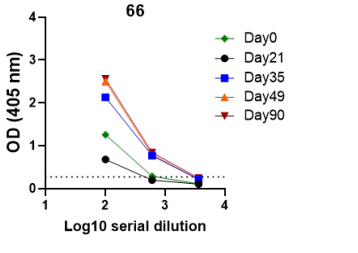

	Day0	Day21	Day35	Day49	Day90
Total Area	445.8	339.5	326.8	413.3	481.3

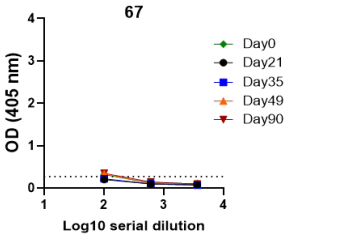

	Day0	Day21	Day35	Day49	Day90
Total Area	479.8	345.5	318.8	427.5	415.0

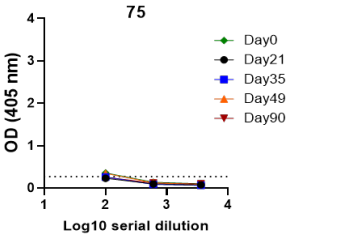

	Day0	Day21	Day35	Day49	Day90
Total Area	365.3	283.8	298.5	414.5	419.8

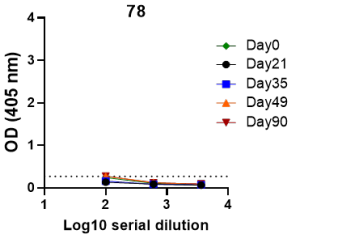

	Day0	Day21	Day35	Day49	Day90
Total Area	453.8	307.0	378.3	453.8	599.3

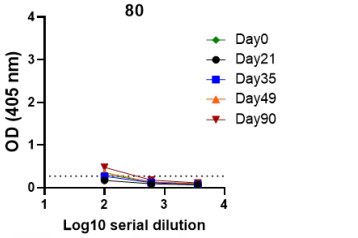

	Day0	Day21	Day35	Day49	Day90
Total Area	614.5	398.8	6257	8056	4532

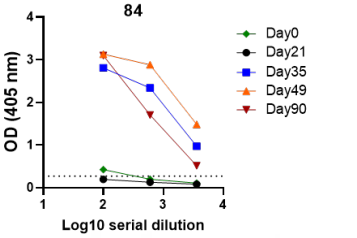

	Day0	Day21	Day35
Total Area	365.5	345.0	1811

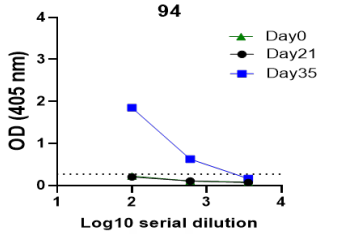

	Day0	Day21	Day35	Day49	Day90
Total Area	308.0	258.3	259.5	341.8	407.5

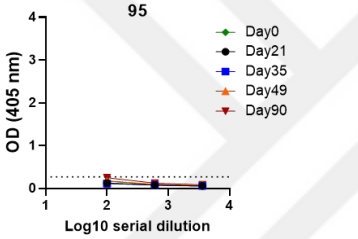

	Day0	Day21	Day35	Day49	Day90
Total Area	443.3	326.8	1332	874.5	540.0

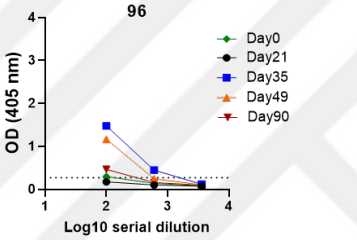

	Day0	Day21	Day35	Day49	Day90
Total Area	525.5	1062	2178	2928	2704

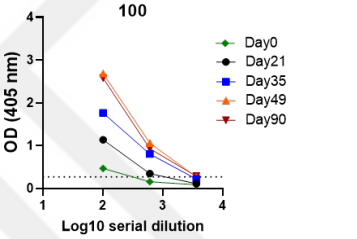

	Day0	Day21	Day35	Day49	Day90
Total Area	523.0	337.8	497.0	548.0	772.3

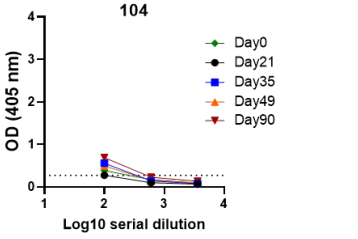

	Day0	Day21	Day35	Day49	Day90
Total Area	806.3	389.8	400.3	532.0	727.8

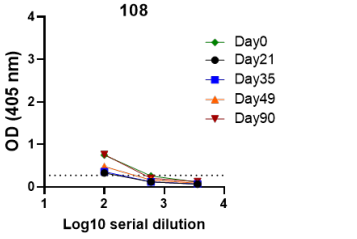

	Day0	Day21	Day35	Day49	Day90
Total Area	618.3	333.5	514.5	668.5	993.3

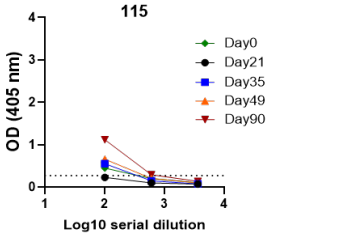

	Day0	Day21	Day35	Day49	Day90
Total Area	524.0	311.0	572.5	1097	738.0

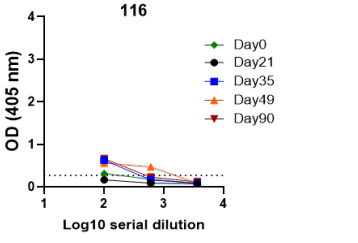

	Day0	Day21	Day35	Day49	Day90
Total Area	444.8	266.8	303.8	377.3	569.5

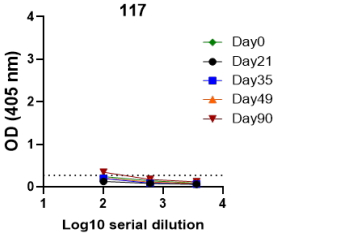

	Day0	Day21	Day35	Day49	Day90
Total Area	422.0	356.3	351.8	540.3	738.5

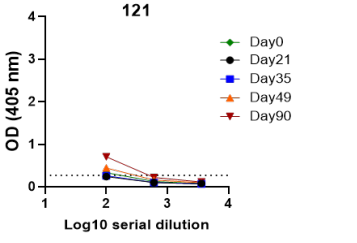

	Day0	Day21	Day35	Day49	Day90
Total Area	294.5	255.3	243.3	321.5	467.0

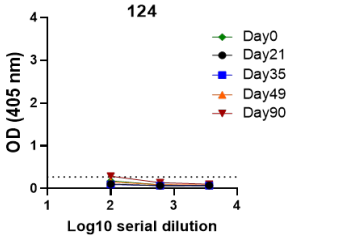

	Day0	Day21	Day35	Day49	Day90
Total Area	378.5	266.3	277.8	384.0	447.3

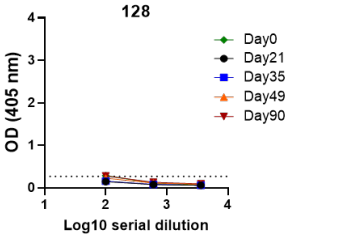

	Day0	Day21	Day35	Day49	Day90
Total Area	441.0	298.8	591.0	748.3	8918

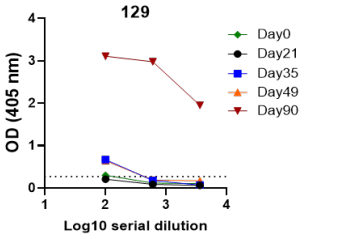

	Day0	Day21	Day35	Day49	Day90
Total Area	652.5	443.0	432.0	506.5	8386

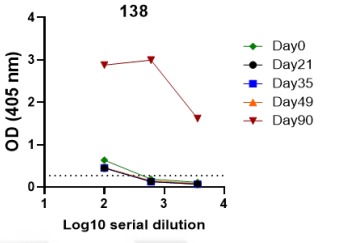

	Day0	Day21	Day35	Day49	Day90
Total Area	473.0	357.0	473.0	936.0	842.8

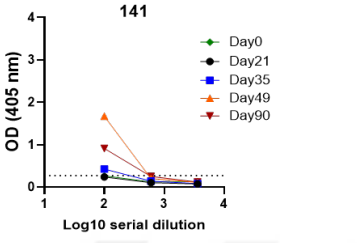

	Day0	Day21	Day35	Day49	Day90
Total Area	487.8	494.5	3139	7826	6754

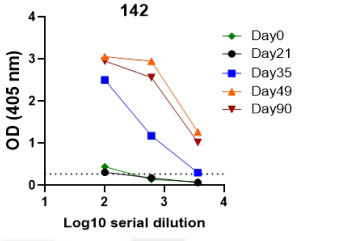

	Day0	Day21	Day35	Day49	Day90
Total Area	289.3	254.3	762.3	626.8	4592

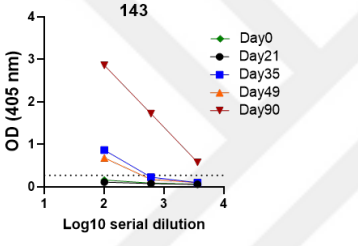

	Day0	Day21	Day35	Day49	Day90
Total Area	551.3	401.5	580.5	644.8	720.8

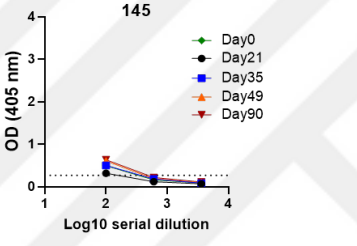

	Day0	Day21	Day35	Day49	Day90
Total Area	743.8	550.3	1108	1336	1125

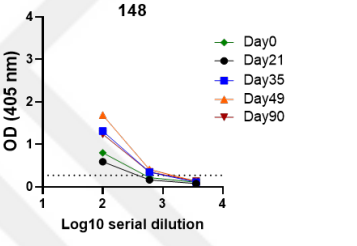

	Day0	Day21	Day35	Day49
Total Area	411.3	343.0	336.0	395.0

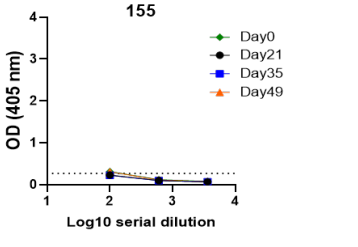

	Day0	Day21	Day35	Day49	Day90
Total Area	381.0	267.5	757.8	450.8	420.3

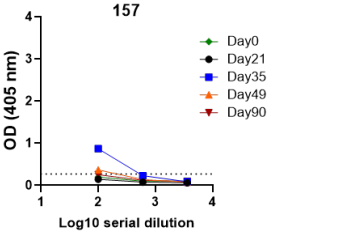

	Day0	Day21	Day35	Day49	Day90
Total Area	351.0	317.0	396.8	472.0	454.5

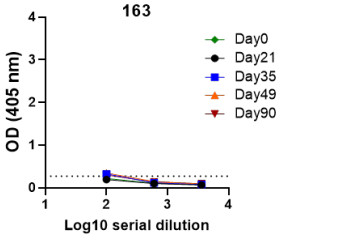

	Day0	Day21	Day35	Day49
Total Area	658.3	373.8	1244	814.8

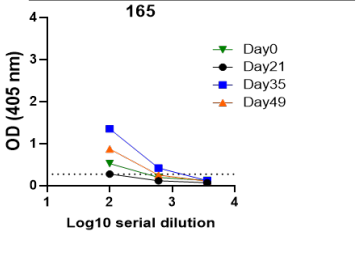

	Day0	Day21	Day35	Day49	Day90
Total Area	336.0	218.8	363.3	407.0	364.8

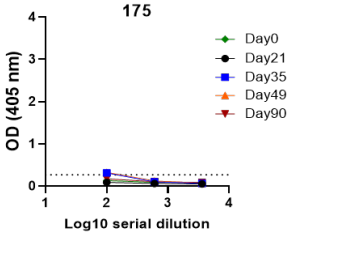

	Day0	Day21	Day35	Day49	Day90
Total Area	393.8	359.8	935.5	2186	1271

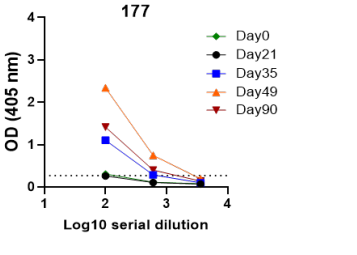

	Day0	Day21	Day35	Day49	Day90
Total Area	401.5	332.8	331.8	442.5	383.3

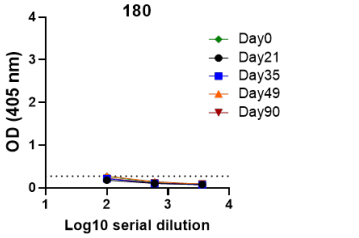

	Day0	Day21	Day35	Day49	Day90
Total Area	607.0	388.5	1747	3556	1125

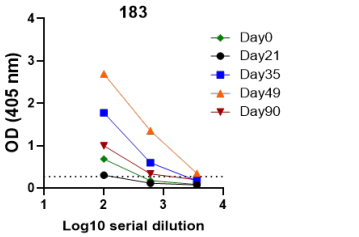

	Day0	Day21	Day35	Day49	Day90
Total Area	535.5	637.0	1141	1003	7932

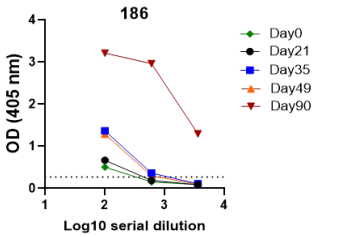

	Day0	Day21	Day35	Day49	Day90
Total Area	316.0	276.3	265.5	273.3	450.3

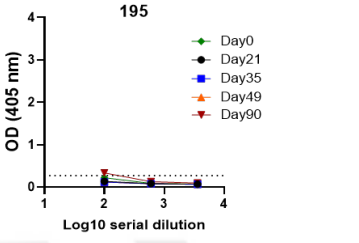

	Day0	Day21	Day35	Day49	Day90
Total Area	817.5	416.3	328.3	675.5	965.5

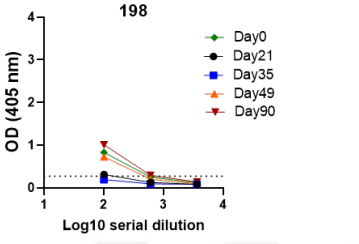

	Day0	Day21	Day35	Day49	Day90
Total Area	389.5	292.0	561.3	666.3	579.8

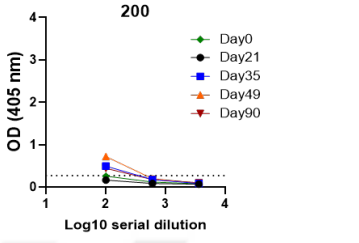

	Day0	Day21	Day35	Day49
Total Area	459.3	313.3	1043	1363

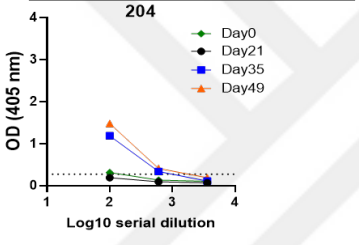

	Day0	Day21	Day35	Day49	Day90
Total Area	450.0	263.3	647.5	1130	1201

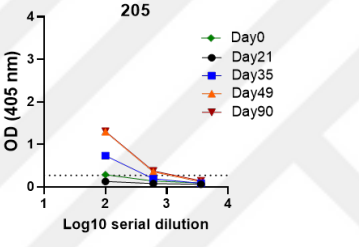

	Day0	Day21	Day35	Day49	Day90
Total Area	429.3	296.3	350.8	526.3	633.0

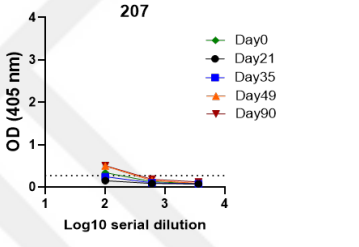

	Day0	Day21	Day35	Day49	Day90
Total Area	989.0	593.0	604.0	831.3	987.5

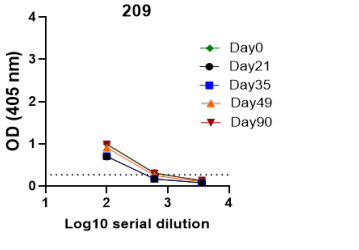

	Day0	Day21	Day35	Day49	Day90
Total Area	838.3	434.0	800.0	1219	1381

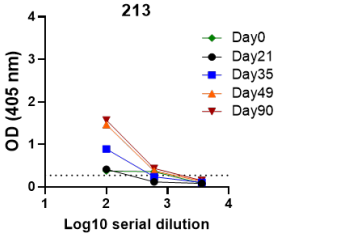

	Day0	Day21	Day35	Day49	Day90
Total Area	583.8	658.3	1252	1748	1511

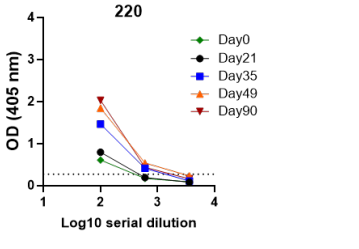

	Day0	Day21	Day35	Day49	Day90
Total Area	396.3	343.0	643.0	393.5	526.3

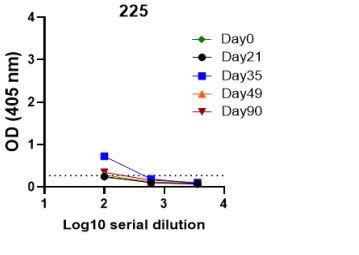

	Day0	Day21	Day35	Day49	Day90
Total Area	453.0	581.0	1028	1596	635.3

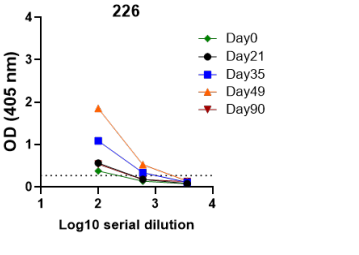

	Day0	Day21	Day35	Day49	Day90
Total Area	2099	1636	1658	1734	11248

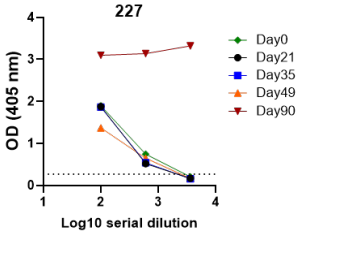

	Day0	Day21	Day35	Day49	Day90
Total Area	1077	637.5	3841	4215	3076

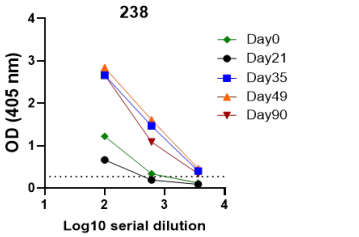

	Day0	Day21	Day35	Day49	Day90
Total Area	511.0	309.0	2392	3601	1387

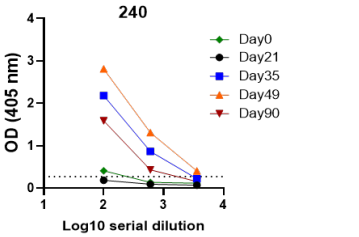

	Day0	Day21	Day35	Day49	Day90
Total Area	316.5	321.0	419.3	534.5	861.3

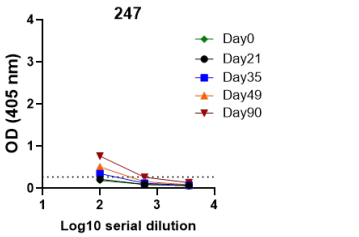

	Day0	Day21	Day35	Day49	Day90
Total Area	547.8	577.8	1769	2170	1272

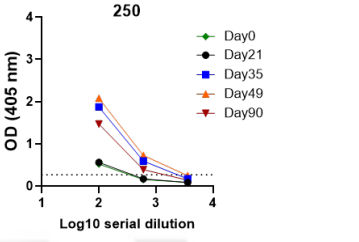

	Day0	Day21	Day35	Day49	Day90
Total Area	360.5	340.5	575.3	709.8	445.3

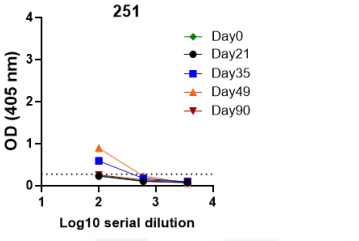

	Day0	Day21	Day35	Day49	Day90
Total Area	493.8	306.8	343.0	497.0	622.3

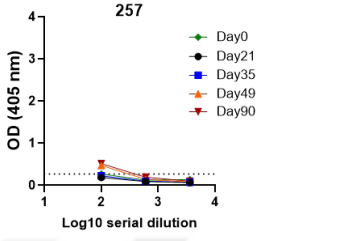

	Day0	Day21	Day35	Day49	Day90
Total Area	538.8	344.5	369.0	731.8	548.8

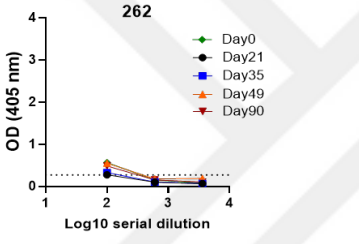

	Day0	Day21	Day35	Day49	Day90
Total Area	419.0	282.5	389.0	754.0	457.5

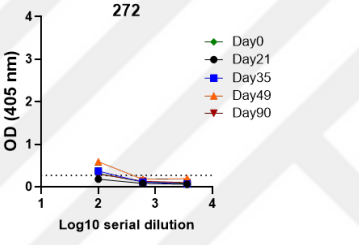

	Day0	Day21	Day35	Day49	Day90
Total Area	511.8	400.8	484.3	581.5	9154

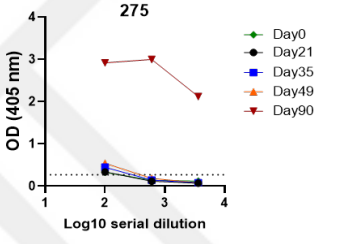

	Day0	Day21	Day35	Day49	Day90
Total Area	746.8	526.3	483.3	706.0	733.3

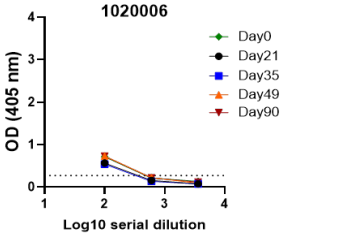

	Day0	Day21	Day35	Day49	Day90
Total Area	603.5	588.3	1619	2361	1319

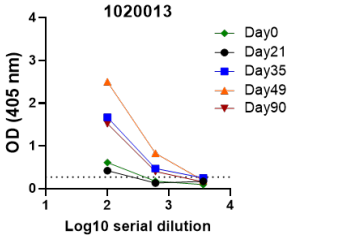

	Day0	Day21	Day35	Day49	Day90
Total Area	301.8	291.5	277.3	433.5	455.3

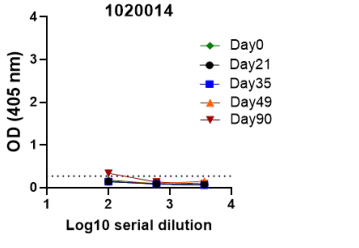

	Day0	Day21	Day35	Day49	Day90
Total Area	699.0	591.3	1098	2020	2394

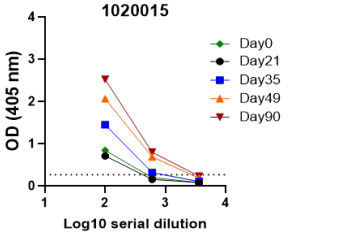

	Day0	Day21	Day35	Day49	Day90
Total Area	417.3	357.0	439.3	658.5	681.0

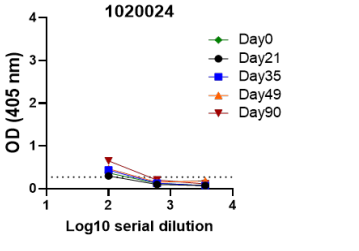

	Day0	Day21	Day35	Day49	Day90
Total Area	923.0	573.3	588.3	655.0	777.5

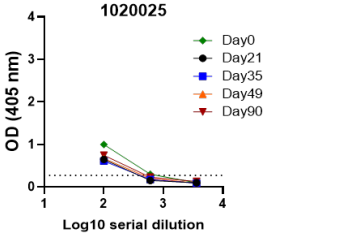

	Day0	Day21	Day35	Day49	Day90
Total Area	711.8	472.5	736.8	1349	1158

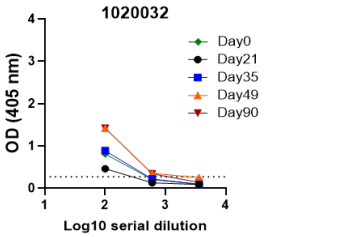

	Day0	Day21	Day35	Day49	Day90
Total Area	677.0	582.0	589.0	813.0	897.3

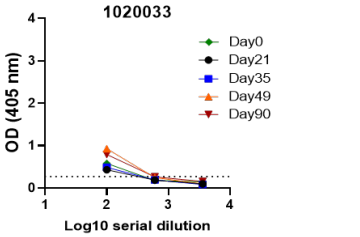

	Day0	Day21	Day35	Day49	Day90
Total Area	373.5	307.5	308.3	337.5	559.5

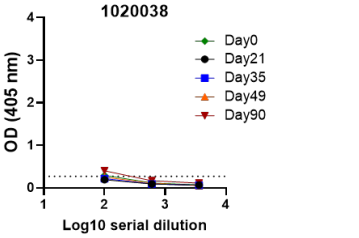

	Day0	Day21	Day35	Day49	Day90
Total Area	399.0	390.0	857.0	2392	399.3

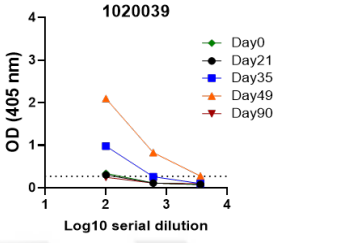

	Day0	Day21	Day35	Day49	Day90
Total Area	1410	1251	1168	1891	9932

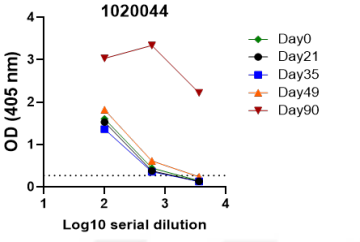

	Day0	Day21	Day35	Day49	Day90
Total Area	324.3	254.3	265.0	348.3	514.0

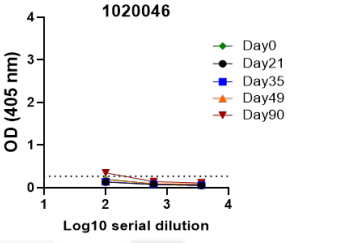

	Day0	Day21	Day35	Day49	Day90
Total Area	392.5	291.5	311.3	500.5	670.5

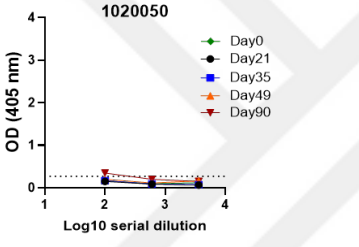

	Day0	Day21	Day35	Day49
Total Area	385.3	358.8	391.5	426.0

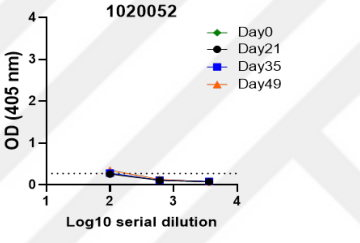

	Day0	Day21	Day35	Day49	Day90
Total Area	394.8	469.8	485.3	366.8	501.3

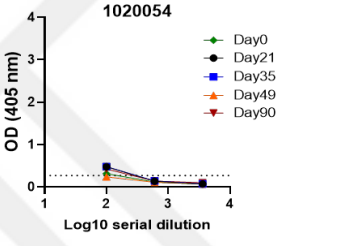

	Day0	Day21	Day35	Day49	Day90
Total Area	1734	567.0	672.8	1022	1202

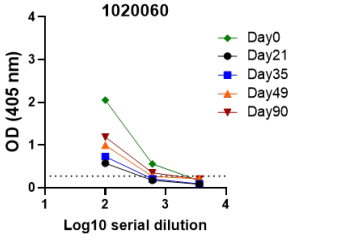

	Day0	Day21	Day35	Day49
Total Area	344.0	356.5	424.5	525.5

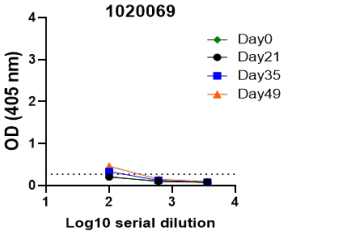

	Day0	Day21	Day35	Day49	Day90
Total Area	447.8	1279	3881	5389	3647

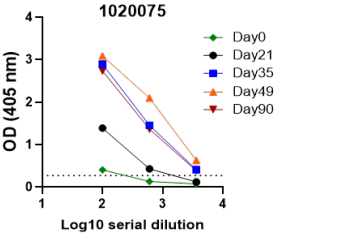

	Day0	Day21	Day35	Day49	Day90
Total Area	447.8	348.0	878.5	3794	1737

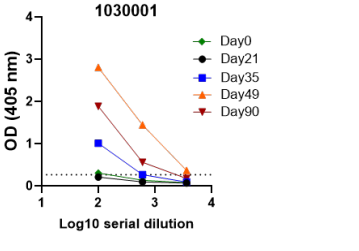

	Day0	Day21	Day35	Day49	Day90
Total Area	373.3	304.3	732.8	960.0	429.8

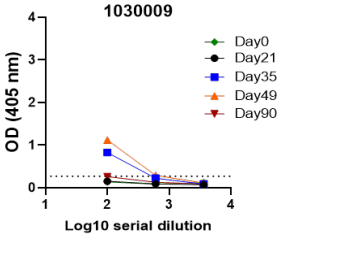

	Day0	Day21	Day35	Day49	Day90
Total Area	367.5	366.5	511.5	612.0	693.0

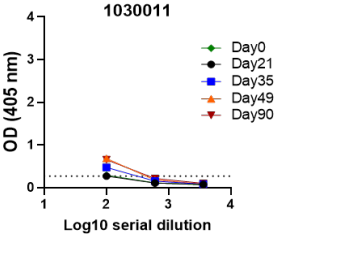

	Day0	Day21	Day35	Day49	Day90
Total Area	321.0	331.3	1171	2192	475.8

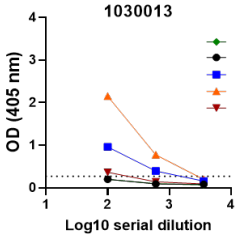

	Day0	Day21	Day35	Day49	Day90
Total Area	285.5	321.8	293.8	307.5	515.8

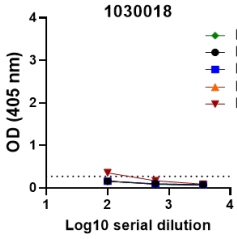

	Day0	Day21	Day35	Day49	Day90
Total Area	830.8	684.0	297.0	844.5	1128

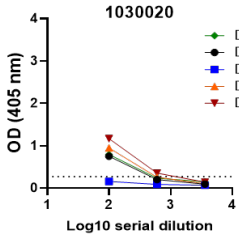

	Day0	Day21	Day35	Day49	Day90
Total Area	355.3	275.0	290.8	420.3	370.0

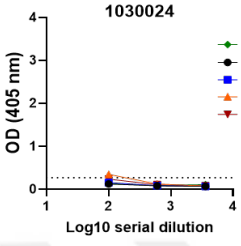

	Day0	Day21	Day35	Day49	Day90
Total Area	376.5	310.0	343.5	7414	3721

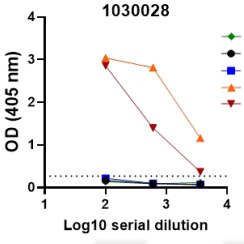

	Day0	Day21	Day35	Day49	Day90
Total Area	538.5	370.8	374.3	403.0	533.0

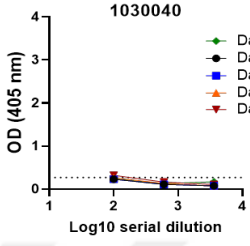

	Day0	Day21	Day35	Day49	Day90
Total Area	399.0	415.8	2607	1085	2608

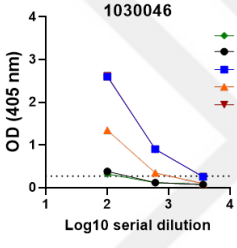

	Day0	Day21	Day35	Day49	Day90
Total Area	322.0	289.8	392.0	513.5	495.3

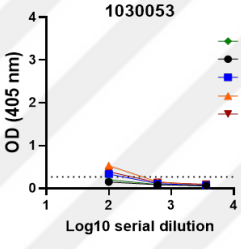

	Day0	Day21	Day35	Day49	Day90
Total Area	475.8	438.8	570.0	550.0	8844

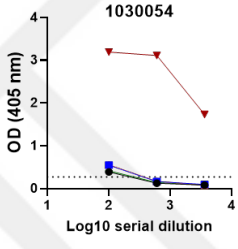

	Day0	Day21	Day35	Day49
Total Area	826.3	2452	3652	4876

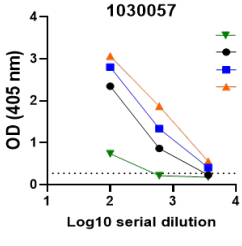

	Day0	Day21	Day35	Day49	Day90
Total Area	432.3	4322	6369	6879	2971

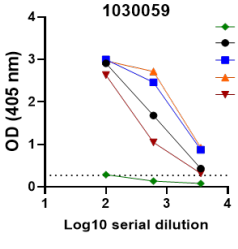

	Day0	Day21	Day35	Day49
Total Area	436.3	396.8	454.5	460.0

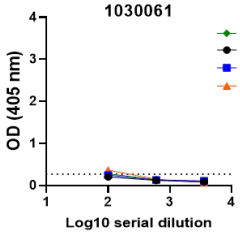

	Day0	Day21	Day35	Day49	Day90
Total Area	355.3	343.5	365.3	489.0	3380

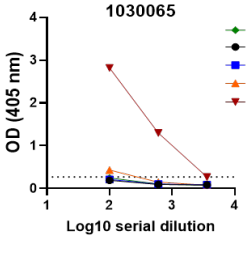

	Day0	Day21	Day35	Day49	Day90
Total Area	541.8	407.5	476.0	527.8	723.3

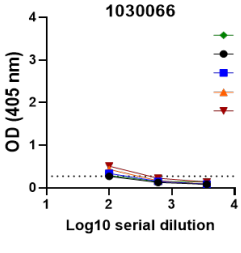

	Day0	Day21	Day35	Day49	Day90
Total Area	355.8	355.8	380.3	504.3	10706

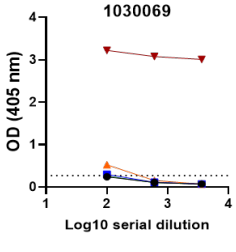

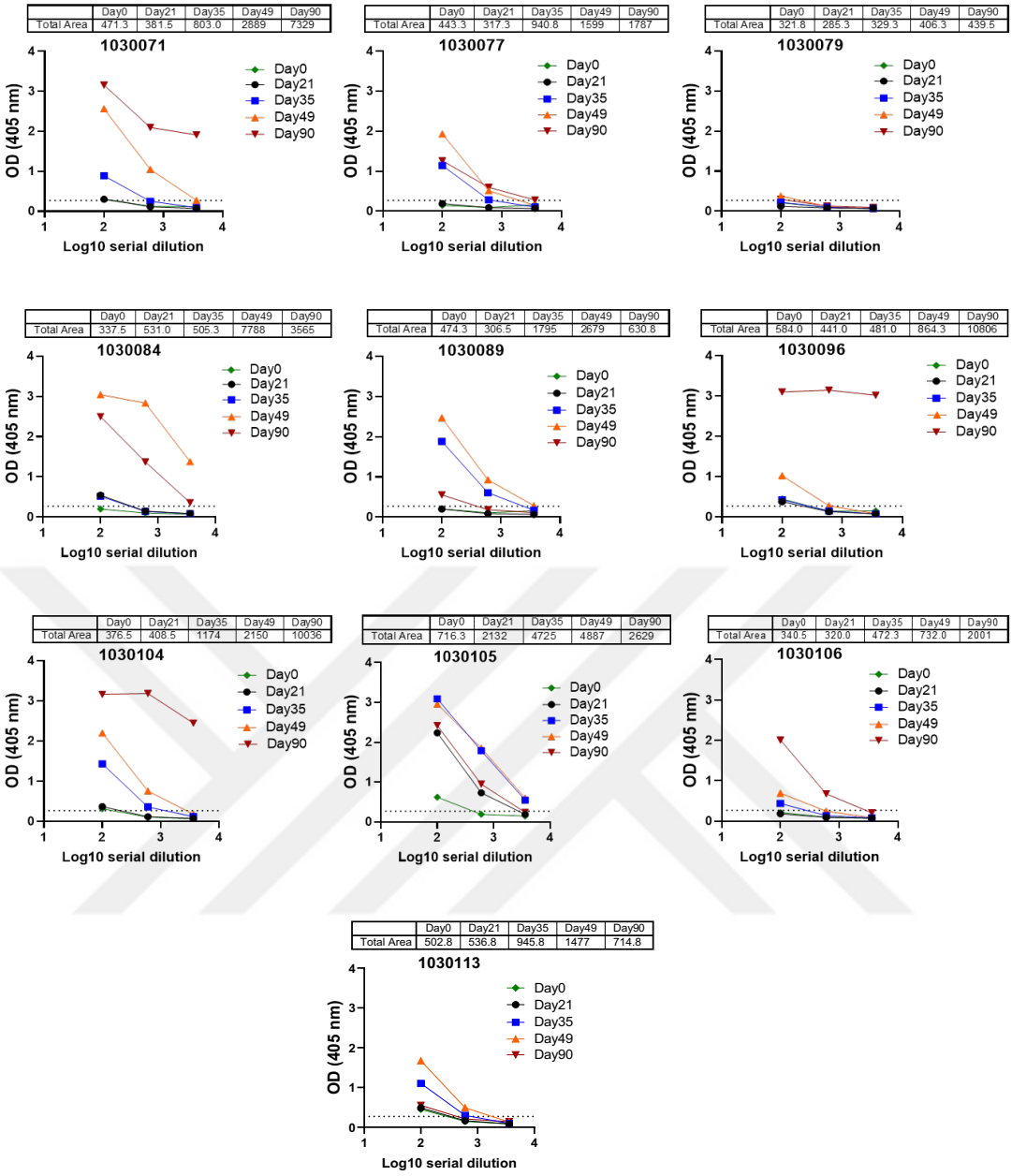

Figure A2. Anti-N IgG Titer demonstrations of Phase II clinical trial volunteers. Serum samples taken from volunteers were diluted 1:100, 1:600 and 1:3600-fold. Area under the curve calculations were used to determine titers of OD405 versus log10 reciprocal serial dilutions graphs.

	Day35	Day49	Day90
Total Area	1454	1900	823.8

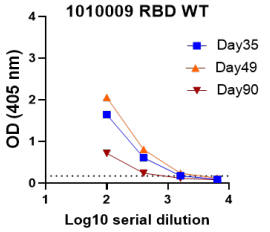

	Day35	Day49	Day90
Total Area	466.4	497.3	590.9

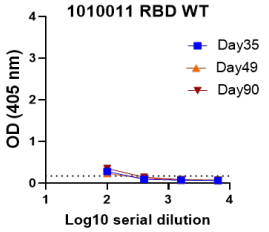

	Day35	Day49	Day90
Total Area	2393	2629	19155

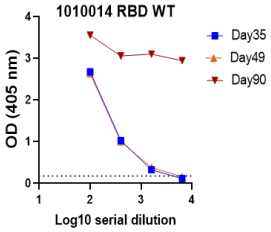

	Day35	Day49	Day90
Total Area	3467	5466	1461

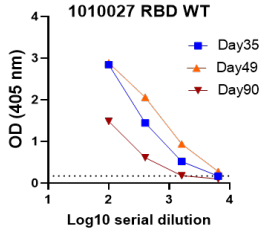

	Day35	Day49	Day90
Total Area	486.3	821.4	15358

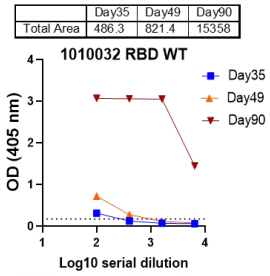

	Day35	Day49	Day90
Total Area	1330	2189	875.9

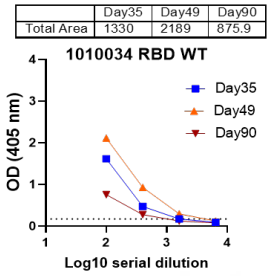

	Day35	Day49	Day90
Total Area	481.8	680.1	534.6

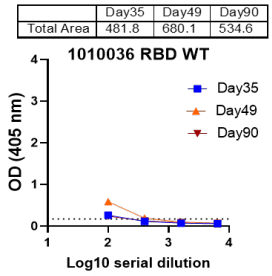

	Day35	Day49	Day90
Total Area	428.3	497.9	518.1

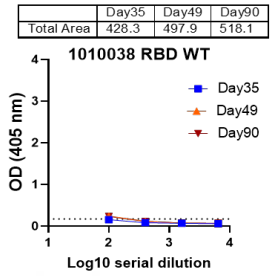

	Day35	Day49	Day90
Total Area	590.4	912.2	1102

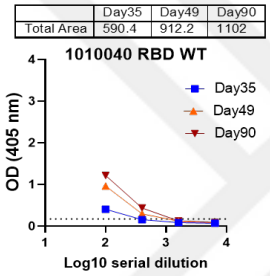

	Day35	Day49	Day90
Total Area	1389	1637	1085

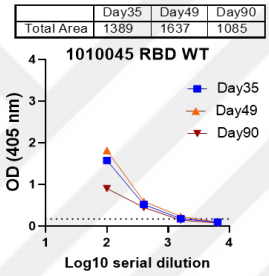

	Day35	Day49	Day90
Total Area	518.3	634.8	641.0

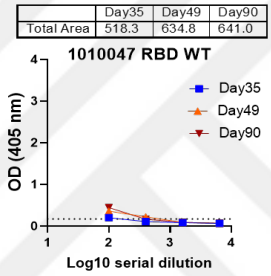

	Day35	Day49	Day90
Total Area	1715	1649	1227

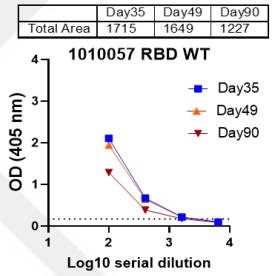

	Day35	Day49	Day90
Total Area	465.8	493.1	659.9

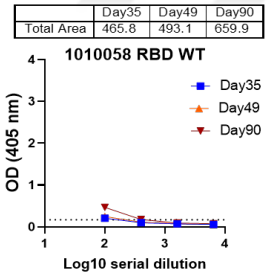

	Day35	Day49	Day90
Total Area	1313	2587	1045

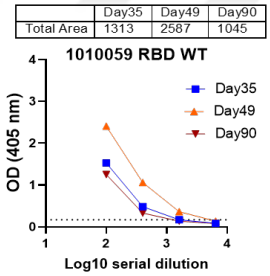

	Day35	Day49	Day90
Total Area	5462	6118	1640

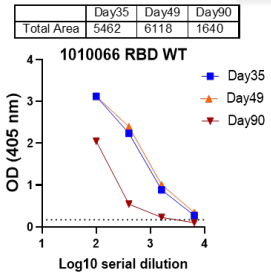

	Day35	Day49	Day90
Total Area	3288	5072	1475

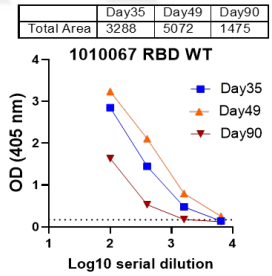

	Day35	Day49	Day90
Total Area	470.3	677.6	624.2

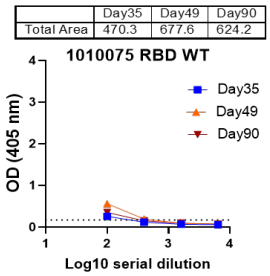

	Day35	Day49	Day90
Total Area	641.0	978.5	710.9

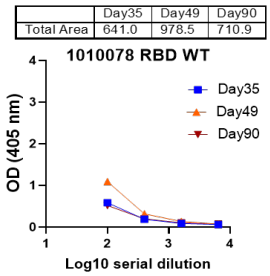

	Day35	Day49	Day90
Total Area	452.3	488.4	618.5

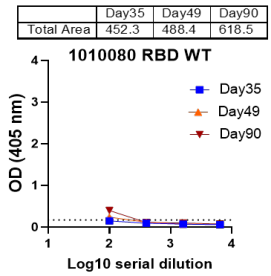

	Day35	Day49	Day90
Total Area	1232	3041	2200

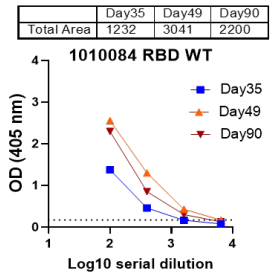

	Day35
Total Area	748.1

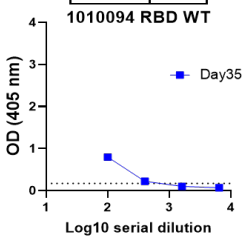

	Day35	Day49	Day90
Total Area	411.3	421.1	616.7

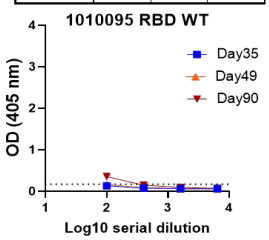

	Day35	Day49	Day90
Total Area	2585	5366	1378

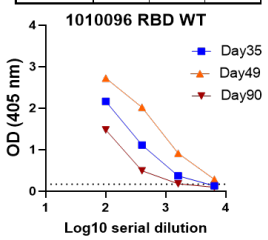

	Day35	Day49	Day90
Total Area	1322	1878	1477

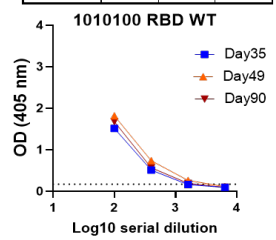

	Day35	Day49	Day90
Total Area	960.2	1973	689.6

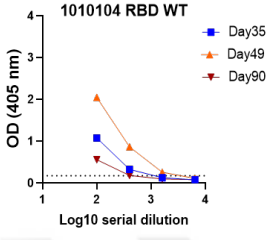

	Day35	Day49	Day90
Total Area	623.3	1044	744.6

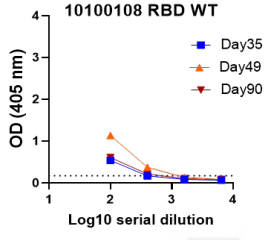

	Day35	Day49	Day90
Total Area	497.3	638.6	799.8

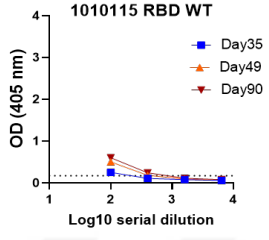

	Day35	Day49	Day90
Total Area	787.2	1363	851.3

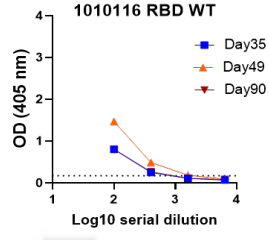

	Day35	Day49	Day90
Total Area	439.7	512.1	612.9

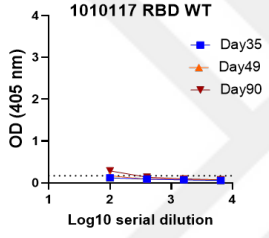

	Day35	Day49	Day90
Total Area	783.8	1482	851.7

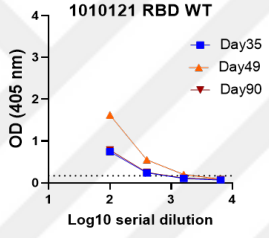

	Day35	Day49	Day90
Total Area	512.7	842.7	900.9

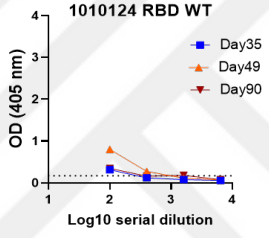

	Day35	Day49	Day90
Total Area	426.8	1392	789.6

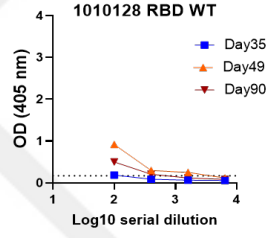

	Day35	Day49	Day90
Total Area	1902	3012	18745

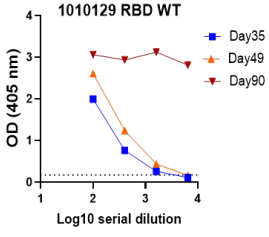

	Day35	Day49	Day90
Total Area	680.3	982.4	15815

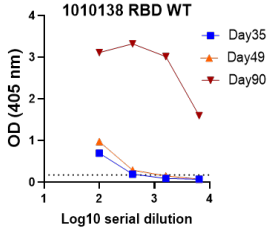

	Day35	Day49	Day90
Total Area	716.6	1086	907.4

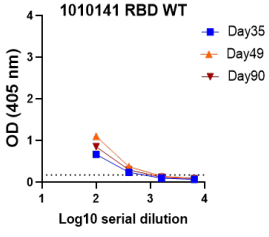

	Day35	Day49	Day90
Total Area	9716	17582	8438

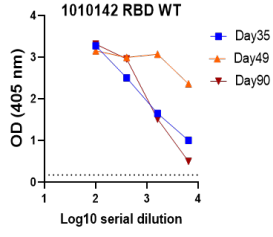

	Day35	Day49	Day90
Total Area	350.4	816.0	15030

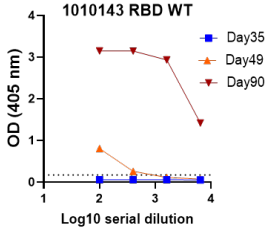

	Day35	Day49	Day90
Total Area	1809	4852	2881

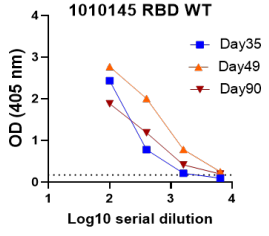

	Day35	Day49	Day90
Total Area	1543	1785	1020

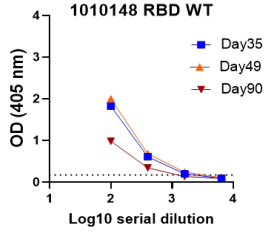

	Day35	Day49
Total Area	1746	2707

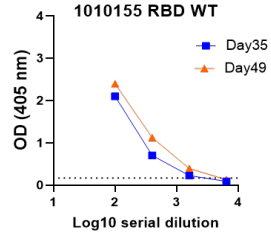

	Day35	Day49	Day90
Total Area	804.8	1162	912.5

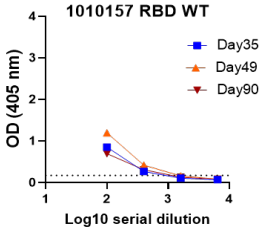

	Day35	Day49	Day90
Total Area	668.9	1003	1008

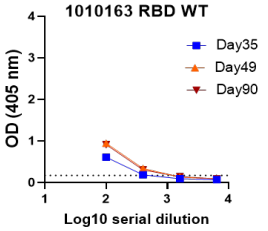

	Day35	Day49
Total Area	590.6	743.1

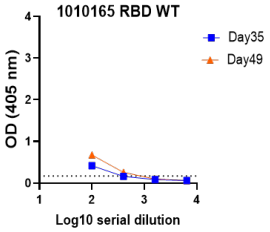

	Day35	Day49	Day90
Total Area	683.1	1483	755.7

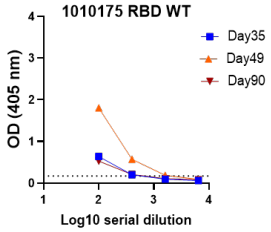

	Day35	Day49	Day90
Total Area	568.4	866.3	727.8

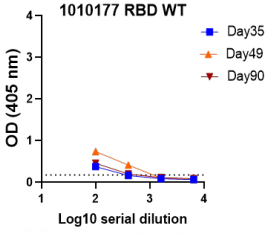

	Day35	Day49	Day90
Total Area	650.9	1138	1247

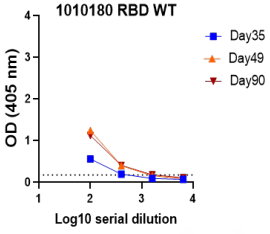

	Day35	Day49	Day90
Total Area	440.9	672.6	832.5

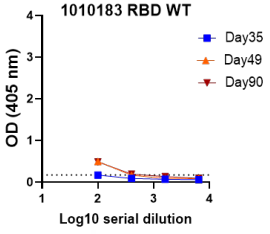

	Day35	Day49	Day90
Total Area	2886	3641	19626

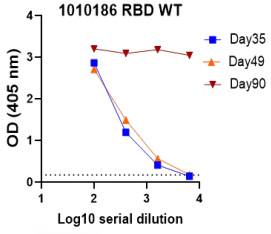

	Day35	Day49	Day90
Total Area	420.5	399.6	780.2

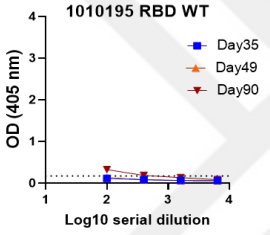

	Day35	Day49	Day90
Total Area	870.6	1657	1662

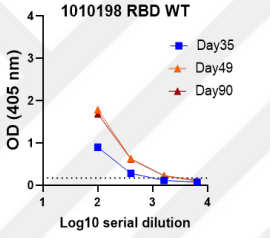

	Day35	Day49	Day90
Total Area	1381	2635	2145

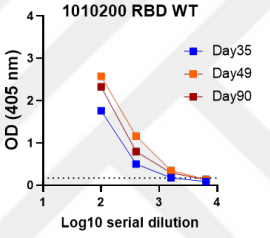

	Day35	Day49
Total Area	1738	3428

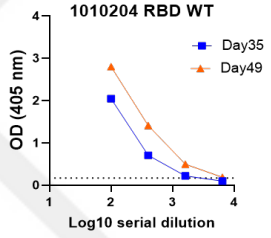

	Day35	Day49	Day90
Total Area	1615	2418	1579

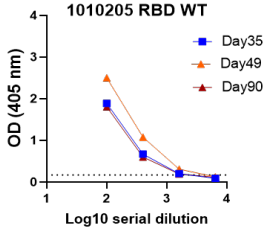

	Day35	Day49	Day90
Total Area	489.0	679.4	820.8

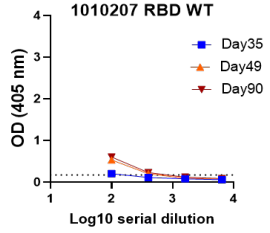

	Day35	Day49	Day90
Total Area	926.3	1614	1815

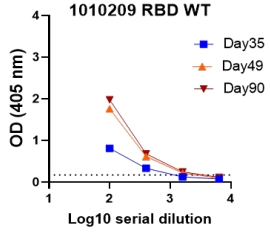

	Day35	Day49	Day90
Total Area	750.8	1699	1556

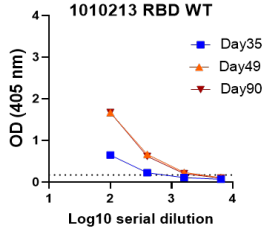

	Day35	Day49	Day90
Total Area	2623	6087	6795

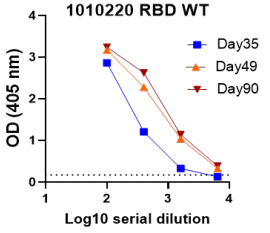

	Day35	Day49	Day90
Total Area	2573	3449	2627

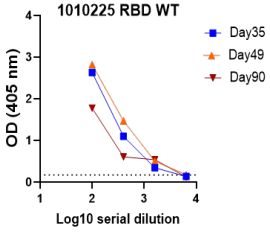

	Day35	Day49	Day90
Total Area	4779	4329	1954

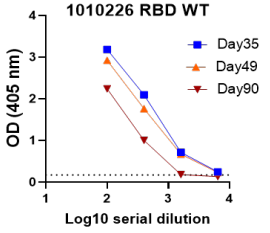

	Day35	Day49	Day90
Total Area	786.8	785.1	19429

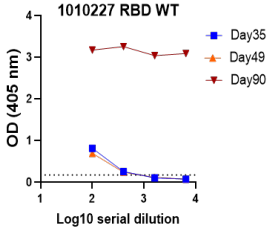

	Day35	Day49	Day90
Total Area	1457	1538	1479

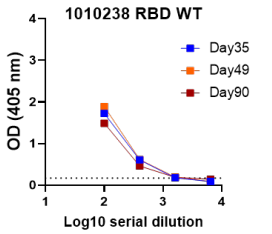

	Day35	Day49	Day90
Total Area	3117	3108	2288

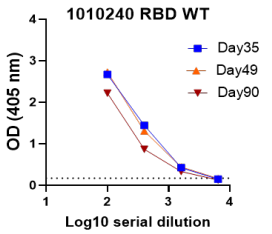

	Day35	Day49	Day90
Total Area	551.3	776.4	892.1

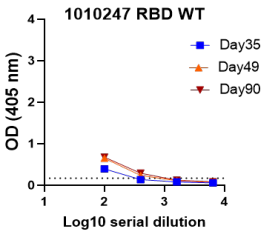

	Day35	Day49	Day90
Total Area	1077	1260	862.8

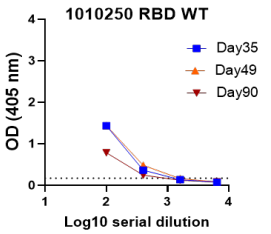

	Day35	Day49	Day90
Total Area	453.3	866.9	932.4

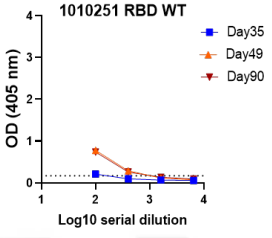

	Day35	Day49	Day90
Total Area	521.3	522.3	829.4

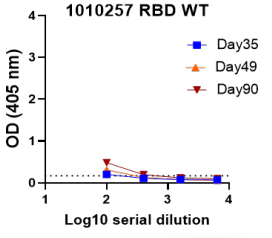

	Day35	Day49	Day90
Total Area	1877	1242	888.6

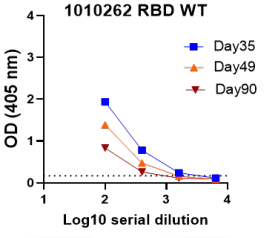

	Day35	Day49	Day90
Total Area	922.1	1216	1430

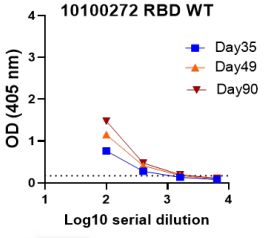

	Day35	Day49	Day90
Total Area	519.2	512.7	19405

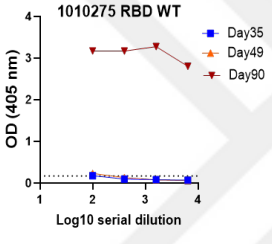

	Day35	Day49	Day90
Total Area	381.2	592.8	767.0

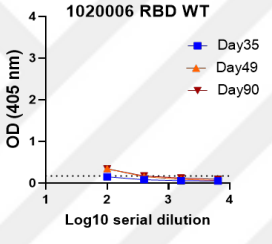

	Day35	Day49	Day90
Total Area	1111	1340	1345

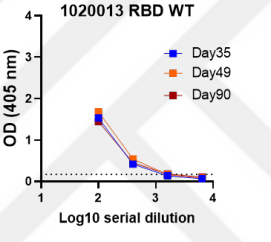

	Day35	Day49	Day90
Total Area	377.6	903.2	560.9

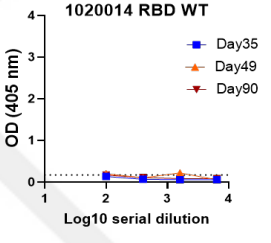

	Day35	Day49	Day90
Total Area	508.4	1514	1297

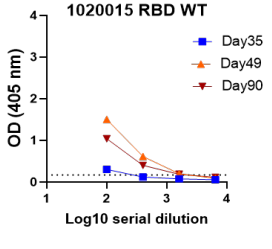

	Day35	Day49	Day90
Total Area	423.8	564.2	708.5

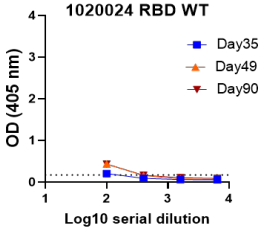

	Day35	Day49	Day90
Total Area	431.0	597.6	956.9

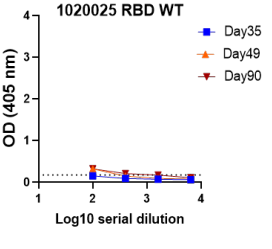

	Day35	Day49	Day90
Total Area	599.4	845.9	849.0

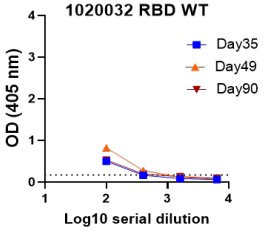

	Day35	Day49	Day90
Total Area	939.2	842.3	770.6

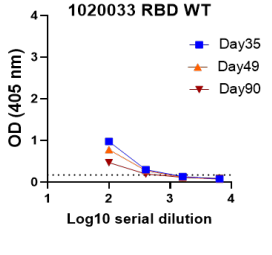

	Day35	Day49	Day90
Total Area	1341	942.3	760.2

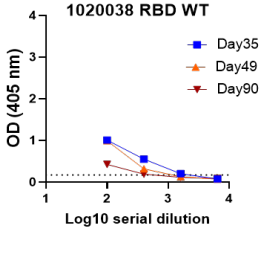

	Day35	Day49
Total Area	1034	1566

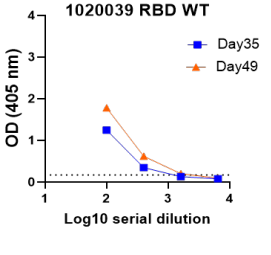

	Day35	Day49	Day90
Total Area	461.3	564.0	16415

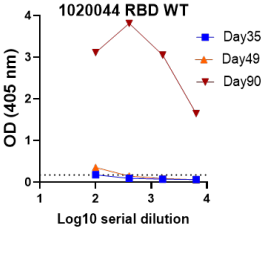

	Day35	Day49	Day90
Total Area	520.8	1120	1109

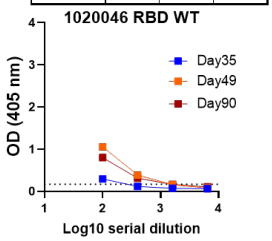

	Day35	Day49	Day90
Total Area	542.0	1173	1388

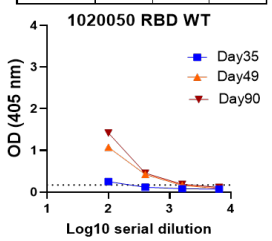

	Day35	Day49
Total Area	502.8	497.1

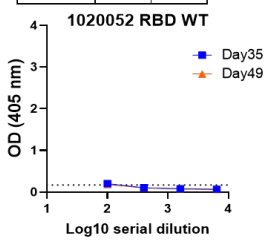

	Day35	Day49	Day90
Total Area	549.5	648.2	729.8

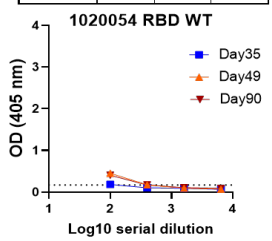

	Day35	Day49	Day90
Total Area	838.7	879.9	855.2

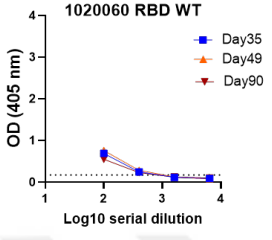

	Day35	Day49
Total Area	591.8	569.4

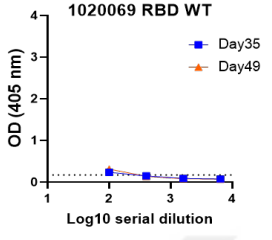

	Day35	Day49	Day90
Total Area	3562	3251	2799

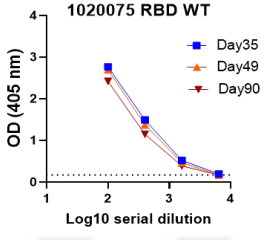

	Day35	Day49	Day90
Total Area	8535	12841	7529

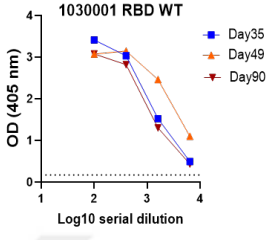

	Day35	Day49	Day90
Total Area	506.4	754.5	860.9

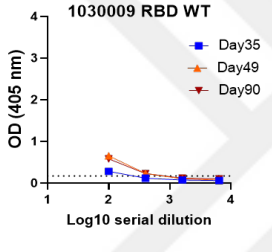

	Day35	Day49	Day90
Total Area	693.2	846.6	851.9

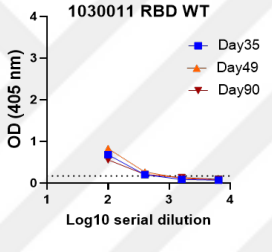

	Day35	Day49	Day90
Total Area	3649	5382	1722

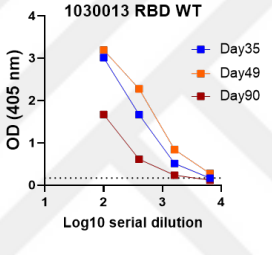

	Day35	Day49	Day90
Total Area	580.1	899.4	1132

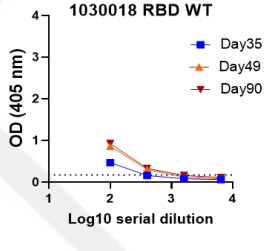

	Day35	Day49	Day90
Total Area	1646	2041	2277

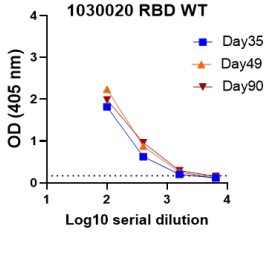

	Day35	Day49	Day90
Total Area	461.6	708.2	825.3

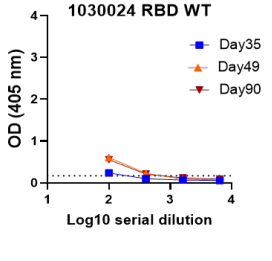

	Day35	Day49	Day90
Total Area	443.1	11795	12412

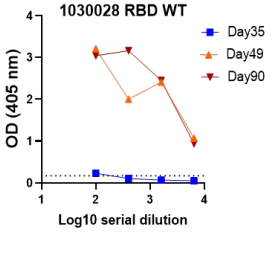

	Day35	Day49	Day90
Total Area	574.7	1279	1012

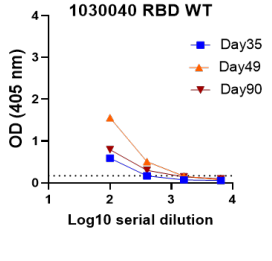

	Day35	Day49	Day90
Total Area	2073	825.3	2193

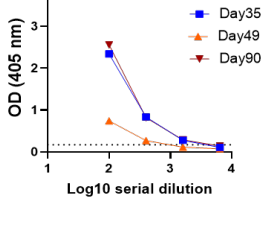

	Day35	Day49	Day90
Total Area	802.7	1720	2187

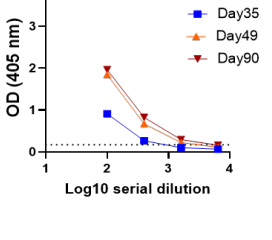

	Day35	Day49	Day90
Total Area	777.2	781.5	18414

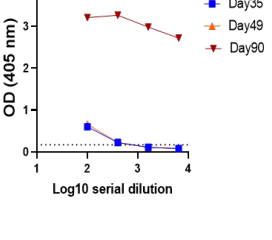

	Day35	Day49
Total Area	2106	2119

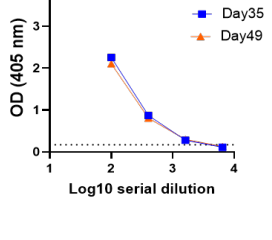

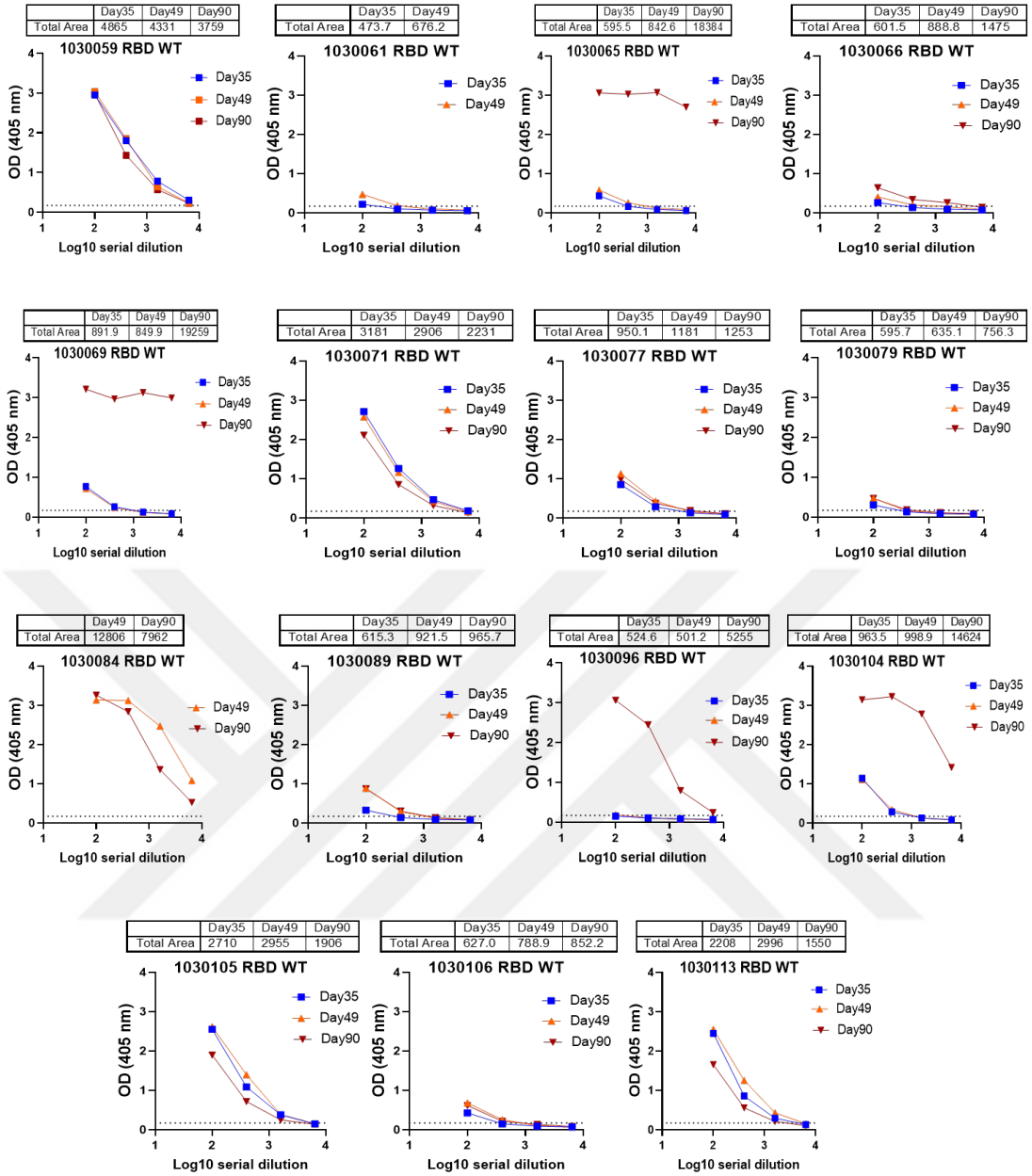

Figure A3. Anti-WT RBD IgG Titer demonstrations of Phase II clinical trial volunteers. Serum samples taken from volunteers were diluted 1:100, 1:400, 1:1600 and 1:6400-fold. Area under the curve calculations were used to determine titers of OD405 versus log10 reciprocal serial dilutions graphs.

	Day35	Day49	Day90
Total Area	1183	2963	1266

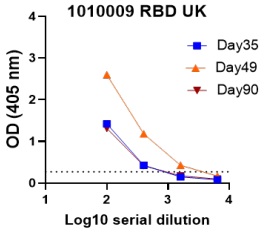

	Day35	Day49	Day90
Total Area	429.6	664.1	629.7

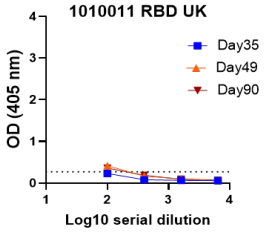

	Day35	Day49	Day90
Total Area	3407	5871	19598

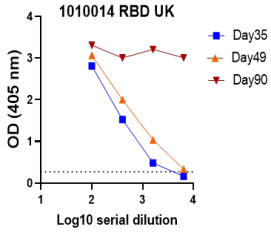

	Day35	Day49	Day90
Total Area	2809	6389	1142

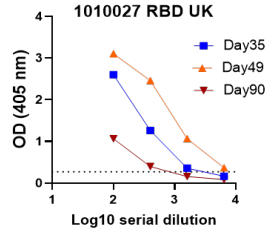

	Day35	Day49	Day90
Total Area	525.2	1957	15222

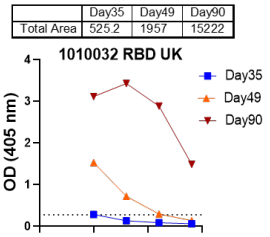

	Day35	Day49	Day90
Total Area	542.4	1112	872.7

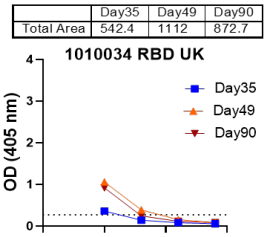

	Day35	Day49	Day90
Total Area	504.0	1071	657.6

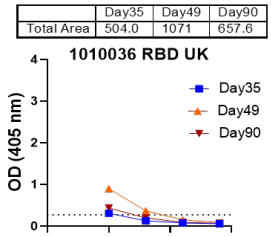

	Day35	Day49	Day90
Total Area	404.3	763.4	576.2

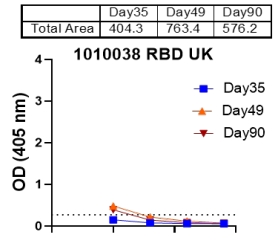

	Day35	Day49	Day90
Total Area	935.6	1841	1932

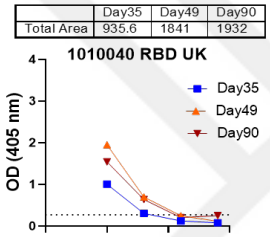

	Day35	Day49	Day90
Total Area	1494	641.3	911.7

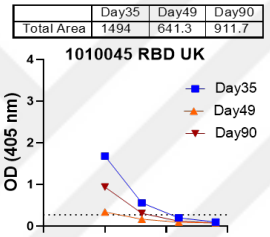

	Day35	Day49	Day90
Total Area	461.1	843.6	670.2

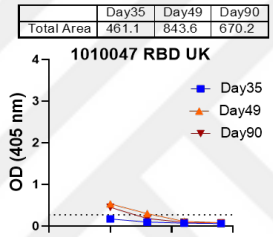

	Day35	Day49	Day90
Total Area	1584	2236	1210

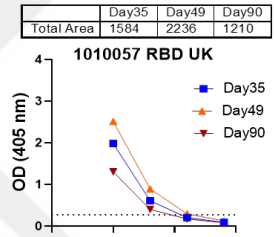

	Day35	Day49	Day90
Total Area	447.6	740.1	678.0

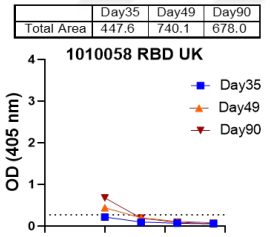

	Day35	Day49	Day90
Total Area	1109	2676	1100

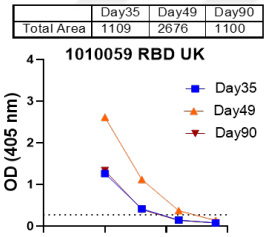

	Day35	Day49	Day90
Total Area	6122	8993	1584

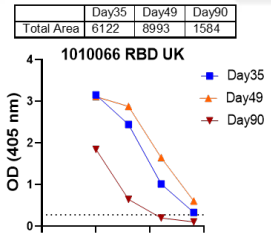

	Day35	Day49	Day90
Total Area	3321	5106	1199

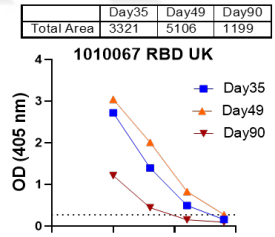

	Day35	Day49	Day90
Total Area	474.9	755.9	496.8

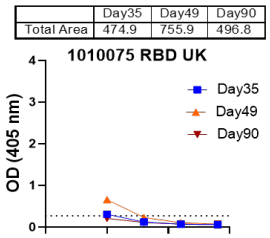

	Day35	Day49	Day90
Total Area	629.6	1018	548.9

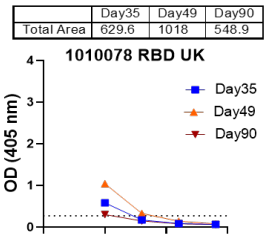

	Day35	Day49	Day90
Total Area	420.6	686.3	674.4

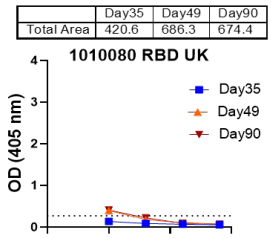

	Day35	Day49	Day90
Total Area	1109	3980	1910

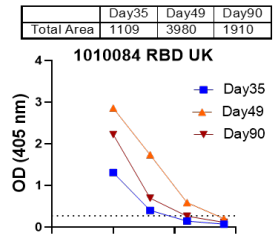

	Day35
Total Area	1095

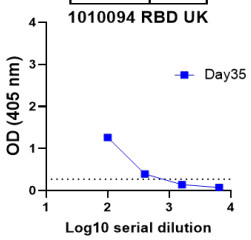

	Day35	Day49	Day90
Total Area	428.1	669.6	511.7

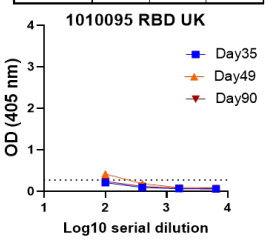

	Day35	Day49	Day90
Total Area	2063	4637	1002

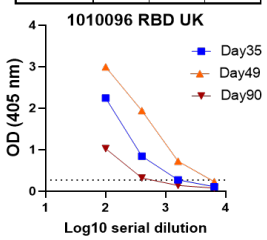

	Day35	Day49	Day90
Total Area	794.1	1685	1113

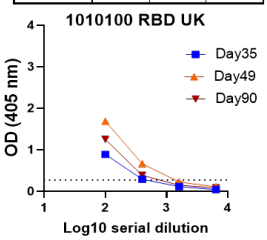

	Day35	Day49	Day90
Total Area	1256	2549	657.2

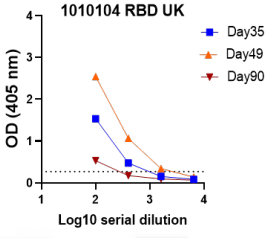

	Day35	Day49	Day90
Total Area	670.5	1359	626.9

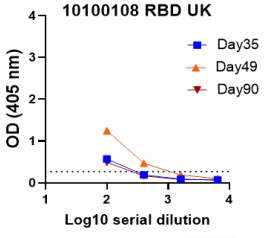

	Day35	Day49	Day90
Total Area	860.9	1493	771.8

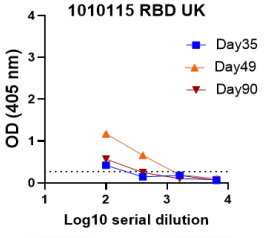

	Day35	Day49	Day90
Total Area	929.0	1947	639.0

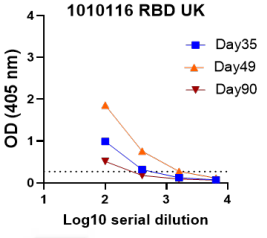

	Day35	Day49	Day90
Total Area	385.8	800.3	454.8

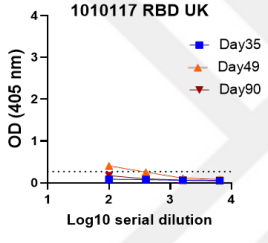

	Day35	Day49	Day90
Total Area	904.4	1988	667.7

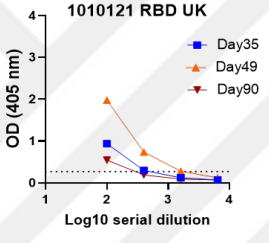

	Day35	Day49	Day90
Total Area	615.9	1177	511.4

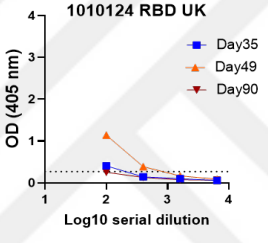

	Day35	Day49	Day90
Total Area	447.5	2158	753.2

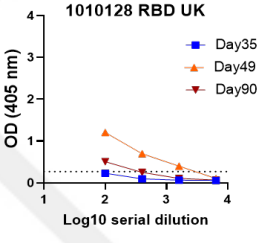

	Day35	Day49	Day90
Total Area	1614	3382	16299

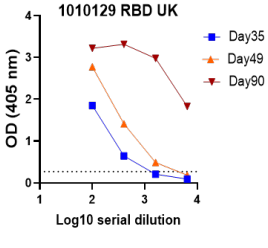

	Day35	Day49	Day90
Total Area	871.4	1366	12325

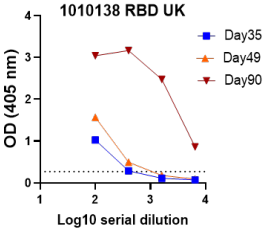

	Day35	Day49	Day90
Total Area	637.8	1871	1450

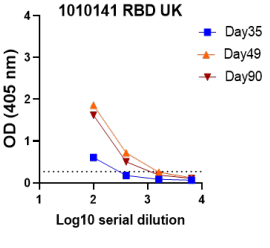

	Day35	Day49	Day90
Total Area	8250	17506	8838

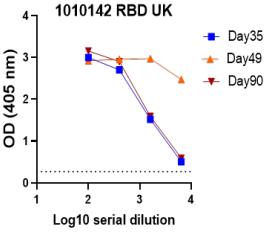

	Day35	Day49	Day90
Total Area	327.5	1257	15326

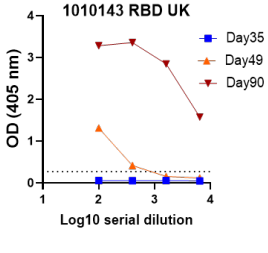

	Day35	Day49	Day90
Total Area	1899	6256	3337

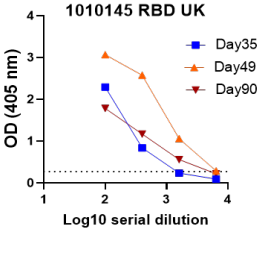

	Day35	Day49	Day90
Total Area	1168	2216	994.2

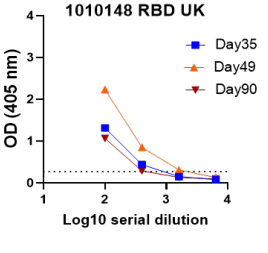

	Day35	Day49
Total Area	1604	3813

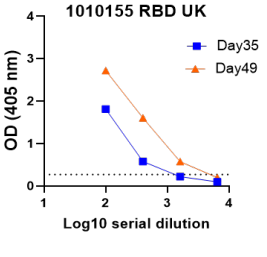

	Day35	Day49	Day90
Total Area	704.0	1493	785.1

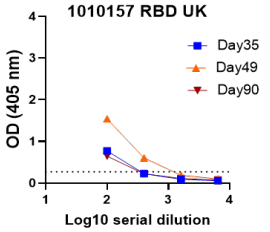

	Day35	Day49	Day90
Total Area	1028	2601	972.2

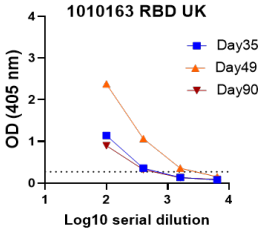

	Day35	Day49
Total Area	624.8	1455

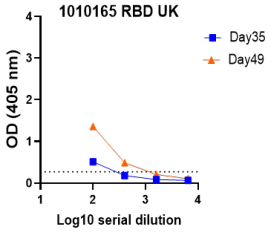

	Day35	Day49	Day90
Total Area	575.7	1683	641.4

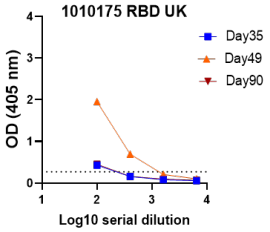

	Day35	Day49	Day90
Total Area	686.9	1610	761.6

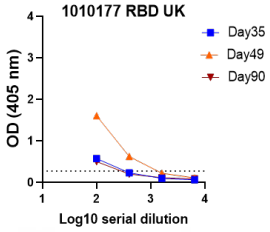

	Day35	Day49	Day90
Total Area	761.4	1844	1377

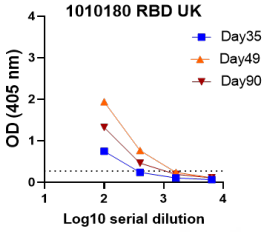

	Day35	Day49	Day90
Total Area	398.7	793.7	878.7

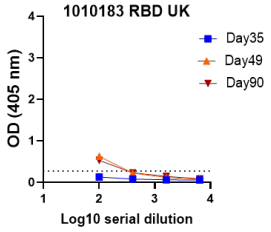

	Day35	Day49	Day90
Total Area	2207	4797	19028

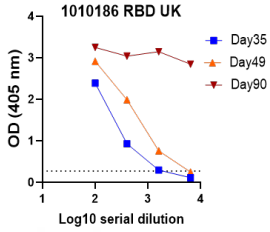

	Day35	Day49	Day90
Total Area	456.3	621.3	710.0

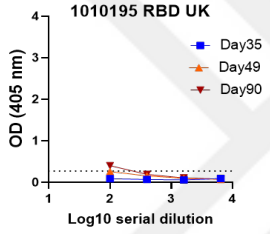

	Day35	Day49	Day90
Total Area	562.2	1907	1515

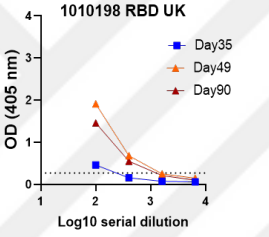

	Day35	Day49	Day90
Total Area	799.1	2662	1901

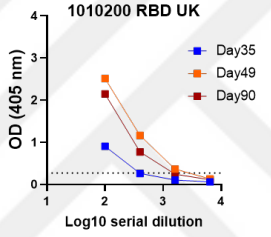

	Day35	Day49
Total Area	1140	4026

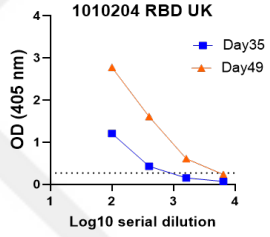

	Day35	Day49	Day90
Total Area	1044	2854	1495

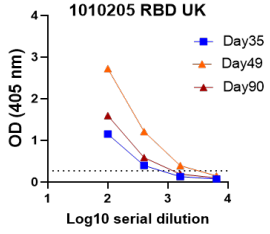

	Day35	Day49	Day90
Total Area	409.7	1052	777.8

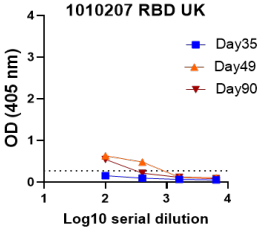

	Day35	Day49	Day90
Total Area	615.8	1621	1665

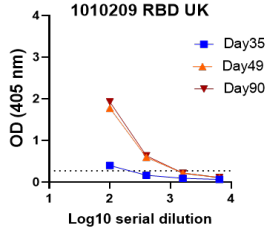

	Day35	Day49	Day90
Total Area	740.7	2332	1396

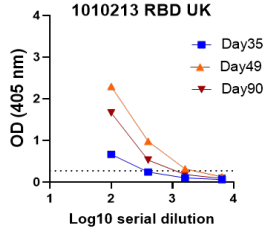

	Day35	Day49	Day90
Total Area	1629	6652	6843

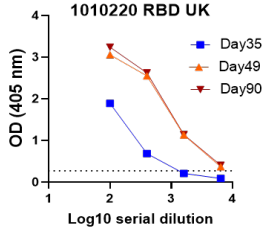

	Day35	Day49	Day90
Total Area	2018	3917	1672

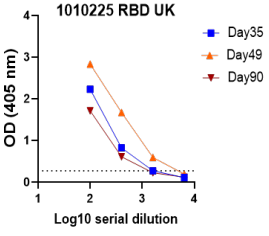

	Day35	Day49	Day90
Total Area	3125	5180	2564

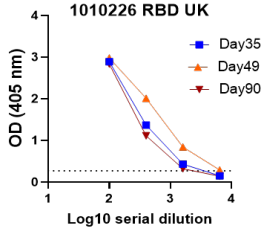

	Day35	Day49	Day90
Total Area	521.7	936.2	19007

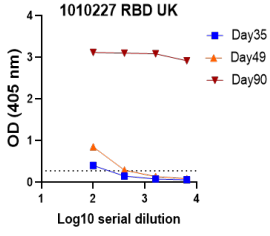

	Day35	Day49	Day90
Total Area	1489	3930	1739

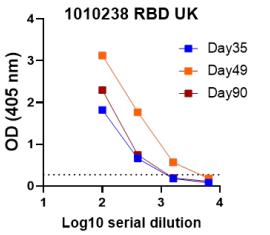

	Day35	Day49	Day90
Total Area	1962	4189	2766

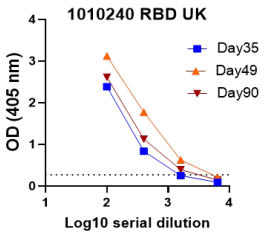

	Day35	Day49	Day90
Total Area	546.6	1269	1026

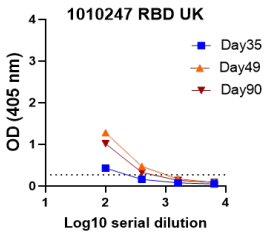

	Day35	Day49	Day90
Total Area	1104	2572	1595

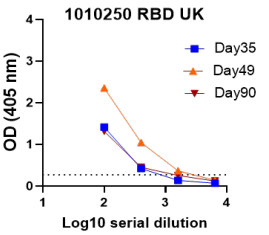

	Day35	Day49	Day90
Total Area	364.8	1170	986.7

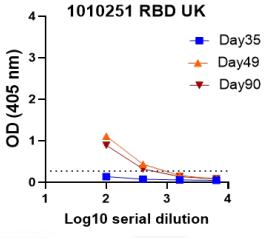

	Day35	Day49	Day90
Total Area	408.8	659.3	822.5

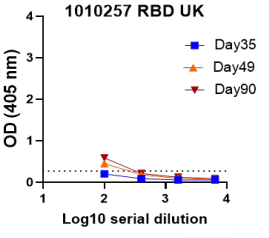

	Day35	Day49	Day90
Total Area	2825	2673	832.4

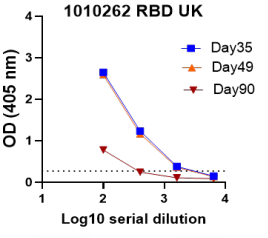

	Day35	Day49	Day90
Total Area	941.9	1547	1411

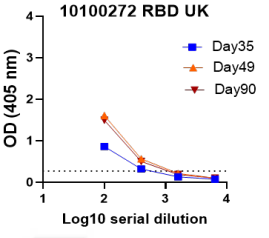

	Day35	Day49	Day90
Total Area	465.6	647.4	18469

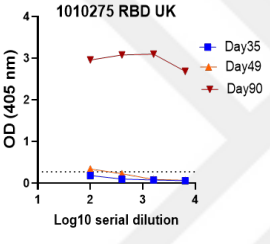

	Day35	Day49	Day90
Total Area	362.4	756.6	747.3

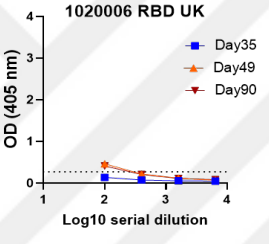

	Day35	Day49	Day90
Total Area	1419	1576	1123

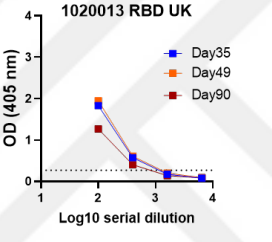

	Day35	Day49	Day90
Total Area	384.3	568.2	537.8

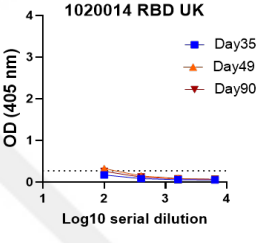

	Day35	Day49	Day90
Total Area	535.1	2312	1232

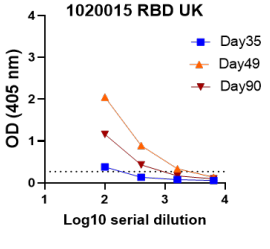

	Day35	Day49	Day90
Total Area	405.0	665.1	515.3

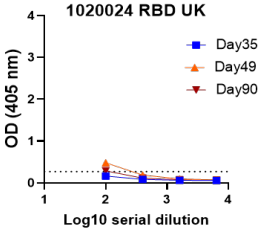

	Day35	Day49	Day90
Total Area	444.8	764.0	856.5

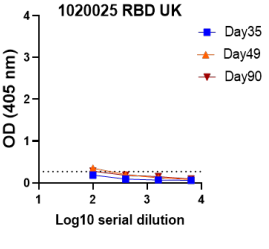

	Day35	Day49	Day90
Total Area	792.8	1493	921.3

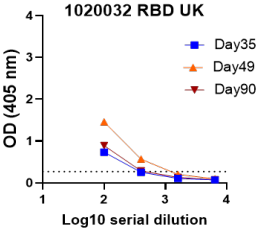

	Day35	Day49	Day90
Total Area	1052	1130	660.6

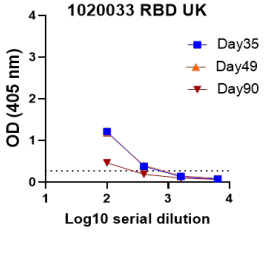

	Day35	Day49	Day90
Total Area	1076	1380	614.4

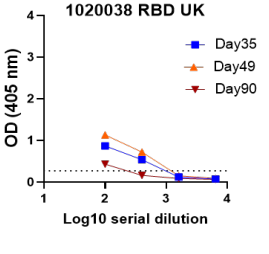

	Day35	Day49
Total Area	1338	1978

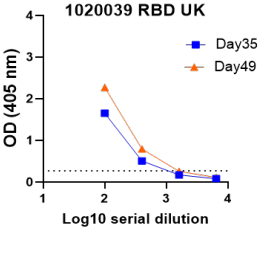

	Day35	Day49	Day90
Total Area	584.9	664.8	12743

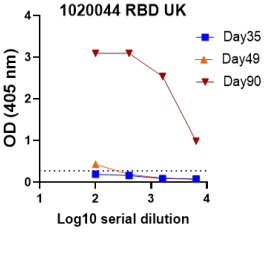

	Day35	Day49	Day90
Total Area	549.9	1224	674.4

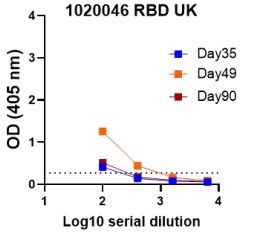

	Day35	Day49	Day90
Total Area	487.2	1306	884.3

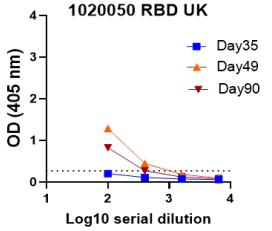

	Day35	Day49
Total Area	481.8	890.0

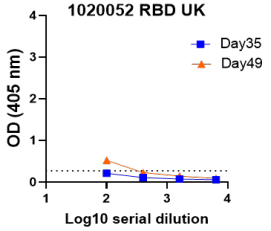

	Day35	Day49	Day90
Total Area	447.6	987.9	691.4

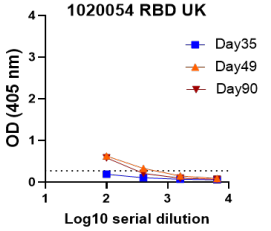

	Day35	Day49	Day90
Total Area	845.0	1300	771.8

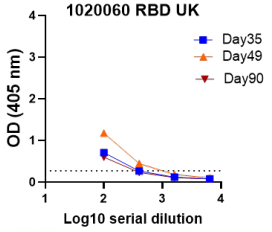

	Day35	Day49
Total Area	684.9	1019

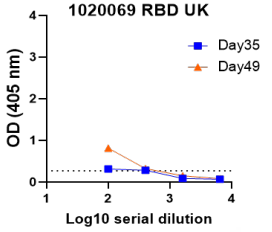

	Day35	Day49	Day90
Total Area	3337	3852	2013

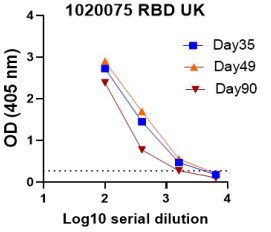

	Day35	Day49	Day90
Total Area	7026	14483	5334

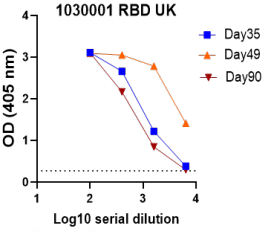

	Day35	Day49	Day90
Total Area	531.9	1166	695.4

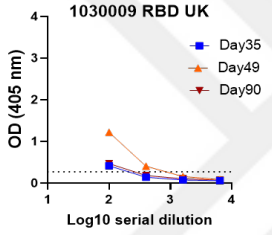

	Day35	Day49	Day90
Total Area	728.7	1199	666.2

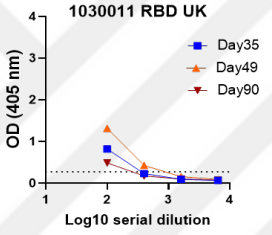

	Day35	Day49	Day90
Total Area	3459	6828	1273

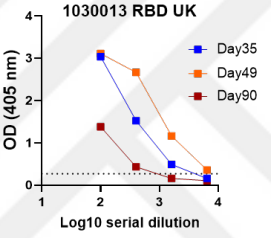

	Day35	Day49	Day90
Total Area	562.1	1211	732.8

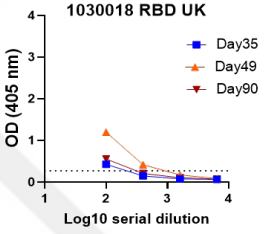

	Day35	Day49	Day90
Total Area	1521	2785	1257

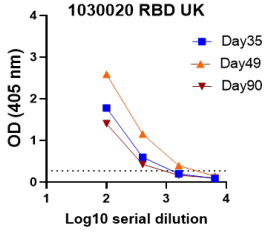

	Day35	Day49	Day90
Total Area	1031	1500	897.3

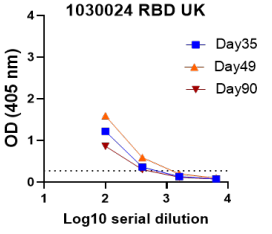

	Day35	Day49	Day90
Total Area	440.0	11361	6718

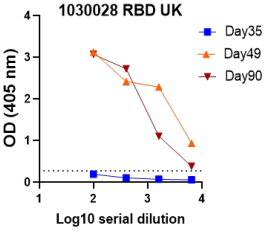

	Day35	Day49	Day90
Total Area	722.0	1667	823.8

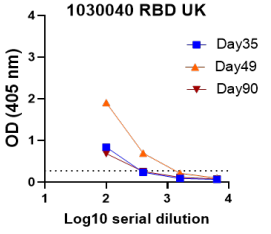

	Day35	Day49	Day90
Total Area	1531	884.7	1615

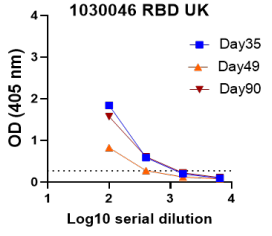

	Day35	Day49	Day90
Total Area	749.6	2022	1684

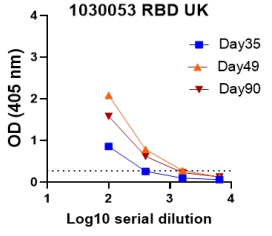

	Day35	Day49	Day90
Total Area	853.5	945.2	18137

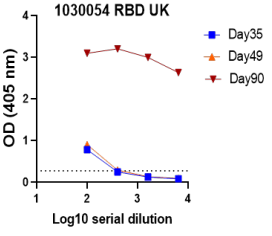

	Day35	Day49
Total Area	1294	1982

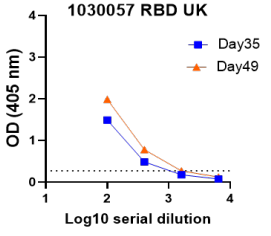

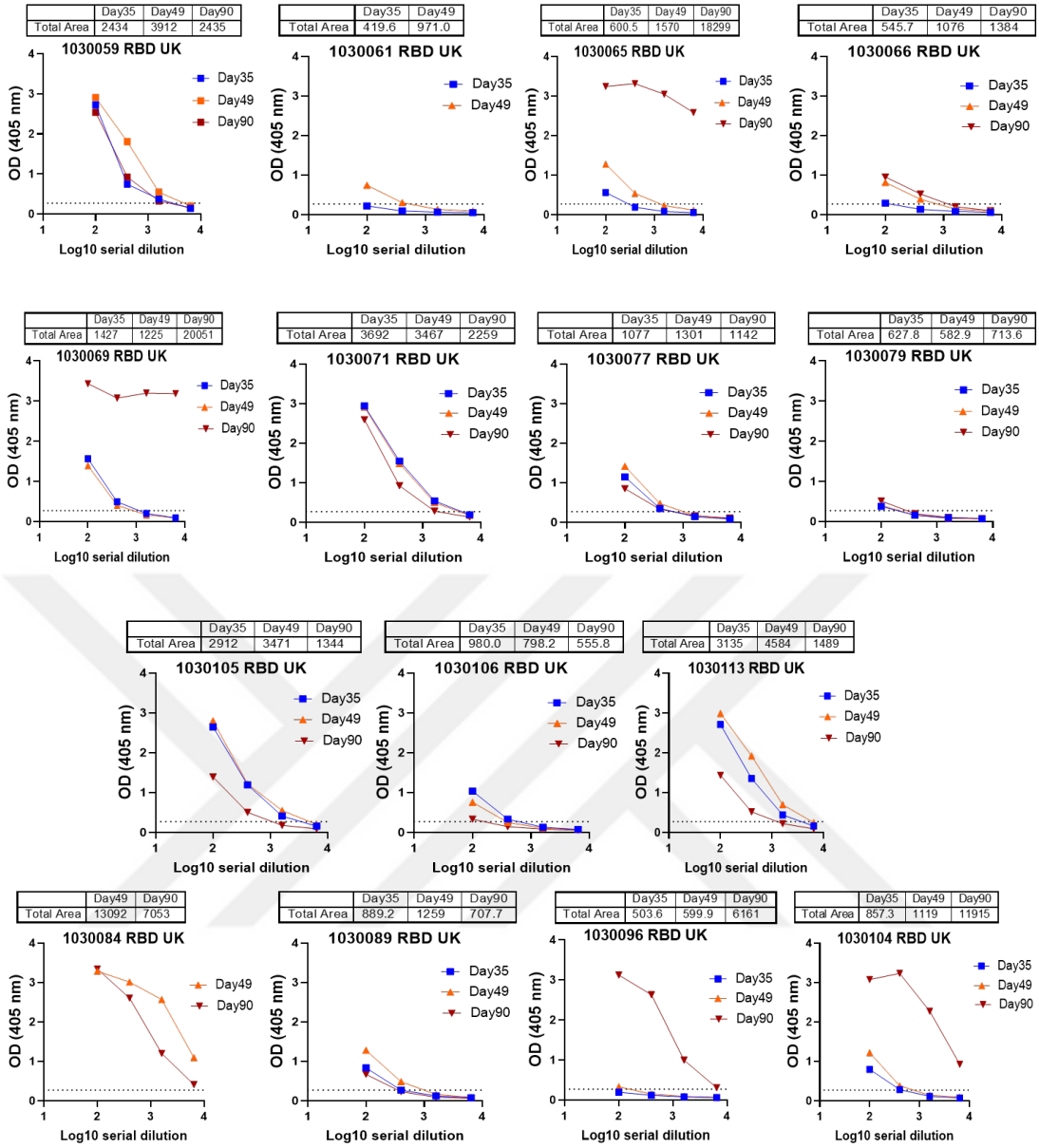

Figure A4. Anti-Alpha RBD IgG Titer demonstrations of Phase II clinical trial volunteers. Serum samples taken from volunteers were diluted 1:100, 1:400, 1:1600 and 1:6400-fold. Area under the curve calculations were used to determine titers of OD405 versus log10 reciprocal serial dilutions graphs.

	Day35	Day49	Day90
Total Area	1006	1900	835.8

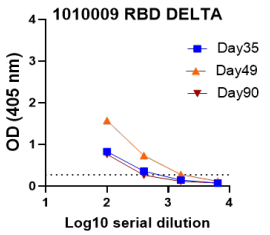

	Day35	Day49	Day90
Total Area	855.0	1232	442.2

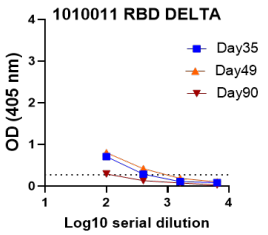

	Day35	Day49	Day90
Total Area	687.9	1550	19618

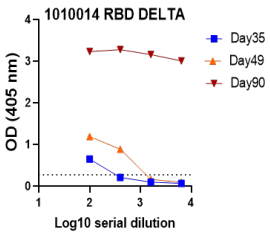

	Day35	Day49	Day90
Total Area	1527	2115	636.3

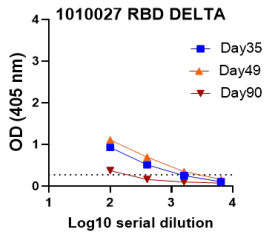

	Day35	Day49	Day90
Total Area	858.2	1881	15724

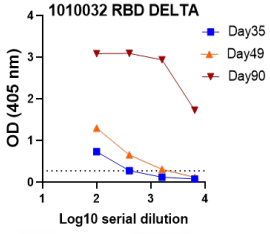

	Day35	Day49	Day90
Total Area	809.4	1428	788.6

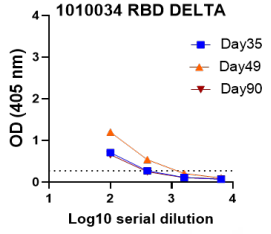

	Day35	Day49	Day90
Total Area	526.1	856.1	493.5

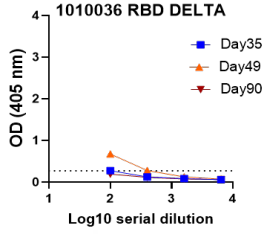

	Day35	Day49	Day90
Total Area	697.7	1305	483.3

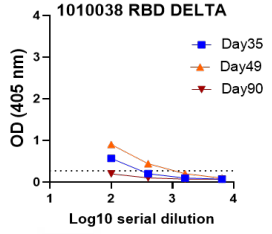

	Day35	Day49	Day90
Total Area	518.9	1032	782.4

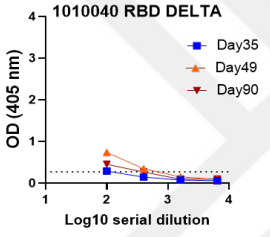

	Day35	Day49	Day90
Total Area	489.0	1136	1013

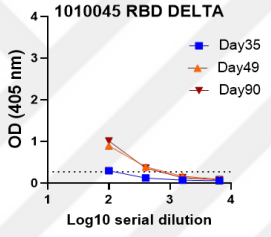

	Day35	Day49	Day90
Total Area	1119	1405	692.9

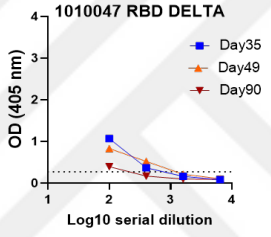

	Day35	Day49	Day90
Total Area	783.8	1466	1177

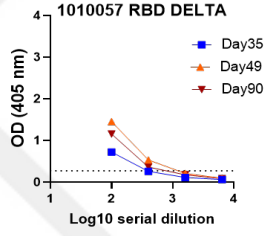

	Day35	Day49	Day90
Total Area	417.5	1054	586.2

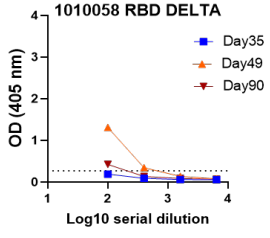

	Day35	Day49	Day90
Total Area	487.7	1476	950.9

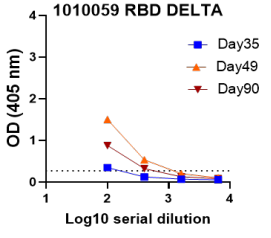

	Day35	Day49	Day90
Total Area	671.4	2054	1056

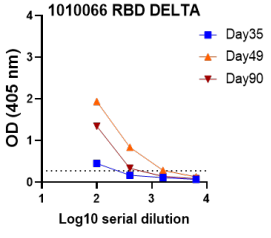

	Day35	Day49	Day90
Total Area	505.8	1023	866.3

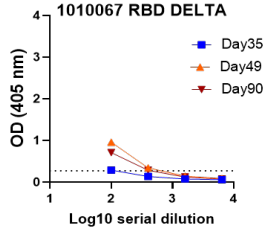

	Day35	Day49	Day90
Total Area	420.9	520.8	537.2

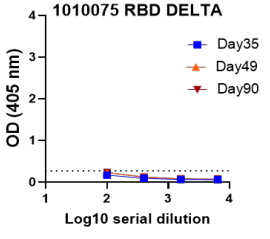

	Day35	Day49	Day90
Total Area	474.8	1114	551.4

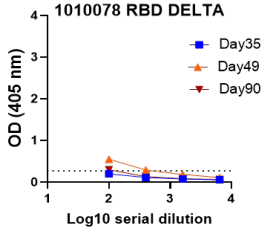

	Day35	Day49	Day90
Total Area	461.3	592.2	555.2

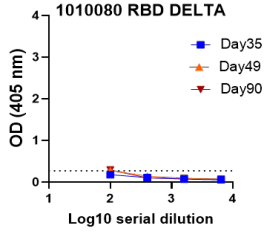

	Day35	Day49	Day90
Total Area	1160	1592	1447

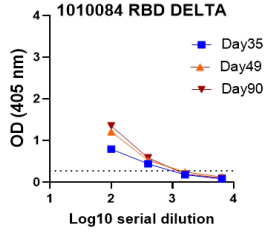

	Day35
Total Area	480.6

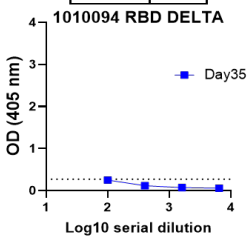

	Day35	Day49	Day90
Total Area	494.1	682.1	512.1

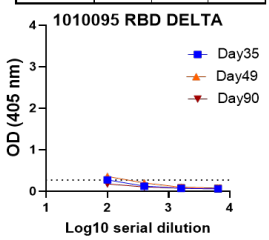

	Day35	Day49	Day90
Total Area	504.5	1342	832.7

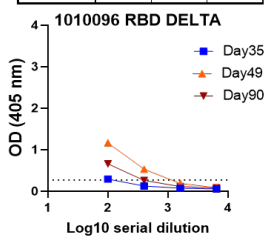

	Day35	Day49	Day90
Total Area	595.1	1326	1235

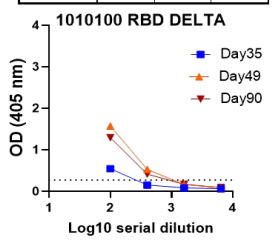

	Day35	Day49	Day90
Total Area	548.3	1028	563.6

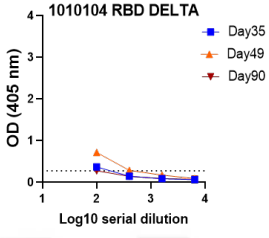

	Day35	Day49	Day90
Total Area	429.9	701.3	613.2

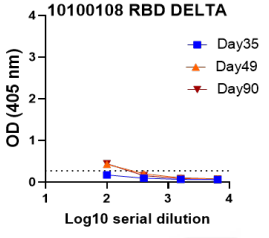

	Day35	Day49	Day90
Total Area	896.9	1110	605.3

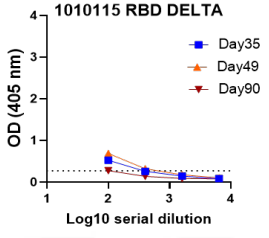

	Day35	Day49	Day90
Total Area	584.4	1228	741.9

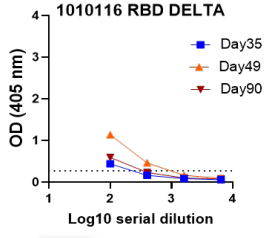

	Day35	Day49	Day90
Total Area	779.6	1258	480.5

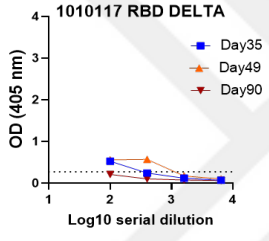

	Day35	Day49	Day90
Total Area	537.2	791.3	674.0

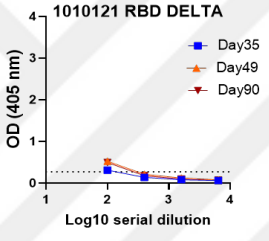

	Day35	Day49	Day90
Total Area	488.7	820.1	728.7

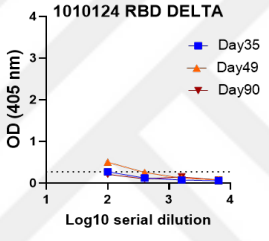

	Day35	Day49	Day90
Total Area	409.7	1155	568.4

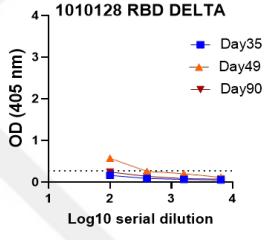

	Day35	Day49	Day90
Total Area	627.5	1070	16676

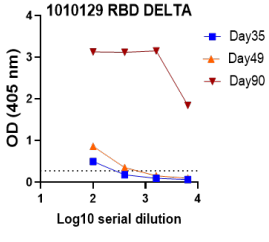

	Day35	Day49	Day90
Total Area	599.0	862.5	13569

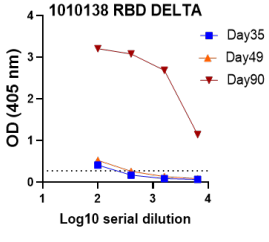

	Day35	Day49	Day90
Total Area	437.0	703.1	834.0

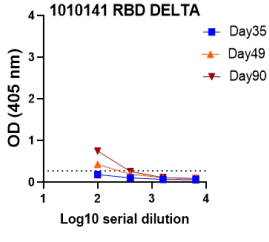

	Day35	Day49	Day90
Total Area	1413	11464	7658

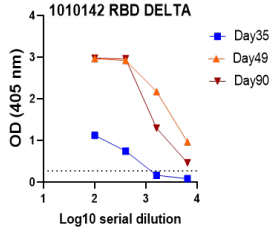

	Day35	Day49	Day90
Total Area	337.7	597.6	14516

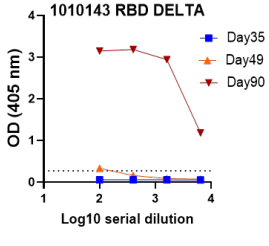

	Day35	Day49	Day90
Total Area	519.2	1651	781.7

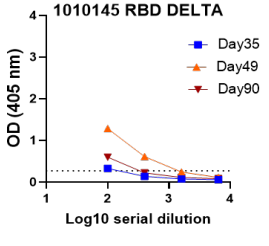

	Day35	Day49	Day90
Total Area	623.3	1348	1046

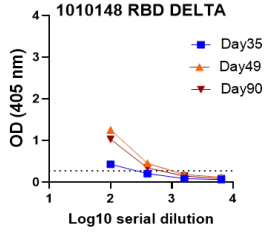

	Day35	Day49
Total Area	853.4	1610

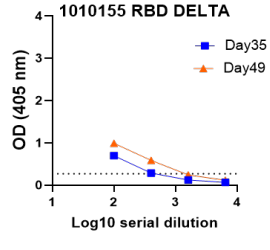

	Day35	Day49	Day90
Total Area	399.8	880.7	756.9

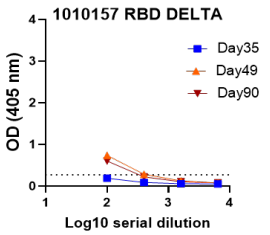

	Day35	Day49	Day90
Total Area	719.3	1602	874.7

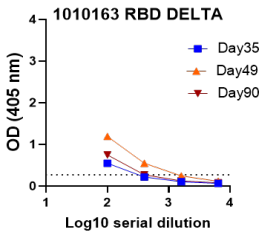

	Day35	Day49
Total Area	440.6	621.8

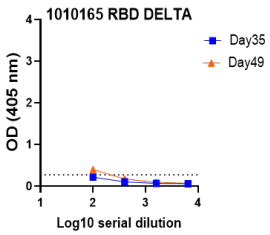

	Day35	Day49	Day90
Total Area	397.5	958.4	1048

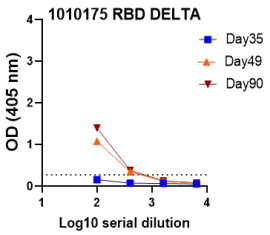

	Day35	Day49	Day90
Total Area	691.5	1250	576.0

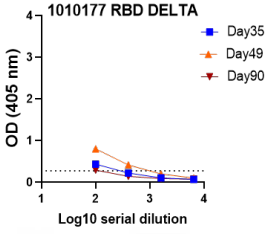

	Day35	Day49	Day90
Total Area	528.9	1098	1232

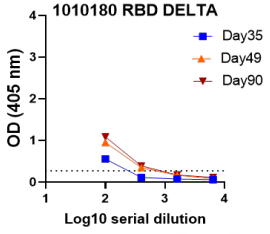

	Day35	Day49	Day90
Total Area	826.8	1105	758.4

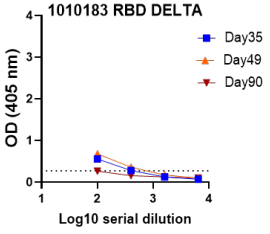

	Day35	Day49	Day90
Total Area	543.2	1835	20058

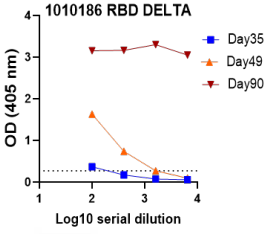

	Day35	Day49	Day90
Total Area	541.4	635.3	699.2

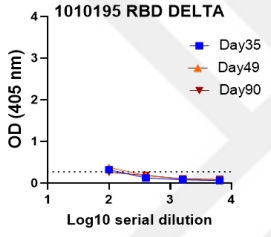

	Day35	Day49	Day90
Total Area	991.8	1690	1879

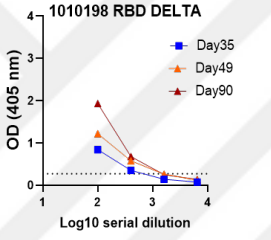

	Day35	Day49	Day90
Total Area	516.9	1041	1360

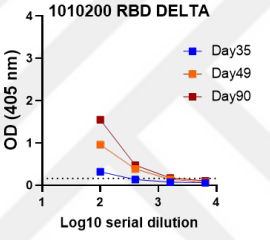

	Day35	Day49
Total Area	638.7	1454

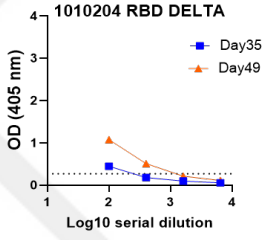

	Day35	Day49	Day90
Total Area	480.3	1119	951.6

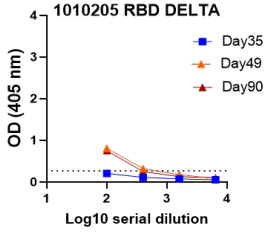

	Day35	Day49	Day90
Total Area	1612	1243	682.2

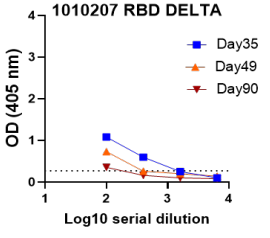

	Day35	Day49	Day90
Total Area	678.3	1327	1399

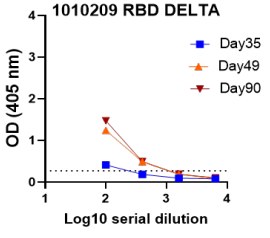

	Day35	Day49	Day90
Total Area	833.4	1840	1462

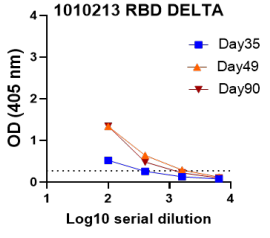

	Day35	Day49	Day90
Total Area	628.4	3373	2706

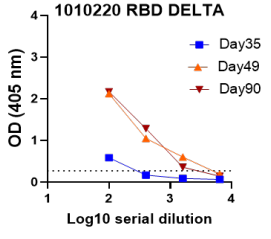

	Day35	Day49	Day90
Total Area	899.7	1621	1099

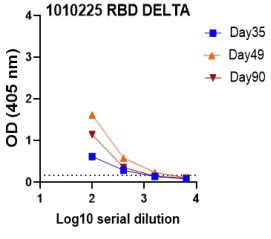

	Day35	Day49	Day90
Total Area	626.4	2040	3176

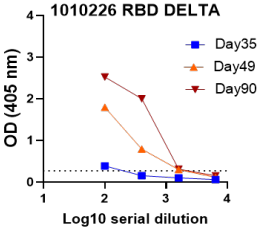

	Day35	Day49	Day90
Total Area	1909	2991	19822

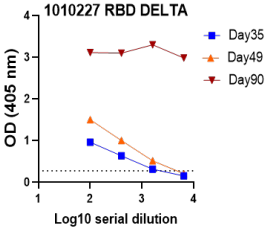

	Day35	Day49	Day90
Total Area	821.7	1500	1376

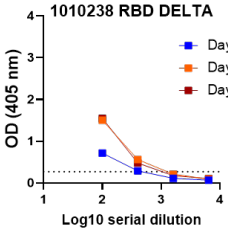

	Day35	Day49	Day90
Total Area	774.8	1521	1635

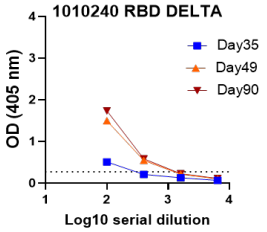

	Day35	Day49	Day90
Total Area	493.5	629.0	837.8

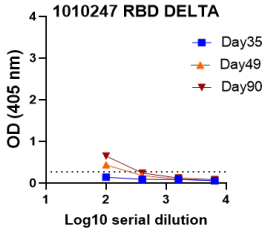

	Day35	Day49	Day90
Total Area	933.5	1253	824.7

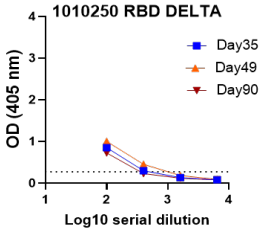

	Day35	Day49	Day90
Total Area	1238	1461	645.2

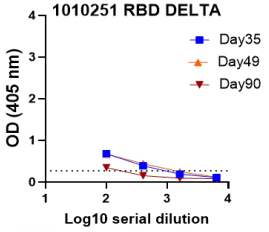

	Day35	Day49	Day90
Total Area	604.2	904.7	791.3

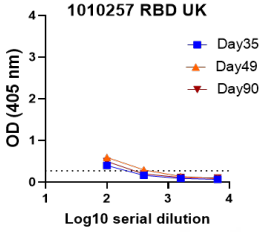

	Day35	Day49	Day90
Total Area	3382	1077	678.8

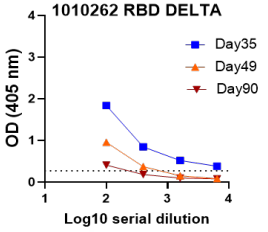

	Day35	Day49	Day90
Total Area	2574	1043	953.1

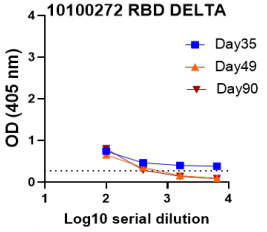

	Day35	Day49	Day90
Total Area	2391	1045	17833

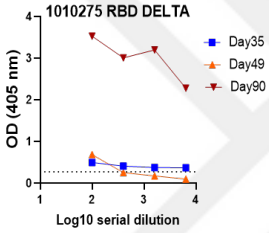

	Day35	Day49	Day90
Total Area	635.3	866.1	746.9

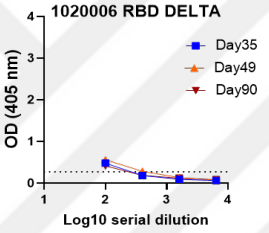

	Day35	Day49	Day90
Total Area	614.1	978.9	619.7

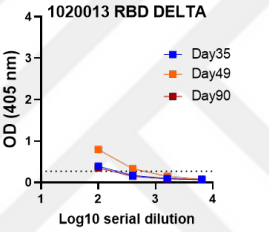

	Day35	Day49	Day90
Total Area	483.9	626.9	521.9

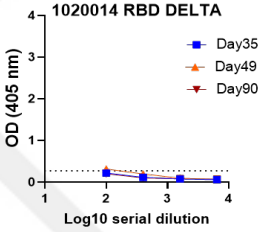

	Day35	Day49	Day90
Total Area	619.8	1354	913.2

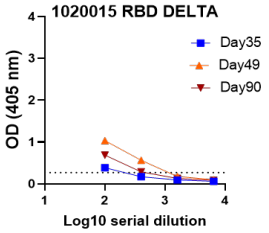

	Day35	Day49	Day90
Total Area	397.1	495.6	611.3

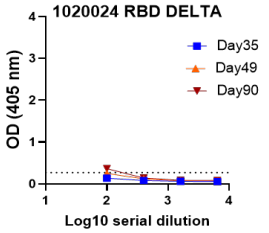

	Day35	Day49	Day90
Total Area	894.3	1632	1033

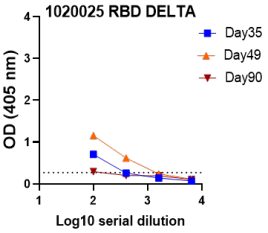

	Day35	Day49	Day90
Total Area	974.1	1318	734.0

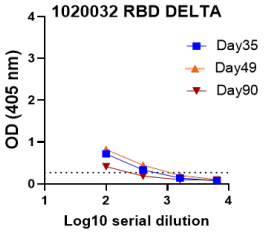

	Day35	Day49	Day90
Total Area	542.6	672.6	688.8

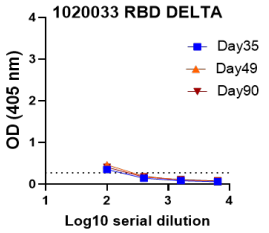

	Day35	Day49	Day90
Total Area	684.5	686.7	587.0

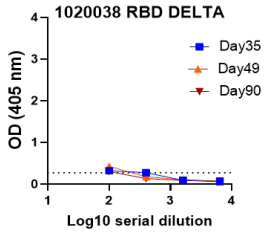

	Day35	Day49
Total Area	554.6	1673

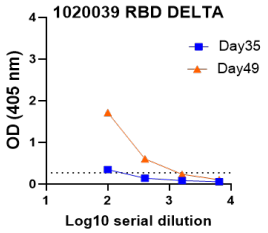

	Day35	Day49	Day90
Total Area	482.9	910.5	14857

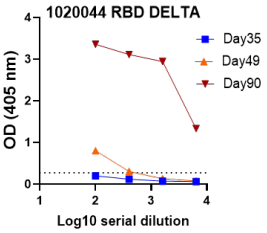

	Day35	Day49	Day90
Total Area	646.1	925.1	668.7

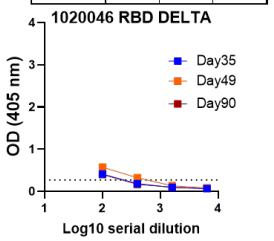

	Day35	Day49	Day90
Total Area	2490	1241	980.0

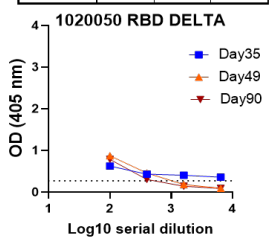

	Day35	Day49
Total Area	2415	985.2

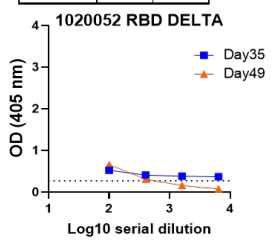

	Day35	Day49	Day90
Total Area	2318	877.7	651.9

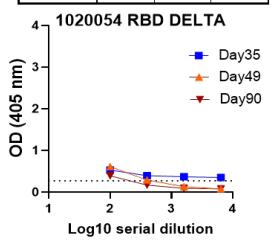

	Day35	Day49	Day90
Total Area	2360	1077	686.6

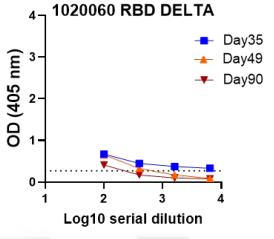

	Day35	Day49
Total Area	2401	713.3

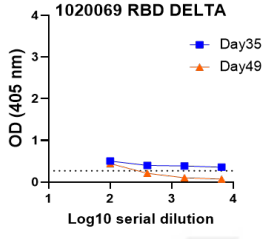

	Day35	Day49	Day90
Total Area	4453	2791	1926

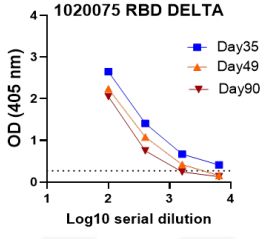

	Day35	Day49	Day90
Total Area	1549	9672	6168

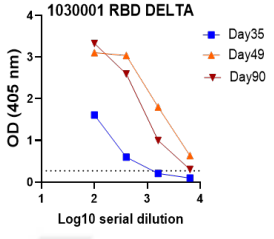

	Day35	Day49	Day90
Total Area	604.4	1871	593.1

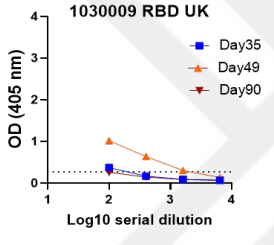

	Day35	Day49	Day90
Total Area	700.1	750.2	740.7

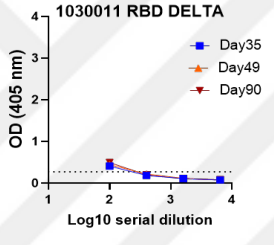

	Day35	Day49	Day90
Total Area	727.2	2098	1023

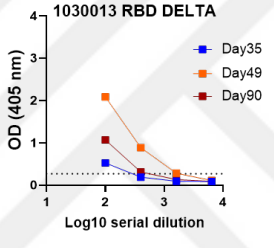

	Day35	Day49	Day90
Total Area	538.1	845.3	645.6

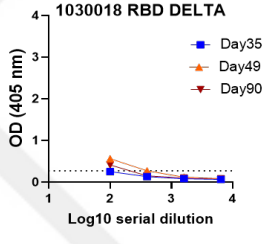

	Day35	Day49	Day90
Total Area	667.1	1153	1238

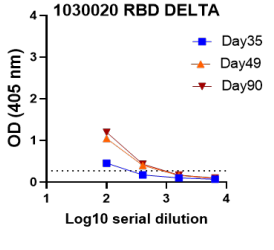

	Day35	Day49	Day90
Total Area	532.2	911.6	614.9

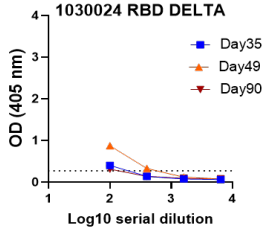

	Day35	Day49	Day90
Total Area	515.0	5887	8350

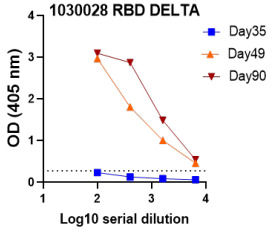

	Day35	Day49	Day90
Total Area	503.7	819.0	822.2

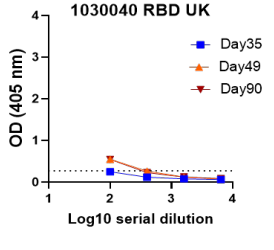

	Day35	Day49	Day90
Total Area	674.9	1069	1107

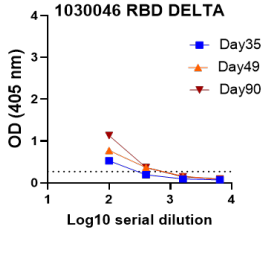

	Day35	Day49	Day90
Total Area	507.6	819.2	1048

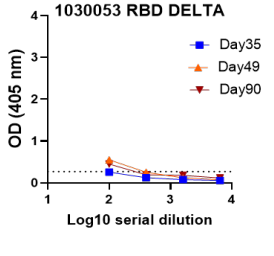

	Day35	Day49	Day90
Total Area	1943	961.2	18750

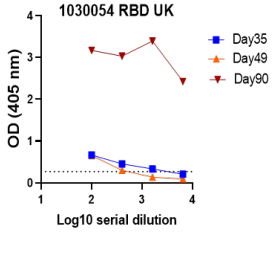

	Day35	Day49
Total Area	774.3	1816

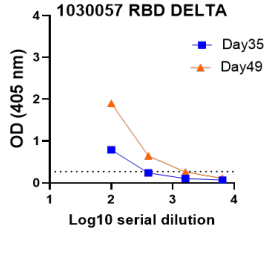

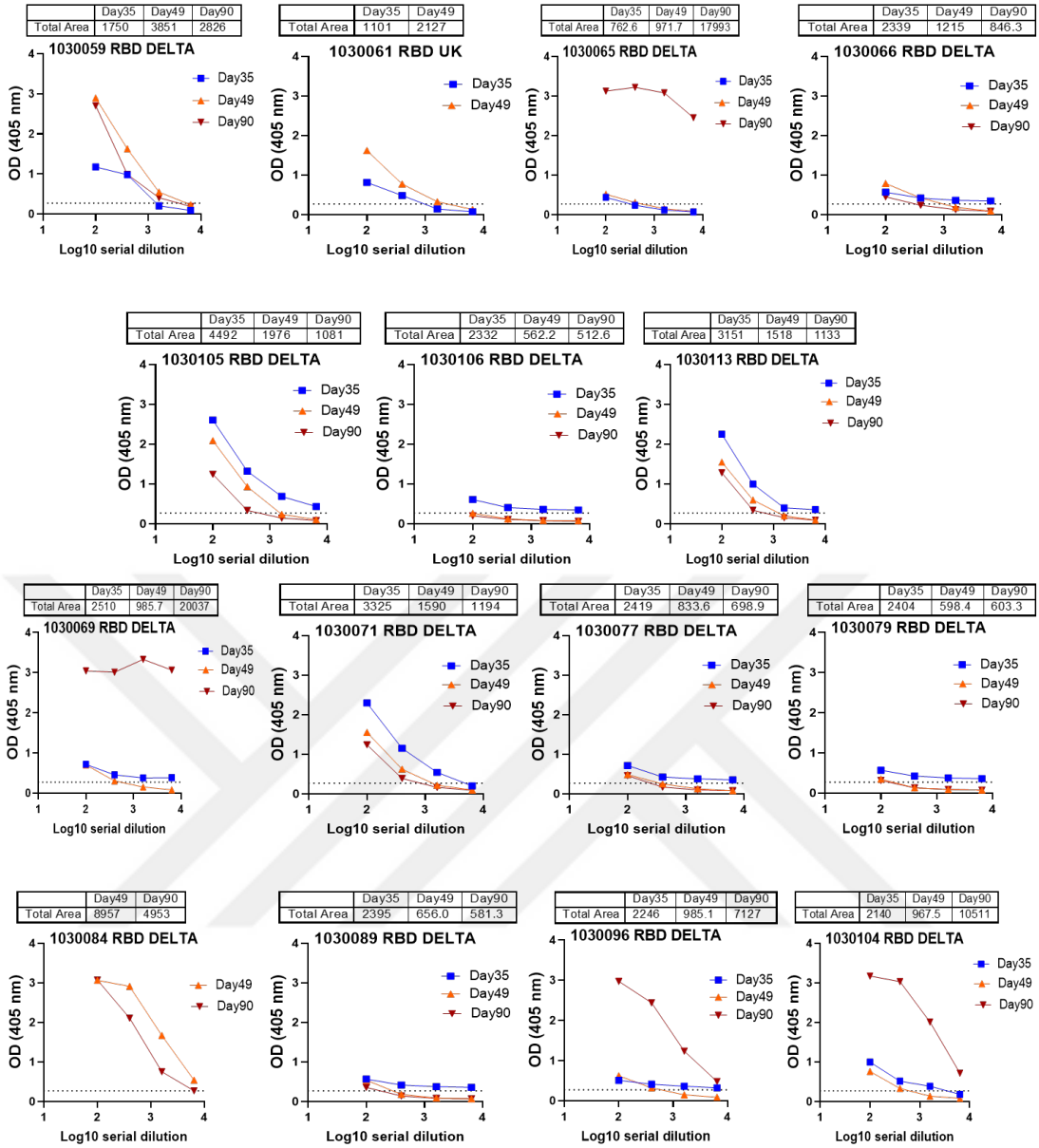

Figure A5. Anti-Delta RBD IgG Titer demonstrations of Phase II clinical trial volunteers. Serum samples taken from volunteers were diluted 1:100, 1:400, 1:1600 and 1:6400-fold. Area under the curve calculations were used to determine titers of OD405 versus log10 reciprocal serial dilutions graphs.

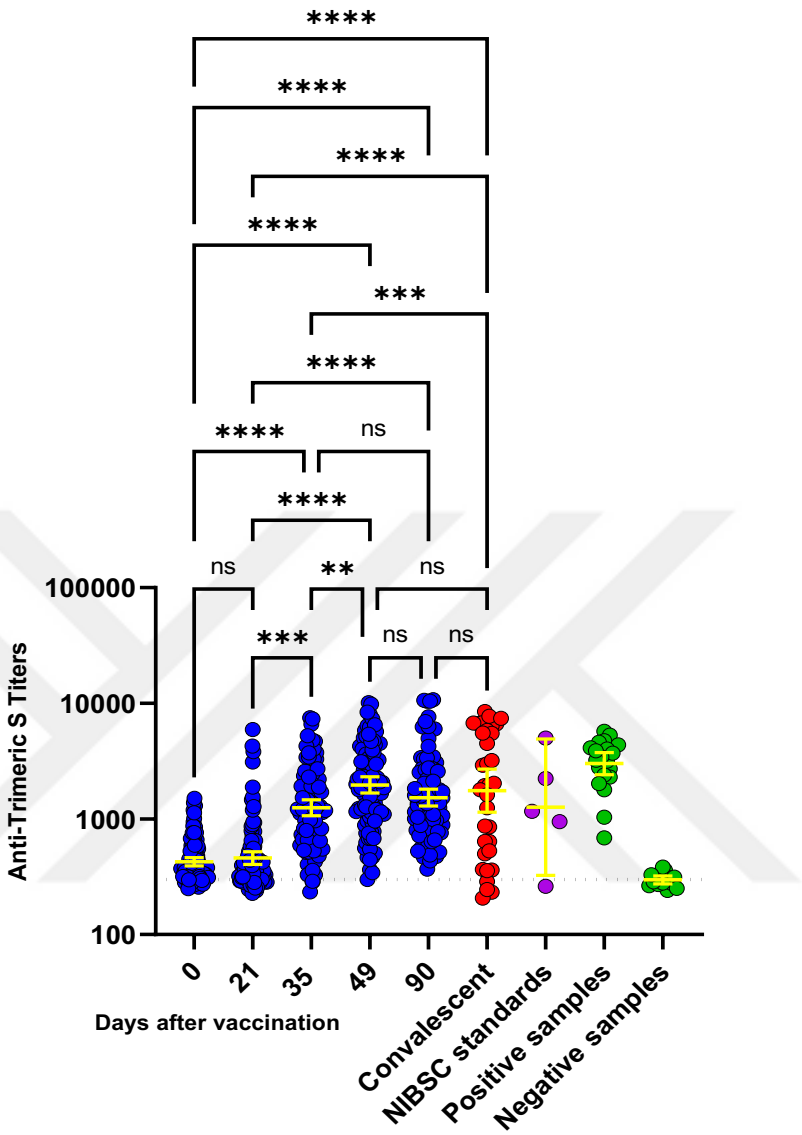

	0	21	35	49	90	Convalescent
Number of values	101	101	101	101	93	35
Geometric mean	426.8	458.4	1248	1969	1529	1756
Geometric SD factor	1.523	1.890	2.253	2.276	2.259	3.485
Lower 95% CI of geo. mean	392.8	404.3	1063	1674	1293	1143
Upper 95% CI of geo. mean	463.8	519.8	1465	2316	1809	2696

Figure A6. Measurement of Anti-Trimeric S IgG responses without volunteers who were positive for COVID-19. Volunteers who were COVID-19 at a given time during the study were excluded. (ns:non-significant, *p≤0.05, **p≤0.01, ***p≤0.001, ****p≤0.0001.)

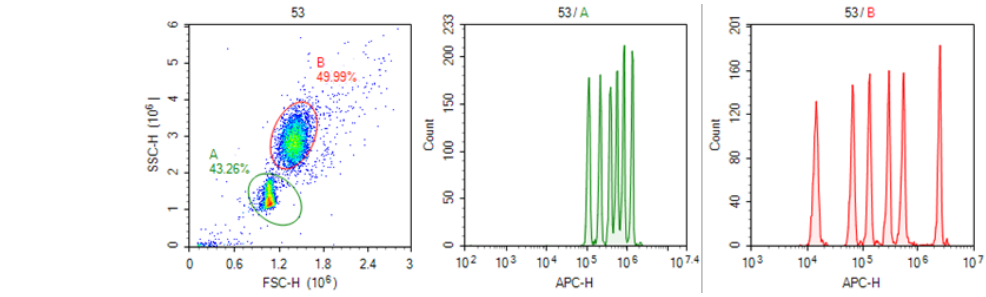
53
B
49.99%
A
43.26%
SSC-H (10^6)
FSC-H (10^6)
53 / A
Count
APC-H
53 / B
Count
APC-H

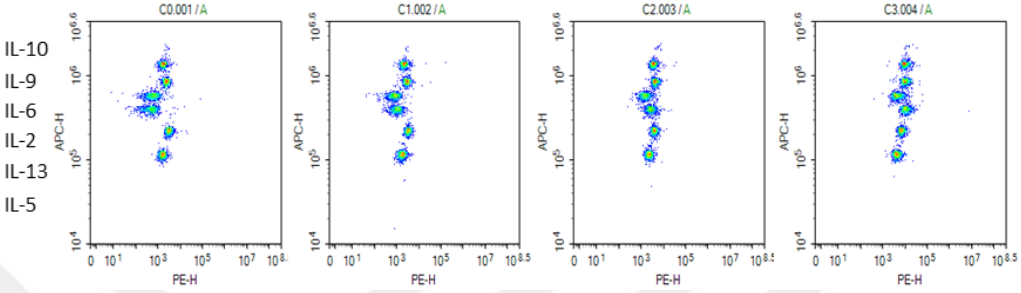
IL-10
IL-9
IL-6
IL-2
IL-13
IL-5
C0.001 / A
C1.002 / A
C2.003 / A
C3.004 / A
APC-H
PE-H

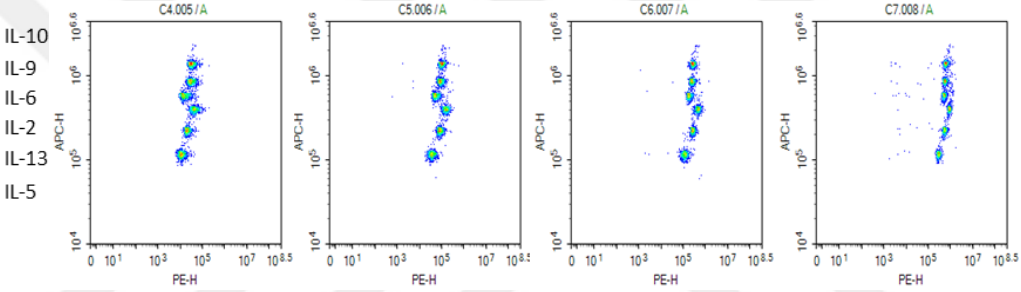
IL-10
IL-9
IL-6
IL-2
IL-13
IL-5
C4.005 / A
C5.006 / A
C6.007 / A
C7.008 / A
APC-H
PE-H

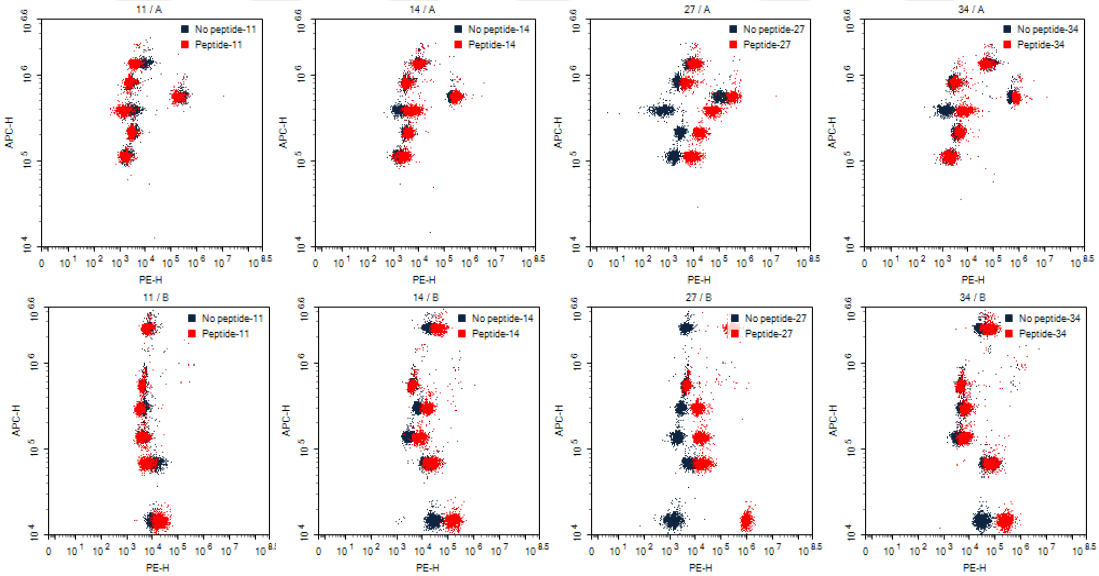
11 / A
14 / A
27 / A
34 / A
No peptide-11
Peptide-11
No peptide-14
Peptide-14
No peptide-27
Peptide-27
No peptide-34
Peptide-34
11 / B
14 / B
27 / B
34 / B
APC-H
PE-H

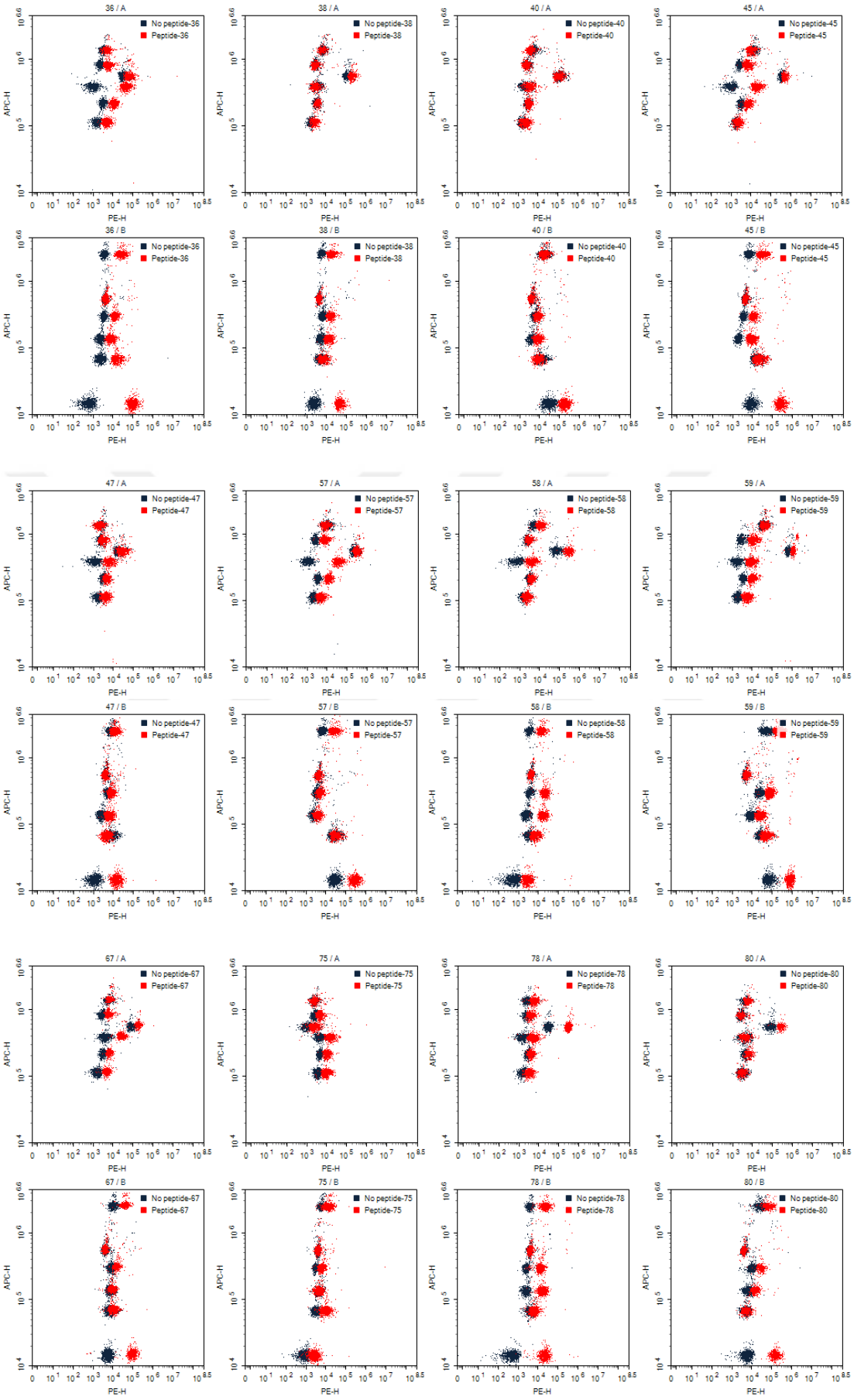
36 / A
No peptide-36
Peptide-36
38 / A
No peptide-38
Peptide-38
40 / A
No peptide-40
Peptide-40
45 / A
No peptide-45
Peptide-45
36 / B
No peptide-36
Peptide-36
38 / B
No peptide-38
Peptide-38
40 / B
No peptide-40
Peptide-40
45 / B
No peptide-45
Peptide-45
47 / A
No peptide-47
Peptide-47
57 / A
No peptide-57
Peptide-57
58 / A
No peptide-58
Peptide-58
59 / A
No peptide-59
Peptide-59
47 / B
No peptide-47
Peptide-47
57 / B
No peptide-57
Peptide-57
58 / B
No peptide-58
Peptide-58
59 / B
No peptide-59
Peptide-59
67 / A
No peptide-67
Peptide-67
75 / A
No peptide-75
Peptide-75
78 / A
No peptide-78
Peptide-78
80 / A
No peptide-80
Peptide-80
67 / B
No peptide-67
Peptide-67
75 / B
No peptide-75
Peptide-75
78 / B
No peptide-78
Peptide-78
80 / B
No peptide-80
Peptide-80
APC-H
PE-H

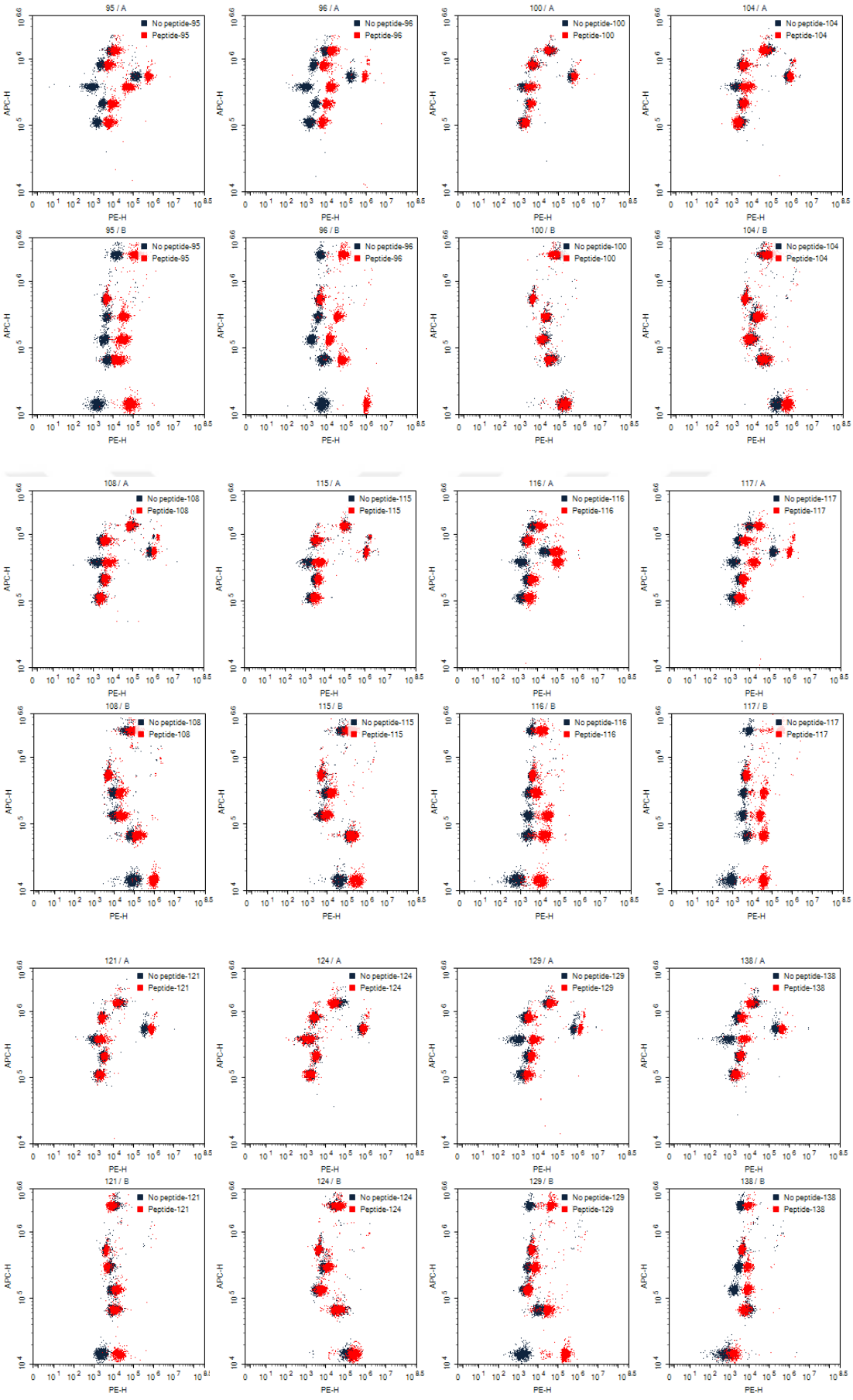
95 / A
No peptide-95
Peptide-95
96 / A
No peptide-96
Peptide-96
100 / A
No peptide-100
Peptide-100
104 / A
No peptide-104
Peptide-104
95 / B
No peptide-95
Peptide-95
96 / B
No peptide-96
Peptide-96
100 / B
No peptide-100
Peptide-100
104 / B
No peptide-104
Peptide-104
108 / A
No peptide-108
Peptide-108
115 / A
No peptide-115
Peptide-115
116 / A
No peptide-116
Peptide-116
117 / A
No peptide-117
Peptide-117
108 / B
No peptide-108
Peptide-108
115 / B
No peptide-115
Peptide-115
116 / B
No peptide-116
Peptide-116
117 / B
No peptide-117
Peptide-117
121 / A
No peptide-121
Peptide-121
124 / A
No peptide-124
Peptide-124
129 / A
No peptide-129
Peptide-129
138 / A
No peptide-138
Peptide-138
121 / B
No peptide-121
Peptide-121
124 / B
No peptide-124
Peptide-124
129 / B
No peptide-129
Peptide-129
138 / B
No peptide-138
Peptide-138
APC-H
PE-H

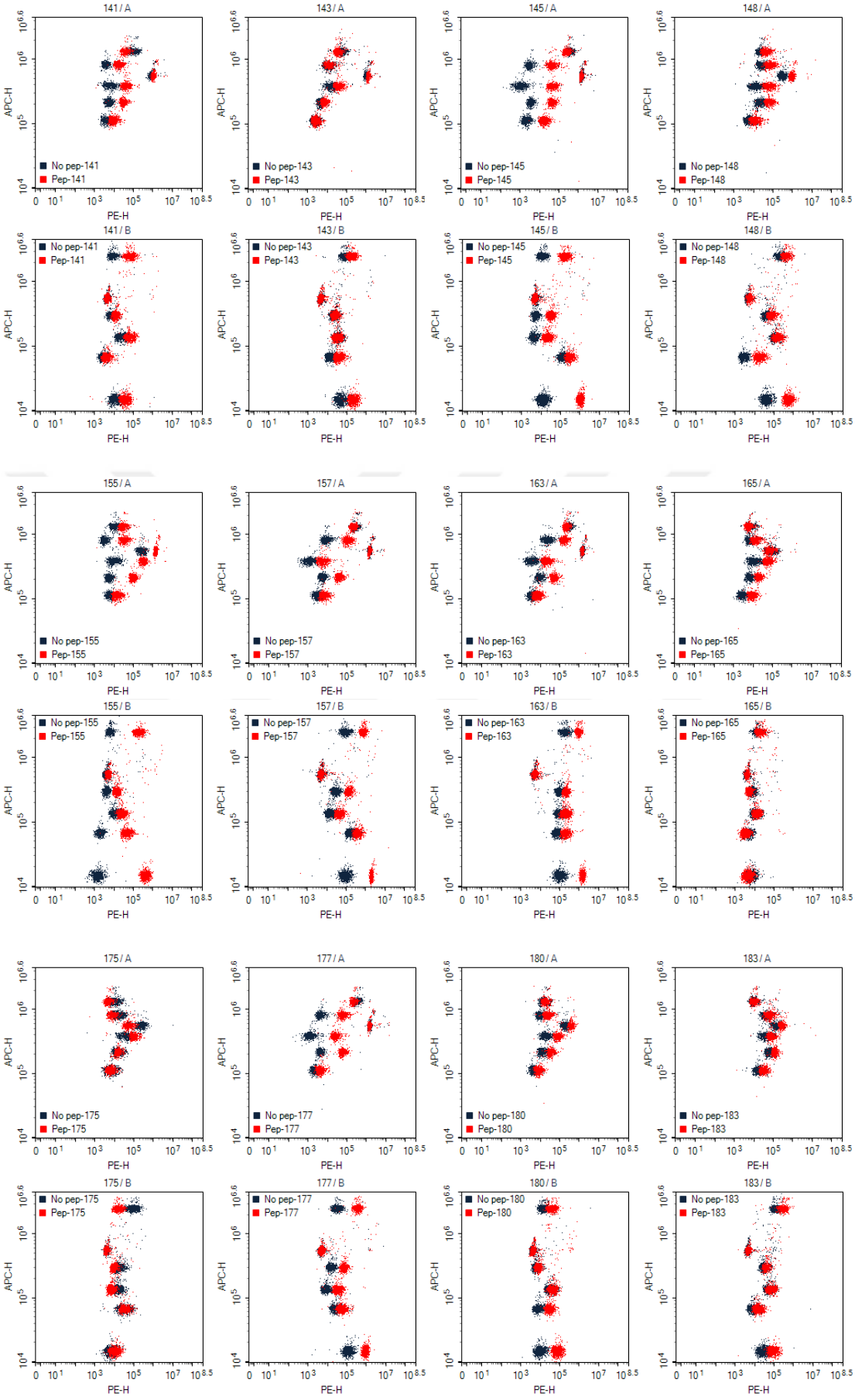
141 / A
No pep-141
Pep-141
143 / A
No pep-143
Pep-143
145 / A
No pep-145
Pep-145
148 / A
No pep-148
Pep-148
141 / B
143 / B
145 / B
148 / B
155 / A
No pep-155
Pep-155
157 / A
No pep-157
Pep-157
163 / A
No pep-163
Pep-163
165 / A
No pep-165
Pep-165
155 / B
157 / B
163 / B
165 / B
175 / A
No pep-175
Pep-175
177 / A
No pep-177
Pep-177
180 / A
No pep-180
Pep-180
183 / A
No pep-183
Pep-183
175 / B
177 / B
180 / B
183 / B
APC-H
PE-H

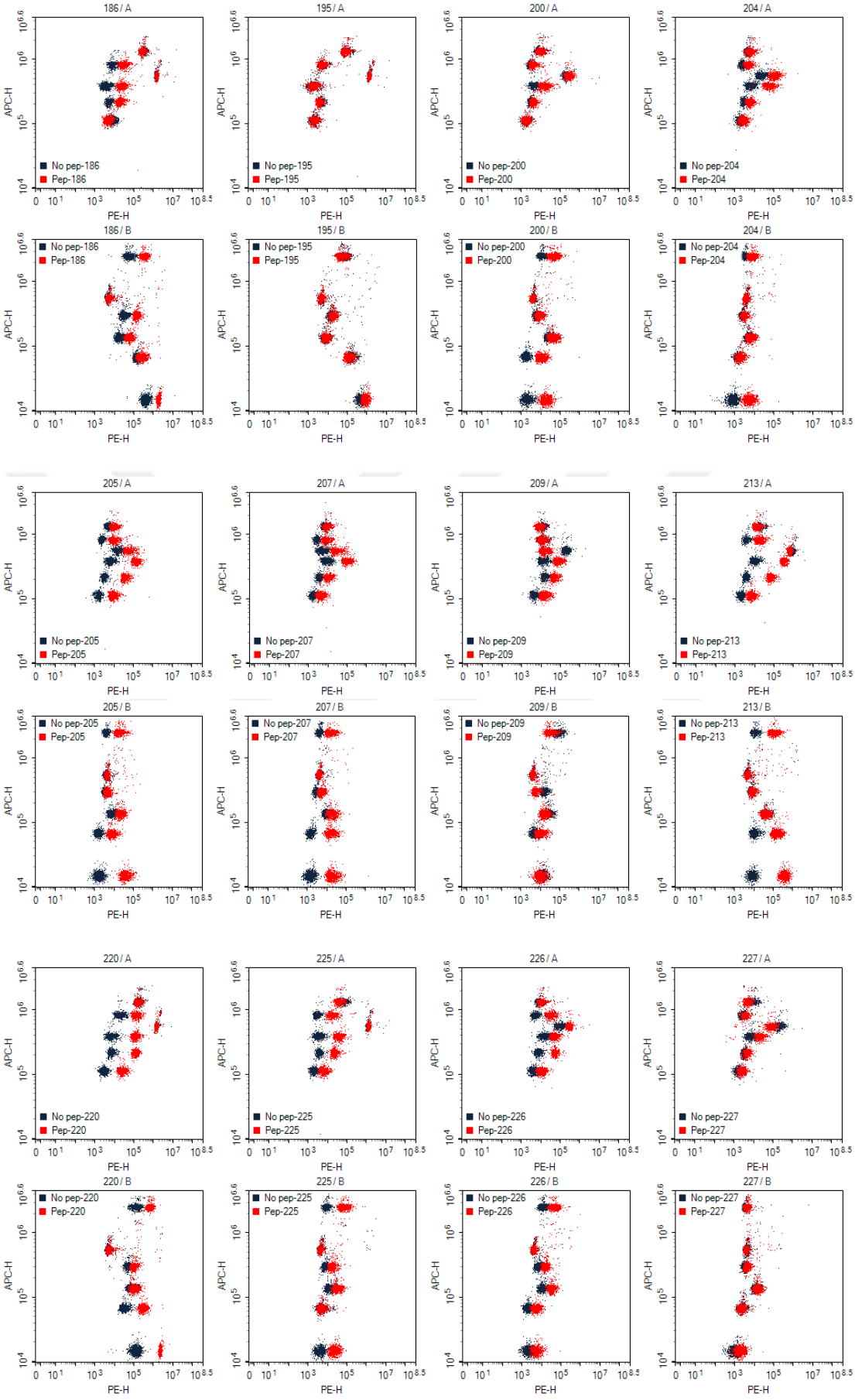
186 / A
No pep-186
Pep-186
195 / A
No pep-195
Pep-195
200 / A
No pep-200
Pep-200
204 / A
No pep-204
Pep-204
186 / B
No pep-186
Pep-186
195 / B
No pep-195
Pep-195
200 / B
No pep-200
Pep-200
204 / B
No pep-204
Pep-204
205 / A
No pep-205
Pep-205
207 / A
No pep-207
Pep-207
209 / A
No pep-209
Pep-209
213 / A
No pep-213
Pep-213
205 / B
No pep-205
Pep-205
207 / B
No pep-207
Pep-207
209 / B
No pep-209
Pep-209
213 / B
No pep-213
Pep-213
220 / A
No pep-220
Pep-220
225 / A
No pep-225
Pep-225
226 / A
No pep-226
Pep-226
227 / A
No pep-227
Pep-227
220 / B
No pep-220
Pep-220
225 / B
No pep-225
Pep-225
226 / B
No pep-226
Pep-226
227 / B
No pep-227
Pep-227
APC-H
PE-H

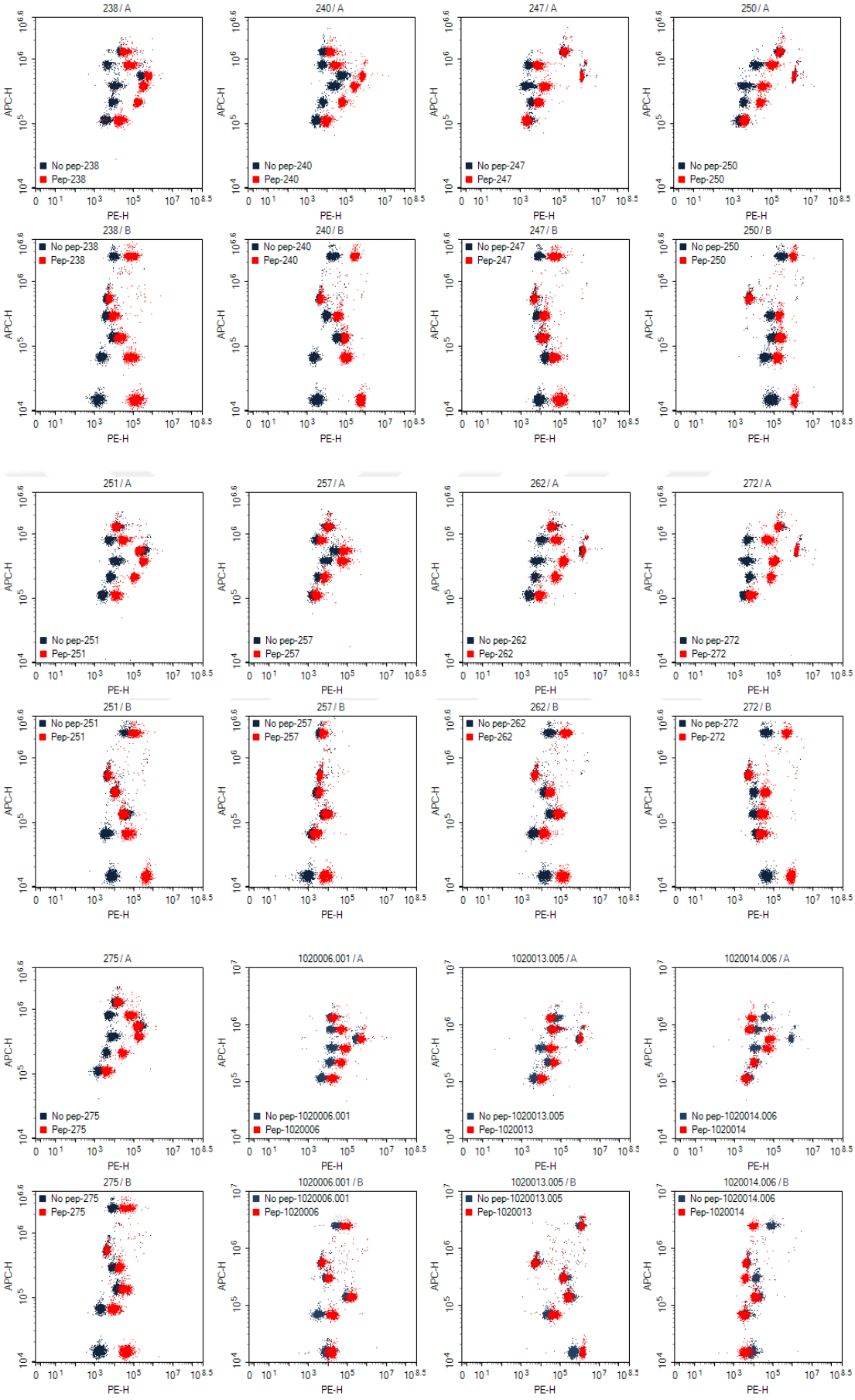
238 / A
No pep-238
Pep-238
240 / A
No pep-240
Pep-240
247 / A
No pep-247
Pep-247
250 / A
No pep-250
Pep-250
238 / B
No pep-238
Pep-238
240 / B
No pep-240
Pep-240
247 / B
No pep-247
Pep-247
250 / B
No pep-250
Pep-250
251 / A
No pep-251
Pep-251
257 / A
No pep-257
Pep-257
262 / A
No pep-262
Pep-262
272 / A
No pep-272
Pep-272
251 / B
No pep-251
Pep-251
257 / B
No pep-257
Pep-257
262 / B
No pep-262
Pep-262
272 / B
No pep-272
Pep-272
275 / A
No pep-275
Pep-275
1020006.001 / A
No pep-1020006.001
Pep-1020006
1020013.005 / A
No pep-1020013.005
Pep-1020013
1020014.006 / A
No pep-1020014.006
Pep-1020014
275 / B
No pep-275
Pep-275
1020006.001 / B
No pep-1020006.001
Pep-1020006
1020013.005 / B
No pep-1020013.005
Pep-1020013
1020014.006 / B
No pep-1020014.006
Pep-1020014
APC-H
PE-H

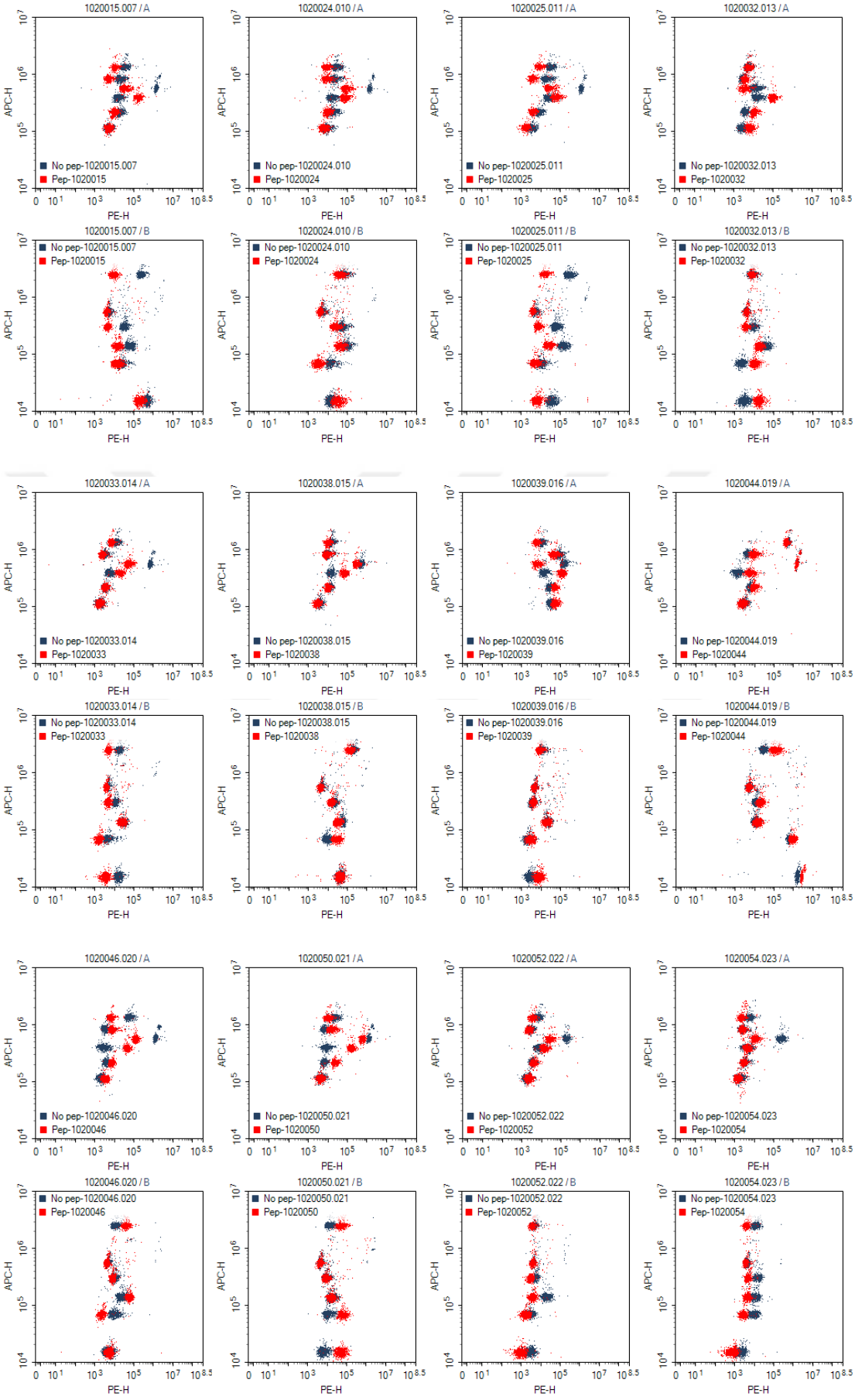
1020015.007 / A
No pep-1020015.007
Pep-1020015
1020024.010 / A
No pep-1020024.010
Pep-1020024
1020025.011 / A
No pep-1020025.011
Pep-1020025
1020032.013 / A
No pep-1020032.013
Pep-1020032
1020015.007 / B
No pep-1020015.007
Pep-1020015
1020024.010 / B
No pep-1020024.010
Pep-1020024
1020025.011 / B
No pep-1020025.011
Pep-1020025
1020032.013 / B
No pep-1020032.013
Pep-1020032
1020033.014 / A
No pep-1020033.014
Pep-1020033
1020038.015 / A
No pep-1020038.015
Pep-1020038
1020039.016 / A
No pep-1020039.016
Pep-1020039
1020044.019 / A
No pep-1020044.019
Pep-1020044
1020033.014 / B
No pep-1020033.014
Pep-1020033
1020038.015 / B
No pep-1020038.015
Pep-1020038
1020039.016 / B
No pep-1020039.016
Pep-1020039
1020044.019 / B
No pep-1020044.019
Pep-1020044
1020046.020 / A
No pep-1020046.020
Pep-1020046
1020050.021 / A
No pep-1020050.021
Pep-1020050
1020052.022 / A
No pep-1020052.022
Pep-1020052
1020054.023 / A
No pep-1020054.023
Pep-1020054
1020046.020 / B
No pep-1020046.020
Pep-1020046
1020050.021 / B
No pep-1020050.021
Pep-1020050
1020052.022 / B
No pep-1020052.022
Pep-1020052
1020054.023 / B
No pep-1020054.023
Pep-1020054
APC-H
PE-H

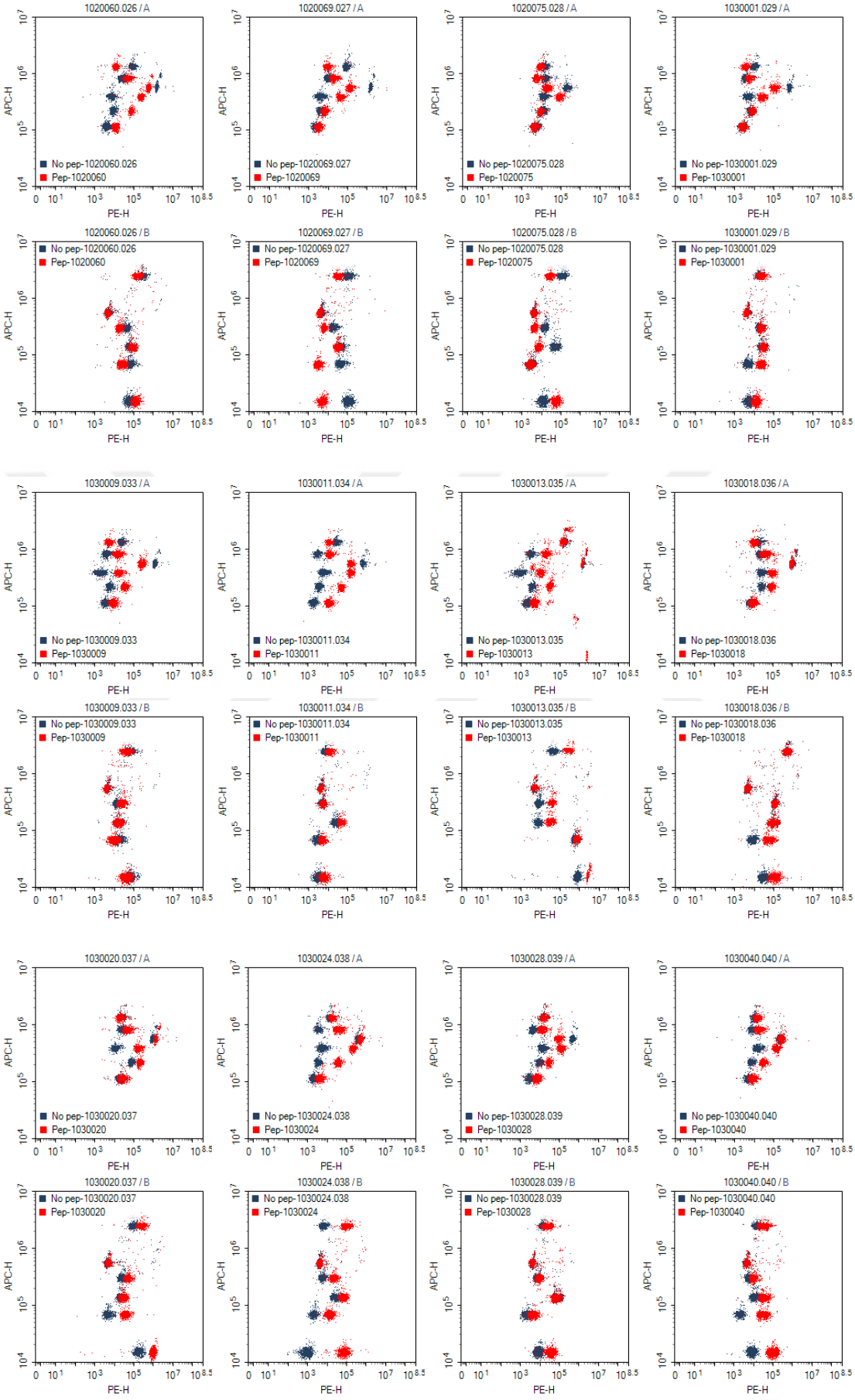
1020060.026 / A
No pep-1020060.026
Pep-1020060
1020069.027 / A
No pep-1020069.027
Pep-1020069
1020075.028 / A
No pep-1020075.028
Pep-1020075
1030001.029 / A
No pep-1030001.029
Pep-1030001
1020060.026 / B
No pep-1020060.026
Pep-1020060
1020069.027 / B
No pep-1020069.027
Pep-1020069
1020075.028 / B
No pep-1020075.028
Pep-1020075
1030001.029 / B
No pep-1030001.029
Pep-1030001
1030009.033 / A
No pep-1030009.033
Pep-1030009
1030011.034 / A
No pep-1030011.034
Pep-1030011
1030013.035 / A
No pep-1030013.035
Pep-1030013
1030018.036 / A
No pep-1030018.036
Pep-1030018
1030009.033 / B
No pep-1030009.033
Pep-1030009
1030011.034 / B
No pep-1030011.034
Pep-1030011
1030013.035 / B
No pep-1030013.035
Pep-1030013
1030018.036 / B
No pep-1030018.036
Pep-1030018
1030020.037 / A
No pep-1030020.037
Pep-1030020
1030024.038 / A
No pep-1030024.038
Pep-1030024
1030028.039 / A
No pep-1030028.039
Pep-1030028
1030040.040 / A
No pep-1030040.040
Pep-1030040
1030020.037 / B
No pep-1030020.037
Pep-1030020
1030024.038 / B
No pep-1030024.038
Pep-1030024
1030028.039 / B
No pep-1030028.039
Pep-1030028
1030040.040 / B
No pep-1030040.040
Pep-1030040
APC-H
PE-H

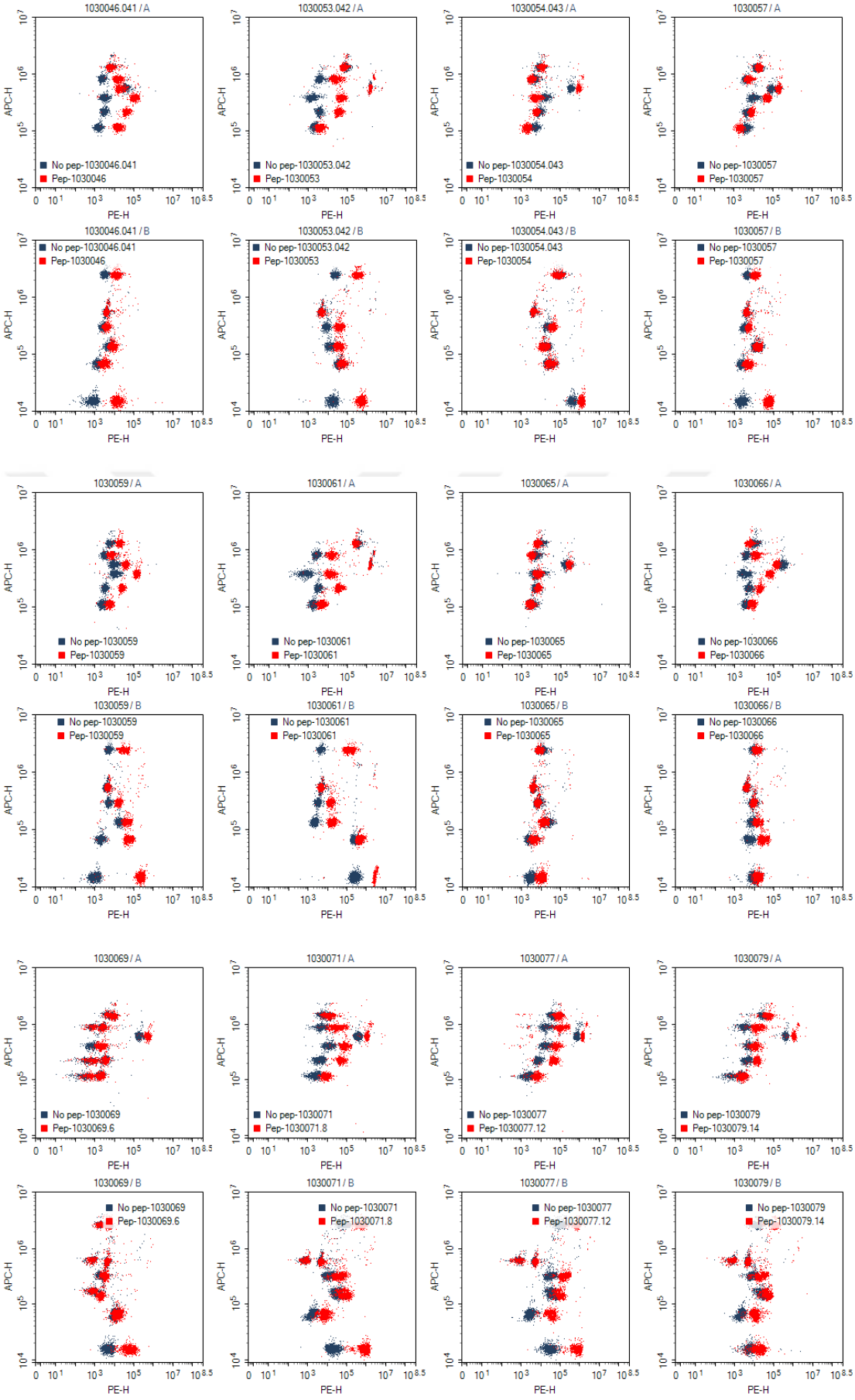
1030046.041 / A
No pep-1030046.041
Pep-1030046
1030053.042 / A
No pep-1030053.042
Pep-1030053
1030054.043 / A
No pep-1030054.043
Pep-1030054
1030057 / A
No pep-1030057
Pep-1030057
1030046.041 / B
No pep-1030046.041
Pep-1030046
1030053.042 / B
No pep-1030053.042
Pep-1030053
1030054.043 / B
No pep-1030054.043
Pep-1030054
1030057 / B
No pep-1030057
Pep-1030057
1030059 / A
No pep-1030059
Pep-1030059
1030061 / A
No pep-1030061
Pep-1030061
1030065 / A
No pep-1030065
Pep-1030065
1030066 / A
No pep-1030066
Pep-1030066
1030059 / B
No pep-1030059
Pep-1030059
1030061 / B
No pep-1030061
Pep-1030061
1030065 / B
No pep-1030065
Pep-1030065
1030066 / B
No pep-1030066
Pep-1030066
1030069 / A
No pep-1030069
Pep-1030069.6
1030071 / A
No pep-1030071
Pep-1030071.8
1030077 / A
No pep-1030077
Pep-1030077.12
1030079 / A
No pep-1030079
Pep-1030079.14
1030069 / B
No pep-1030069
Pep-1030069.6
1030071 / B
No pep-1030071
Pep-1030071.8
1030077 / B
No pep-1030077
Pep-1030077.12
1030079 / B
No pep-1030079
Pep-1030079.14
APC-H
PE-H

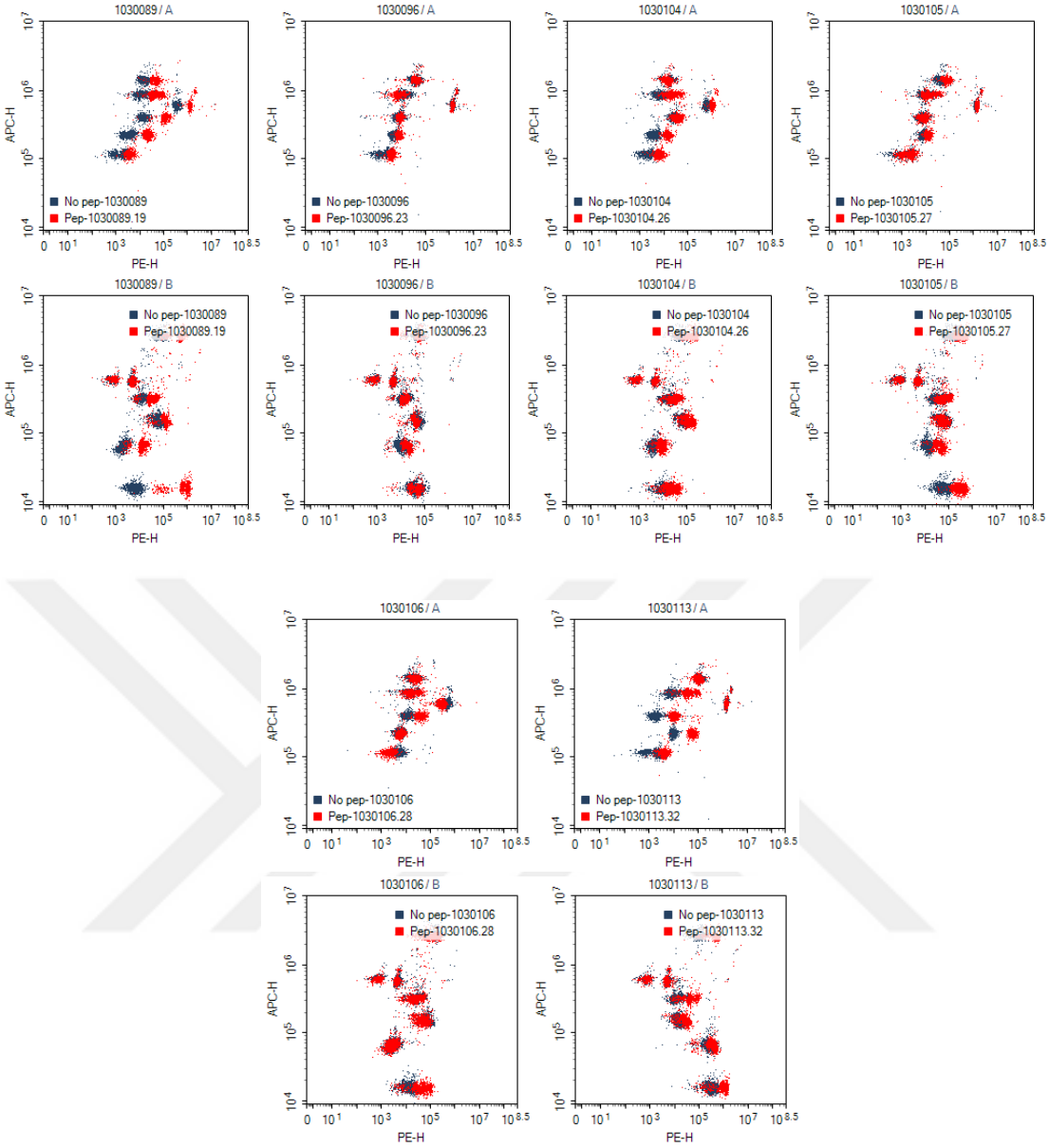

Figure A7. 12 cytokines production in response to SARS-CoV-2 peptide stimulation of Phase II clinical trial volunteers. Each dot represents a cytokine and dot plot overlays indicates whether volunteer produced this cytokine after SNMO peptide pool stimulation. No peptide was shown as black color and peptide stimulated cells were labeled as red color.

APPENDIX B

Recipes of Cell Culture Media and Buffers

1. 10X Phosphate Buffered Saline (PBS):

• 80 g NaCl

• 2 g KCl

• 8.01 g $Na_2HPO_4.2H_2O$

• 2 g KH_2PO_4

• 1 L dH2O

pH is set to 6.8 and the buffer is autoclaved before use.

2. 1X PBS:

• 100 ml 10X PBS

• 900 ml dH2O

pH is set to 7.4.

3. ELISA Blocking Buffer:

• 500 ml 1X PBS

• 25 g bovine serum albumin (BSA)

• 250 µl Tween-20

4. ELISA Washing Buffer:

• 500 ml 10X PBS

• 2.5 ml Tween-20

• 4.5 L dH2O

5. Wash Buffer (ELISA)

• 4.5 lt distilled H2O

• 0.5 lt 10X PBS

• 2.5 ml Tween20

6. RPMI-1640 Media

For %2:

• 500 ml RPMI-1640 Media

• 10.64 ml FBS

• 5.32 ml HEPES

• 5.32 ml Penicillin/Streptomycin

7. RPMI-1640 Media

For %10:

• 500 ml RPMI-1640 Media

• 58 ml FBS

• 5.8 ml HEPES

• 5.8 ml Penicillin/Streptomycin

• 5.8 ml Non-essential Amino acid

• 5.8 ml Sodium-Pyruvate

COPYRIGHT PERMISSIONS

License Details

This Agreement between Berfu Saraydar ("You") and Springer Nature ("Springer Nature") consists of your license details and the terms and conditions provided by Springer Nature and Copyright Clearance Center.

Print Copy

License Number	5373060184486
License date	Aug 20, 2022
Licensed Content Publisher	Springer Nature
Licensed Content Publication	Nature Reviews Immunology
Licensed Content Title	Expanding roles for CD4 T cells in immunity to viruses
Licensed Content Author	Susan L. Swain et al
Licensed Content Date	Jan 20, 2012
Type of Use	Thesis/Dissertation
Requestor type	non-commercial (non-profit)
Format	print and electronic
Portion	figures/tables/illustrations
Number of figures/tables/illustrations	1
High-res required	no
Will you be translating?	no
Circulation/distribution	200 - 499
Author of this Springer Nature content	no
Title	INVESTIGATION OF PRE-CLINICAL AND PHASE II CLINICAL STUDIES OF VLP-58-1023-AL-K3-PII VACCINE FOR ALPHA VARIANT
Institution name	Bilkent University
Expected presentation date	Aug 2022
Portions	Box 1
Requestor Location	Berfu Saraydar Bilkent University main campus science faculty B block Ankara, other Turkey Attn: Miss Berfu Saraydar
Total	**0.00 USD**

BACK

License Details

This Agreement between Berfu Saraydar ("You") and Springer Nature ("Springer Nature") consists of your license details and the terms and conditions provided by Springer Nature and Copyright Clearance Center.

Print Copy

License Number	5375350721528
License date	Aug 24, 2022
Licensed Content Publisher	Springer Nature
Licensed Content Publication	Nature Reviews Immunology
Licensed Content Title	A guide to vaccinology: from basic principles to new developments
Licensed Content Author	Andrew J. Pollard et al
Licensed Content Date	Dec 22, 2020
Type of Use	Thesis/Dissertation
Requestor type	non-commercial (non-profit)
Format	print and electronic
Portion	figures/tables/illustrations
Number of figures/tables/illustrations	1
High-res required	no
Will you be translating?	no
Circulation/distribution	200 - 499
Author of this Springer Nature content	no
Title	INVESTIGATION OF PRE-CLINICAL AND PHASE II CLINICAL STUDIES OF VLP-58-1023-AL-K3-PII VACCINE FOR ALPHA VARIANT
Institution name	Bilkent University
Expected presentation date	Aug 2022
Portions	Figure 3
Requestor Location	Berfu Saraydar Bilkent University main campus science faculty B block Ankara, other Turkey Attn: Miss Berfu Saraydar
Total	**0.00 USD**

BACK

License Details

This Agreement between Berfu Saraydar ("You") and Springer Nature ("Springer Nature") consists of your license details and the terms and conditions provided by Springer Nature and Copyright Clearance Center.

Print Copy

License Number	5373060184486
License date	Aug 20, 2022
Licensed Content Publisher	Springer Nature
Licensed Content Publication	Nature Reviews Immunology
Licensed Content Title	Expanding roles for CD4 T cells in immunity to viruses
Licensed Content Author	Susan L. Swain et al
Licensed Content Date	Jan 20, 2012
Type of Use	Thesis/Dissertation
Requestor type	non-commercial (non-profit)
Format	print and electronic
Portion	figures/tables/illustrations
Number of figures/tables/illustrations	1
High-res required	no
Will you be translating?	no
Circulation/distribution	200 - 499
Author of this Springer Nature content	no
Title	INVESTIGATION OF PRE-CLINICAL AND PHASE II CLINICAL STUDIES OF VLP-58-1023-AL-K3-PII VACCINE FOR ALPHA VARIANT
Institution name	Bilkent University
Expected presentation date	Aug 2022
Portions	Box 1
Requestor Location	Berfu Saraydar Bilkent University main campus science faculty B block Ankara, other Turkey Attn: Miss Berfu Saraydar
Total	**0.00 USD**

BACK